Asteroid Provided In-situ Supplies (APIS):

A Breakthrough to Enable an Affordable NASA Program of Human Exploration and Commercial Space Industrialization

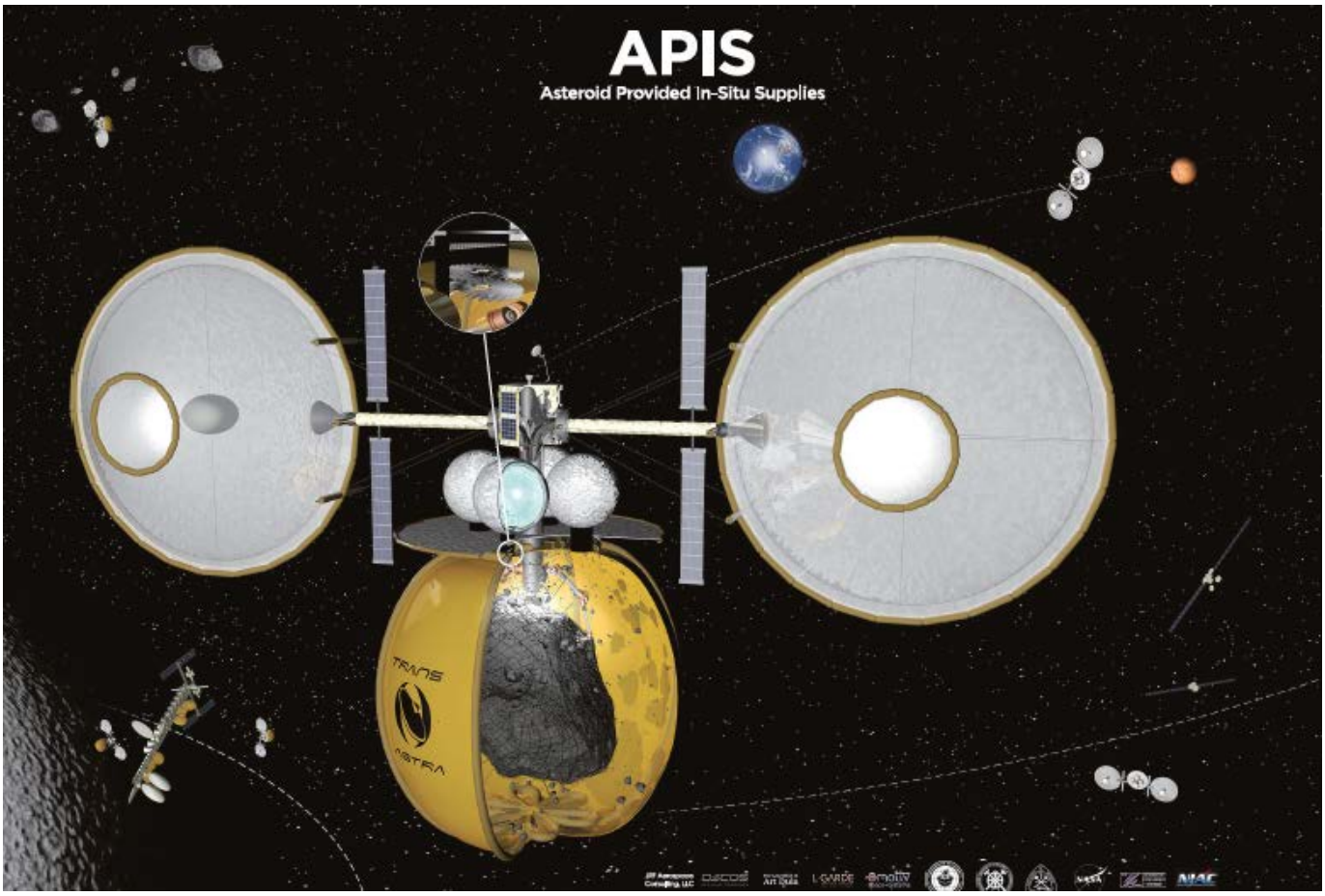

NIAC Phase I Final Report

29 February 2016

Joel C. Sercel, PhD
Principal Investigator
sercel@transastracorp.com

ICS Associates Inc.
Lake View Terrace, CA 91342

APIS

Asteroid Provided In-Situ Supplies

Apis is the genus for Honey Bees

Multiple Honey Bee Missions Will Be In Progress Simultaneously Providing a Constant Stream of Resources to Cis-Lunar Space

TransAstra Has Patents Pending For Passive Thermal Volatile Collection and Dust Separation Technology

TransAstra Is Working with NASA, ISS, and CASIS Planning an Early Optical Mining Demo on ISS

Reusable Worker Bee Space Tugs Provide Commercial Transport for NASA Astronauts in Deep Space

Optical Mining Exploits Inflatable Structures Technology Developed for NASA and the DoD

High Lunar Orbit is an Ideal Location for a Propellant Depot Supplied from Asteroids

Patent Pending Optical Mining Technology Uses Concentrated Sunlight To Excavate Asteroids and Extract Gases

Commercial Applications Include Delivering Satellites from LEO to GEO, Asteroid Mining, and Space Tourism Beyond LEO

Honey Bee Mining Technology Builds On NASA Technology Invested in the ARM Mission

Abstract

The vision of using asteroids as the stepping stones to the solar system has been shared by many for over a century beginning with Konstantin Tsiolkovsky first postulating the idea in 1903. Other space technology pioneers who considered practical applications of asteroid resources include Robert Goddard in 1918 and Gerard K. O'Neill in the 1970s. In the 1990s the well regarded planetary scientist John Lewis proposed asteroids as the source of in-space propellant for space operations. More recently, privately backed startup companies have worked on small prospecting spacecraft with an eye toward someday returning precious metals to the Earth. To move beyond being just a vision, the study of asteroid resource utilization needs a clear and technically rigorous plan for how to cost effectively extract and use asteroid resources as an economically viable approach to supporting space operations. This Phase I NIAC project provides that needed plan. **The Apis™ architecture is a clear and technically viable way to build an in-space transportation network that can reduce the cost of space operations so NASA can accomplish its vision of human exploration of space within a politically realistic budget.** To do this, the Apis architecture comprises several elements including the Honey Bee™ asteroid mining vehicle, the Worker Bee™ reusable deep space tug, and the Hive™ consumables depot in lunar distant retrograde orbit (LDRO). Together, these systems form a cost-effective reusable cis-lunar transportation network supplied by asteroid resources to eliminate the need for launching large quantities of consumables to support human exploration of deep space beyond LEO. Lightweight, thin film solar concentrators, structures, and optical systems are key features of all elements of the Apis™ architecture which relies on raw solar thermal power in place of electrical power for all materials processing and propulsion functions.

The work described in this report has proven the feasibility of three critical technologies: Optical Mining™; the Omnivore™ solar thermal engine; and technical means to determine the quantity and accessibility of asteroid resources that support cis-lunar operations. In addition we have performed conceptual level vehicle design and performance analysis showing the viability of the Apis™ approach. Optical Mining™ is a breakthrough method of asteroid ISRU which avoids the need for costly and complex electric power systems or intricate and massive robotic digging equipment. Instead, in Optical Mining™ asteroid material is loosely encapsulated in tough, thin-film bags with ports that permit the introduction of telescopic optics to deliver highly concentrated solar thermal power to the surface of the asteroid. We have experimentally demonstrated that such radiation can excavate rock and breakup asteroid material though spalling. The passive storage of the resulting evolved gases as ice in thin film bags is enabled through the use of second surface mirror coatings on thin film enclosures. The Omnivore™ solar thermal rocket is a breakthrough propulsion technology invented under this Phase I NIAC effort. Not just a solar thermal rocket, the Omnivore™ thruster is a fundamentally new propulsion capability that will be able to use raw, unprocessed, dirty, volatile products from the Optical Mining™ process directly as propellant to deliver approximately 100 times the thrust of a correspondingly massive solar electric propulsion system, but without the need for expensive propellant to be launched into space from the Earth.

Credits and Acknowledgments

The work reported here was performed under NASA Innovative Advanced Concepts (NIAC) grant NNX15AL93G between June 2015 and February 2016. The author gratefully acknowledges the support of the NIAC Program and the professionals in the NIAC Program Office.

The Principal Investigator for this effort was Dr. Joel C. Sercel, the Founder and Chief Engineer of ICS Associates Inc, and TransAstra Corporation. The world class team of Co-Investigators on this effort included Mr. James R. French of JRF Aerospace Consulting LLC, Dr. Robert Jedicke of the University of Hawaii, Prof. Leslie Gertsch of the Missouri University of Science and Technology, noted author and scientist Dr. Donald Rapp (expert on ISRU), and asteroid scientist-astronaut Dr. Stanley Love. Mr. French reviewed the mission systems analysis and conducted performance analysis and design of the Omnivore™ solar thermal rocket. Dr. Jedicke led the statistical analysis of asteroid availability and resource content. Prof. Gertsch provided technical consultation related to asteroid, meteorite, and simulant properties especially from the perspective of mining engineering. Dr. Rapp provided technical review and consultation and developed a library of supporting documentation. Dr. Love consulted on several aspects of this work especially as it related to asteroid physical properties and mission operations.

Scaling relationships for low mass, thin film inflatable structures and reflectors and some of the optical ray trace analysis were provided by L'Garde corporation of Tustin California. Dr. Jeffrey Gillis-Davis of the University of Hawaii provided information mapping asteroid taxonomic type to albedo and main belt source region analysis for the resource availability analysis. Ms. Karen Morenz assisted with code development for the resource analysis work while an intern at the University of Hawaii. CAD visualization support was provided by Mr. Teodros Hailye and Mr. McKenzie Wilder Read and CAD animations were developed by Mr. Teodros Hailye. Prof Daniel Britt of the University of Central Florida provided a large sample of asteroid simulant for our full scale Optical Mining™ demonstration at no cost. The Army White Sands Missile Range provided their large scale solar furnace facility for the demonstration under contract with TransAstra Corporation. Design of the full scale Optical Mining™ apparatus was provided under a related but distinct SBIR contract managed by the Johnson Space Center while the Optical Mining™ apparatus itself was provided by TransAstra Corporation under private sponsorship. Mr. Erik Rosdorff provided laboratory assistance and photographic services for the full scale demonstration. The work described in this report was enhanced through a no funds exchange collaboration with TransAstra Corporation.

Table of Contents

1.0 Introduction and Background

In this Phase I NIAC research effort ICS Associates with its partners and coordinated related research efforts has accomplished the following:

- Performed a full-scale proof of concept demonstration of Optical Mining™, our innovative breakthrough method of solar thermal asteroid ISRU, which promises to allow extraction of tens of tons of water and carbon dioxide per week from 1,000 ton class asteroids based on a required plant mass of less than 2,000 kg.
- Invented and analyzed the performance of a new breakthrough propulsion technology called the Omnivore™ thruster which promises to use, concentrated solar power in conjunction with the raw, unprocessed effluents of Optical Mining™ to deliver thrust levels up to 100 times that of solar electric propulsion but without the need for large, costly solar electric power systems or tons of propellant launched from the Earth at high cost.
- Demonstrated a statistical method of analysis that allows the estimation of available asteroid ISRU resources as a function of return trip ΔV and trip time. Completed the conceptual design and performance analysis of the Apis reusable cis-lunar transportation architecture which is supplied from asteroid resources and which can be developed as a public-private partnership to reduce NASA's cost for human exploration while establishing a new commercially viable industry in space.
- Planned an integrated research and development roadmap to mature Apis™ component and systems level technologies based on rapid, agile ground based technology maturation concurrent with an innovative, early flight demonstration of Optical Mining™ technology on ISS followed quickly by a low-cost, subscale demonstration of the end-to-end Apis flight system technology in LEO concluding with a full scale demonstration mission to harvest up to 100 tons of ice from a NEO and return it to cis-lunar space with a trip time of about 3 years based on the launch of a single Falcon 9.

1.1 Overview of Report

This report is organized into six Sections. Section 1 is this introduction and gives the reader the background information needed to place the rest of the report in context. Section 1 includes the above summary of accomplishments and contains subsections which include this overview; a description of the problems the Apis™ architecture is designed to solve; a description of both the long term and near term potential of asteroid resources to enhance human activities in space; a qualitative description of the primary features of the Apis™ architecture; and an overview of related work by TransAstra, ICS Associates, and our partners as needed to understand the accomplishments of the work reported here. Section 1 is provided as a high level summary without technical detail to orient the reader. Technical detail is provided in later sections. Section 2 reports on the results of our research and technology analysis to include our demonstration of Optical Mining™; our analysis of the quantity of material and accessibility of the most easily

reached asteroids; our analysis and design of the optical system needed to enable both the Optical Mining™ system and the Omnivore™ thruster; our design and performance analysis for the Omnivore™ thruster; and the development plan for the Omnivore™ thruster. Section 3 provides the mission-systems analysis and includes a quantitive description of the architecture described in Section 1. Section 4 provides a description of the path forward to develop the Apis™ system architecture including an assessment of technology readiness and risks and the steps ahead for technology development and demonstration. Section 4 also includes a simplified roadmap for an improved approach to space exploration based on a public-private partnership that will enable both an affordable program of human exploration for NASA and the development of important new industries in space. We provide a summary of key findings and conclusions in Section 5 and we provide the community with a large bibliography encompassing literature related to asteroid resources in Section 6.

1.2 Problem and Motivation

In the summer of 2014 the NASA Advisory Council Committee on Human Exploration and Operations noted that, "a mismatch between NASA's aspirations for human spaceflight and its budget" is "the most serious problem facing the Agency" (see Squires NASA Advisory Council, 2014)". Since that time, the NASA Human Exploration and Operations Mission Directorate (HEOMD) has redoubled its work to address this issue. Their effort culminated in an announcement in October of 2015 that NASA's strategy for human exploration of space will transition from the current focus on Earth reliant research aboard the ISS to one of using cis-lunar space as a *Proving Ground* for future human exploration in deep-space and then transitioning to *Earth Independent* activities to enable human exploration beyond cis-lunar space. In its announcement and the attendant report NASA made it clear that: "A pioneering approach enables a sustained expansion of human presence into the solar system, rather than a once-in-a-generation expedition". Likewise, NASA's Advanced Exploration Systems (AES) division within HEOMD has announced that it is "pioneering innovative approaches and public-private partnerships to rapidly develop prototype systems, advance key capabilities, and validate operational concepts for future human missions beyond Earth orbit." Key aspects of the AES strategy include providing "Opportunities for US commercial business to further enhance their experience and business base" and "Resilient architecture featuring multi-use, evolvable space infrastructure, minimizing unique major developments, with each mission leaving something behind to support subsequent missions." The "Evolvable Mars Campaign" (see Crusan, July 2014) uses cis-lunar space as a proving ground to develop the techniques and knowhow for human exploration of Mars and beyond. Key elements of the Campaign include the use of Lunar Distant Retrograde Orbit (LDRO) as a staging area, high-orbit outposts, and human missions to

asteroids as precursors to human expeditions to Mars. We applaud NASA for this approach because only with Earth independence can American industry move into space on a large scale and enable the homesteading of the solar system. The Apis™ architecture and the technologies and the business models that will enable Apis™ fit hand in glove with NASA's new strategy. Apis™ will be a key enabler in making NASA's vision of pioneering the space frontier a reality.

To aid NASA in solving its "most serious problem" associated with the future of human exploration of space, Apis™ focusses squarely on reducing space mission and operations cost and building a sustainable cis-lunar infrastructure that is a viable commercial entity in its own right. We understand that the cost of human exploration missions is strongly driven by the need to launch large quantities of rocket propellant, drinking water, oxygen, and radiation shielding. If plentifully available in cis-lunar space, water and carbon dioxide can be used as radiation shielding, to replenish other consumables, or directly as propellant in the Omnivore™ solar thermal rocket we have invented under this contract. Unfortunately, independent analysis shows that Lunar ISRU cannot be cost-effective (see Rapp, 2012) beyond its use to support surface operations due to the Size, Weight, Power, and Cost (SWAP-C) of ISRU equipment, the large round trip ΔV to get to the lunar surface, and the logistical issues of working on the lunar surface. Likewise, publications on asteroid mining by a prior NIAC-funded team concluded that they "could not find any scenario for a realistic commercial economic return from such a mission" (see Cohen and Zacny, 2013). We understand why these prior efforts failed and we believe we have solved the problems. To substantially reduce the cost of developing and sustaining exploration missions to cis-lunar space and beyond, NASA urgently needs an innovative new system architecture for cost-effectively extracting H_2O from near-earth asteroids and delivering it to a depot in cis-lunar space. We are optimistic that Apis™ will succeed where others have failed (Zegler 2010, Wilhite 2012) owing to the major innovation in ISRU technology of Optical Mining™ in which innovative optical systems made from light-weight, thin film inflatable reflectors direct concentrated solar power onto asteroid surfaces to excavate solid material by spalling and extract water and other volatiles by thermal dissociation. Wherever explorers go in the solar system there will always be asteroids available to supply water and other resources. NASA needs a way to harvest and use these materials. Apis™ will meet the goal of providing the capability to extract, process, transport, and use asteroid resources to make the Evolvable Mars Campaign affordable within realistic budget projections, thereby enabling human exploration within cis-lunar space, to the asteroids, to the surface of the Moon, to Mars, and beyond. This will lead to the creation of large new industries in space and homesteading of the solar system.

1.3 The Potential of Asteroid Resources

Supporting The Long-Term Vision: Although our focus is on near-term, realistic technologies and systems to aid NASA in its missions of human exploration within just a few years, our *vision* and *motivation* are to enable an unlimited future for human civilization in space. For humans to live in space with normal health, they will require habitats that provide artificial gravity through rotation and radiation shielding at least two meters thick. Such habitats were designed historically by Prof. Gerard Kitchen O'Neill in the 1970s and more recently and with more technically feasibility due to a breakthrough in mechanical design using tensegrity structures by NIAC Fellow Robert Skelton. Skelton's work, like ours, is based on a long term vision but is grounded in practical first steps that can support NASA's near-term plans for human exploration. Figure 1-1 is an artist's concept of an interior view showing what a 16 km diameter space habitat might look like as an example of the kinds of living spaces we envision eventually being built in space. Skelton estimates that a habitat such as that depicted in Figure 1-1 could provide a usable land surface area of about 8 km^2 and support a population of about a 100,000 people at a typical Californian suburban population density. The colony itself would mass about 14 million tons mostly to provide the radiation shielding needed to support the population.

Figure 1-1: Interior View of the Type of Space Colonies That Will Someday Be Built From Asteroid Resources.

The asteroid belt represents an industrial resource of nearly unimaginable scope that will allow mankind to grow and thrive as a species spreading throughout the solar system without limits to fulfill this vision. To understand why, consider that the best statistical estimates are that there are approximately one million (±50%) asteroids in the solar system with diameters of 1 km or more which each mass at least a billion tons. We estimate that there are over 100,000,000 asteroids larger than 100 meters in diameter orbiting within the inner solar system, each one of which has a mass of about a million tons. Together these objects constitute a total mass of available resources of about a trillion tons. If we count only 10 meter class asteroids which are small enough to be addressed by the first generation technology described in this report, there are probably over 75 billion potential targets, each with a mass of about a thousand tons. The total mass of material in the asteroid belt is on the close order of 10^{18} tons, which is enough to make millions of the colonies depicted in Figure 1-1 with a total land surface area of thousands of times the land area of the Earth. Such a collection of space colonies could take thousands of years to build and could potentially support a population of thousands of times the current population of the Earth. This is not to suggest that we *should* use the *entire* mass of the asteroids to build habitats to grow the population humanity into the trillions, it is to suggest that the potential of the asteroid belt is to completely eliminate practical limitations on the growth and development of the human species and do so without endangering the biosphere of the Earth *or any other planet* using only sustainable resources including the gigawatts of solar energy streaming through every square kilometer of space at 1 AU from the Sun and the trillions of tons of lifeless and inert rocks called asteroids that tumble around in the solar system.

The Near-Term Potential of Asteroid Resources: **While our vision is far ranging, our work focuses on near-term, realistic technologies and systems to aid NASA in its missions of human exploration within just a few years.** For our immediate concern we consider not the whole population of asteroids across the vast expanse of the solar system, but just those that are most accessible to Earth in terms of the propulsive ΔV required to get to the target and return to a useful location in cis-lunar space such as Lunar Distant Retrograde Orbit (LDRO). Although the science community has long known that there is a large population of small asteroids in orbits that are far more accessible to the Earth than is the surface of the Moon, this fact has recently been presented in a clear and compelling way in the scientific literature. For example, Figure 1-2, reproduced with permission from a Nature article from Oct. 30, 2014 (R. Binzel), provides a clear summary of the accessibility advantage afforded by asteroids for ISRU. We have annotated Figure 1-2 to show where Lunar Distant Retrograde Orbit (LDRO) falls in the ΔV-trip time space. The important conclusions from this plot are that there are many near Earth asteroids that are far more accessible than either the Moon or Mars which will make ideal targets for resource missions and

Figure 1-2 - Missions to near-Earth asteroids will require less propulsion and comparable mission duration than missions to the Moon. Binzel (Nature Oct 2014) shows that a dedicated survey filling in the yellow-hatched region would reveal abundant asteroid stepping stones as a gateway to the solar system. Figure 1-reproduced with permission with annotation showing Lunar Distant Retrograde Orbit (LDRO) added. Note that all ΔVs in this plot are round trip to LEO except the Asteroid Redirect Mission, which ends at LDRO

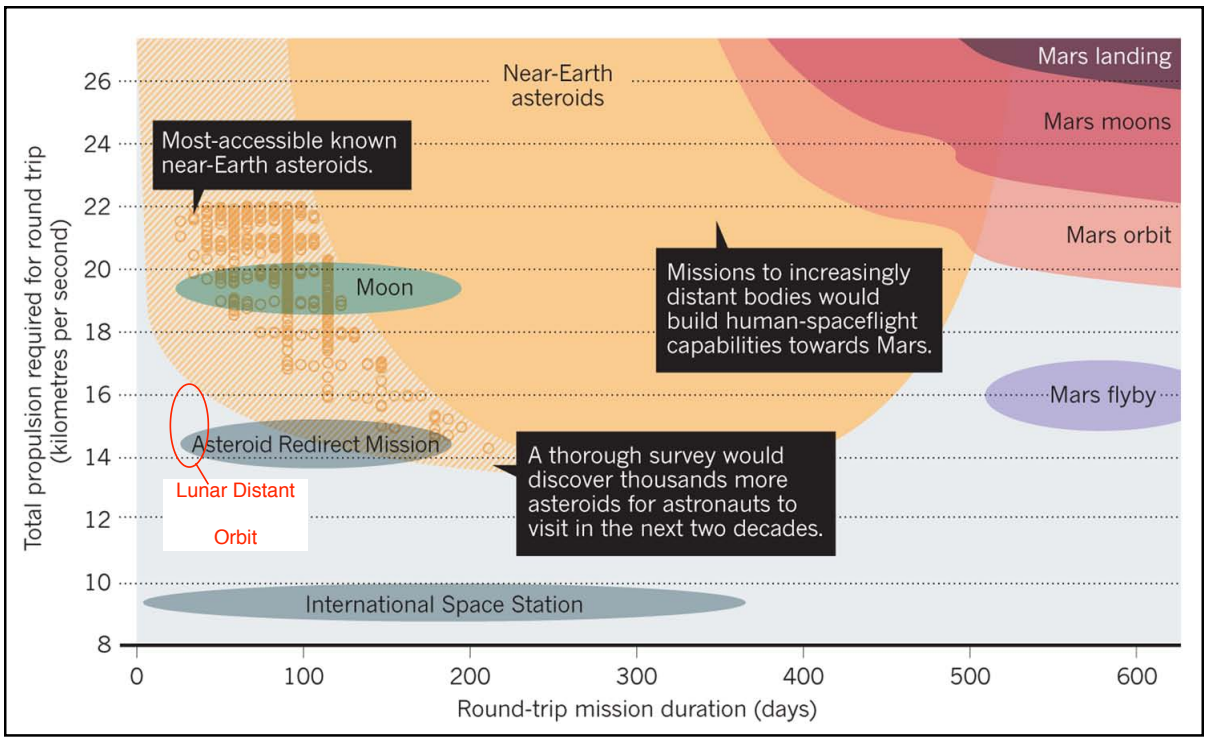

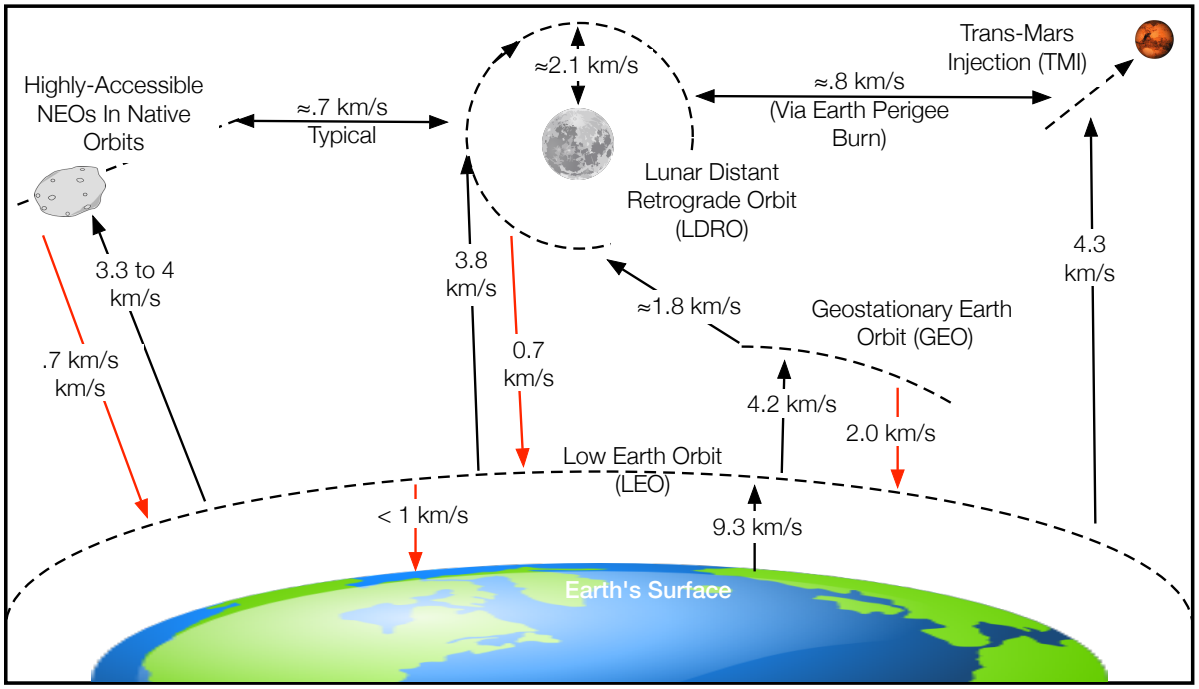

Figure 1-3 - Typical ΔV's Between Nodes in A Cis-Lunar Transportation Network. Impulsive ΔV's Overwritten on Black Lines, ΔV's With Aerobraking or Aerocapture On Red Lines. Highly Accessible NEOs in Native Orbits Represents A Theoretical Population of the Most Accessible Objects

human missions of exploration. In addition, the most accessible near-Earth asteroids can be expected to be virtually in contact with LDRO energetically, and therefore ideally suited as supply sources for an outpost at LDRO. Figure 1-3 provides a ΔV map for transportation between nodes in a cis-lunar transportation network and shows that LDRO is energetically close to all the destinations NASA is considering in its Evolvable Mars Campaign. The impulsive ΔV to go from LDRO to some highly accessible NEOs in their native orbits or to Trans-Mars Injection (TMI) can be expected to be less than 1km/s, as is the ΔV to go from LDRO to LEO with aeroassist. The population and statistics of this accessible group are discussed in more detail in Section 2.3 of this report.

The most important resources we seek in the near-term are volatile materials including water and carbon dioxide because these materials have myriad potential uses in human exploration. Most importantly and immediately they can be used as propellant in solar thermal rockets effectively eliminating the need for rocket upper stages to support cargo missions in human exploration. In addition, water in liquid or solid form is an excellent radiation shielding material and can be purified in liquid form to make potable for consumption by astronauts. The ISS currently uses the Sabatier process to chemically react waste water and CO_2 to produce oxygen for breathable air. A byproduct of this process is methane which is disposed of on ISS. For deep space human exploration, the same process at a larger scale could be used to produce oxygen and methane which could subsequently be liquified and used as chemical propellants in high performance, high thrust propulsion systems for rapidly transporting human crews through cis-lunar space or for Lunar or Martian landing vehicles. Although we have not analyzed the LOX-methane high thrust propulsion option in the present work, it is part of our strategic plan.

CI and CM type carbonaceous chondrite meteorites are known to comprise as much as 20%, and typically 10% water by weight. At least one sample of the Ivuna CI meteorite was measured to be 43.5% water by weight. The bulk density of that sample was about 2 g/cm^3, so the density of water in that sample was 80% of the volumetric density of liquid water. Meteoriticists have known since the 1960s that gradual or sudden heating to increase temperature causes release of water from meteorites with sudden heating causing not only release, but also disintegration. Water of space origin begins to be driven out at temperatures as low as 250º C, about half is driven out by 400º C, and all is extracted by 900º C. Figure 1-4 (Court and Sephton 2009) shows typical volatile content extracted from samples and the temperatures at which the relative quantities of water are driven out (also see Garenne et al. 2014) in vacuum.

This effect is graphically demonstrated in Figure 1-5 which is a photo of a demonstration performed by Dr. Dan Durda of the Southwest Research Institute for an episode of "How the

Universe Works" which was aired on *The Science Channel*. This demonstration showed the release of water from a ~1 cm^2 chip of CM2 meteorite. Dr. Durda placed the chip in a test tube and heated it over a burner. Water bubbled out of the chip and condensed onto the walls of the tube, which can clearly be seen in the photo. Figure 1-6 is a screen grab of a video of a hydrated rock chemically similar to the water bearing constituents of carbonaceous asteroids being exposed to the focus of a multimeter diameter solar concentrator at White Sands New Mexico. This sample is roughly the size of a soccer ball. As is shown in the image, chips of rock are rapidly spalling off the surface. From the research we have preformed on Optical Mining™, we now know that this spalling is driven by thermal

Figure 1-4 - Volatiles extracted from meteorite samples (Court & Sephton 2009)

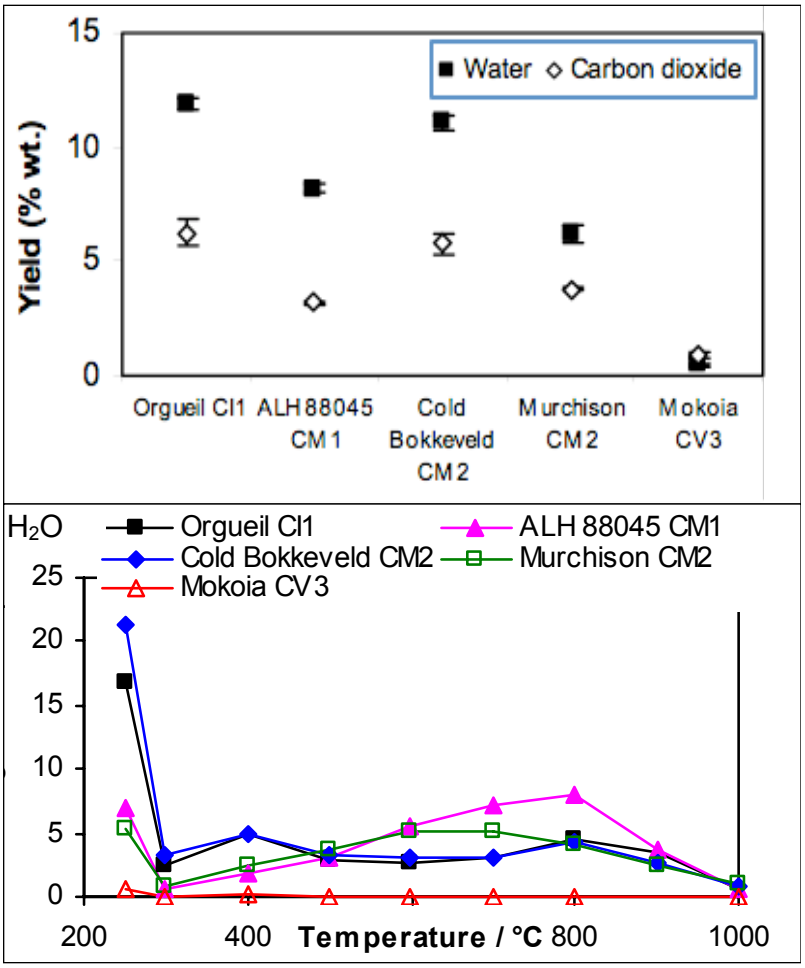

Figure 1-5 - Demonstration of Thermal Dehydration of Meteorite Sample

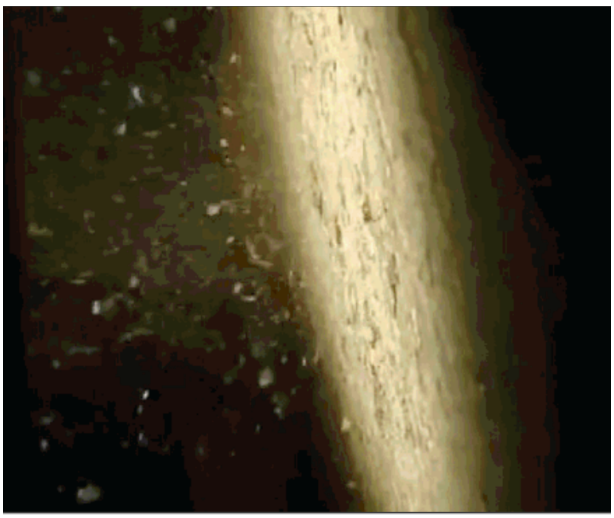

Figure 1-6 - Video Image of Solar Furnace Ablating Hydrated Rock
(click link to view video)

shock and the outgassing of volatiles which separates chips of rock from the surface and drives them away. In the 10^{-4} atmosphere pressure of the Apis™ containment bag (described in Section 1.3 of this report), gas expansion will be 10,000x greater than at one atmosphere, so excavation produced by gas movement will be even more effective.

We started this research expecting that concentrated sunlight could be used to dig holes in asteroids. During this effort we have demonstrated that this is true as described in Section 2.2 of this report. While robotic scoops, augers and arms will be largely useless for digging in a microgravity environment without the benefit of gravitational anchors for purchase, we have shown that it will be possible to breakup, disrupt and mine the water and other volatile materials from asteroids largely without moving parts through the intelligent use of highly focussed sunlight. One process we have invented and demonstrated to do this is called Optical Mining™ and it is a key part of the architecture for deep space transportation we call Apis™ along with a new propulsion technology called the Omnivore™ thruster.

1.4 Solution: The Apis Architecture

Apis™ is named for the honeybee genus because like bees Apis efficiently gathers and returns useful resources and then utilizes those resources to perform useful work. In this case the resources are volatile materials from highly accessible asteroids and the useful work is transportation services for NASA's missions of human exploration of space. To do this, the Apis™ architecture comprises several elements including Honey Bee™ asteroid mining vehicles, Worker Bee™ reusable deep space tugs, and the Hive™ consumables depot and outpost in lunar distant retrograde orbit (LDRO) as shown in Figure 1-7. Together, these systems form a cost effective reusable cis-lunar transportation network supplied by asteroid resources which eliminate the need for launching large quantities of consumables to support human exploration of deep space beyond LEO. Lightweight, thin film solar concentrators, structures, and optical systems are a key features of all elements of the Apis™ architecture which relies on raw solar thermal power in place of electrical power for all materials processing and propulsion functions.

We have created a concept-level, technically rigorous design of a first full-scale project using the Apis™ architecture. Details of this design are reported in Section 3 of this report. In this first Honey Bee™ mission, a version 1.0 of the Apis™ architecture will enable a spacecraft launched on **a single Falcon 9 class rocket to harvest and return to LDRO approximately 100 tons of water from an ARM-like NEO.** Depicted conceptually in Figure 1-8, the first Honey Bee™ mission operations start with a Falcon 9 or equivalent launch to a low C3 transfer to a low ΔV

Figure 1-7 - Top-Level Diagram of Apis™ Architecture

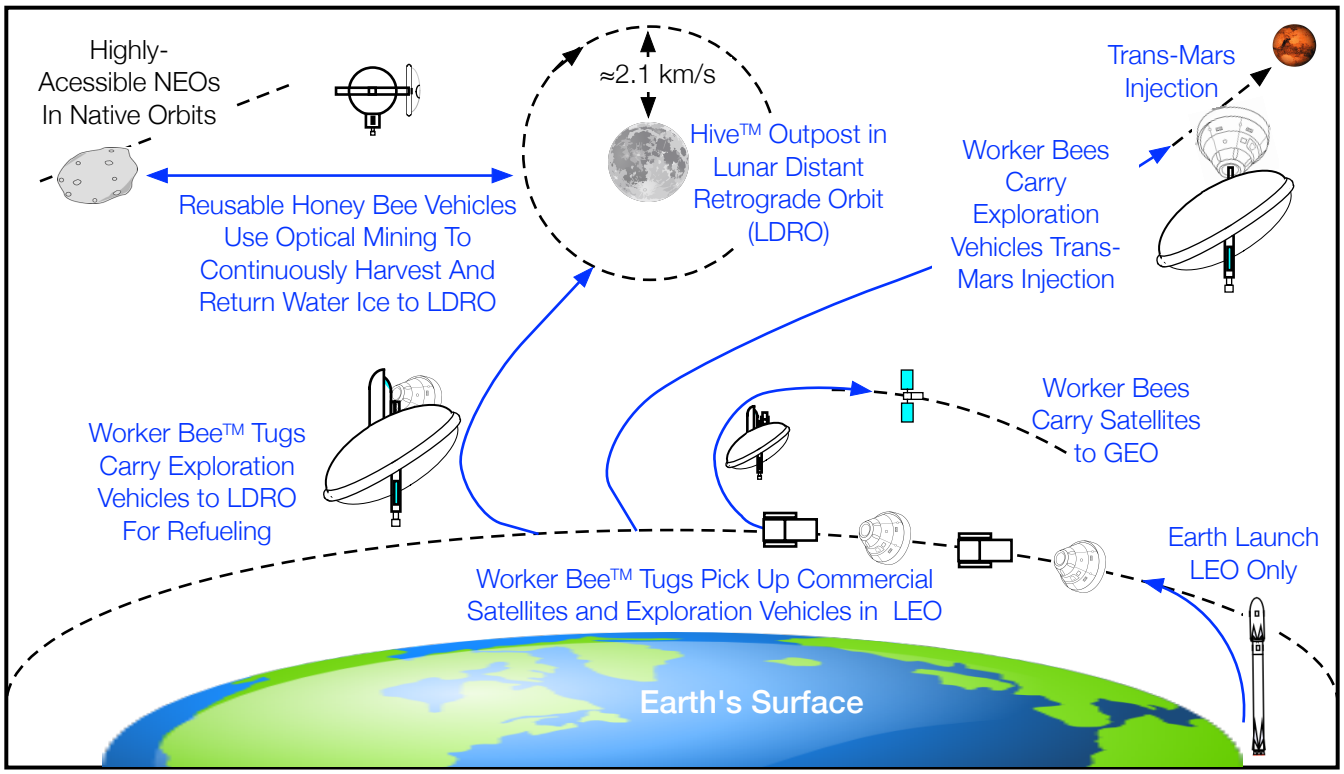

volatile-rich NEO (step 1 in the figure). After launch, solar arrays are deployed and the Honey Bee™ vehicle performs a deep space cruise to the target. Once at the target (step 3), an inflatable capture system similar to that proposed for the Option "A" ARM (see Brophy 2012 and Wilcox 2015) mission, but designed to enclose the target with a nearly hermetic seal, is used to capture and control the asteroid. Note that NASA and JPL spent millions of dollars on this thin film inflatable capture mechanism and concluded that it was ready to be baselined on the ARM mission as documented in Wilcox 2015. JPL has published work showing extensive modeling, simulation, and engineering demonstrations of large scale hardware proving the feasibility of this approach at TRL-4. After the asteroid is encapsulated and the system de-spun (step 4), inflatable solar concentrators currently at TRL 3-4 provide direct solar thermal heat to the asteroid (step 5).

Inflatable optical and structural elements including light-tubes and optical baffles provide a combination of highly concentrated and diffuse solar thermal power to heat the asteroid material (step 6) in a controlled way to force the H_2O and CO_2 to outgas into the enclosing bag at low pressure (10^{-4} to 10^{-5} atm). Other optical elements in the system design include turning mirrors and sapphire Fresnel lenses. The highly concentrated sunlight is directed through the optical elements to spall and excavate within the enclosure bag without the need for impractical mechanical excavation equipment. It is important to note that the requirements for optical quality of the reflectors and other optical elements in this system are not stringent. This is not a diffraction

Figure 1-8 - Concept of Operations for First Honey Bee™ Mission

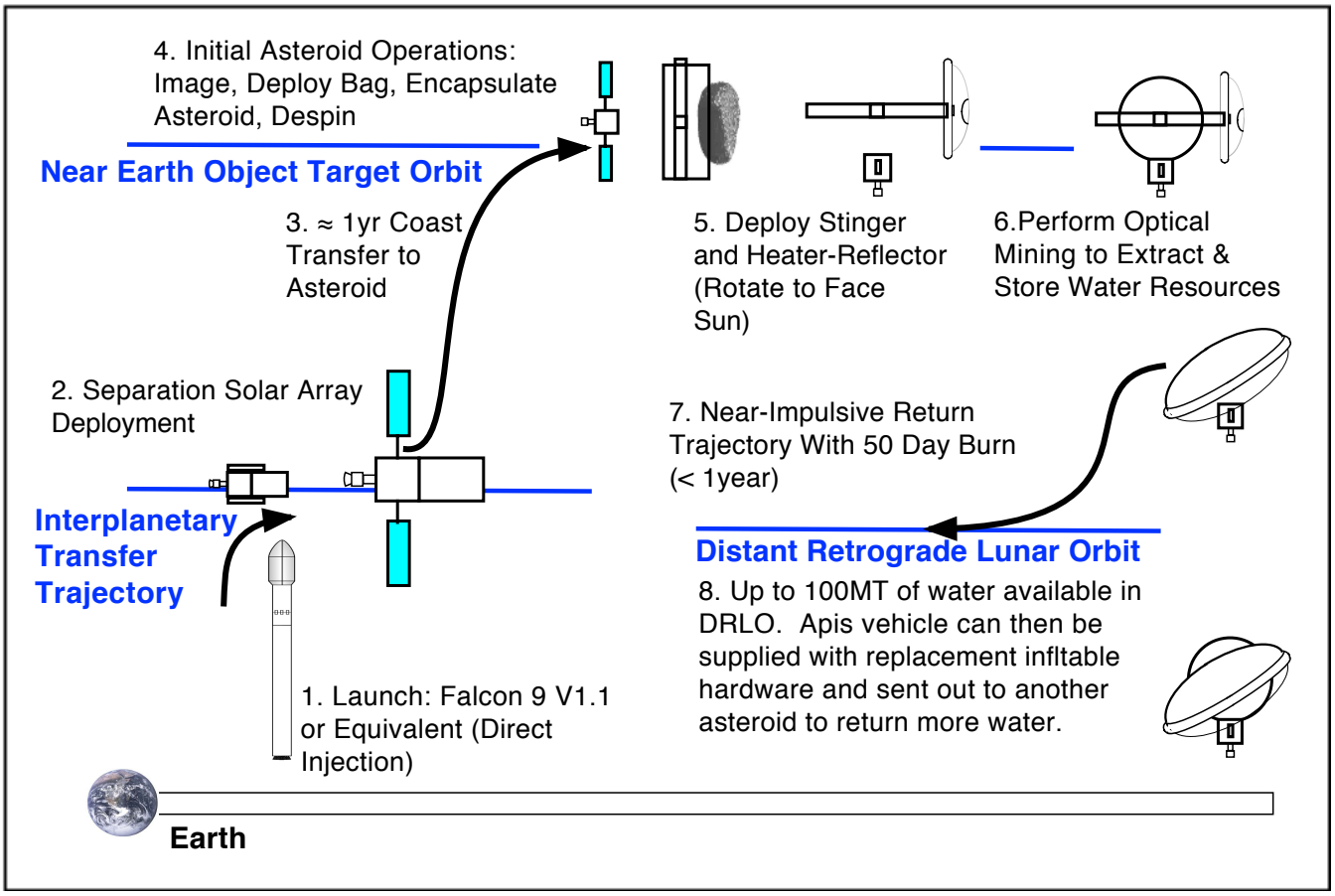

limited physical optical system like a telescope. By optical standards this is a crude light bucket operating in the gross geometric optical domain with allowable RMS slope errors of multiple mrad over a 15 m diameter primary aperture corresponding to maximum allowable surface deformations of centimeters. This level of surface accuracy for inflatable structures has been demonstrated in the laboratory since the 1980s and was achieved in ground tests of a 14 m diameter reflector flown in space in the 1990s. Many geometries are possible for state of the art inflatable structures technology including on-axis and off-axis reflectors in both Newtonian and Cassegrain configurations as shown in Figure 1-9.

Outgassed volatiles are cryopumped at moderate temperatures into passively cooled thin film storage enclosures. Because the water is stored as solid ice, there is no need for hard-shell hermetic storage and the storage containers can mass less than 1% of the mass of ice they contain. After a few months of resource collection, the Apis vehicle nominally leaves the asteroid behind (step 7). Depending on the particular target's return-trip ΔV, 10 to 20 percent of the collected water is used in a Solar Thermal Rocket (STR) burn to initiate a typically ≈1yr return trip flight to bring the water to LDRO (step 8) for utilization. Alternatively, Apis could bring back the

Figure 1-9 - Some Of Many Possible Large Inflatable Reflector Configurations

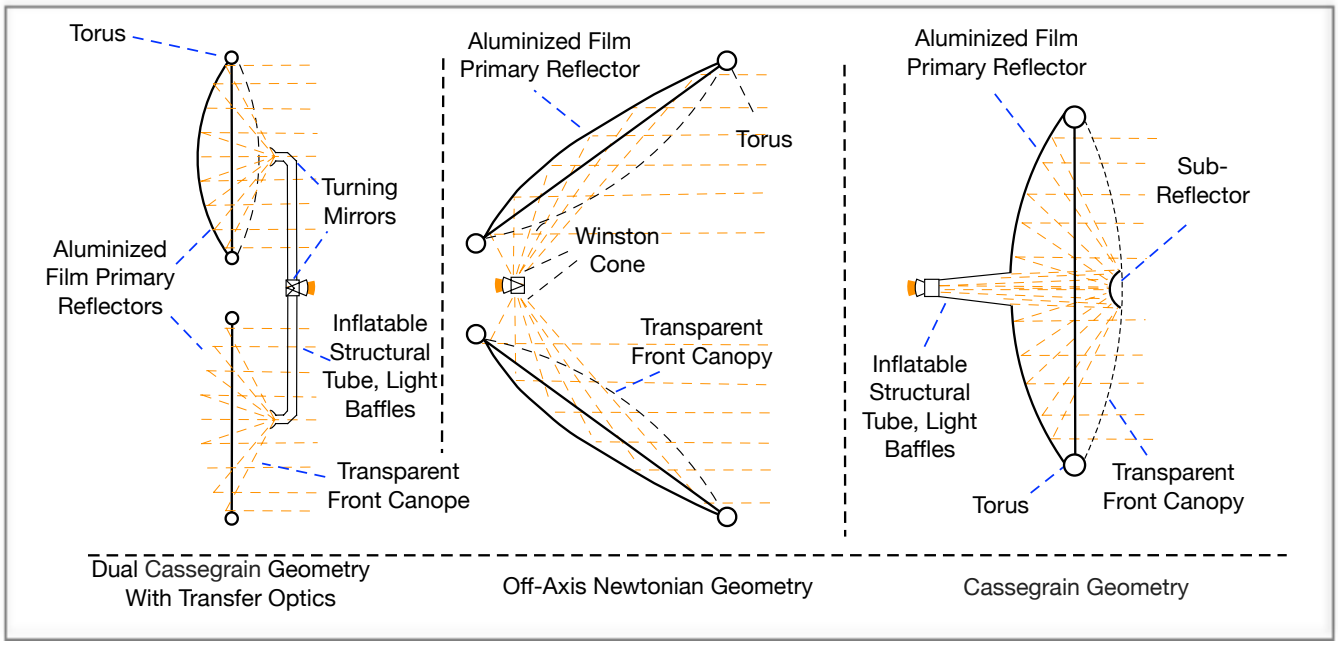

entire asteroid with a ≈1yr flight time. In this optional scenario, half to two-thirds of the extracted water would be used to propel the asteroid to LDRO.

Apis™ Technologies: The Apis™ system architecture is enabled by five key technologies which overlap in function and structure and work together in unique ways to provide a disruptive game changer for NASA: i) thin film precision inflatable structures, ii) our breakthrough Omnivore™ solar thermal rocket, iii) innovative optical design, and iv) Optical Mining™ with passive thermal processing and resource storage.

Since the Echo program of the early 1960s (Staugaitis, C. & Kobren, 1966), numerous engineering studies, sub-scale tests, full-scale tests, and flight tests of inflatable structures in space have been conducted under the sponsorship of NASA, the Air Force, and other agencies. Feasible concentrator design options exist for Cassegrain, Newtonian, off-axis, and on-axis geometries for both imaging and non-imaging or anidolic geometries. Figure 1-9 depicts some of these options. Such reflectors comprise the storage and release mechanism that holds the structure prior to deployment; the inflatant gas storage and handling system; makeup gas to account for leakage; the lenticular structure; a torus to support the lenticular structure; and struts. Of these, the torus, struts, and lenticular structure are all made of thin films or membranes, but on long duration missions only the lenticular structure is typically inflated. The lenticular structure includes a transparent front surface and a reflective back surface.

Figure 1-10: 14 m Diameter Off-Axis Inflatable Reflector Flown on A Space Shuttle Mission In Orbit in 1996

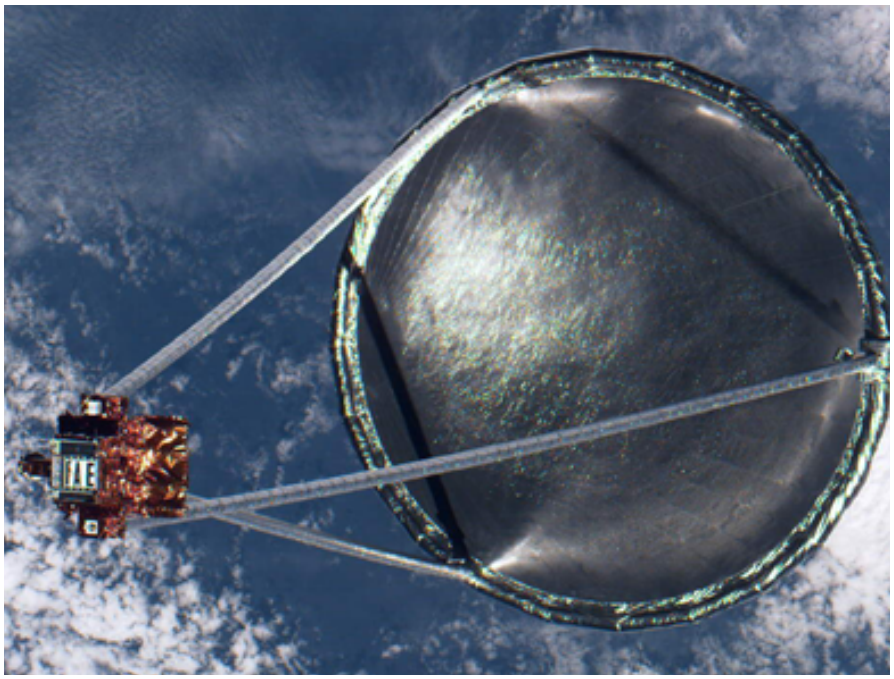

Because of the higher structural rigidity required by the torus and struts it typically does not make sense to use inflation pressure to provide them strength once they are deployed because the pressures, and hence leakage rates, would be too high. In one method of rigidification the torus and struts are fabricated from polyamide films bonded to a metallic foil. These are inflated into position, and then the inflating pressure is increased to a level that provides yield but not rupture stress to the metallic foil. This causes the foil to undergo plastic deformation and rigidify in place eliminating the need for makeup gas. In another method of rigidification the torus and struts are fabricated from shape memory materials that are structurally deformed within the elastic limit in the stowed configuration. In this variant of the technology the membrane is fabricated from a composite material in which carbon structural fabric is impregnated with a low-outgassing silicone resin. Structural tubes can be stowed in retractable motor driven reels with rollers that permit deterministic deployment and re-stowage in space. The design and analysis work performed in this study suggests that the shape memory materials are both lower in mass and higher in structural precision, so we have baselined that approach.

The lenticular structure, by contrast, is not rigidified, but is made of extremely lightweight (typically 0.25mil) films and requires an inflation pressure of only 10^{-5} Pa to provide the ≈500 psi film stress needed to pull out wrinkles and provide optimal shape and curvature. At this low pressure, only 100s of grams of gas are present in a lenticular structure at any one time. Even after worst case micrometeoroid punctures as calculated with standard models, leakage is less than 5kg/yr after several years for a 20 m diameter reflector. The surface precision, reflectivity, and other optical properties of these devices have been measured on the ground many times. A full-scale 14 m diameter inflatable reflector was flown in space on the space shuttle as a technology demonstrator (Figure 1-10).

Likewise, rigidification and deployment approaches have been investigated and tested on the ground in sub-scale and full-scale systems. Surface accuracy and precision have been measured and validated in multiple programs from the 1960s through the 1990s. Figure 1-11 shows the projected mass of inflatable reflectors adapted from the literature (Sercel, 1985). Note that a 1,000 m^2 reflector with an optical efficiency of 50% provides over 600 kW_t of solar power for a performance figure of merit of more than 2 kW_t/kg: more than 10x better than the best *realistic* projection of any solar array technology. For example, NASA ARM missions studies typically assume an optimistic 900 kg for an electric power system that produces less than 50kWe. Another important metric for solar concentrator technology is surface accuracy. A series of analysis and ground based tests with full-scale and sub-scale engineering units starting in the 1950s has consistently confirmed that deviations from ideal parabolic, or other specified doubly curved surface shape are in the range of approximately 1mrad angular error (see for example, Ehricke 1956, Etheridge 1979, Grossman, 1990, Veal 1991, and Cassapakis, 1996) resulting in the ability to provide solar concentration ratios of several thousand to one. Section 2.3 of this report provides detailed calculations and updated mass scaling relationships confirming these general trends.

Figure 1-11: Inflatable Reflector System Mass Scaling

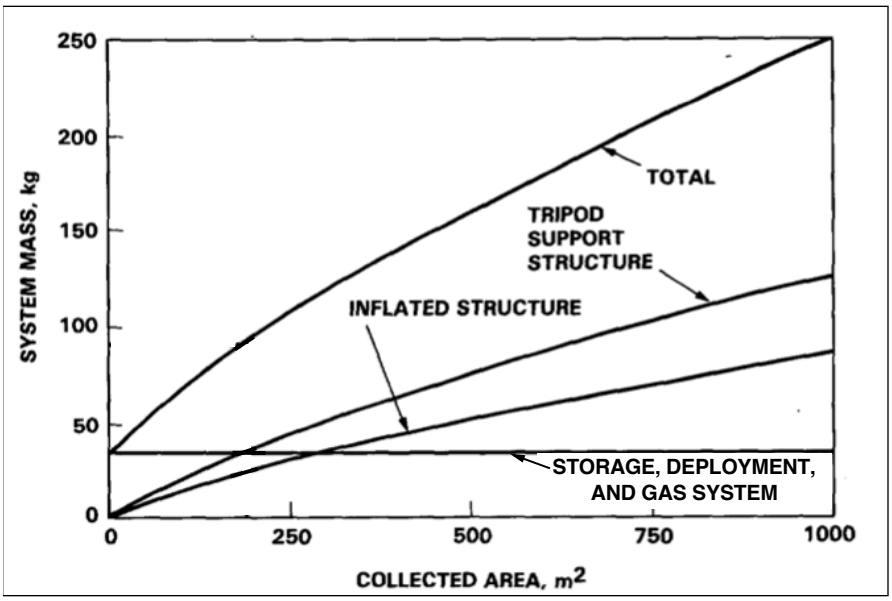

Solar Thermal Rocket (STR): Solar thermal propulsion has been under consideration and development since the early days of the space program and performance can be

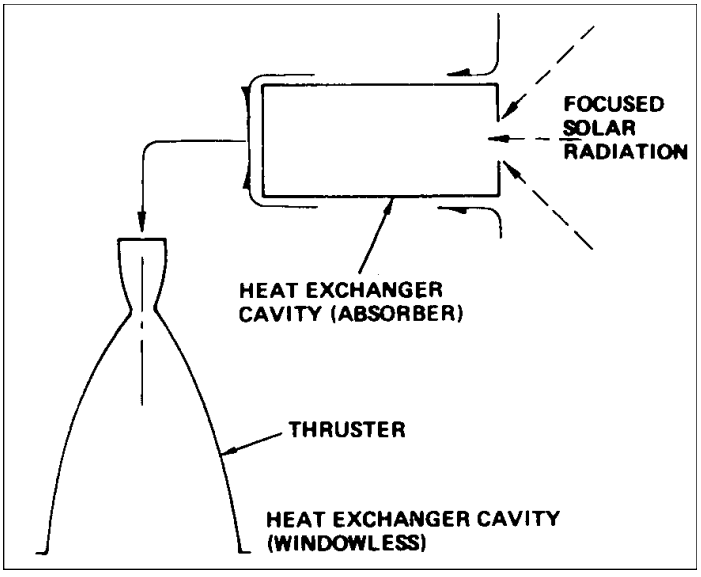

Figure 1-12: Solar Thermal Rocket Concept of Operation (Etheridge 1979)

Figure 1-13: Solar Thermal Rocket on A Test Stand In the 1990s

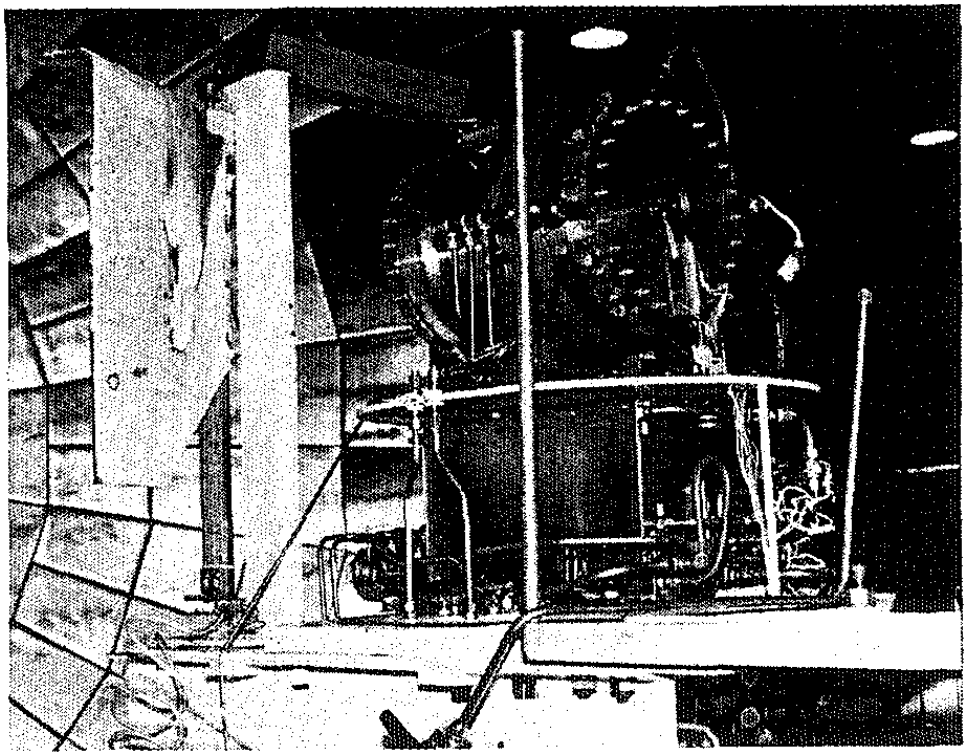

confidently projected. Figure 1-12 shows a design concept for a solar thermal rocket while Figure 1-13 shows an STR on a test stand at an Air Force facility. For the Apis application, the propellant is water extracted from the asteroid. In operation, concentrated sunlight is focused into a hollow cavity and propellant is flowed through a heat exchanger. We have run ODK rocket performance analysis and performed standard rocket engine derating on that analysis based on real-world experience. We have also compared our results to results claimed in the literature. Our findings are shown in Figure 1-14 which predicts real-world, de-rated performance. Ideal ODK and ODE analysis suggests somewhat higher performance. At a chamber temperature of 2750 K we are confident that STR can achieve 350 s. However, in the spirit of conservatism, we assume 335 s.

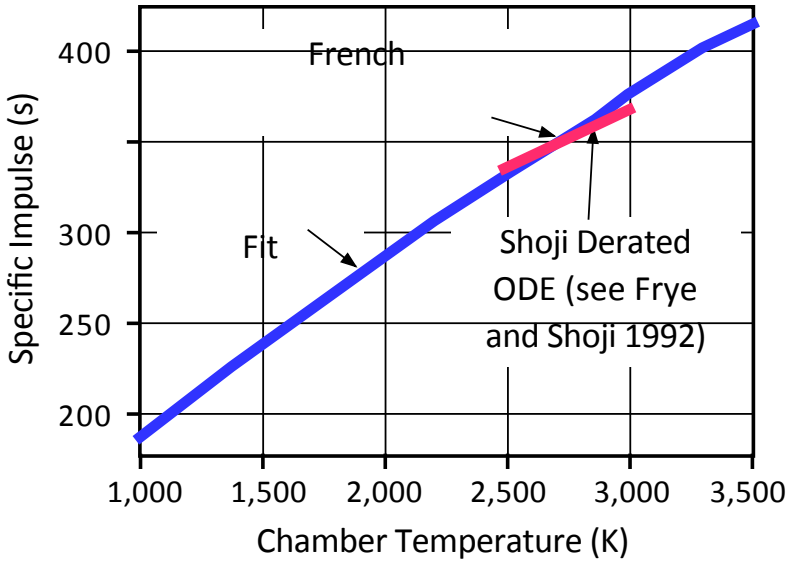

Figure 1-14: Specific Impulse Performance of Solar Thermal Propulsion With Water Propellant

In the course of performing this study we found that a difficulty to be overcome with the design of solar thermal rockets for use with asteroid ISRU is associated with the fact that normal rocket propulsion technology requires the propellant to be highly purified and typically not variable.

There are two ways to address this problem: one could design the ISRU system to produce only highly purified, clean propellants, or one could design a thruster that can handle "dirty" propellants of variable composition. For a first generation system, we concluded that the latter option is preferable and therefore have solved the problem of how to make a rocket engine work on raw, unprocessed effluent of asteroid ISRU with an invention called the Omnivore™ thruster which is described in Sections 2.4 and 2.5 of this report.

1.5 Related Work by TransAstra and ICS Associates

This NIAC study is closely related to several other activities that have been carefully planned and coordinated by the PI of this work to form a coherent research program with the goal of rapidly maturing the Apis™ technologies and starting down the path of developing the vehicles and systems needed to harness asteroid resources to support NASA missions of human exploration. ICS is executing this NIAC study and a clearly distinct but related SBIR contract focussed on aspects of Optical Mining™ not addressed under this grant. TransAstra Corporation is a sister company to ICS that has been established to do related privately funded work, also related but distinct, and the two organizations have a partnership agreement to share intellectual property and collaborate where it is in the best interest of both their sponsors. In addition to ICS and TransAstra there are several other organizations involved in this work as enumerated in the credits and acknowledgments section of this report, with most of these organizations acting as subcontractors to ICS. The integrated research and development program that starts with theoretical studies at ICS Associates and University of Hawaii linked to experimental efforts at ICS, TransAstra, Missouri University of Science and Technology (Missouri S&T), and Colorado School of Mines (CSM). Under SBIR sponsorship ICS has developed a model of surface spalling and outgassing in Optical Mining™ that accounts for heat penetration into the surface, thermal gradient driven stress, gas release, vapor pressure driven tensile stress, and gas migration through the bulk material.

Related experimental efforts include:

- The development and use of a kilowatt-scale thermal oven for bulk, up to unitary kilogram level, material heating studies at Missouri S&T (ICS is a subcontractor on this NASA ESI funded activity),
- A subscale Optical Mining™ simulator based on the use of a 2 kW_e class xenon arc lamp at CSM sponsored by a NASA SBIR effort, and
- A large-scale Optical Mining™ apparatus using a 10 kW class solar thermal furnace with a vacuum chamber and cryotrap developed by TransAstra. In this full-scale demonstration, the design of the apparatus was performed by ICS and sponsored by NASA under an SBIR contract. The hardware was paid for and assembled by TransAstra under private sponsorship, and the full scale demonstration was performed by ICS with NASA approval under this NIAC grant.

Summary of Theory Of Optical Mining™ Excavation: The first related effort we will recap here is the analytical work on the theory of the excavation process in Optical Mining™ . This work was conducted by ICS under SBIR sponsorship. It is important for readers of this NIAC report to be aware of the theoretical work as it places the full scale demonstration of Optical Mining™ performed under this NIAC grant in context. Before describing the model of the physics of the process, we will review the larger system concept. Optical Mining™ involves encapsulating the asteroid in a tough, thin film bag and introducing an optical tube through a port in the bag. The tube serves as a debris shield for optical elements, a light baffle, and as the structural support for a sapphire Fresnel lens which provides the final solar concentration near the asteroid surface to deliver highly concentrated solar power (light) to the surface of the asteroid to excavate the exterior, breakup the asteroid (while containing debris within the bag), and outgas the volatiles. Outgassed volatiles are cryopumped through a filter and an inflatable tube into a passively cooled thin film enclosure where the gases freeze out for storage and transport. This process is depicted in Figure 1-15. Figure 1-15a (on the left) shows the initial configuration. Figure 1-15b shows an intermediate condition, and Figure 1-15c (on the right) shows the final stage of the system when the accessible volatiles have been completely removed from the asteroid. Our thermal design and analysis shows that the passive storage of ice in a thin film bag as depicted is enabled through the use of a second surface mirror coating which emits IR radiation and reflects sunlight. This is a standard method used in cooling cryogenic instruments and various other surfaces in space.

The mathematical model of the spalling and outgassing process which produces the excavation is based on optics, geophysics, and gas-dynamic considerations to include scaling laws and empirical factors to account for variability in material properties. The complete model of surface spalling accounts for radiative heat transfer, conductive heat transfer, endothermic phase change

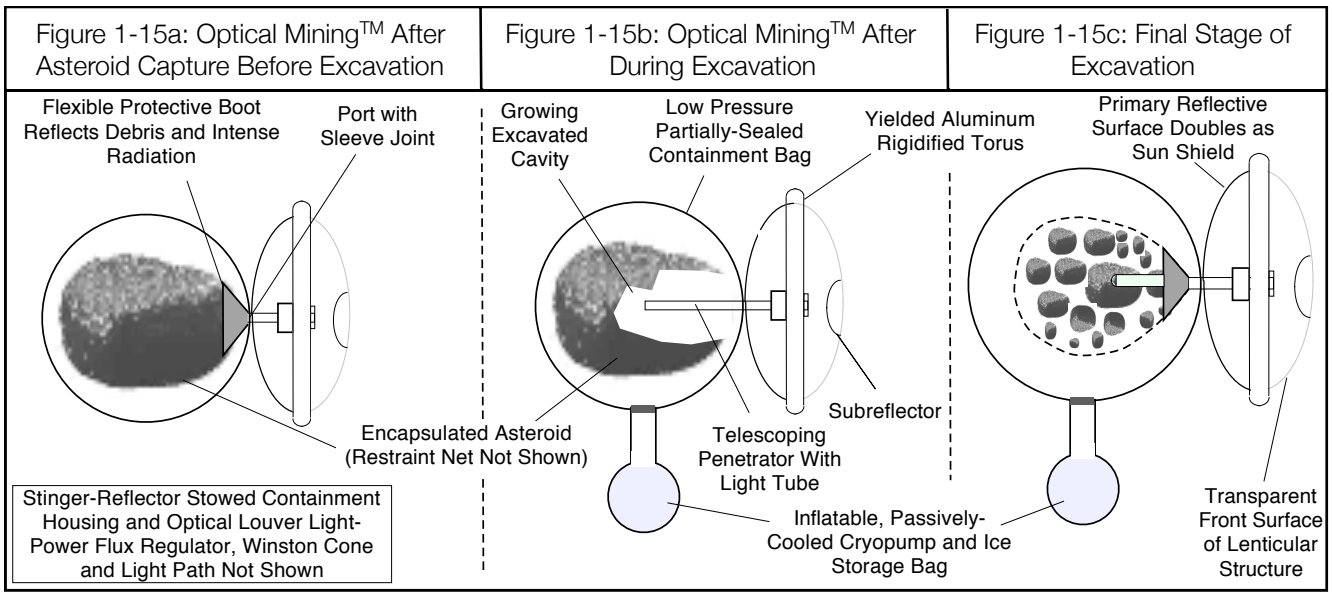

Figure 1-16 - Summary of Insights Gained From Analytical Modeling of the Spalling Process

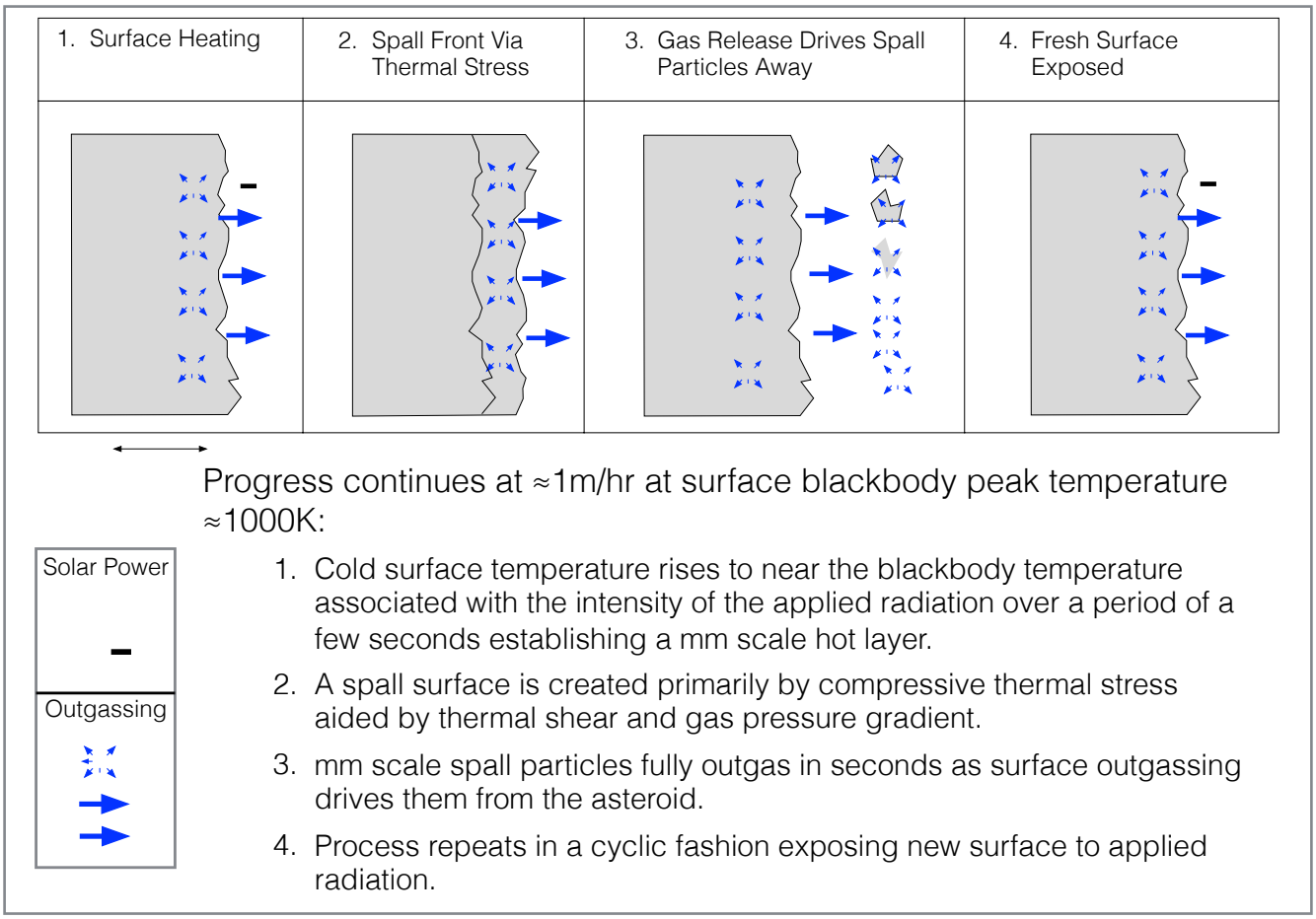

processes, rock structural properties, and occlusion of incoming radiation. The model is based on theoretical considerations with empirical factors for unknown quantities, and has been refined to account for observations and findings from the subscale SBIR experimental effort and the full scale NIAC demonstration. As depicted in Figure 1-16, highly concentrated sunlight is directed onto the surface of the target asteroid. Our experiments and analytical work have provided new insights into the physics of what this highly concentrated sunlight will do. The concentrated sunlight will cause extreme local heating of the asteroid surface to a temperature of up to 1000 K over an area of several square inches (for an Optical Mining™ apparatus working at power levels of tens of kilowatts). This will cause heat to conduct into the structure of the asteroid only to a depth of a few millimeters before thermal shock fractures the surface material while the intense heating causes outgassing of the volatiles. The resulting gas release produces a pressure gradient that drives fractured material away from the surface thereby exposing new cold surface material to the incoming radiation. The quantity of gas liberated in this process can be expected to be 5 to 40 percent of the total mass of the rock material. Based on our experiments thus far, this liberated gas can be expected to be about half to two-thirds H_2O with the other half dominated by CO_2

and SO_2, so the yield of water will be in the range of 5 to 15 percent of the total mass of rock heated depending on the quality of the ore. If the liberated gas constitutes only 10 percent of the rock mass, once it is released from its bound state it will increase in volume by a factor of several hundred times relative with geometric density it was stored at as hydrates and carbonates.

Although the target type of asteroids, the source bodies for CI and CM meteorites, can be expected to be permeable, they are often structurally weak with low tensile strength. Hence, the massive increase in gas volume inside the permeable rock structure will cause an internal pressure gradient driving the diffusion of the gas out of the rock. This gradient will cause tensile stress to build up in the rock. The experimental evidence shows that this internal gas-pressure driven tensile stress in combination with the thermal shock of rapid heating fractures the material locally and causes it to spall and shed small pieces or chips. Once these pieces are separated from the surrounding rock, the expanding and escaping gases will drive them away from the surface exposing fresh new, still cold surface below and the excavation process will continue.

Note that our review of the literature has shown that the volatile release reaction for hydrated silicate minerals is about 2,800 kJ/kg and is approximately the same for release of carbon dioxide and sulfur dioxide from carbonates and sulfates. This large enthalpy is one reason why simple heating without highly focussed spalling in a bag will not work for ISRU. As depicted in Figure 1-17, our model shows that the thermal time constants for even small asteroids in the 10 meter class range from years to decades due in large part to the dehydration enthalpy. By applying heat locally and fracturing the rock, Optical Mining™ avoids the thermal time constant problem and can breakup and mine a thousand tonne asteroid in only a few months with modestly sized solar concentrators. However, the raw power requirements are still so high as to make electrically driven approaches infeasible. Note that the spalling of rock surfaces in the presence of concentrated sunlight does *not require* the presence of significant quantities of volatiles in the rock. Our modeling shows that thermal shock can cause spalling on its own and can significantly enhance spalling in combination with volatile release driven tensile stress. For a more complete description of the details of the analytical model, the reader is referred to our SBIR final report which is available to NASA personnel under contract NNX15CJ35P.

Overview Of Subscale Optical Mining™ Tests: ICS Associates and CSM collaborated under SBIR contract NNX15CJ35P on an experimental program that culminated in 38 subscale tests and demonstrations of Optical Mining™ The experimental apparatus we used (Figure 1-18) includes a xenon arc lamp with an aspheric lens that can provide highly concentrated optical radiation through a windowing system into a small vacuum chamber equipped with several ports for performing mass spectrometry, spectrography, and high resolution photography, and video. The

Figure 1-17: Typical Asteroid Material Thermal Time Constant As a Function of Size

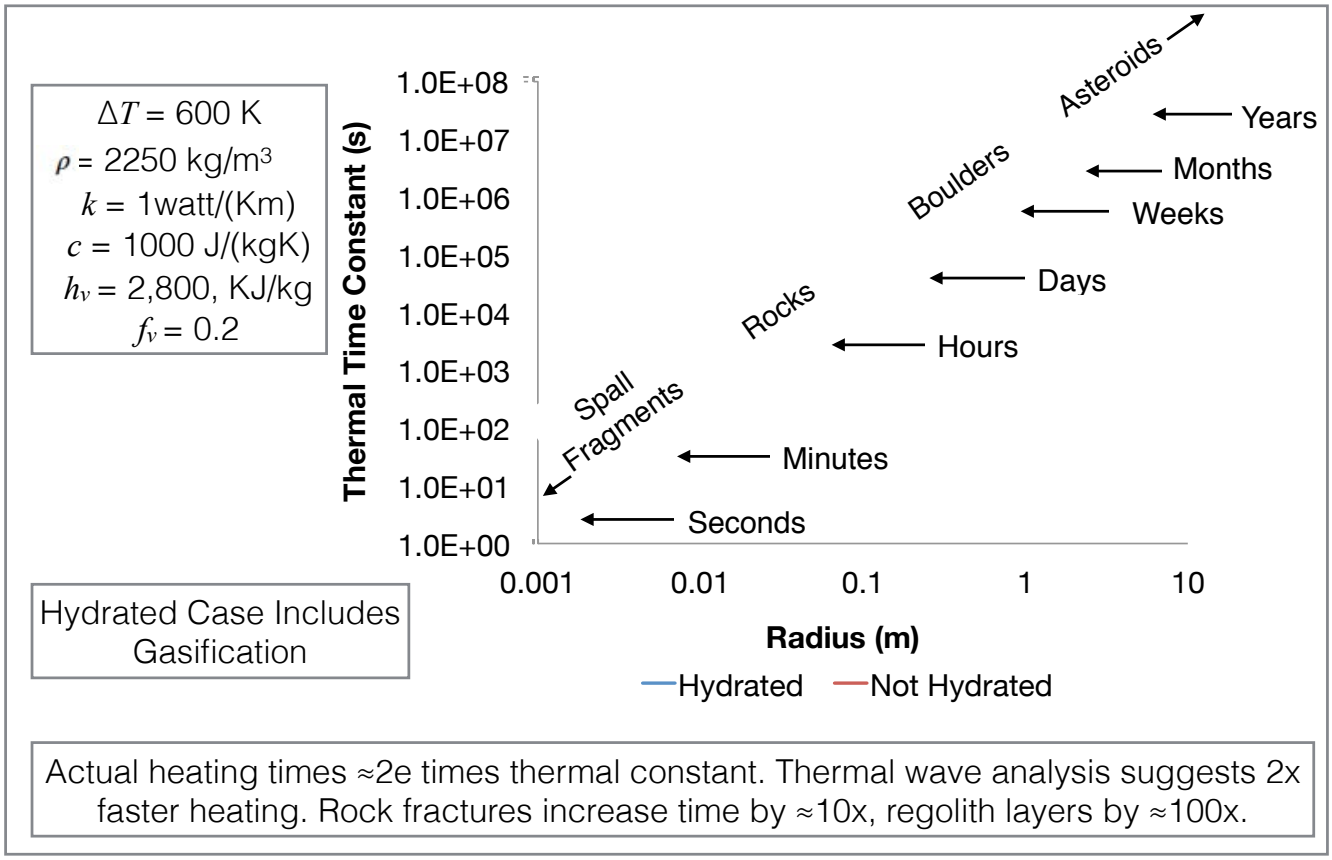

system was reconfigured to include a mass spectrometer with sampling valve. Facility capabilities include:

- Xenon Arc Lamp, nominally 1000 W
  (Focus variable from ~10 to 1000 W/cm^2)
- Video: 1280 x 720, 240 fps
- Mass Spectrometer (1-200 amu)

This apparatus is installed in a frame for use on microgravity aircraft and has flown on multiple times to investigate micro-gravity metals combustion (Abbud-Mardid, et al, 1996). For our NASA SBIR Phase I experiments the apparatus was installed in a 1500 sq. ft. laboratory run by our partners Prof. Christopher Dreyer and Prof Angel Abbud-Mardid of the Center for Space Resources (CSR).

The xenon arc lamp from ILC Technology has an input power level of 1 kW_e and a manufacturer specified output optical power level of 250 watts, which we measured during Phase I efforts at 150 watts delivered to the sample. Approximately 42% of the lamp's output power is in the 800-1150 nm range and the rest between 300-800 nm. The lamp is equipped with a parabolic,

Figure 1-18: Apparatus Use In Subscale Test and Demonstration Effort

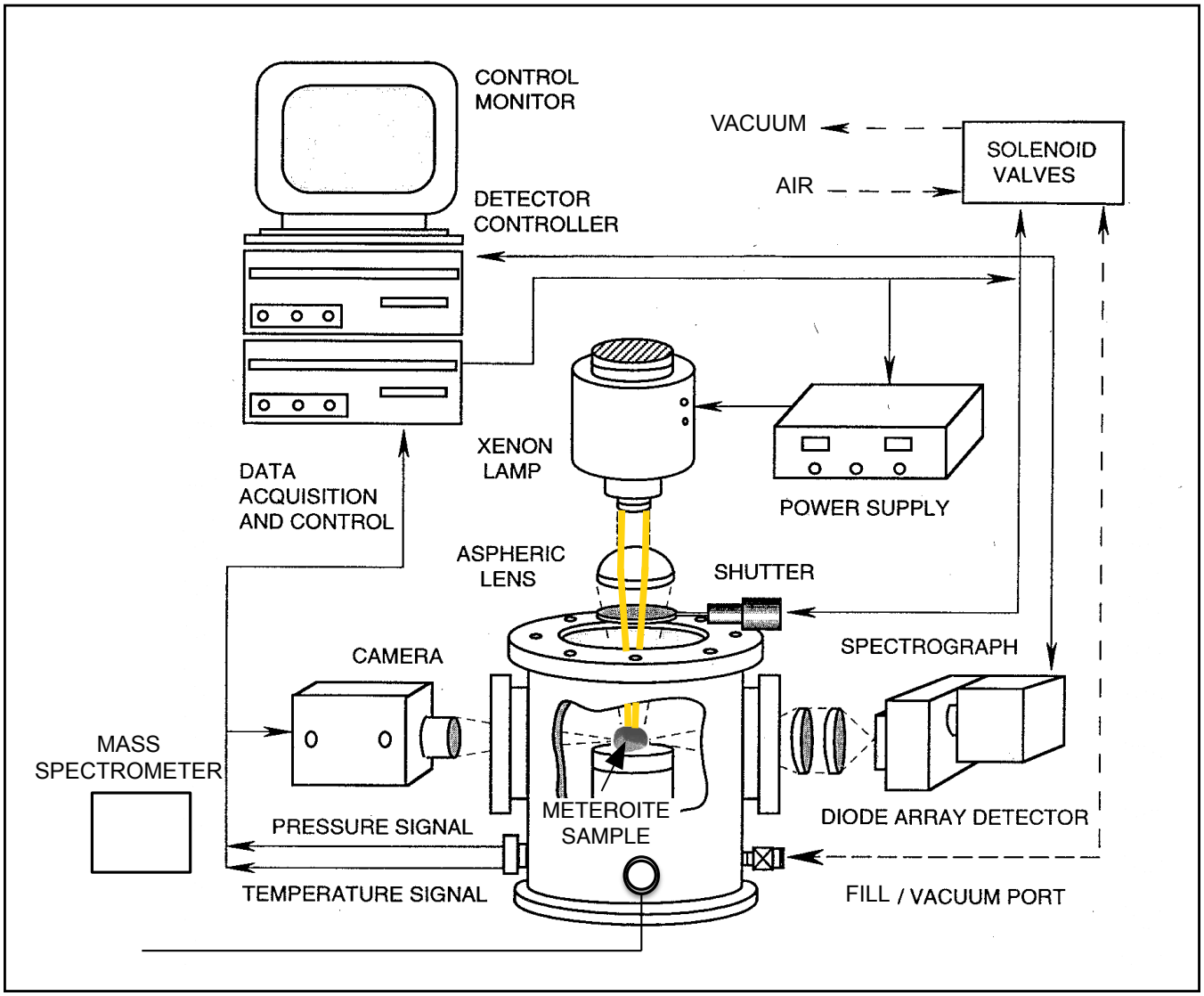

light-collection reflector that is silver-coated to eliminate UV radiation below 300 nm for user safety on the micro-g aircraft flights. The high-intensity, non-coherent light comes out of the lamp in a highly collimated beam (4° half-angle) with a gaussian profile. A shutter placed between the Xe lamp and the top window of the experiment chamber effectively blocks the light beam for sample-heating control.

Once the shutter opens, the beam goes through the 25-mm thick, quartz top window of the chamber and is intercepted by an aspheric lens (Melles Griot®, model 01LAG025) of 84 mm diameter and 60 mm focal length. The low f-number of the lens (f/# = 0.94) provides the maximum light-collection efficiency for the available focal length under these conditions. The lens focuses down the beam to the top surface of the sample. High-speed video was recorded with a

GoPro Hero 4+ at 240 fps in 1280x720 pixel resolution. The GoPro in the standard GoPro camera body was mounted on a frame and set to view the sample in the center for the chamber through a window. A macro lens was fitted to the GoPro for close in imaging of the samples. A polarizing filter and 2.0 neutral density filter were attached to reduce glare and light intensity during sample runs illumination. Many tests include before and after photographs without the neutral density filter. A tablet or smart phone was used to start and stop video acquisition. A mass spectrometer was attached to the sample chamber. The mass spectrometer was based on a Stanford Research Systems Residual Gas Analyzer (RGA) (model RGA-200). Gas is introduced to the spectrometer through a sampling valve. This valve provides fine control of gas flow into the mass spectrometer. A dedicated turbo pump in the mass spectrometer draws a small flow of gas into the mass spectrometer. Pressure in the mass spectrometer is monitored with an Inficon MPG-400 multifunction pressure gauge. The chamber was pumped down before tests using a roughing pump. A second Inficon MPG-400 gauge was used to measure chamber pressure. Both Inficon vacuum gauges were recorded with a National Instruments myDAQ at 20 samples per second.

Simulants: Several types of carbonaceous chondrite asteroid simulants were used in the experimental program. The simulants were designed to represent a range of material properties. In reviewing the literature and consulting with the planetary science community we have determined that the best meteorites to use to simulate water-rich asteroids are CI and CM chondrites. Multiple samples of the CM chondrites Jbilet-Winselwan and Murchison were purchased. A reasonable terrestrial analog of water rich asteroid rock, albeit with very different density and porosity, was found to be a type of serpentine called lizardite, which we purchased in kilogram quantities. The chemical formula for lizardite is $Mg_3(Si_2O_5)(OH)_4$ and it is approximately 13 percent water by weight which is approximately the same as Murchison. Moreover lizardite releases water at temperatures very close to the temperature Murchison releases its water. In addition to these natural materials we also worked with the University of Central Florida (UCF) to formulate bulk asteroid simulants. The UCF simulants consist of smectite clay, kerogen, magnetite, pyrrhotite, and olivine. In addition water is added to the mixture as part of fabricating the samples. These ingredients are ground up and moistened to make a mud-like mixture that can be molded to shape. Then the samples are placed in molds and dried, either with a heater or in a vacuum chamber.

The results of the subscale Optical Mining™ tests are detailed in a conference paper and in our SBIR Phase I Final Report. A few key highlights are provided here to place the full scale demonstration in context. One example of phenomenon observed is explosive spalling on a small scale. In one test an asteroid surface simulant made from a solid block of lizardite explosively

fractured into several fragments. Figure 1-19 shows six sequential frames of high speed video shot during explosive spalling. A jet of material can be seen coincident to the rock fracturing due to the tensile force of the gas release. Another interesting example involved an asteroid surface simulant produced by Prof. Britt of the University of Central Florida to simulate a carbonaceous chondrite. This simulant was the result of an iterative effort of refinement and was an especially good model of the actual meteorites we had in the lab. This sample showed significant fracturing and mass loss from the surface directly exposed to the focused light immediately as exposure began. Before and after images of the sample are shown in Figure 1-20. The light remained on the sample following spalling causing melting of the surface only when all the volatile content had been removed. Several frames during spalling are shown in Figure 1-21. Spalling is complete in 60 seconds. The video of this test clearly shows a stream of macroscopic particles being lifted off the sample and being carried away by outgassing volatiles thereby excavating a hole in the sample. As soon as spalling stopped the surface melted and excavation stopped. This critical demonstration proves the feasibility of key aspects of Optical Mining™.

Solar Thermal Oven Development: The NASA funded Early Stage Innovation (ESI) project titled "Laboratory Demonstration and Test of Solar Thermal Asteroid ISRU" is being conducted under the leadership of PI Prof. Leslie Gertsch of the Missouri University of Science and Technology. This program is designed to evaluate the volatile yield and the changes in properties of meteorites and asteroid simulants from steady and stepwise slow heating of carbonaceous chondrite material in vacuum. One of the primary deliverables of this ESI effort is an instrumented laboratory facility that can carefully control the temperatures of large (up to multiple kilogram) samples of material over a

Figure 1-19: High speed video frames of asteroid surface simulant explosive spalling. Spalling event begins at 1 and proceeds sequentially. Frames are separated by ≈4 ms.

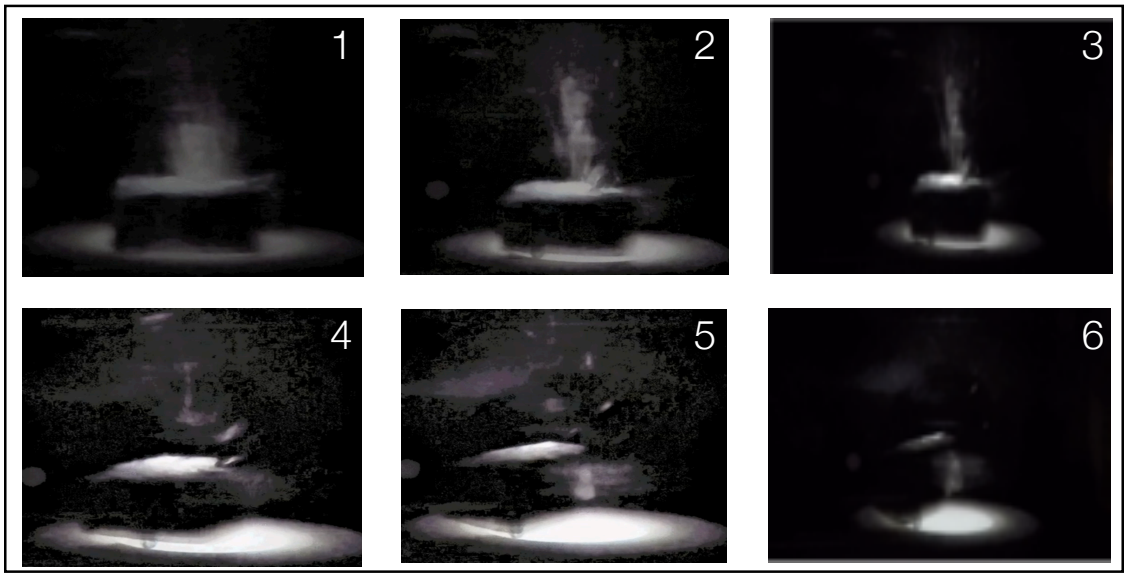

Figure 1-20: Simulant spalling – Before (left) and after (right). The light has bored a hole into the sample. The color change is typical of dehydration of hydrated materials.

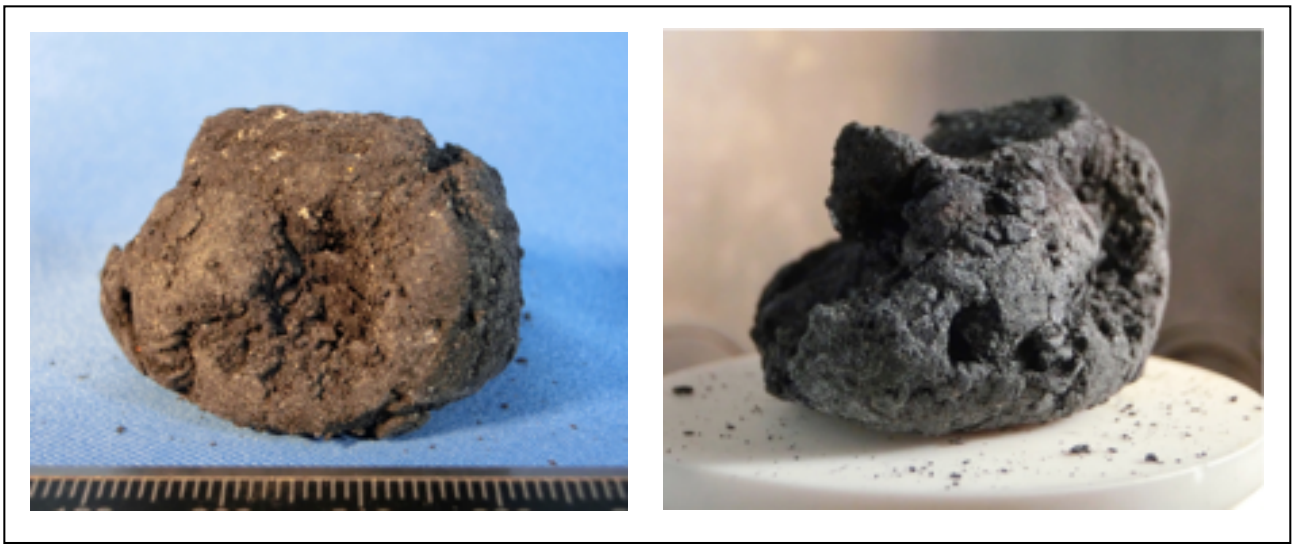

Figure 1-21: Asteroid surface excavation of a sample composed of simulant. Frames span 60 seconds. In the video, surface spalling can be seen with a stream of macroscopic particles being lifted off the sample and being carried away by outgassing volatiles thereby excavating a hole in the sample.

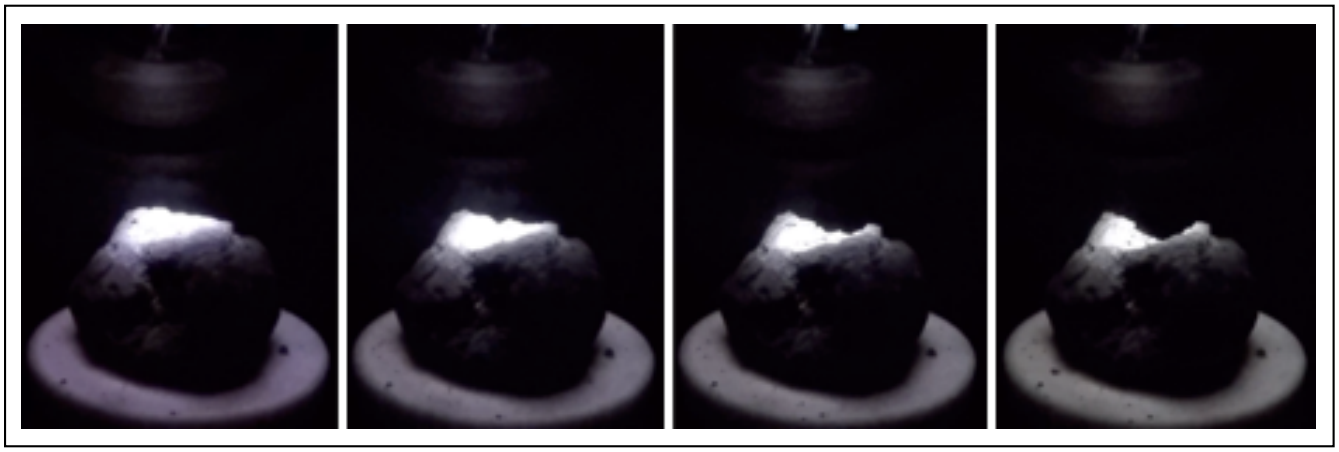

very wide range of temperatures to examine the material effects of thermal volatilization. In addition, the facility will include a LN2 cryotrap that can capture evolved volatiles in solid form for post test chemical analysis. A schematic diagram of this facility is provided in Figure 1-22 and photographs of the oven that has been built under this effort are provided in Figure 1-23.

In 2015 this project concentrated on building or adapting and testing the laboratory equipment which included vacuum chamber, furnace, and cold trap, and beginning a numerical model of the expected volatiles production function with temperature. In 2016 the project began to apply stepwise heating to kilogram scale samples of terrestrial simulants of carbonaceous chondrite meteorites and to compare the results to the completed numerical model. Strong synergy exists

Figure 1-22: Schematic diagram of MO S&T ESI Solar Thermal Oven Simulator

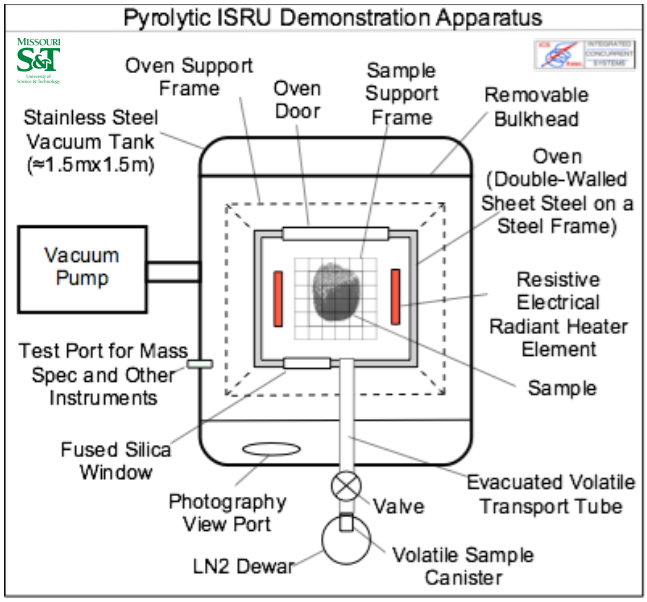

Figure 1-23: Photographs of the MO S&T Oven

between these efforts due to the co-location of the MO S&T oven in the same CSM laboratory as the arc lamp for the present effort. Most importantly, the solar thermal oven simulator will allow evaluation of the effects of bulk heating separately from the effects of intense surface heating and it will allow for the use of larger sample size. In combination these two facilities will allow us to independently control for many more variables and therefore study a wider experimental trade space with more rigorous experimental methods.

Asteroid Redirect Mission (ARM) FAST Membership: Dr. Sercel has recently completed his role as a member of the ARM FAST and has been working with the ARM Project team and the FAST to ensure that ISRU research is included in the ARM technology demonstration opportunities. This work has already been mutually beneficial with the SBIR effort and the present NIAC effort. For example, ARM FAST deliberations on the physics of the boulder the ARM mission will pick up has produced useful insights into the material properties of solid asteroid material that will benefit our modeling and simulation work. Likewise, AMR FAST deliberations focussed on ISRU experiments to be performed both on the ARM mission and on the boulder after its return to Lunar Distant Retrograde Orbit (LDRO) provide useful insights into eventual follow-on work stemming from this SBIR to include flight demonstrations in LDRO. It is becoming clear that a nearly full scale optical mining mission to the boulder in LDRO may be possible as a follow-up to ARM.

2.0 Research and Technology Results

The research and technology results reported in Section 2 of this report acting together prove the scientific feasibility of the Apis architecture™. We have accomplished the following:

- performed a large scale multi kilowatt demonstration of the Optical Mining™ method of excavation of asteroid material,
- developed and exercised a new technology to analytically determine the availability of asteroid resources as a function of return trip ΔV and trip time,
- performed detailed optical design and analysis showing that low mass thin film structures can be used to collect and deliver the solar thermal power needed for Optical Mining and high performance solar thermal propulsion,
- invented and analyzed *Omnivore™*, a new breakthrough type of solar thermal rocket ideally suited for use with asteroid derived propellants, and
- invented a new type of test apparatus to cost effectively demonstrate Omnivore™ propulsion technology.

2.1 Large Scale Optical Mining Demonstration

The goal of the demonstration effort was to perform a large scale (≈10 kW) demonstration of Optical Mining™ on a kilogram scale sample of a high fidelity asteroid simulant as a way to show that Optical Mining™ can be used to excavate large rocks in vacuum without physical contact with digging equipment and to obtain practical insights into Optical Mining™ paving the way for further technological maturation. This large scale demonstration was needed to confirm that the 38 tests and demonstrations performed in the related SBIR work did not perform as expected only due to some unknown scale factor effect. The full scale NIAC funded demonstration was successful in meeting these goals. We demonstrated the following: spalling of the large high fidelity simulant prepared for this purpose by the University of Central Florida; survival of our fused quarts window through nearly 15 minutes of combined operation at power levels in excess of 8 kW in a dirty environment with copious spall products and outgassing; and cryotrapping of outgassed water from a low fidelity sample.

This demonstration was performed at the solar thermal test facility at the White Sands Missile range in White Sands New Mexico. Figure 2-1 is a photograph of the facility which shows the geometric configuration. The furnace has four primary components: a sun tracking heliostat with a collection area of approximately 140 m^2, a digitally controlled louver system that allows modulation of the solar flux, the primary parabolic reflector with an area of approximately 80 m^2, and an elevated laboratory test area (open at the left in the photograph) to allow concentrated

Figure 2-1: Exterior View Solar Furnace Facility at White Sands Missile Range

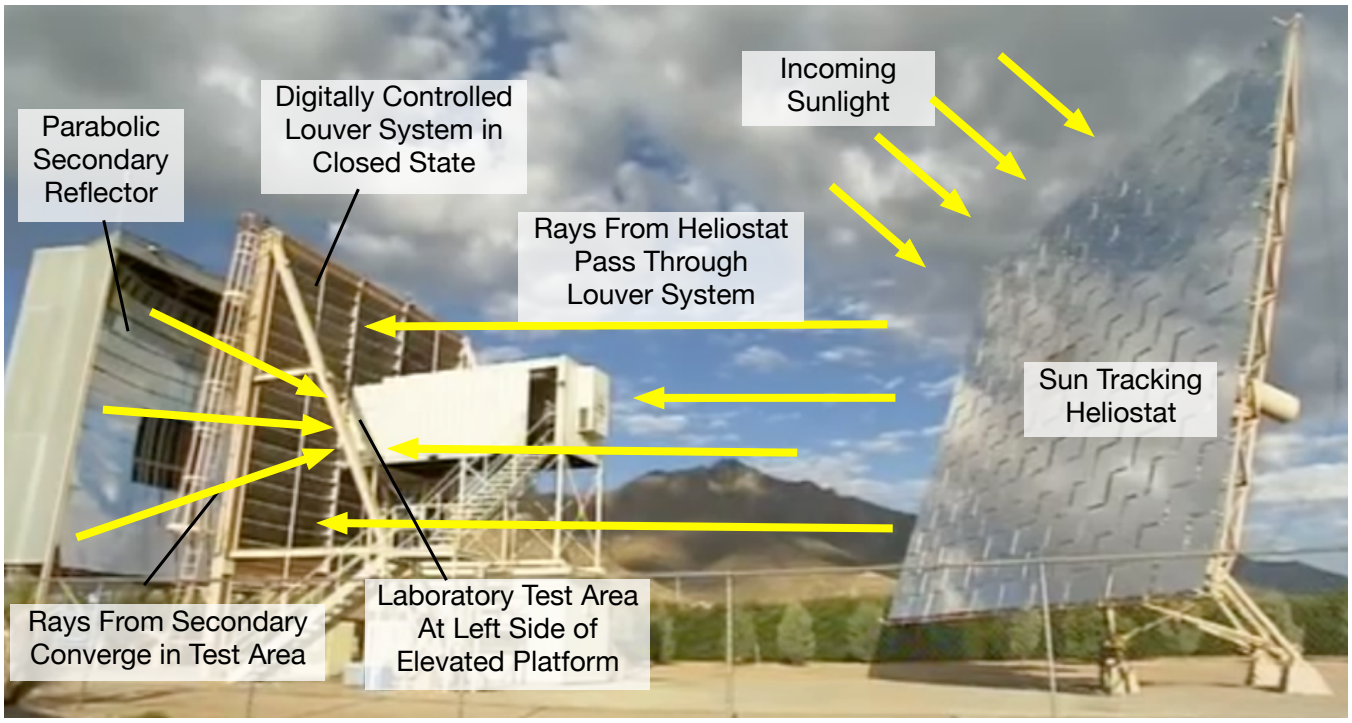

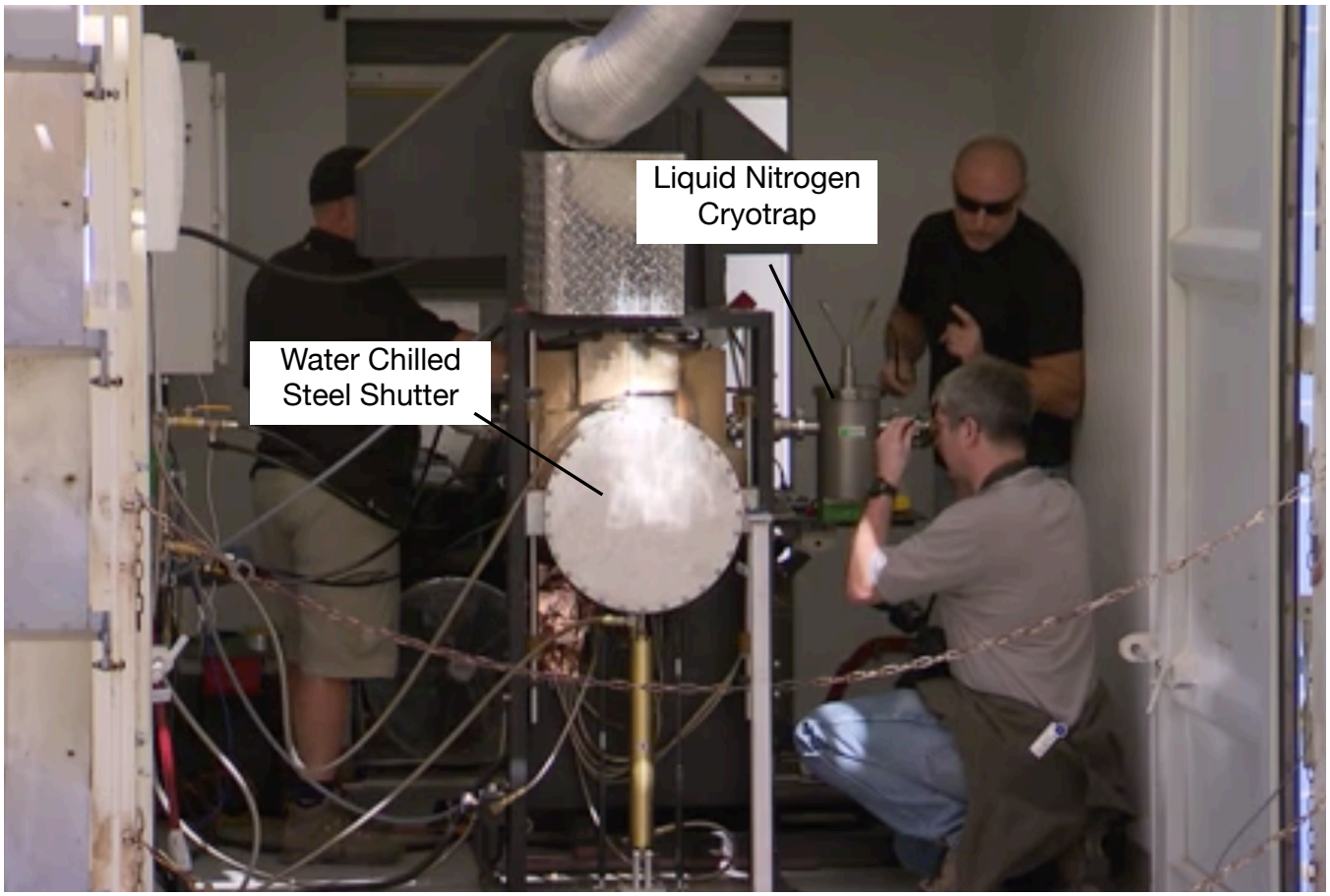

Figure 2-2: Laboratory Test Area As Viewed From the Center of the Parabolic Reflector

solar radiation into the facility. Note that the parabolic reflector has a square area on centerline without reflectors. This central area is shadowed by the test laboratory so it does not require reflectors and it provides a platform which allows viewing into the laboratory from centerline on the parabolic reflector. Figure 2.2 is a view of the test area from this platform showing both a water chilled steel shutter which can be raised and lowered pneumatically to allow flux into the test area and the liquid nitrogen cryotrap that was successfully used to trap volatiles from some of the Optical Mining™ experiments during this demonstration effort.

The White Sands solar furnace provides a peak power flux which is somewhat variable due to weather effects, mirror alignment, and elevation angle effects but is generally 150 ± 50 W/cm^2 corresponding to an in-space solar concentration ratio of about 1,000 Suns. This intensity level corresponds to a maximum spot temperature due to radiative heat balance of approximately 2,500 Kelvin. Actual spot temperatures are always less than this due to convective and conductive cooling effects and phase change phenomenon. This solar intensity level is about a factor of three less than we expect to be able to achieve in space with thin film reflectors but high enough for demonstration purposes for Optical Mining™. It is high enough to operate a low performance solar thermal rocket, but not high enough to demonstrate the performance we expect to get from high performance solar thermal rockets. As discussed later in this report, this limitation is one of the reasons we will not be using ground based solar concentrators in our Phase II work.

Figure 2-3 shows photographs of the test equipment we used at White Sands. The upper left image shows the equipment we built for this demonstration (under private funding) during assembly and test in Pasadena California. The upper right image shows a view of a small portion of the primary reflector as seen through welding goggles during a test after topping off the liquid nitrogen dewar. The lower left image shows the apparatus installed in the laboratory at White Sands, and the lower right image shows successfully cryotrapped water from a test of a low fidelity asteroid simulant. The primary cylindrical vacuum chamber for these tests is made of stainless steal and is 14 inches in diameter and 8 inches deep. It has a double wall construction with two independent water cooling chambers to prevent chamber melting during tests. The pumping system is a dual roughing and turbo-molecular plant that allows the system to achieve an ultimate vacuum of 10^{-8} torr with a pumpdown time of about 20 minutes. In the image on the upper left of the figure, a small adjustable stainless steal platform can be seen inside the tank onto which samples are placed during tests. The front window on the tank is an optically polished fused silica slab 3/4 of an inch thick. Note that there are two mechanical valves in the system, one leading to the pumping station and one leading to the cryotrap. The line between

Figure 2-3: Photographs of Apparatus Used in The Full Scale Demonstration Effort

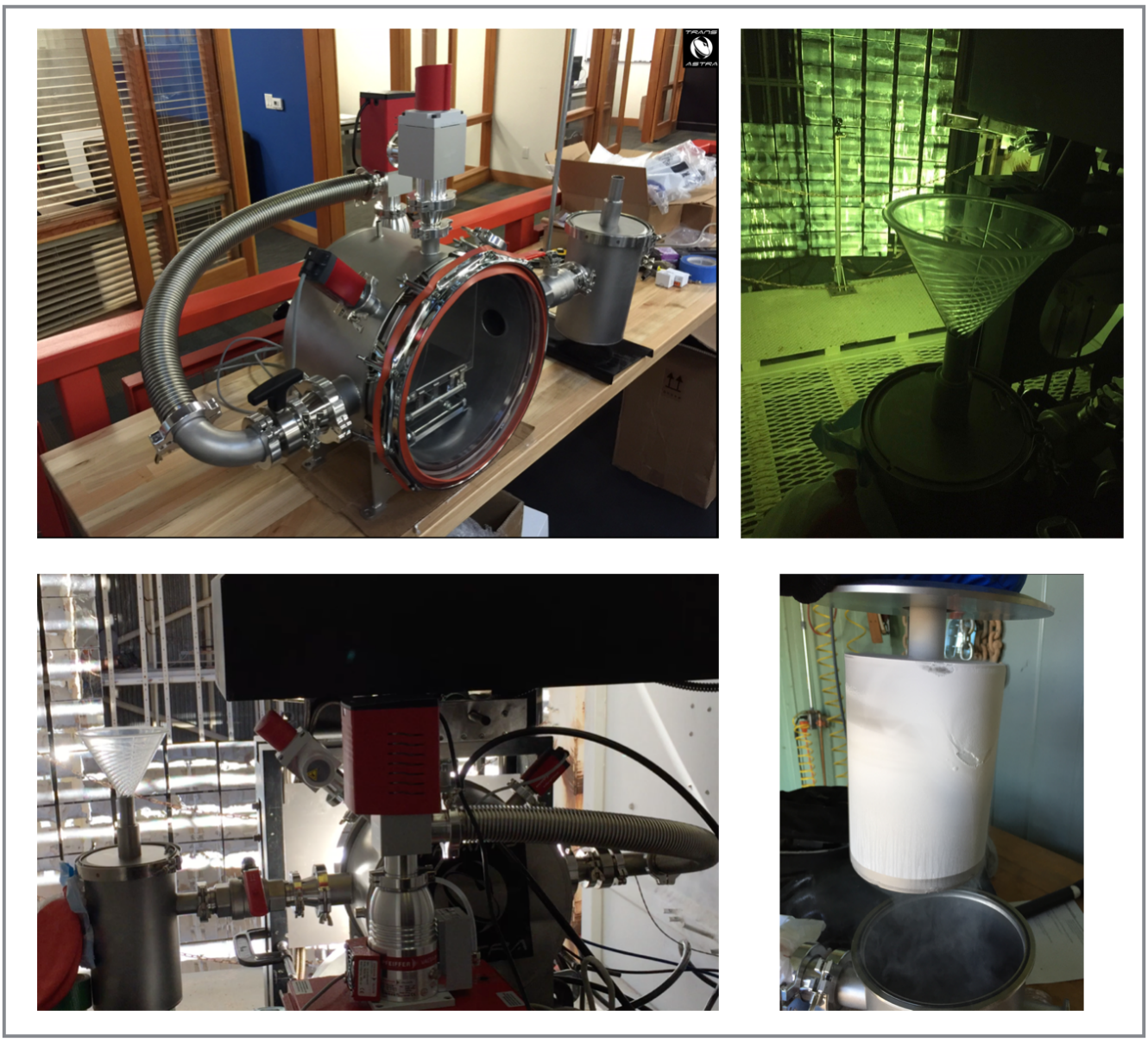

the tank and the pumping system includes two dust filters in parallel to protect the pumping station from debris during Optical Mining™. Even with these filters in place we do not operate the turbo pump while heat is applied to samples and we close valves prior to applying sunlight.

In operation, the first step after cleaning the tank from a prior test is to place a sample on the adjustable stand and center it before clamping the window in place over an o-ring seal. Both valves start in the nominally open position and then the system is pumped down. After pump down the valve to the turbo pump is closed and liquid nitrogen is added to the cryotrap, first pre-chilling, and then topping off to compensate for boil off. After the cryotrap has been chilled and

topped off, the movable shutter shown in Figure 2-2 is opened to allow solar flux through the window into the tank and onto the surface of the sample. During these early proof of concept demonstrations instrumentation was minimal to include monitoring vacuum system pressure versus time and taking video imagery of the sample during the tests to observe spalling and other physical effects. Samples were weighed and photographed before and after tests and trapped effluent was observed on the cryotrap. Extensive instrumentation including residual gas analysis was included in our related subscale experiments, and was therefore not critical to this scale factor confirmation demonstration.

Figure 2-4 provides images of the high fidelity asteroid simulant prepared by Prof. Daniel Britt of the University of Central Florida for this demonstration. Before this demonstration the simulant had a mass of 1.32 kg. After the test 220 grams of spall material was collected in the vacuum tank and the mass of the primary body was reduced to 998 grams (1.0 kg) for a total after-test dry mass of 1.19 kg. The remaining 130 grams of mass loss was volatile material. Additional post test analysis measuring the total volatile content of both the main body of the sample and the

Figure 2-4: Before And After Images Of Simulant From Full Scale Demo With Data Regarding Mass Loss

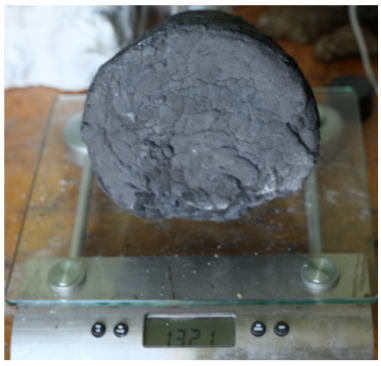

Image Before Test:
1.32Kg

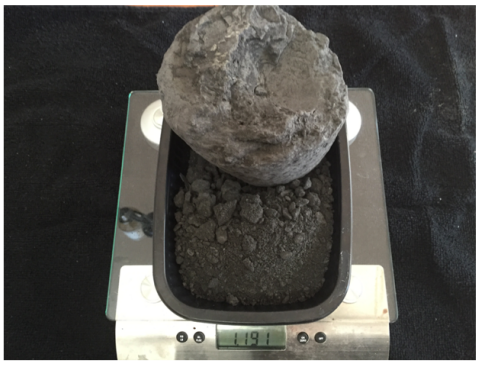

Image After Test
1.19Kg with Spall

After Removal From
Vacuum Chamber

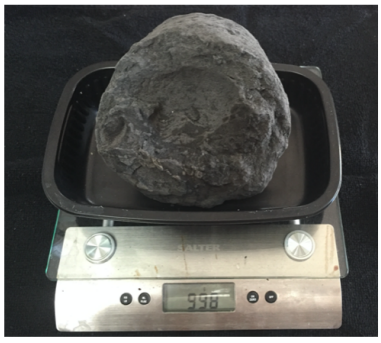

Image After Test: 1.0Kg

Spall Product 0.22kg

130 Grams Of Volatile Mass Lost Out Of 220 Grams Of Spall Production (Or 350 Grams Of Source Material). Suggests 37% Volatile Yield By Weight

spall debris will be required to determine how much of this volatile loss came from the spall debris and how much came from the primary body of the sample. Our analytical model suggests that the thermal wave does not propagate far into the sample so we expect the vast majority of volatile loss to come from the spall debris. We plan to perform this measurement as well as many more higher fidelity tests in future work.

Table 2-1: Asteroid Simulant Ingredients

Ingredient	Weight %
smectite clay	37.7%
kerogen	1.1%
magnetite	24.3%
pyrrhotite	7.2%
olivine	29.7%

The recipe for the simulant of Figure 2-4 is provided in Table 2-1. Note that in addition to the ingredients in Table 2-1, the fabricator also adds liquid water to the mixture. These ingredients are ground up and moistened to make a mud like slurry that can be molded to shape. Then the samples are placed in molds and dried with a heater and a vacuum chamber. Note that the primary role of the water in simulant production is to act as a lubricant causing the microscopic clay particles to adhere to one another for molding. The fact that the water was removed in vacuum prior to our tests is critical to understanding the validity of this formulation. In our other collaborative work with UCF we have tried several different formulation processes and the procedure has improved making samples that behave more and more like actual meteorite samples.

The spalling process can be clearly viewed in video we took through heavy welding goggle like filters during the test. Figure 2-5 is a series of screen grabs from the video. Without motion the screen grabs don't clarify the spalling process much. The water cooled aperture stop (the round circle) the video was taken through is 4 inches in diameter. Due to alignment issues, the beam was not perfectly centered on the aperture stop, but rather in the upper right hand quadrant of the exposed circular area. We estimate that only 8 kW of the 12 kW beam was on target during this test. Spalling was primarily in an elliptically shaped area approximately 1.5 by 2.5 inches in diameter. Post test measurements of the depth of the excavation in the sample show an excavation rate of 0.7 mm/s. This is in excellent agreement with the theoretically predicted excavation rate from our analytical model which is documented in our SBIR Phase I final report and which predicts 0.3 mm/s for material of this type. Given the heterogeneous nature of these materials and uncertainties in material properties, a factor of four agreement between theory and experiment can only be deemed excellent.

Figure 2-5: Video Screen Grabs Of The High Fidelity Sample At 10 Second Intervals. Times shown are after initiation of solar beam.

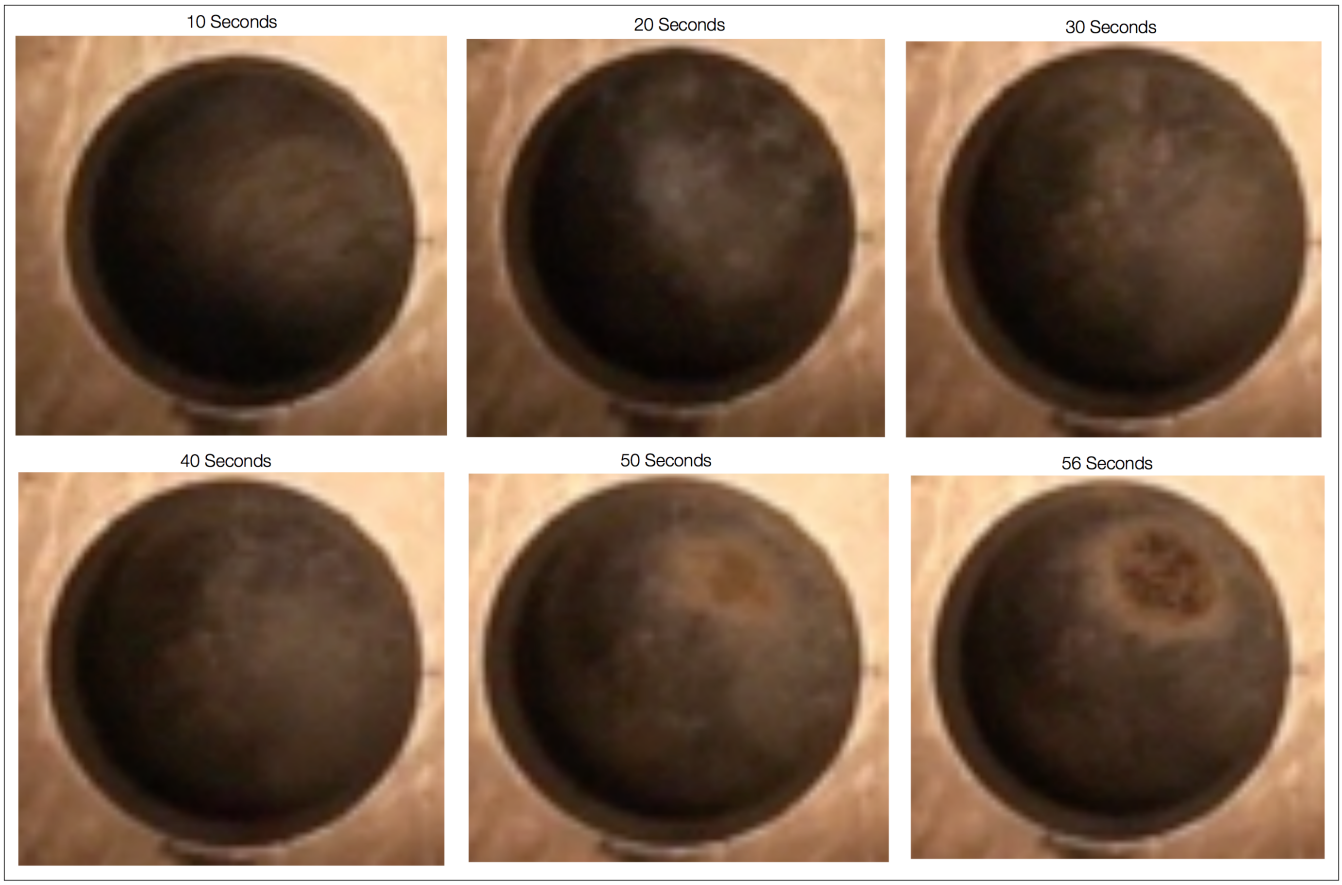

While the White Sands demonstration was a technical success, there were important practical lessons learned during the week of testing that led up to the demonstration that have caused us to radically improve our plans for both our Phase II SBIR and our Phase II NIAC. Recall that during the Phase I SBIR effort we used a small xenon arc lamp and vacuum system at Colorado School of Mines. We found the lamp to be easy to use and it allowed us to quickly iterate tests and adjust as we moved forward. Such agility is vital to an effective technology development effort, especially for an adaptive test methodology such as ours. By contrast, the White Sands tests were interrupted by weather, made slow and difficult by the extreme large size of the facility, and slowed by cramped working conditions in the test laboratory. We have concluded that it would not be practical to mount a successful Phase II program using the White Sands facility. We searched several alternatives including a solar concentrator site at Marshall Space Flight Center and several different types of solar furnaces. We decided that the best way to proceed for Phase II will be to build a ≈30X larger version of the xenon lamp we used at Colorado School of Mines, the design of which is documented later in this report.

2.2 Resource Availability Analysis

One of the technological needs associated with the Apis architecture and the general field of asteroid ISRU is that of determining the accessibility and quantity of useful materials that are available from the asteroids. There are many ways to define accessibility, but the natural approach if given the human and computational resources to perform a full mission optimization study would be to include an aggregate of several parameters to define accessibility. These parameters would include the spacecraft mass that a given rocket can launch to each target (which is calculated from the launch vehicle performance curves and the C_3 or V_∞ of a trajectory to get to the target), the waiting period before launch opportunities, the ΔV to return from the target to some given orbit, the waiting period at the target before the return window opens, and the return trip time. The problem is made challenging by the fact that the best target bodies for modestly sized missions to return tons to hundreds of tons of resources based on modestly sized spacecraft that can be affordably launched in the near term are probably in the 4 to 10 meter diameter range, and most of the asteroids in that size range have not yet been discovered. Hence, we are dealing with a statistical population model, not a well established list. Another challenge is the fact that the composition of asteroids is variable and determining the distribution of composition of objects in a statistically generated population requires modeling the history of each object all the way back to each object's source region in the main asteroid belt to determine taxonomic type. One would prefer to couple all of these variables with a fully optimized mission model. Finally, one would prefer to model the discoverability of new asteroids as a function of time given the performance of existing telescopes and the projected performance of telescopes that will be coming on line in the search for asteroids in the coming years.

These ideal goals are well beyond the scope of this Phase I effort, especially given that resource availability analysis is only one aspect of this work. Instead, as per our NIAC Phase I proposal, we sought only to develop and prove a simplified approach that can give useful engineering results but not require an exhaustive mission optimization effort. Several workers have attempted to address this practical problem in the past starting with Shoemaker and Helin in 1978 who published a closed form equation for estimating asteroid return ΔV based on a statistical analysis of several hypothetical asteroid missions. While the Shoemaker equation is handy and easy to use, it has also been known by engineers to be grossly inaccurate. In spite of this, the science community has used this equation for rough estimates and it has passed refereed publication several times (for a recent example see Elvis 2013). It is interesting to note that an academic review of the Shoemaker equation in 2015 mentored by Elvis found the flaws with the Shoemaker equation (see Murphy 2015).

We have developed a simplified mission model to estimate ΔV, Earth-return trip time, and quantity of material available per year in near-Earth objects (NEOs). Our model is designed to be analytically simple, to err on the conservative side of over-estimating ΔV, and to be close enough to optimal to provide a useful assessment of mission viability from the perspective of ΔV requirements and resource availability. We treat Earth's heliocentric orbit as circular with a semi-major axis of 1 au and zero inclination. Since only 0.00001% of all NEOs with diameters greater than about 4 m are known, our ΔV calculation is performed on members of a synthetic population of one million randomly generated objects according to the NEO orbit distributions estimated by Granvik 2016. In the work we report here, we show that we can exercise the Granvik model for millions of synthetic targets and tie them to main belt source regions and spectroscopic data regarding known targets as well as meteorite composition data to predict water content as a function of accessibility. With these results and methods in hand, we can confidently plan our Phase II activities to include a survey of resource materials other than just water and which takes advantage of more available funding to provide more optimal and complete results with an accessibility model more like the list provided in the first paragraph of this subsection.

Our model divides the mission into five distinct phases separated by four time ordered independent propulsive ΔV maneuvers using the method of patched conics for efficiency:

ΔV_{plane}
The first maneuver rotates the asteroid's trajectory into the ecliptic plane (henceforth the "ecliptic orbit"). Performing the plane change maneuver separately from other maneuvers is suboptimal, but doing so simplifies the remaining problem with a boundable mission performance penalty.

$\Delta V_{\text{transfer}}$
The second maneuver places the asteroid onto an elliptical "transfer orbit" trajectory that is tangent to Earths orbit at one extrema and ensures that the asteroid and Earth rendezvous at the same heliocentric ecliptic longitude at the same time. We require that the maneuver take place when the object is opposite from Earth relative to the Sun.

ΔV_{LGA}
The third maneuver takes place near the Earth and enables a Lunar Gravity Assist (LGA) for capture in the Earth-Moon system from the transfer orbit.

ΔV_{DLRO}
The fourth and final maneuver is a generously allocated 100 m/s for capture into distant lunar retrograde orbit (DLRO) from the low energy departure from the LGA.

Table 2-2: Orbit Element Definitions

			orbit		
symbol	element	unit	original	ecliptic	transfer (eqn. #)
a	semi-major axis	au	a	a	a_T (11)
e	eccentricity		e	e	e_T (12)
i	inclination	deg	i	0.0	0.0
Ω	ascending node	deg	Ω	Ω	0.0
ω	argument of perihelion	deg	ω	ω	$\omega\tilde{}_T$
$\tilde{\omega}$	longitude of perihelion	deg	$\Omega+\omega$	$\Omega+\omega$	$\omega\tilde{}_T = \lambda(T_M)$ or $\lambda_{t_M} + \pi$ (5) $M_{0,T} = 0$
M_0	mean anomaly at epoch	deg	M_0	M_0	
t_0	epoch	MJD	t_0	t_0	

The total estimated ΔV is the scalar sum of the four components. Our technique is conservative because broken plane maneuvers and optimized plane changes combined with adjustments to eccentricity and semi-major axis always result in lower actual mission $\Delta V < \Delta V'$. We take this approach for expediency in this Phase I effort and because it is computationally far less expensive. We will now provide the derivation for each of the first three ΔVs in which we use the orbit element definitions and variables provided in Table 2-2. In this model, all propulsive maneuvers are treated as impulsive, which is a good approximation for heliocentric applications of the solar thermal propulsion technology we are proposing.

Calculating ΔV_{plane}: As shown in Figure 2-6, the plane change maneuver rotates an NEO's orbit into the ecliptic plane resulting in an *ecliptic orbit* with $i = 0^{\circ}$, without affecting any of the other orbital elements. Once the orbit is in the ecliptic, the ascending node becomes degenerate and the orbit can be described by just 4 elements: (a, e, ω, M_0) but our ecliptic orbits are defined by (a, e, $\tilde{\omega}$, M_0) where $\tilde{\omega} = \Omega + \omega$. Since the plane change maneuver must take place when the object is in the plane of the ecliptic (the instant at which it passes through the ascending or descending node) it requires that $\nu + \omega = 0$ or π and we can solve for the eccentric anomaly E using

$$2\arctan\left[\sqrt{\frac{1+e}{1-e}}\tan\frac{E}{2}\right] + \omega = 0 \text{ or } \pi. \quad (1)$$

Figure 2-6: An example of a plane change maneuver that rotates the plane of the (red) original orbit with $a = 0.8$ au, $e = 0.5$ and $i = 45°$ into the (mauve) ecliptic orbit with $a = 0.8$ au, $e = 0.5$ and $i = 0$. The blue curve represents Earth's idealized circular orbit with $a = 1$ au, $e = 0$ and $i = 0$. The yellow circle at the center represents the Sun and the straight black line extending from it to the right represents the direction of the vernal equinox. The ΔV_{plane} for this example is either ≈ 82 km/s or ≈ 27 km/s depending on whether the maneuver takes place at the ascending or descending node (represented by the red filled and unfilled circles respectively).

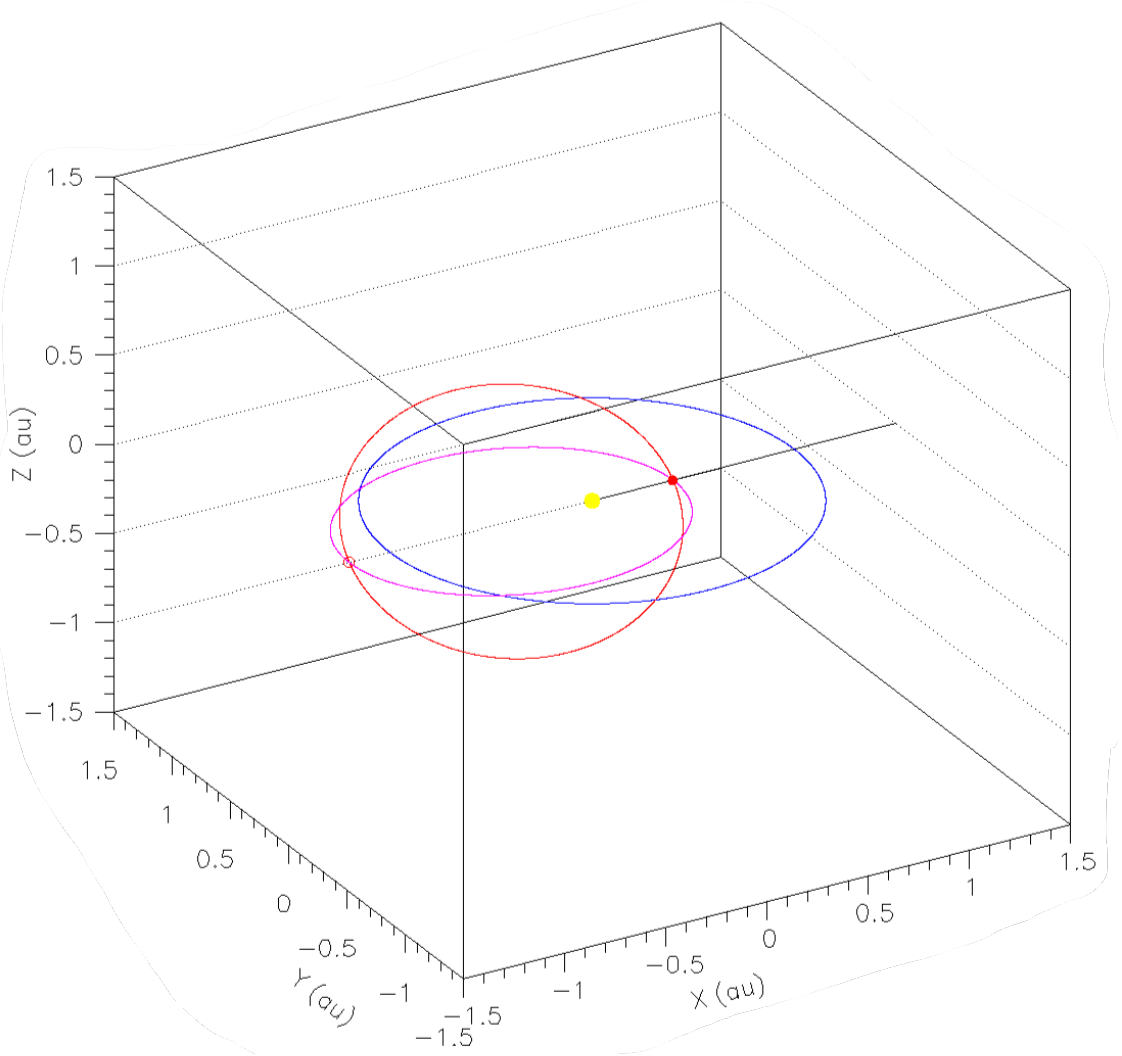

Letting the eccentric anomaly at the two nodes be represented by E_j, with $j = 1$ or 2 corresponding to the ascending and descending nodes respectively, the object's heliocentric distance and speed at the times of node crossings are given respectively by

$$r_j = a\,(1 - e\,\cos E_j) \tag{2}$$

and

$$v_j = \sqrt{\mu\ \left(\frac{2}{r_j} - \frac{1}{a}\right)}' \tag{3}$$

where μ is the solar gravity constant. We then apply the standard ΔV equation for a pure plane change of magnitude $\Delta i = i$ (because our intent is to remove all the original orbit's inclination),

$$\Delta v_{plane,j} = 2\, v_j\, \sin\left(\frac{i}{2}\right), \left(\tag{4}$$

where v_j is the orbital speed at the time of the maneuver. The two $\Delta V_{\text{plane},j}$ values will not be equal in general and we will use both values for our final ΔV distributions.

Calculating $\Delta V_{\text{transfer}}$: The second propulsive maneuver places the asteroid onto a 'transfer orbit' with one extrema (periapsis or apoapsis) tangent to Earth's orbit with the correct orbit phasing so that it arrives at Earth's orbit when the Earth is also at that location. We have made the design choice that the extrema of the transfer orbit opposite to Earth arrival must be the location of the $\Delta V_{\text{transfer}}$ maneuver on the ecliptic orbit (Figure 2-7). This design choice is suboptimal but simplifies the analysis consistent with our Phase I philosophy with future optimization in Phase II.

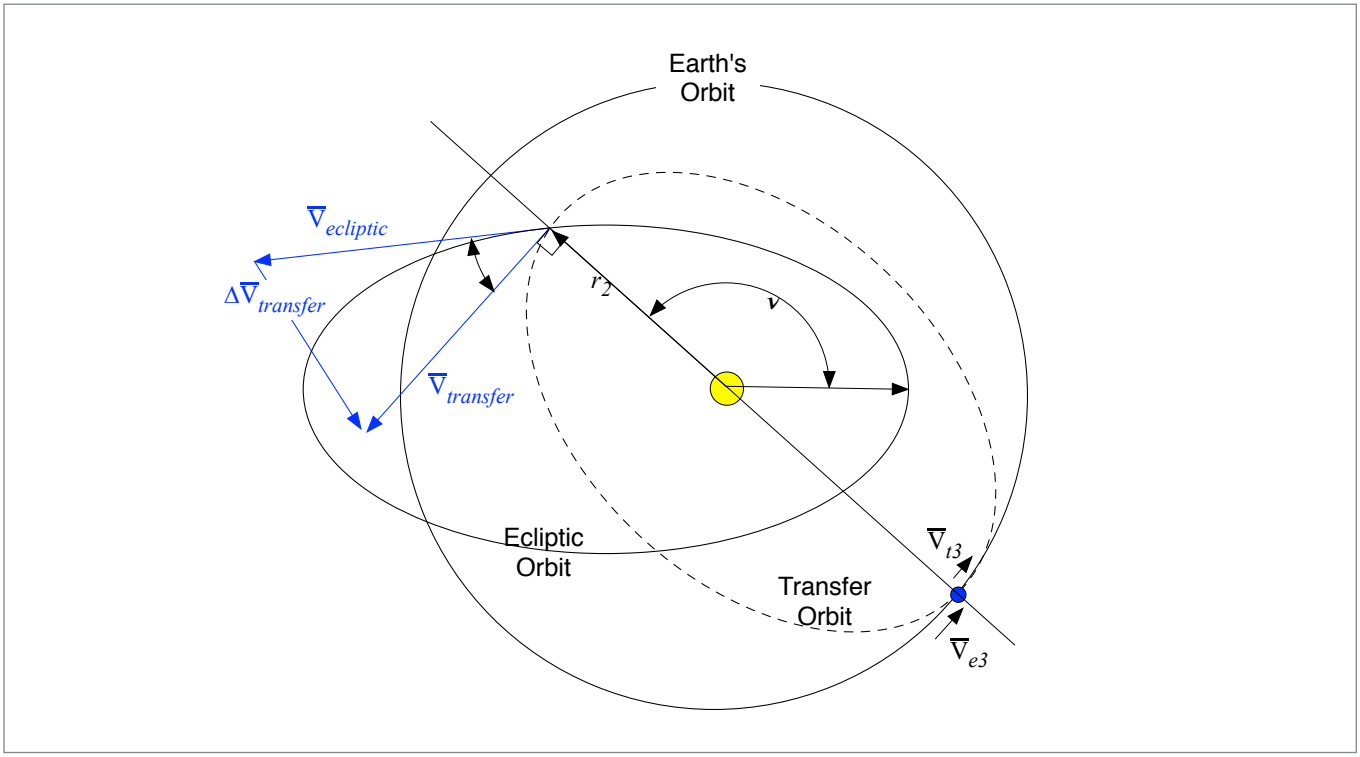

Figure 2-7: Definition of vectors in the $\Delta V_{\text{transfer}}$ maneuver between the ecliptic and transfer orbit.

Thus, with t_M representing the time of the maneuver on the object's ecliptic orbit and $T_T(t_M)$ the orbital period of the transfer orbit if the maneuver occurs at time t_M, we require that:

$$\lambda_E\left(t_M + \frac{T_T(t_M)}{2}\right) = \lambda_e(t_M) + \pi \tag{5}$$

where $\lambda_E(t)$ and $\lambda_e(t)$ are, respectively, the heliocentric ecliptic longitude as a function of time of Earth and the object on its ecliptic orbit. We use the capital E subscript for Earth, the small '*e*' subscript to refer to the object's ecliptic orbit, a capital T subscript to reference the transfer orbit, and orbital elements without subscripts refer to the object's original orbit. This equation can be solved for the maneuver time, t_M, because all other terms are known. With the simplifying assumption that Earth is on a circular, zero inclination orbit, its heliocentric ecliptic longitude at time (t) is:

$$\lambda_E(t) = M_E(t) = M_{E,0} + n_E\,(t - t_0) + \omega_E \tag{6}$$

where $M_{E,0}$ is Earth's mean anomaly at the orbit epoch (t_0), n_E is Earth's mean angular rate of motion, and ω_E is Earth's argument of perihelion. In our model, since we use synthetic objects and an idealized Earth, we define $M_{E,0}=0$, $t_0=0$, and $\omega_E = 0$, without loss of generality. Since the object is in an ecliptic orbit, its heliocentric ecliptic longitude is

$$\lambda_e(t) = \nu_e(t) + \omega \tag{7}$$

where ω is its argument of perihelion and its true anomaly (ν_e) can be calculated from the standard formulae (Green 1985)

$$E_e(t) - e\sin E_e(t) \;=\; M_0 + n(t - t_0) \tag{8}$$

$$\tan\frac{\nu_e(t)}{2} \;=\; \sqrt{\frac{1+e}{1-e}}\tan\frac{E_e(t)}{2}. \tag{9}$$

Similarly, the object's heliocentric distance is given by

$$r_e(t) = a\big[1 - e\cos E_e(t)\big]. \tag{10}$$

When the transfer maneuver takes place at time t from the object's ecliptic orbit, its transfer orbit will have perihelion $q_T=r_e(t)$, the heliocentric distance at which the transfer maneuver takes place, and aphelion at Earth's orbit, $Q_T=a_E=1$ au. Alternatively, the transfer orbit has perihelion at Earth's

orbit, q_T=a_E=1 au, and aphelion where the transfer maneuver takes place, Q_T = $r_e(t)$. Thus, the semi-major axis and eccentricity of the transfer orbit are given by

$$a_T(t) = \frac{a_E + r_e(t)}{2} \tag{11}$$

and

$$e_T(t) = \frac{|a_E - r_e(t)|}{a_E + r_e(t)} \tag{12}$$

respectively.

Note that we use the absolute magnitude of the difference in the numerator in eq. 12 so that the eccentricity calculation is symmetric regardless of whether the transfer orbit intersects Earth's orbit at perihelion or aphelion. The period of the transfer orbit in years is then

$$T_T(t) = a_T(t)^{\frac{3}{2}}. \tag{13}$$

In summary, we solve for the transfer maneuver time t_M in eq. 5 so

$$n_E \left[t_M + \frac{T_T(t_M)}{2} \right] = \nu_e(t_M) + \omega + \pi \tag{14}$$

where:

$$E_e(t_M) \quad e \sin E_e(t_M) \;=\; n\, t_M, \tag{15}$$

$$\tan \frac{\nu_e(t_M)}{2} \;=\; \sqrt{\frac{1+e}{1 \quad e}} \tan \frac{E_e(t_M)}{2}, \tag{16}$$

$$r_e(t_M) \;=\; a\big[1 \quad e \cos E_e(t_M)\big], \tag{17}$$

$$a_T(t_M) \;=\; \frac{a_E + r_e(t_M)}{2}, \tag{18}$$

$$T_T(t_M) \;=\; a_T(t_M)^{\frac{3}{2}}. \tag{19}$$

Then, if the transfer maneuver occurs at t_M on the object's elliptical orbit, it will arrive at the Earth a half-period later on the transfer orbit.

The speed of the object on its ecliptic orbit at the instant before the maneuver time is

$$v_e(t_M) = \sqrt{\mu \left(\frac{2}{r_e(t_M)} - \frac{1}{a} \right)}. \tag{20}$$

The speed of the object on its transfer orbit at the instant after the maneuver time is

$$v_T(t_M) = \sqrt{\mu \left(\frac{2}{r_e(t_M)} - \frac{1}{a_T(T_M)} \right)}. \tag{21}$$

From vector addition using the Law of Cosines, the required ΔV is then given by

$$\Delta v^2_{transfer} = v_T^2 + v_e^2 - 2\, v_T\, v_e\, \cos\phi \tag{22}$$

where ϕ is the angle between the velocity vectors on the two orbits at the maneuver time, the 'flight path angle' (Figure 2-7). Since the velocity vector on the transfer orbit is, by definition, purely tangential to the Sun-object line because the transfer occurs at perihelion or aphelion on the transfer orbit, the angle between the two orbits at the maneuver time is simply the flight path angle of the ecliptic orbit at the maneuver time where

$$\cos\phi(t_M) = \frac{h_e}{r_e(T_M)\, v_e(T_M)} = \frac{\sqrt{\mu\, a\, (1-e^2)}}{r_e(T_M)\, v_e(T_M)} \tag{23}$$

and h_e is the orbital angular momentum of the ecliptic orbit.

The orbital elements of the transfer orbit are completely specified above except for the longitude of perihelion $\tilde{\omega}_T$, mean anomaly $M_{0,T}$, and epoch. The epoch is simply the maneuver time. If the transfer maneuver takes place at perihelion then $\tilde{\omega}_T$ is the heliocentric ecliptic longitude at which the maneuver takes place and $M_{0,T}$=0. Alternatively, if the transfer maneuver takes place at aphelion, then $\tilde{\omega}_T$ is the heliocentric ecliptic longitude at which $M_{0,T}=180^o$ (see Table 2-2).

Calculating ΔV_{LGA}: Strange et al. (2014) performed a study of LGA capture trajectories and calculated the maximum C_3 that can be captured into Earth orbit using a LGA as a function of the right ascension and ecliptic declination of the approach asymptote. They show that objects that approach Earth at ecliptic right ascension and declination of zero can be captured with $\Delta V_{LGA} \approx 0$

Figure 2-8: Physical Picture for the Conditions at Earth Arrival. The mauve ecliptic orbit and Earth's orbit appear as in Figure 2-6. The transfer orbit is illustrated by the green curve. The open circles in 3 related colors indicate the position of the relevant object on its orbit at the time of the $\Delta V_{transfer}$ maneuver. (The location at the time of maneuver on the ecliptic and transfer orbit are identical, as designed.) The filled circles indicate the respective positions of the asteroid and Earth at the time of Earth encounter i.e. they are coincident. In the case shown in the figure, $\Delta V_{transfer} \approx$ 9.5 km/s and $\Delta V_{LGA} \approx$ 11.6 km/s.

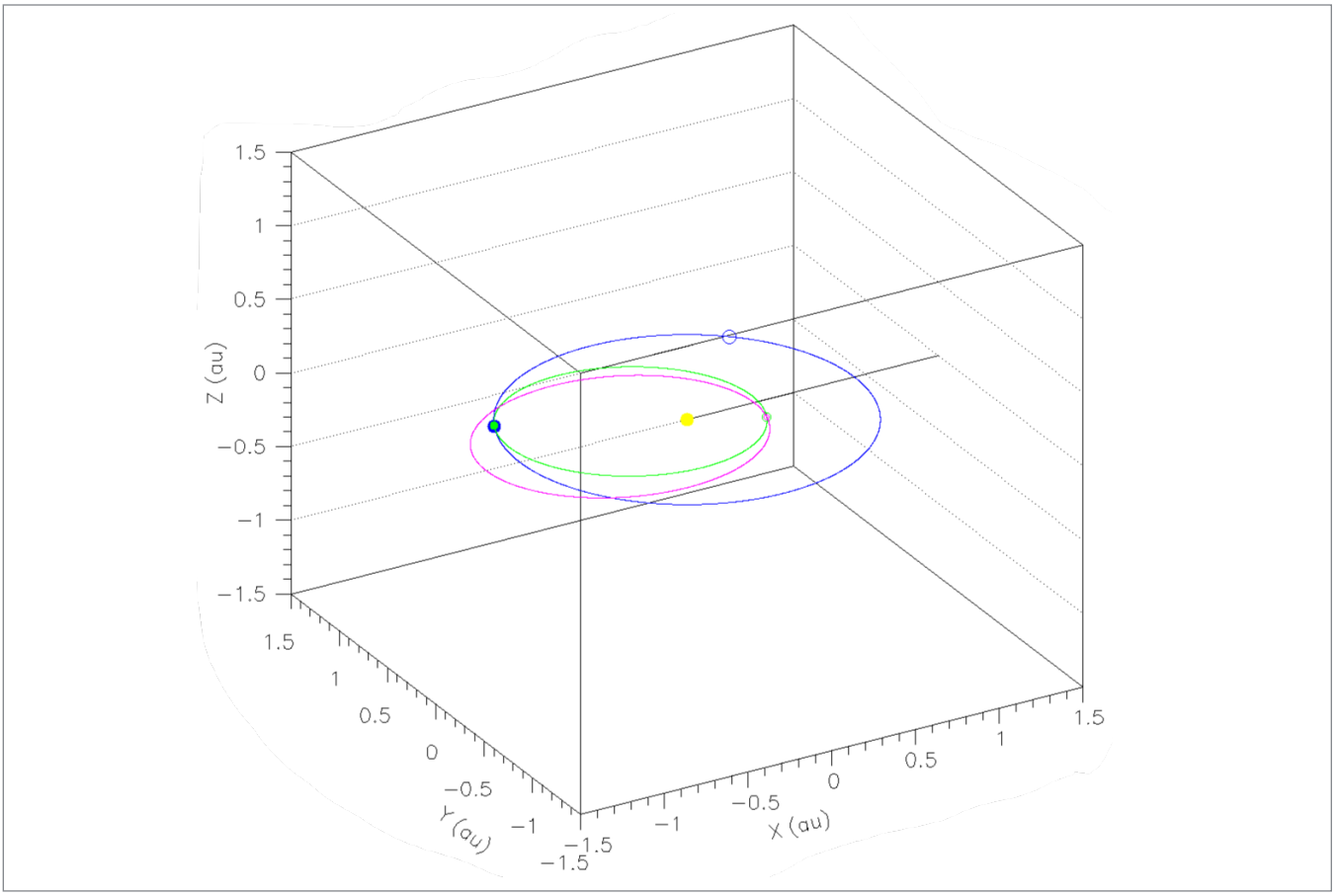

for C_3 up to 3 (km/s)^2 corresponding to v_∞ less than a critical value of approximately 1.73 km/s (see their Fig. 2). For the purpose of this Phase I study therefore we take ΔV_{LGA} to be zero for all $v_\infty \leq$ 1.73 km/s. After corresponding with one of the authors (Landau) of the Strange paper, we concluded that a reasonable estimate for the value of ΔV_{LGA} for values of $v_\infty >$ 1.73 km/s is that the ΔV required to capture is one half the residual approach velocity in excess of the critical value, or:

$$\Delta v_{LGA} = \begin{cases} \frac{1}{2}(v_\infty - v_0) & \text{if } v_\infty > v_0 \\ 0 & \text{otherwise} \end{cases} \quad (24)$$

.

Since the transfer orbit is tangent to Earth's orbit, the hyperbolic excess speed, v_∞ of the transfer at Earth encounter is simply the difference in speeds between the Earth and the arriving asteroid encounter time (t_R):

$$v_\infty = |v_E - v_T(t_R)| \tag{25}$$

where v_E is Earth's (constant) orbital speed and $v_T(t_R)$ is the object's orbital speed at encounter,

$$v_T^2 = \frac{\mu}{a_T}\left[\frac{2}{1 \pm e_T} \quad 1\right] \tag{26}$$

where the ± depends on whether the rendezvous occurs at aphelion or perihelion respectively.

Calculating Transfer Time: The relevant total transfer time (t_{xfer}) is the time from the ΔV_{plane} maneuver to Earth encounter, which is the time spent on the ecliptic orbit between the plane change and the transfer maneuver, plus half the period of the transfer orbit:

$$t_{xfer,j} = \Delta t_{ecl,j} + \frac{T_{T,j}}{2} = (t_{M,j} - t_j) + \frac{_{T,j}}{2}. \tag{27}$$

The subscript $j = 1{,}2$ accounts for the plane change maneuver occurring at either the ascending or descending node and the transfer orbit period, $T_{T,j}$, is given by eq.19. The transfer maneuver times, $t_{M,j}$, are the solutions to eq.14 and we can solve for the times of the plane change maneuver because the eccentric anomaly at the times that an object is in the ecliptic is given by E_j from eq. 2 so that t_j can be calculated from

$$M_j = E_j - e\sin E_j = M_0 + n_0\,(t_j - t_0) = M_0 + n_0\,T_{plane,j} \tag{28}$$

where we ensure that $t_j > t_0$.

Application of the NEO Model to Estimating Resource Accessibility: The asteroids that may provide a source of water for ISRU near the Earth and Mars mostly derive from the population of asteroids in our solar system termed near-Earth objects (NEOs). NEOs are either asteroids or comets, respectively icy dirt balls or dirty ice balls, that can approach to within 1.3 au of the Sun. Despite the term, these objects may only rarely or never be *near* Earth and, if they are near Earth, they are usually not accessible with low ΔV. The NEOs are a transient population of objects with

each member having a half-life in the NEO population of about 10 Myr with their orbits constantly changing due to many factors, chief among them multi-body gravitational effects from the planets and a radiation dynamic called the Yarkovsky effect. NEOs are constantly lost from the population by these dynamical effects or collisions with planets. New NEOs are supplied mostly from the main belt to maintain the steady-state population. The orbital element phase space within the main belt that supplies the new NEOs are called *source regions*. The main belt asteroids' orbits in the source regions are slowly perturbed by the effect of solar radiation and the gravitational effects of (typically) Jupiter and Saturn such that their orbital eccentricities increase, resulting in their perihelion distance dropping close enough to the Sun to introduce them into the NEO population. Once the objects enter the inner solar system they experience frequent interactions with planets that cause their orbits to evolve such that they either hit the Sun, a planet, or are ejected entirely from the solar system.

Table 2-3: Percentage Of Asteroids From Class (C) As A Function Of Source (K).

	Source						
Class	Hun	Pho	ν_6	3:1	5:2	2:1	JFC
S	17.	48.	55.	47.	17.	4.3	0.0
C	9.6	23.	18.	26.	43.	57.	0.0
D	0.0	0.3	0.3	0.5	0.6	1.6	1.0

The so called Granvik model (Granvik et. al. 2015) includes a mapping of the major NEO source regions grouped into seven primary sources referred to as Hungaria, Phocaea, ! $_6$, 3:1, 5:2, 2:1, and JFC. The first two source regions are located near the inner edge of the main belt and are related to the Hungaria and Phocaea dynamical families, associations of asteroids that are separated from the remainder of the belt due to dynamical (gravitational) interactions with Jupiter and Saturn. The last source, the Jupiter family comets, is particularly water-rich as it contains objects that have migrated into the inner solar system from beyond the orbit of Neptune where temperatures have never been warm enough for water sublimation. Finally, the other four sources are denoted by the primary dynamical resonance that drove them into NEO space. The ! $_6$ region is a secular resonance due to the long term combined effects of Jupiter and Saturn's gravitational influence while the other three are mean motion resonances with Jupiter. For example, asteroids in the 3:1 resonance make three revolutions around the Sun in the same time that Jupiter makes one revolution.

Asteroids have a broad range of mineralogies and water content, but for the purpose of this study we restrict the analysis to three principal taxonomic classes that dominate the main belt and Jupiter family comet (JFC) NEO sources — the S, C and D classes. We will show later that the low ΔV NEO population is dominated by the water-poor S class asteroids while the water rich D

class asteroids are extremely rare, comprising only about 0.2% of the population. The most promising population for ISRU of NEO water resources are therefore the C class asteroids that are thought to correspond to meteorite classes that have about 5% to 15% water content by weight. Table 2-3 provides the relative fraction from each class as a function of source derived from the literature (see DeMeo and Carry, 2013). Note that fractional percentages for the JFC source is not provided in the table as this data is not yet in the literature.

Granvik et al. (2015) modeled the number density of NEOs as

$$n_k(a, e, i, H) = n_k(H)\ R_k(a, e, i) \tag{29}$$

where *(a,e,i)* represent the NEOs' heliocentric semi-major axis, eccentricity, and inclination respectively, H is their absolute magnitude in the range $15 < H < 25$, k represents the NEO source region, $n_k(H)$ is the number density of NEOs from source k, and $R_k(a,e,i)$ is the normalized 'residence time' distribution of NEOs from each source, essentially the probability of an NEO of absolute magnitude H having orbital elements *(a,e,i)*. Thus, the number of NEOs within a range *da, de, di,* and *dH* of *(a,e,i,H)* that came from source k is

$$N\ (a, e, i, H; \mathrm{d}a, \mathrm{d}e, \mathrm{d}i, \mathrm{d}H) = n\ (a, e, i, H)\ \mathrm{d}a\ \mathrm{d}e\ \mathrm{d}i\ \mathrm{d}H \tag{30}$$

The fraction of NEOs from each source varies as a function of *(a,e,i,H)*:

$$f_k(a, e, i, H) = \frac{n_k(a, e, i, H)}{\sum_k n_k(a, e, i, H)} \tag{31}$$

The fraction of asteroids of class c from source k is denoted as f_{ck} where $\sum_c f_{ck} = 1 \forall k$ (see Table 2-3).

ISRU requires that the asteroid be large enough to have a high probability of containing enough water to propel the next stage of the process, yet small enough that it can be processed by a flight system of reasonable size. For the purpose of this study, these two requirements limit consideration to NEOs in the diameter range of four to ten meters. The diameter and absolute magnitude of an asteroid of class c are related (Fowler and Chillemi 1992) by the albedo, A_c, such that

$$\frac{d(H, A_c)}{\text{meters}} = \frac{1.329 \times 10^6}{\sqrt{A_c}} 10^{-H/5}. \tag{32}$$

Table 2-4: Asteroid taxonomic class, bulk density, probable meteorite association, meteorite density, water weight percentage, macro-porosity, and albedo adopted in this work. Only S, C, and D classes were considered in Phase I. In Phase II we will determine whether other water bearing classes of asteroids justify consideration.

Tholen Taxonomic class (c)	SMASSII Taxonomic class (c)	Bulk density[a] $(\mathrm{g\,cm^{-3}})$ $[\rho_{Mc}]$	Associated Meteorite	Meteorite density $(\mathrm{g\,cm^{-3}})$ $[\rho_c]$	Water Weight[g] % $[f_{H_2O}, c]$	Bulk porosity[j] $[P_c]$	NEO Albedo[l] $[A_c]$
S	L	2.7 ± 0.7	CV3[b]	2.95 ± 0.26[h]	1	$.08 \pm 0.02$	0.26
C	Ch	1.4 ± 0.7	CI[b]	2.12 ± 0.26[h]	13-20	$.34 \pm 0.18$	0.13
			CM[d]	2.26 ± 0.02[g]		$.38 \pm 0.20$	
D	D	9.6 ± 0.2	Tagish Lake[e]	1.6[i]	13-20	undef.[k]	0.02
			CI[b]	2.26 ± 0.02[g]		undef.[k]	

Most asteroids have albedos in the range 0.03 <A_c< 0.20 so that our limited diameter range corresponds to absolute magnitudes in the range 27.4 <H< 30.4; much smaller and fainter than the applicable range of the Granvik et al. (2015) NEO model.

We treat the asteroids as spherical with a class-dependent macro-porosity P_c (Table 2-4) so that the mass of water available in NEOs within *(da,de,di,dH)* of *(a,e,i,H)* is

$$m_{H_20}(a, e, i, H; \mathrm{d}a, \mathrm{d}e, \mathrm{d}i, \mathrm{d}H) \tag{33}$$

$$= \frac{\pi}{6} \sum_k \sum_c f_{ck}\, \rho_c\, (1 - P_c)\, f_c^{H_2O}\, d(H, A_c)^3\, n_k(a, e, i, H)\, \mathrm{d}a\, \mathrm{d}e\, \mathrm{d}i\, \mathrm{d}H \tag{34}$$

where ρ_c is the class-dependent microscopic density (Table 2-4).

Three recent publications show good agreement on the NEO Size Frequency Distribution (SFD), which in general is given as a power law over the entire size range down to the few meter scale

[a] From Table 3, Carry (2012) but given here with reduced precision; ρ50 for S and C types, ρ∞ for D type.
[b] Trigo-Rodrıguez et al. (2014)
[d] Cloutis et al. (2011), Cloutis et al. (2011)
[e] Hiroi et al. (2001)
[g] Mason (1963)
[h] Britt and Consolmagno (2003)
[i] Grady et al. (2002)
[j] Pc =1−ρMc/ρc
[k] Undefined since the reported asteroid density is up to 6× higher than the constituent meteorite!
[l] Thomas et al. (2011)

(see: Lilly 2016, Harris 2015, Brown 2014). We use the three SFDs to characterize the systematic uncertainty in our assessment of water ISRU in NEOs.

A more difficult consideration is to account for the changing fraction of objects from each source, and therefore from different taxonomic classes, as a function of asteroid size. Granvik et al. (2015) provides the only debiased estimate of the fraction of material from each source region for $H < 25$ but this is significantly larger than the objects we consider suitable for ISRU. We will first assume that the source/class fraction in the diameter range 4 m < d < 10 m is identical to the last 'measured' fraction by Granvik et al. (2015) for the smallest objects in their study with H_{max} = 24.875. i.e. in the 4 m < d < 10 m range the fraction of material from source k with (a, e, i) is:

$$f_k(a, e, i, H_{max}) = \frac{n_k(a, e, i, H_{max})}{\sum_k n_k(a, e, i, H_{max})}. \tag{35}$$

So the cumulative number density of objects with (a, e, i) from source k for $H > 25$ is

$$n_k^{cum}(a, e, i, \leq H) = f_k^A(a, e, i, H_{max}) \left[\sum_j \int^{25} n_j(a, e, i, h)\, \mathrm{d}h \right] N(H) \tag{36}$$

where the term in square brackets is the number density of objects at (a, e, i) with $H \leq 25$ from all sources. The mass of water available as a function of (a, e, i, H), $g(a, e, i, H)$, is then

$$m_{H_20}(g^*) = \int_a \int_e \int_i \int_H m_{H_20}(a, e, i, H)\, \delta\Big[g^* - g(a, e, i, H)\Big]\, \mathrm{d}a\, \mathrm{d}e\, \mathrm{d}i\, \mathrm{d}H \tag{37}$$

where we have introduced the Dirac delta function, δ.

In particular, the mass of water as a function of the Δv is:

$$m_{H_20}(\Delta v^*) = \int_a \int_e \int_i \int_H m_{H_20}(a, e, i, H)\, \delta\Big[\Delta v^* - \Delta v(a, e, i, H)\Big]\, \mathrm{d}a\, \mathrm{d}e\, \mathrm{d}i\, \mathrm{d}H \tag{38}$$

and the mass of water available as a function of ΔV in objects with diameters in the range $[d_{min}, d_{max}]$ is

$$\begin{aligned} & m_{H_20}(\Delta v^*; d_{min}, d_{max}) \\ = & \int_a \int_e \int_i \int_H m_{H_20}(a, e, i, H)\, \delta\Big[\Delta v^* - \Delta v(a, e, i, H)\Big]\, B[d(H, A_c); d_{min}, d_{max}]\, \mathrm{d}a\, \mathrm{d}e\, \mathrm{d}i\, \mathrm{d}H \end{aligned} \tag{39}$$

and we have introduced the boxcar function with the property that $B(x;\ x_{min},\ x_{max}) = 1$ if $x_{min} \leq x \leq x_{max}$ and $B = 0$ otherwise. Note that diameter is dependent on the absolute magnitude and the albedo (A_c) but class dependence is implicit in $m_{H20}(a, e, i, H)$ from eq. 34.

Results and Discussion: Keeping in mind that this ongoing and still preliminary work is intended primarily to show that we can integrate the Granvik model with a mission design model in a computationally tractable way and that the method we used for convenience is by design highly conservative, our work (Figure 2-9) suggests that there are about 1,000 NEOs that can be

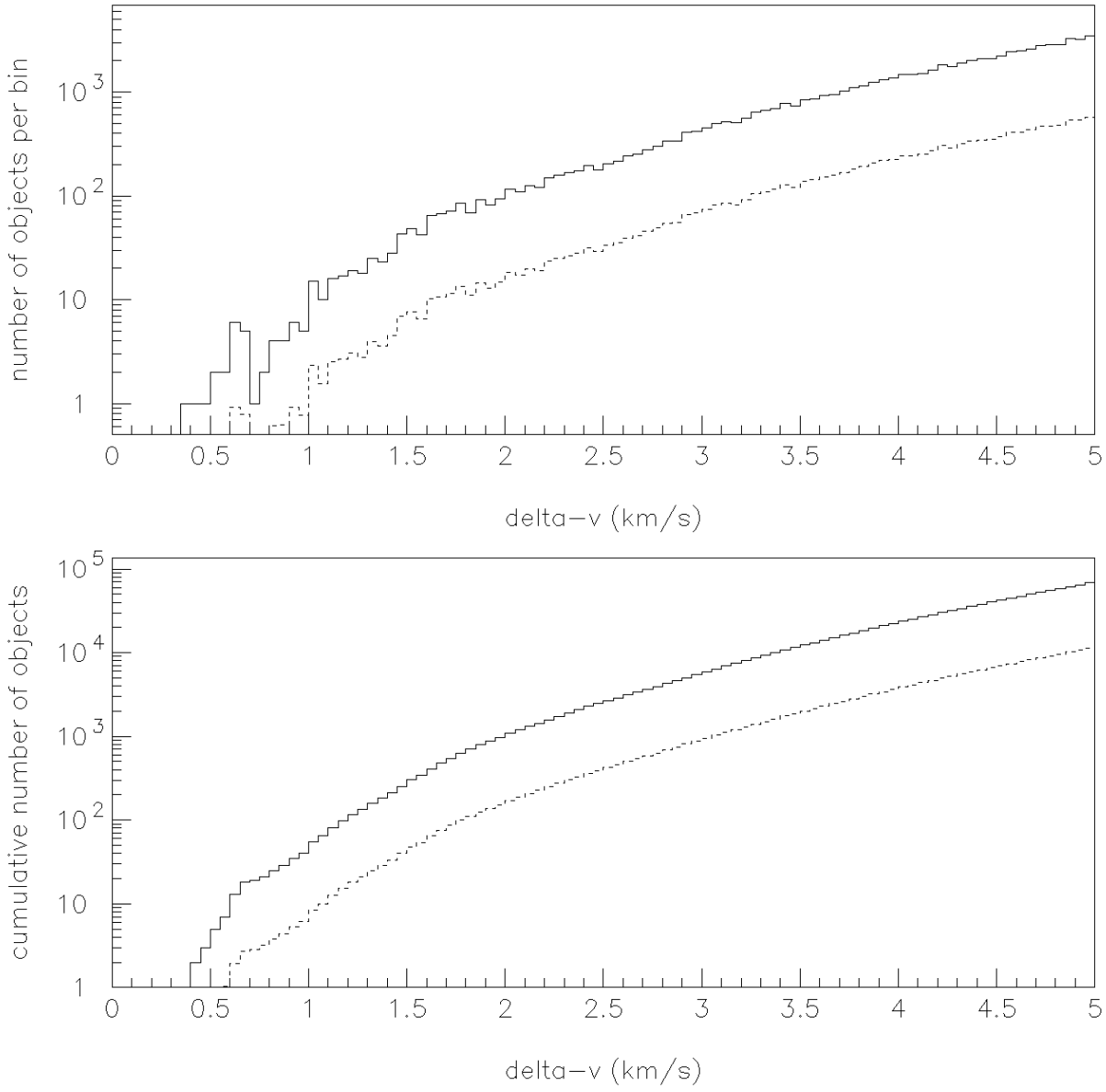

Figure 2-9: (top) Incremental number of NEOs with D > 4 m and total ΔV < 5 km/s per 0.05 km/s bin. The solid line represents all objects while the dashed line represents the distribution for water-bearing C class asteroids. (bottom) Cumulative number of NEOs with D > 4 m and total ΔV < 5km/s as a function of total return trip ΔV. Note that there are about 1,000 objects with total $\Delta V \leq$ 2 km/s in this conservative model.

brought to Earth with $\Delta V \leq 2$ km/s. In the mission design section of this report we show that 2 km/s return trip ΔV can be cost effective for supplying propellant to cis-lunar space for NASA missions of human exploration or commercial activities. It should be emphasized that the estimate of 1,000 commercially viable NEOs should be considered a lower limit to the number given that our ΔV calculation was designed to be conservative. Our model also suggests that the most accessible objects most likely have return trip ΔVs of about 0.5 km/s, which is consistent with the results of the JPL Option "A" ARM missions studies. Although it is speculative at this point, a

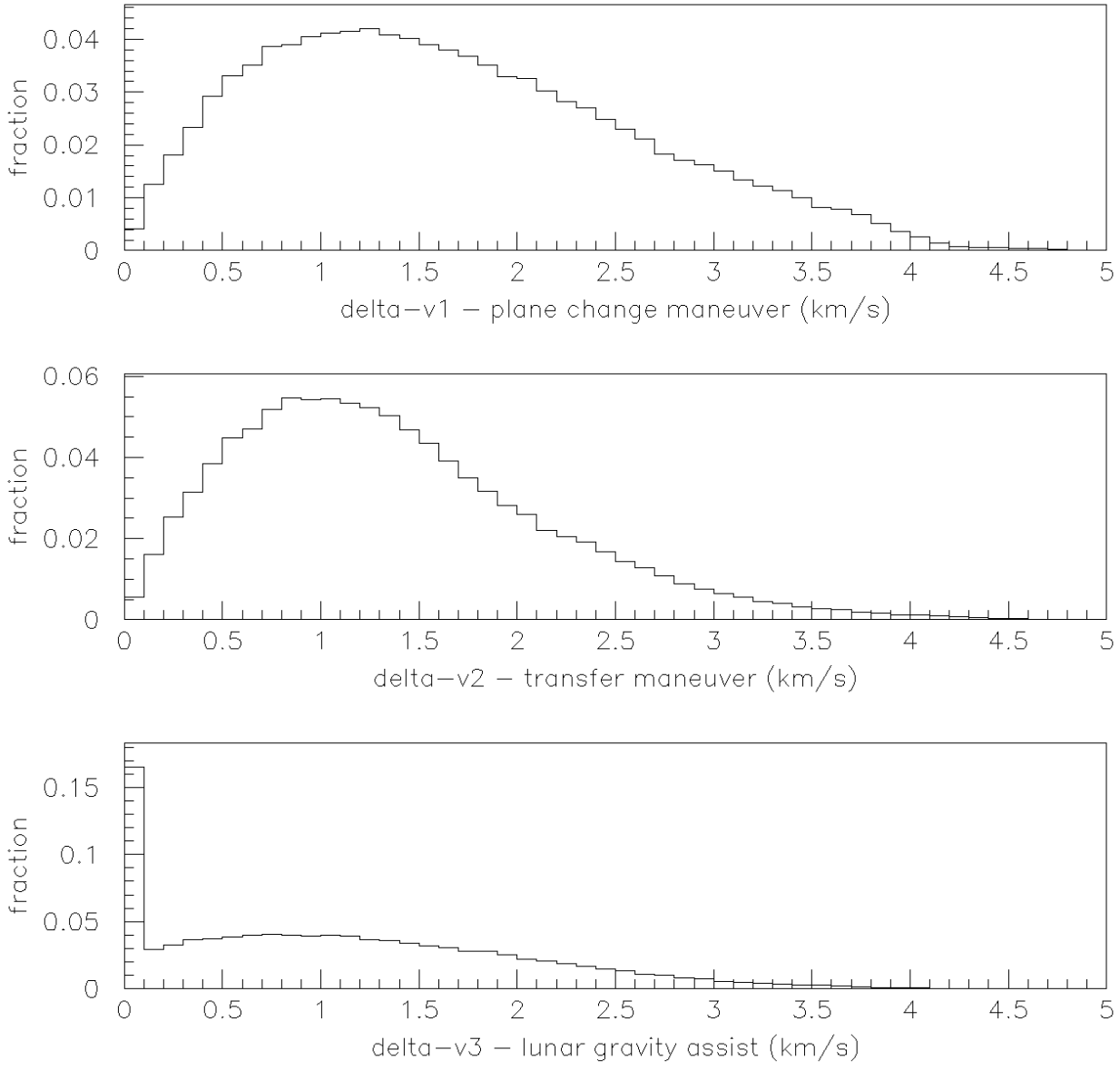

Figure 2-10: Incremental fraction of NEOs with total return trip $\Delta V \leq 5$ km/s per 0.1 km/s bin as a function of (top) ΔV_{plane}, (middle) $\Delta V_{transfer}$, and (bottom) ΔV_{LGA}.

semiempirical analysis of our results to date suggest that a more optimized mission design approach will likely show three to four thousand commercially accessible asteroids and several hundred that are water rich. Firm confirmation of these estimates is very important and points out the importance of our proposed Phase II effort.

The results of our Phase I asteroid resource availability modeling effort are presented graphically in Figures 2-9 though 2-15 which follow. Figure 2-10 shows that the allocation of the total ΔV to each of the plane change, transfer orbit, and lunar gravity assist maneuvers is roughly comparable

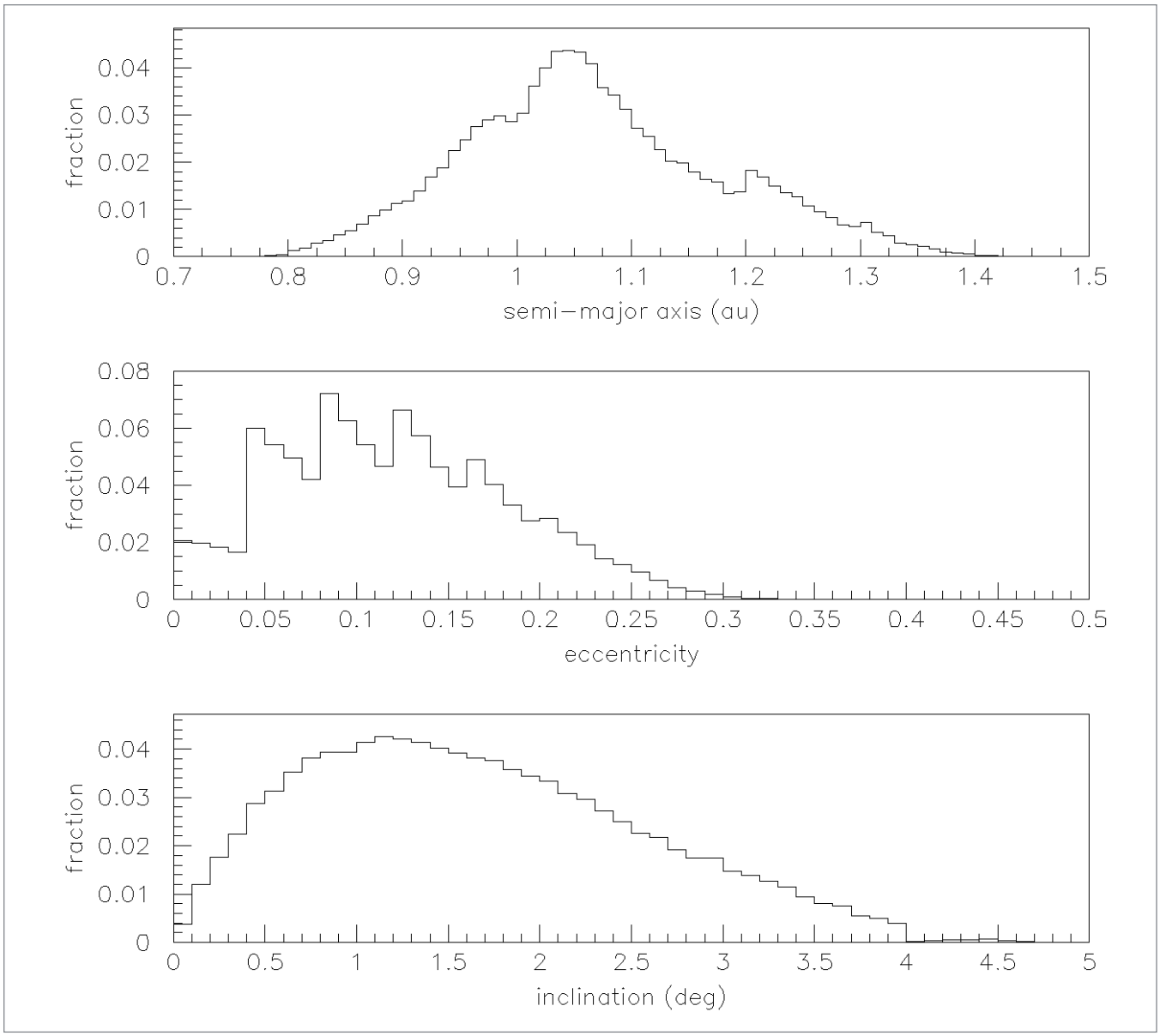

Figure 2-11: Incremental fractional (top) semi-major axis, (middle) eccentricity, and (bottom) inclination distributions of NEOs with a total $\Delta V \leq 5$ km/s. The residual binning effects in the semi-major axis and eccentricity panels are artifacts of binning in the Granvik 2016 NEO model that will be fixed in Phase II along with an optimized mission design and broader ranges of targets.

Figure 2-12: Relative distribution of orbital semi-major axis and eccentricity for NEOs with a total $\Delta V \leq 5$ km/s. The size of each box is proportional to the number of objects in the (a, e) bin. The solid curve on the left ending at a = 1.0 au represents objects with aphelion of Q = 1.0 au (roughly at Earth's orbit) while the solid curve on the right beginning at a = 1.0 au represents objects with perihelion of q = 1.0 au (roughly at Earth's orbit). The dashed curve beginning at a = 1.3 au represents the NEO limit with q = 1.3 au and the fact that some objects have q > 1.3 au suggests that a few more objects could be available with $\Delta V \leq 5$ km/s outside of the arbitrarily defined NEO orbital parameter space (this issue will be address in Phase 2).

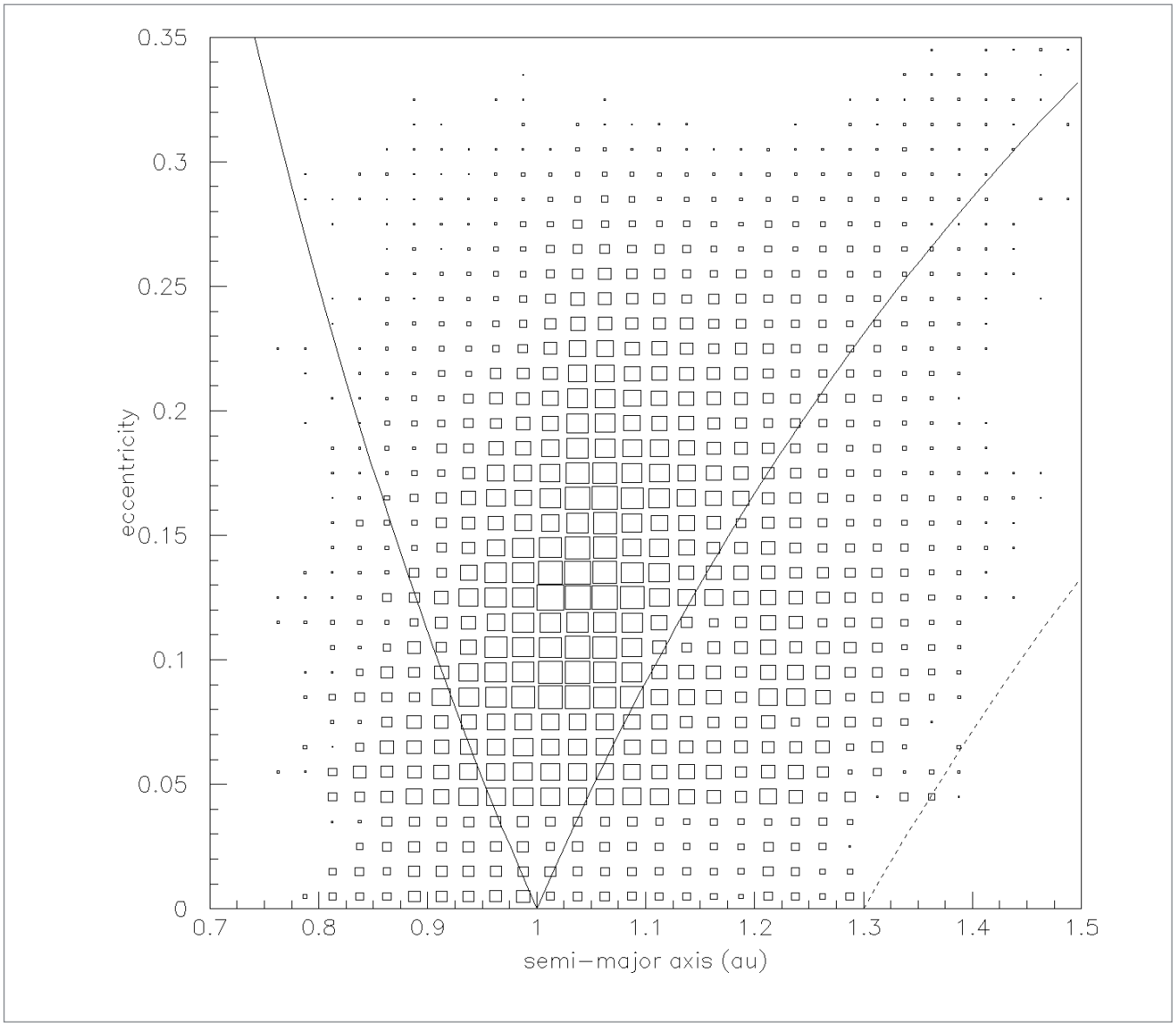

with poisson-like distributions with means of 1.7 ± 0.9 (rms) km/s, 1.4 ± 0.8 (rms) km/s, and 1.1 ± 0.9 (rms) km/s respectively for the three maneuvers. The LGA maneuver has a spike at 0.0 due to its definition (eq. 24). Not including the zero values yields a mean of 1.3 ± 0.8 (rms) km/s for this maneuver. Total ΔV is slightly dominated by the plane change maneuver.

Figure 2-13: Fractional incremental distribution of transfer times for NEOs with a total $\Delta V \leq 5$ km/s. The bi-modal distribution is due to objects with $a < 1$ au and $a > 1$ au, for the left and right peaks respectively. The minimum between the peaks corresponds to about half a year showing the effect of a relative paucity of targets near $a = 1$ au.

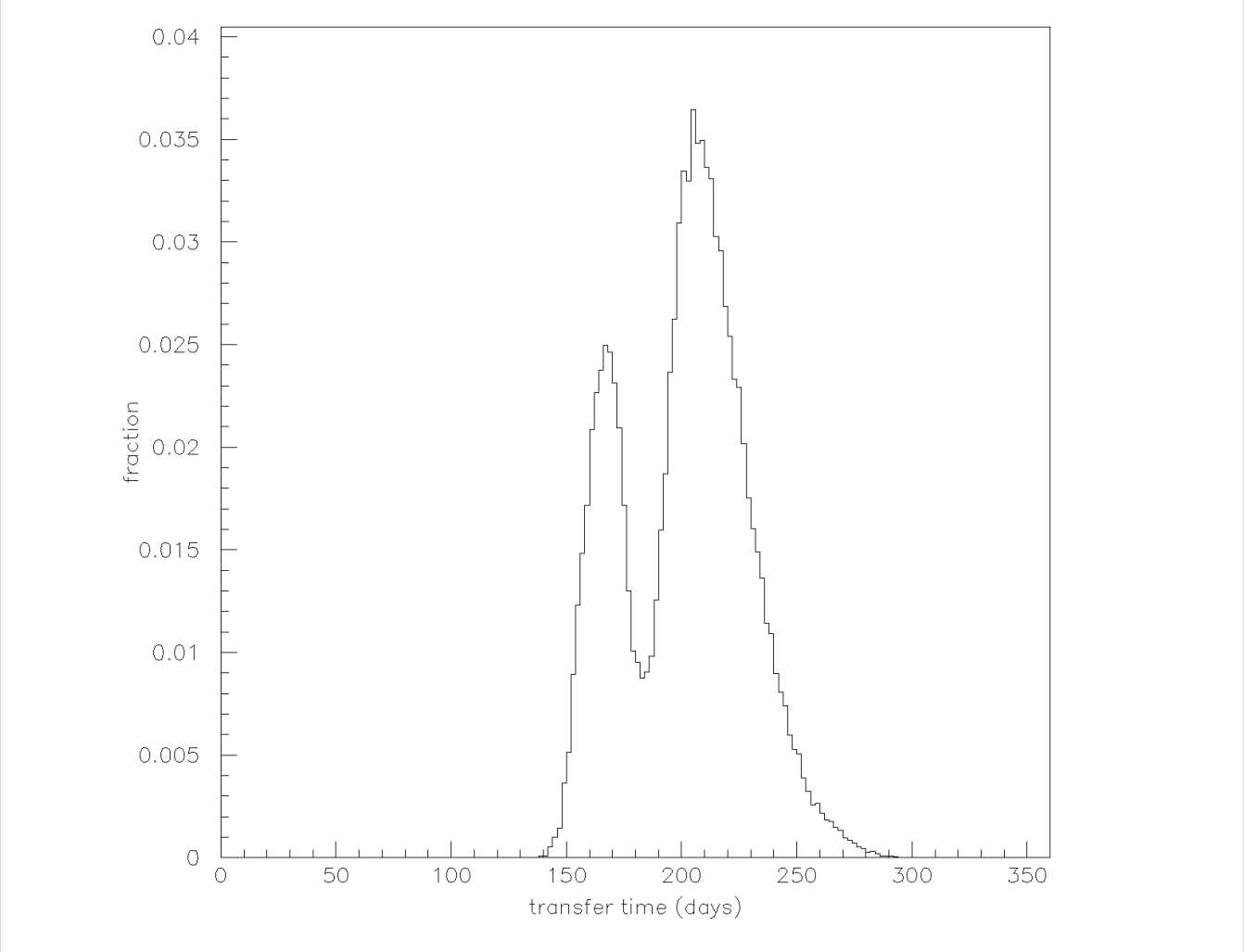

Figure 2-11 shows that the orbit element distribution of ISRU accessible objects with $\Delta V \leq 5$ km/s is restricted to inclinations of 5° but encompasses a wide range of semi-major axis and eccentricities in NEO orbital element phase space. The inclination restriction is about half the theoretical limit for objects with semi-major axes and about equal to Earth's according to eq. 4 since objects with a ≈ 1 au have orbital speeds of about 30 km/s. i.e. an NEO on an Earth-like orbit could have an inclination of up to about 10° and still have $\Delta V \leq 5$ km/s but in practice we find the limit to be about 5°. Note that there are some residual binning effects evident in the semi-major axis and eccentricity distributions (Figure 2-11) which are numerical artifacts resulting from our application of the Granvik 2016 model. The generated (and detected) distribution of both orbital parameters should not have this behavior and we will address the issue in Phase II. We have already fixed a similar issue with the inclination distribution because not doing so allowed for

Figure 2-14: Fractional incremental distribution of the time spent on the ecliptic orbit after the plane change maneuver and before the transfer maneuver for NEOs with a total $\Delta V \leq$ 5km/s. The time can be up to ten years because our simple model requires that the NEO and Earth be directly opposite each other relative to the Sun at the transfer maneuver time. Given that we are working with a synthetic population of targets, this parameter is an approximate surrogate for the waiting period for any given target prior to launching a minimum ΔV mission. The peak near ten years is a result of the fact that low ΔV targets are in highly Earth-like orbits with large synodic periods relative to Earth.

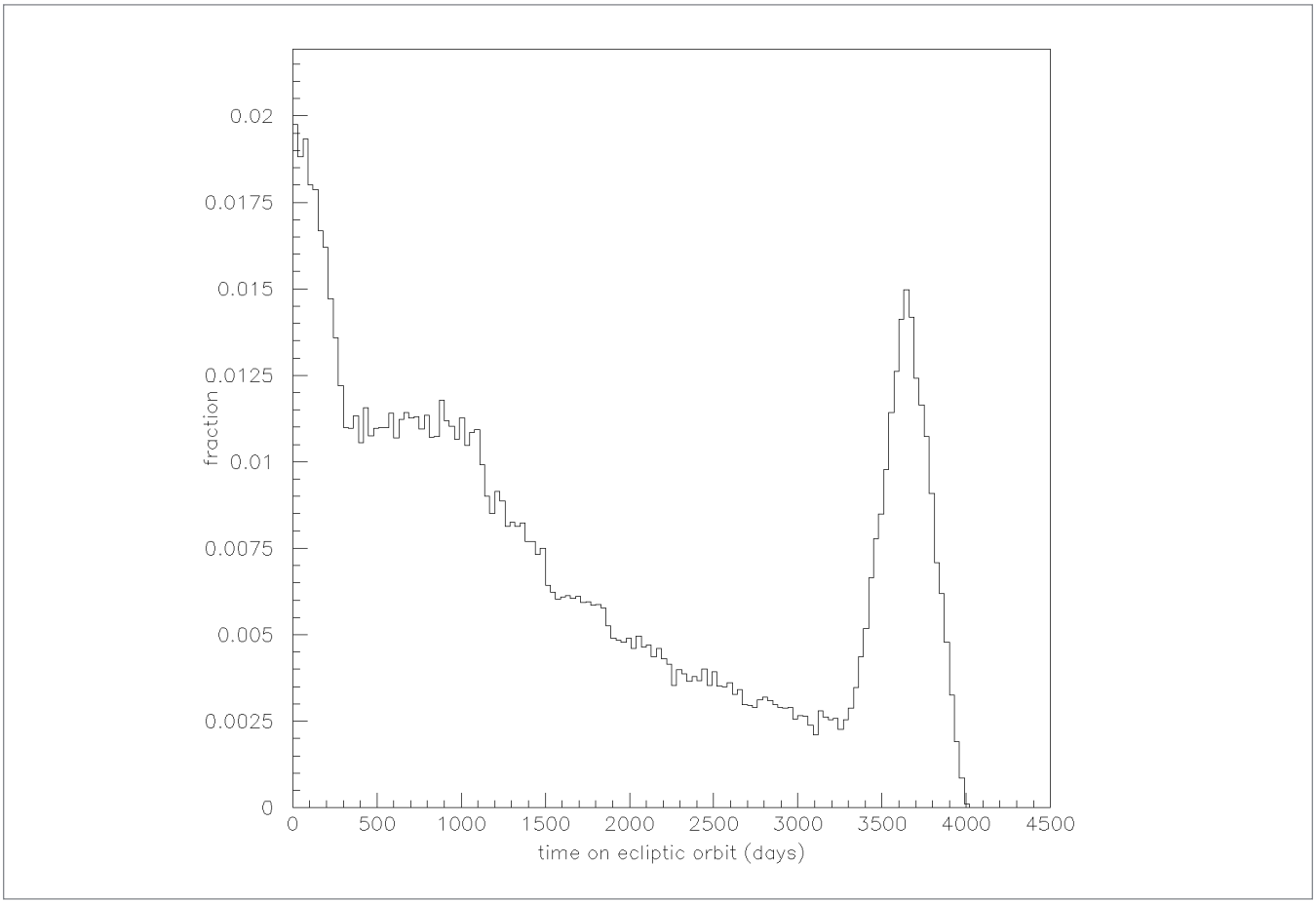

the creation of a non-physical number of low inclination objects to pass the $\Delta V \leq 5$ km/s requirement and created an unphysical inclination distribution. The requirement that $\Delta V \leq 5$ km/s preferentially selects objects out of the NEO population with a ≈ 1 au and modest eccentricities (Figure 2-12) with the typical low ΔV NEO having a ≈ 1 au, e ≈ 0.13, and i ≈ 1.2 deg.

We define transfer time as the time spent on the transfer orbit between the transfer maneuver and Earth intercept. This period is typically about half a year because the typical NEO has an Earth-like semi-major axis of 1au as shown in Figure 2-13. NEOs with semi-major axis interior to Earth typically require less than a half year while those exterior to Earth require more. Since there is a larger number of objects exterior to Earth the mean transfer time is 201 ± 27 (rms) days. Another important time period is the waiting period between the plane change ΔV and the transfer ΔV. We have calculated mission performance for this parameter and present it in Figure 2-14. The time

Figure 2-15: Incremental fractional distribution of the probability that NEOs with a total $\Delta V \leq 5$ km/s that derive from the S, C, D or 'other' classes ('other' classes refer to any class other than S, C, or D). In Phase II we will investigate the water content of "other" classes and will investigate the availability of valuable resources other than water.

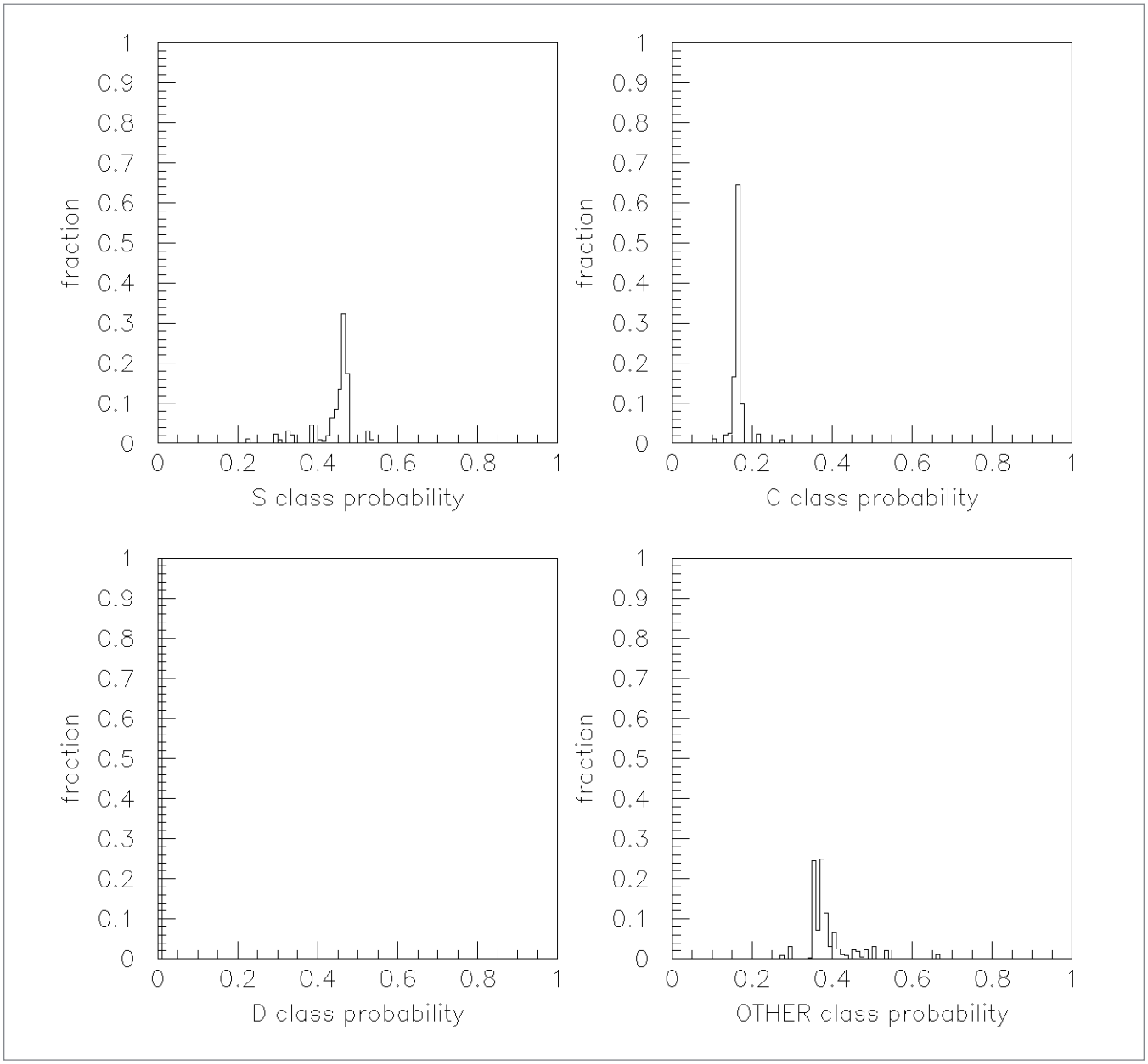

can be up to ten years because our simple model requires that the NEO and Earth be directly opposite each other relative to the Sun at the transfer maneuver time. Given that we are working with a synthetic population of targets, this parameter is an approximate surrogate for the waiting period for any given target prior to launching a minimum ΔV mission. The peak near ten years is a result of the fact that low ΔV targets are in highly Earth-like orbits with large synodic periods relative to Earth.

Our model also allows us to determine the fraction of objects that are water-bearing (Figure 2-15). We find that about 20% of the objects are of the water-bearing C class and essentially none of them are the water-rich D class of objects. This is because most of the low ΔV objects escape from the $\nu 6$ main belt source region that crosses through the inner region of the belt where S class asteroids dominate. In Phase II we will investigate the uncertainty in the fraction of objects in these types of orbits by performing exactly the same calculations using different H bins from the Granvik et al. (2015) NEO model. Since about 20% of the low ΔV objects are C class and these objects inhabit a narrow range of orbit elements, it is no surprise that the shape of the ΔV distribution for the C class asteroids mirrors the entire size distribution. We conservatively estimate that there are about 200 water-bearing asteroids of diameter greater than 4 m with $\Delta V \leq 2$ km/s available in the NEO population but will refine this estimate in Phase II. Within the uncertainty of our model and the inherent conservatism in our simplified approach, the number of highly accessible water rich asteroids could be substantially higher.

Next Steps (Phase II Population Accessibility Analysis): The purpose of our Phase I effort in this area was to demonstrate that a mission design model can be integrated with the Granvik model and taxonomic estimates of resource content to produce an assessment of asteroid resource availability with enough computational efficiency to allow modeling the millions of synthetic targets needed to confidently asses the statistics of the relatively small population of the few most accessible likely targets. We have been entirely successful in this effort, but our primary effort was focussed on how to integrate the Granvik model with a mission model, not in finding optimal results. Hence, our preliminary results over estimate both ΔV and trip time. Other limitations in our work to date in this area are the limited range of asteroid sizes considered (4 meters to 10 meters in diameter), the limit of addressing only water as a resource for extraction, and the limit of addressing only the resources available in three taxonomic types. In addition, we did not address the outbound trip and/or launch vehicle requirements. A final important limitation in this early Phase I work is the semi-empirical approach we took to calculating the Earth arrival ΔV in the presence of a lunar gravitational assist capture. Now that we have proven our method and its basic technological feasibility, addressing these issues is a matter of time and effort. In our Phase II work we will apply a higher fidelity, more optimized mission model, a larger range of target asteroid sizes, a larger range of taxonomic types, and a model based approach to calculating Earth arrival ΔV with lunar gravitational assist.

Given that the inherent uncertainty in the asteroid population is on the close order of a factor of two, we still will not be seeking results of extreme high precision, so the method of patched conics will continue to be accurate enough for our purposes and we will capitalize on this fact to

use analytical methods that are fast enough to allow a full exploration of millions of test objects with reasonable computational cost. Even for modeling the cis-lunar phase of the mission plan, the method of patched conics will be sufficient because although patched conics are known to give poor results for trip time in cis-lunar space, they yield ΔV values within a few percent of high fidelity, computationally intensive multibody optimization, and the duration of the cis-lunar phase is typically at most a few months and is therefore a small fraction of the overall trip time.

The first and most important improvement in our Phase II mission model will be to substitute a broken plane type trajectory maneuver for our grossly suboptimal two deep space burn strategy. Figure 2-16 shows the mission concept we are planing to employ. Note in Figure 2-16 that to avoid confusion with the equations and methods of Phase I we have changed notation. As before we define three propulsive maneuvers but in this case we refer to them as ΔV_1, ΔV_2, and ΔV_3. ΔV_1 changes energy of orbit as needed to intercept Earth and "part" of the inclination change. ΔV_2 is the broken plane maneuver which provides the rest of the inclination change at line of nodes of return trajectory (halfway to Earth). ΔV_3 is as needed for Earth capture from heliocentric space using a LGA.

Note that from Figure 2-11 we know that the most interesting low ΔV targets are in nearly circular orbits with a mode at an eccentricity of just 0.13. Hence, we think we will be able to pick the time of departure from the asteroid's natural orbit based solely on orbit phasing considerations without paying a significant ΔV penalty. In other words, we think it likely that because the asteroids we are interested in are in such nearly circular orbits we can approximate an optimal return as a Holman transfer without having to resort to computationally expensive iterative application of Lambert's problem. One of the first things we will do in Phase II is test this hypothesis on a variety of low ΔV targets and compare a purely orbit phasing based return strategy to an optimal return. If the error is small, as we suspect, we will forego the Lambert optimization problem.

In the terrestrial fossil fuel and mineral industries the term *proven reserves* means the quantity of sources estimated with reasonable certainty, from the analysis of geologic and engineering data, to be recoverable from known reservoirs with the specified equipment and under specified operating conditions. Other terms of art related to proven reserves are in-place reserves, technically recoverable reserves, and economically recoverable reserves. The mining and fossil fuel industries have established technologies for the statistical assessment of each of the subsets of total reserves and they are calculated using standard methods with a combination of scientific, engineering, and economic tools. It is important to emphasize that the work we are doing on modeling resource accessibility is not just systems engineering or mission analysis: it is part of the

Figure 2-16: Planned Broken Plane Mission Concept for NIAC Phase II Mission Analysis. Top: As Viewed From Above the Plane of the Ecliptic. Bottom: As Viewed From an Oblique Angle.

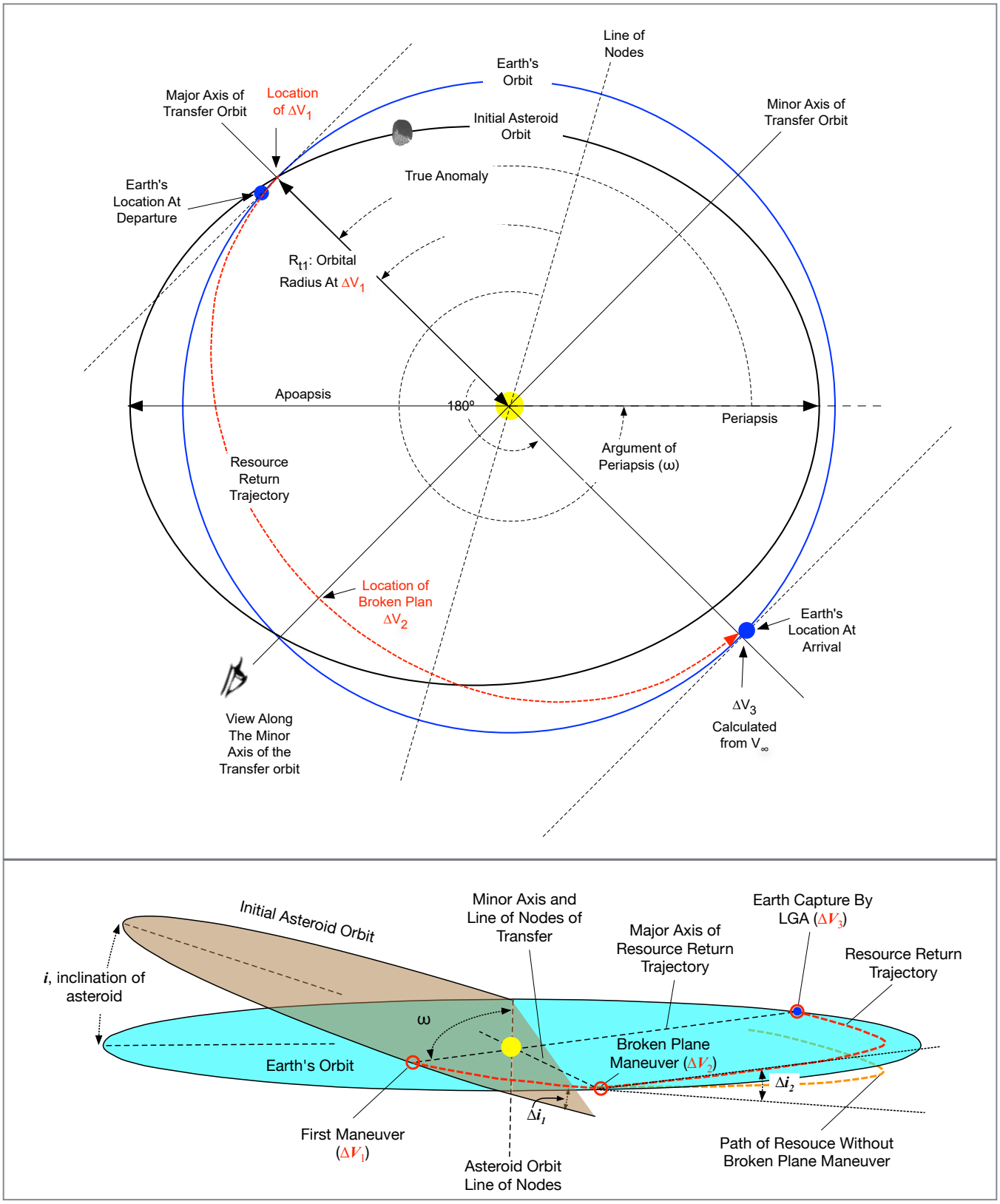

technology development that is needed to enable cost effective asteroid ISRU. Just as the terrestrial mining and fossil fuel industries have developed the technology for estimating the size of reserves in a given land mass, as we move toward asteroid resource exploitation in space, we are developing the technology for estimating various parameters associated with the economic viability of different populations of resources.

2.3 Optical System Design and Analysis

Overview of Optical Design and Analysis: A fundamental aspect of the Apis™ architecture is the use of raw solar thermal power in place of processed electric power whenever possible. This is motivated by the goal of reducing system mass and cost to the absolute minimum while maximizing the productive value of the system in terms of the quantity of resources extracted from target asteroids and in terms of the mass of payload the transportation network can deliver for given missions over a given time. To understand why we minimize the use of electric power, consider that a 20 kW_e state of the art flexible solar array would have a development cost of about $50M, a recurring cost of about $10M, and mass in the hundreds of kilograms. For the same hundreds of kilograms of mass on orbit, we project that a thin film inflatable reflector could produce up to a megawatt of raw thermal power with a recurring cost in the hundreds of thousands of dollars. Because of the current low technology readiness (TRL 3-5) of thin film inflatable solar reflectors it might cost tens of millions of dollars to flight qualify the first megawatt class long life reflector, but after that, nonrecurring development costs should be on the order of a few million dollars each.

The two primary applications of highly concentrated solar thermal power in the Apis™ architecture are for solar thermal propulsion and Optical Mining™. Chief among the design goals of our optical system are:

- maximize the amount of solar thermal power available to mining and propulsion operations within a limited launch mass and stowage volume while maintaining flexible mission operations;
- maximize the power density at the focal point of the optical system for the propulsion system while allowing modulation of intensity on the mining side;
- minimize spacecraft attitude knowledge and control pointing requirements while allowing fabrication tolerance on the thin film structural components to be as lax as possible.

After considering several possible optical configurations for the Honey Bee Optical Mining vehicle to meet these goals, we selected the layout shown in Figure 2-17 for technology analysis and planning purposes. The point design is a dual Cassegrain configuration with two 15 m diameter

Figure 2-17: Honey Bee™ Optical Mining™ vehicle configuration sketch showing primary spacecraft elements and key features of optical train.

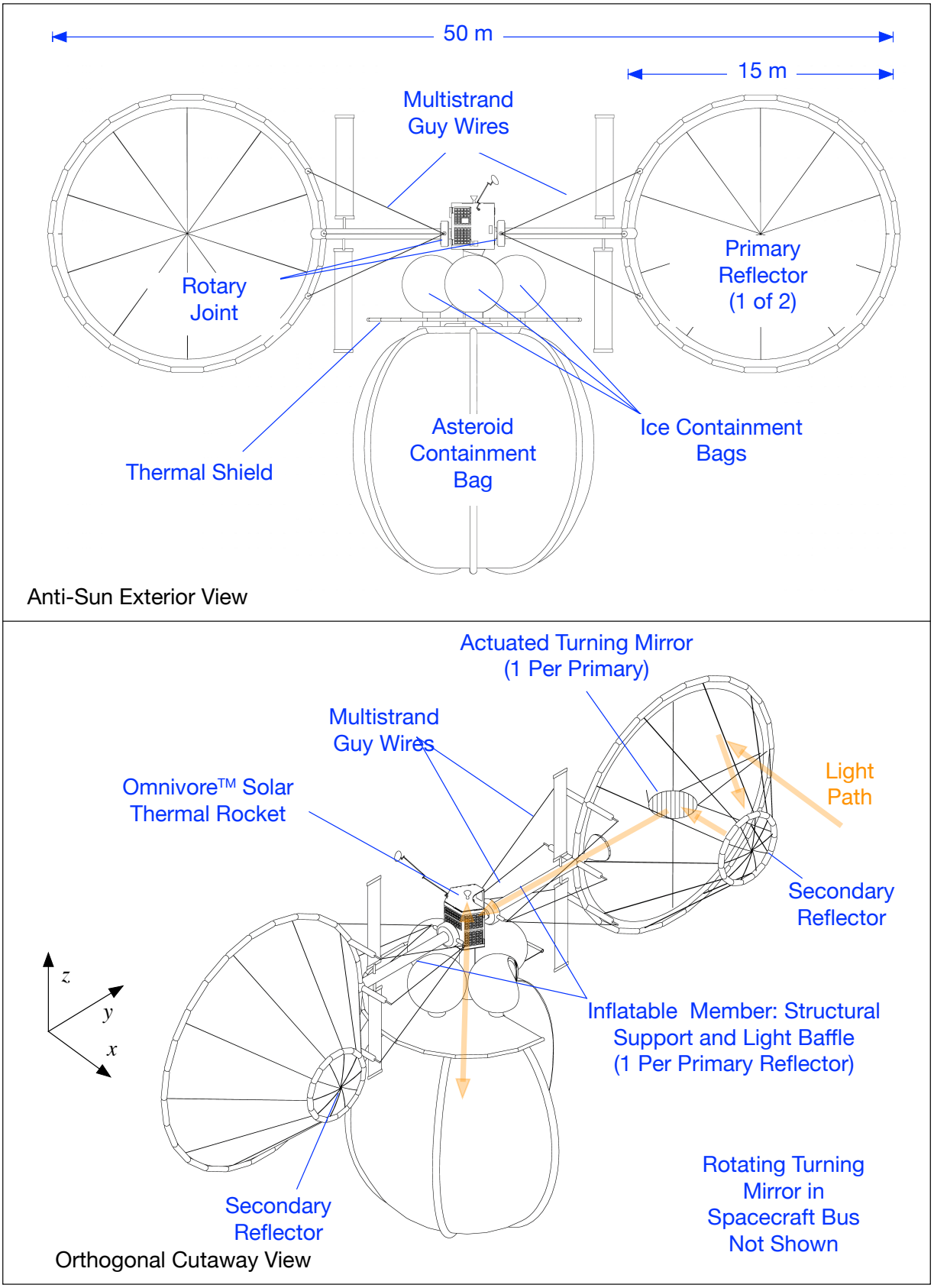

primary reflectors. Each primary feeds a convex secondary reflector which directs the solar radiation onto a curved actuated turning mirror which compensates for low frequency spacecraft pointing errors and directs the solar beam through the structural support and baffle tube.

There are two rotary optical assemblies on the vehicle, one for each primary reflector. Each comprises a primary reflector, a secondary reflector, two turning mirrors, a guy wire support system, and a rotary actuation joint. The joint allows the spacecraft to rotate around the structural support tube, which is aligned with the y-axis in the drawing, while the solar concentrators and arrays remain sun-pointed. Note that with the rotary joint allowing rotations around the y-axis and the spacecraft free to rotate around the x-axis, the thrust vector can be pointed in any direction while keeping the primary reflectors Sun pointed. Rotation around the z-axis is not permitted during mining or primary propulsive operations, but by allowing articulation of the four solar arrays shown around the z-axis, electric power can be maintained in virtually any orientation bearing in mind that the front (Sun pointed) canopies of the lenticular structures are transparent.

Not shown in the drawing are additional optical components internal to the spacecraft bus structure or hidden from view in the diagram by the asteroid containment bag. These internal optical components include:

- two rotatable turning mirrors in the spacecraft bus that allow light to be directed either "up" toward the Omnivore™ thruster or "down" toward the Optical Mining™ apparatus,
- four afocal, numerically optimized reflectors, two for propulsion and two for mining that are detailed below and are required to converge the beams,
- a telescoping structural tube that penetrates into the asteroid containment bag that allows the final focussing lens to be moved in and out in the bag to allow drilling, disruption, and excavation of the asteroid,
- two refracting Fresnel lenses, one for propulsion near the thruster, and one for mining inside the containment bag that provide high terminal beam convergence and brightness as needed to reach peak temperature at focus.

The telescoping tube inside the bag also includes a debris shield and gas handling system that permits counterflow gas near the lens to prevent lens contamination. As a note to the reader, the dual 15 m configuration shown in Figure 2-17 allows over 200 kW_s of solar thermal power to be delivered to the propulsion or mining apparatus. This will be over four times the highest electric power level being considered for the impressive NASA ARM mission which is based on a spacecraft several times more massive than the Honey Bee™ system. Apis™ spacecraft are designed to be compatible with medium class launch vehicles such as the Falcon 9 rather than heavy lift system like the SLS or Falcon Heavy. The relative mass reduction compared to a less capable electric propulsion vehicle is enabled through the use of inflatable structures and the

elimination of the need to carry many tons of electric propulsion propellant, instead capitalizing on ISRU and in space resources.

We have performed a rigorous quantitive optical design and analysis of the configuration shown in Figure 2-17 for the purpose of technology maturation. To do this we started with closed form analytic equations that can be used to model the concentration of sunlight from imperfect reflectors and lenses. Using these analytical methods we were able to create an optical layout of the system in multiple stages at increased levels of fidelity to obtain the basic layout. Then we modeled a simple Cassegrain optical train and introduced a parametrically variable distortion of the primary reflector and calculated the theoretical intensity at the focal spot with both analytical equations and with ray trace analysis using the Zemax optical design package. This validation step was critical as we found in reviewing past work that often the ray trace analysis is done incorrectly with an inadequate number of rays that leads to erroneous results. Following the Zemax analysis of a simple configuration, we developed a more complete model of the end-to-end optical train in Zemax and modeled the following effects:

- parametrically variable distortion of the primary reflector based on past experimental measurements of inflatable reflectors,
- transmissivity of the transparent front cavity,
- the reflectivity of the different optical surfaces,
- all of the secondary and turning mirrors,
- the effects of the sapphire Fresnel lens,
- the distortion effect caused by the elliptical turning mirror compensating for low frequency attitude control errors of the primary structure.

Closed Form Analysis: The theory of geometric optics provides simple closed form equations that allow the calculation of achievable solar concentration ratios as a function of the gross geometric proportions of the solar concentrator, the surface irregularities in the reflector, and the angular size of the Sun's disk. For a reflector with aperture diameter a, and focal length f, the rim angle ϕ can be defined as

$$\phi_r = \tan^{-1}\left[\frac{8\left(\frac{f}{a}\right)}{16\left(\frac{f}{a}\right)^2 - 1}\right] . \tag{40}$$

We characterize the surface quality of the reflector with the parameter δ, the dispersion angle under the assumption that surface irregularities give rise to a uniform dispersion between zero and δ. With these definitions in place we can calculate the maximum theoretical concentration ratio, $C_{\max}$, of a circular parabolic focusing solar concentrator onto a flat plate receiver using

$$C_{\max} = \frac{\sin^2 \phi_r \cos^2\left(\phi_r + 0.267 + \frac{\delta}{2}\right)}{4\sin^2\left(0.267 + \frac{\delta}{2}\right)} - 1 \quad . \tag{41}$$

Note in eq. 41 that 0.267 is a numerical parameter that accounts for the angular size of the solar disk in this case at the Earth's 1 au distance from the Sun. An incident beam of sunlight is a cone with an angular width of 0.534°, or a half-width of 0.267°. Using this equation we performed a simple parametric study of solar concentrator performance as a function of f-number, defined her ratio of the focal length of the reflector to the aperture of the reflector. The results are shown in Figure 2-18.

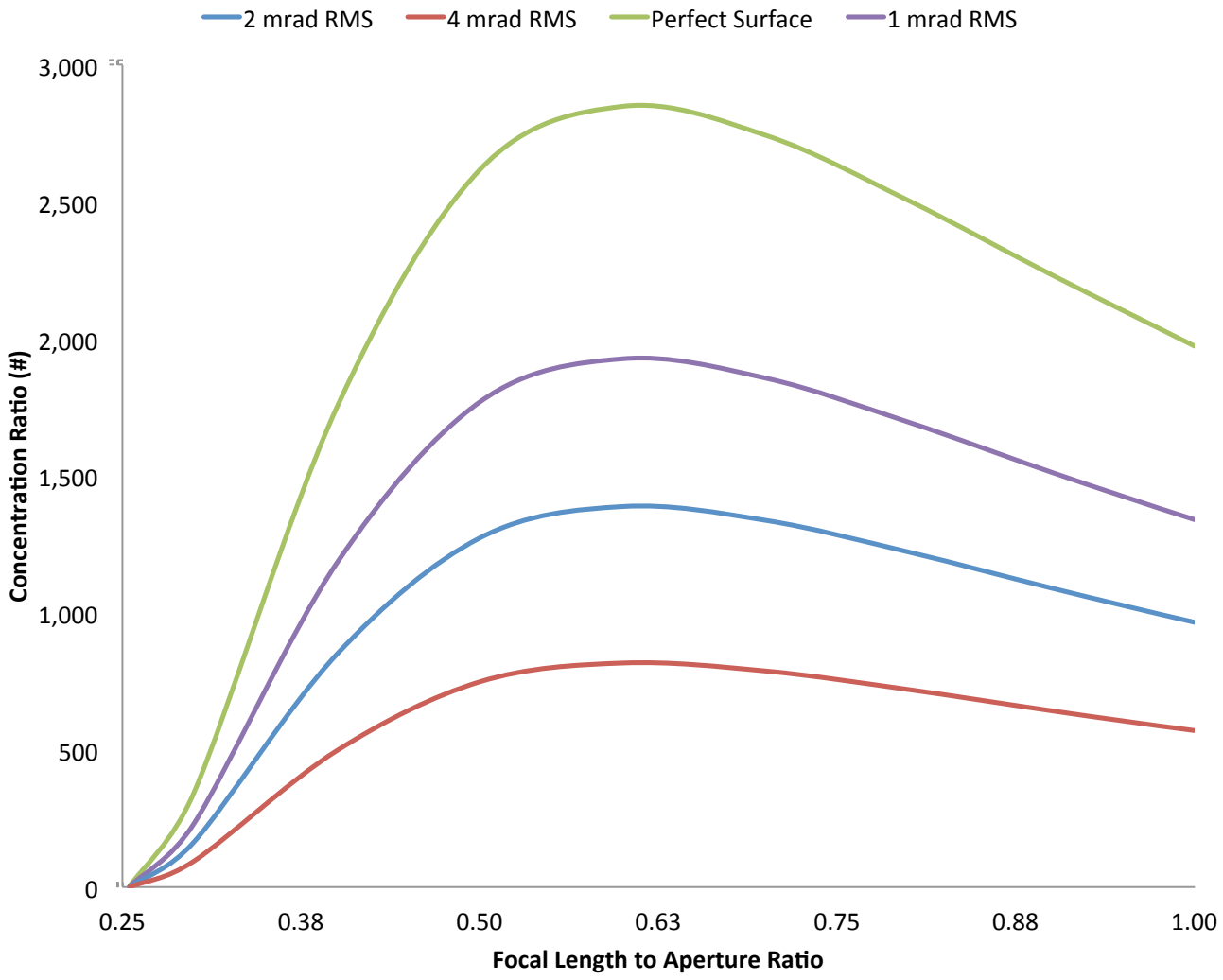

Figure 2-18: Parametric Study Of Solar Concentrator Performance Varying Surface Accuracy And F-Number

In Figure 2-18 we see that for flat plate receivers peak intensity is achieved at moderate f-number. This is because at very low f-number the reflector nearly wraps around the receiver and so much of the light hitting the receiver does so from very wide angles causing any dispersion due to finite solar disk size or reflector surface irregularities to be exaggerated. Likewise, at very large f-number the receiver is farther away from a given sized reflector so dispersion effects increase spot size directly. This later effect is closely related to the concept of *étendue* which places a theoretical upper limit on C_{max} of $C_{max} = 1/\sin^2\alpha$ where α is the total dispersion in the system. This shows that for a perfect optical system in which all dispersion is due to finite solar disk size of 0.53º, in free space, the highest theoretical concentration ratio achievable through geometric optics is approximately 46,800:1 which is the same as the ratio of the area of sphere with a radius of 1 au to the surface area of the Sun. At this concentration ratio the radiative equilibrium spot temperature would be 5,500 Kelvin, the same as the surface of the Sun. This is also the highest spot temperature that can be achieved without violating the second law of thermodynamics.

Note that the flat plate single reflector system of Figure 2-18 produces a C_{max} of 2,850:1 which drops to less than 2,000:1 with a realistic surface accuracy of 1 mrad RMS even without considering shadowing effects, finite reflectivity, and other losses. Our goal is to have a system with realistic loss factors with a concentration ratio well over 3,000. Such a single optical element design is problematic so we must consider more sophisticated concepts. However, to analyze such systems we will require a sophisticated computational tool.

Optical Analysis: The numerical analysis in this study started with the use the Zemax package to do ray trace modeling of the simple Cassegrain optical system depicted in Figure 2-19. Recalling that the solar radiation constant is 1,361 W/m^2, in this simulation the Sun was modeled as a uniformly bright circular disk subtending 9.16 mrad. We modeled several cases starting with ideal surfaces for both the primary and secondary and then modeled perturbed surface. We addressed 3 cases: 0.726, 3.275, and 3.381 mrad RMS. In one case we perturbed the secondary reflector

Parameter	Value
Primary Aperture Diameter	15 m
Primary Focal Length, f1	7.5 m
Primary to secondary separation	6 m
Secondary Aperture Diameter	3.3 m
Secondary Focal Length, f2	2 m

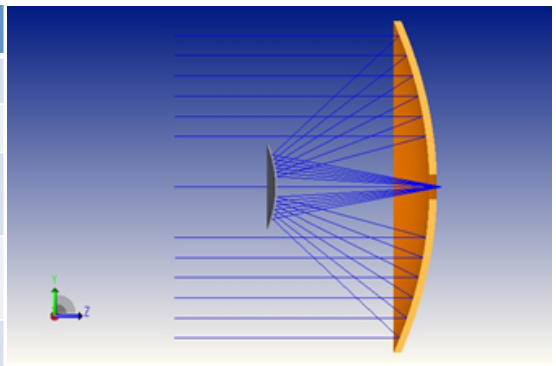

Figure 2-19: Simple Cassegrain Optical Configuration Modeled In Zemax

Figure 2-20: Form of Surface Perturbation Used In Modeling and Simulation

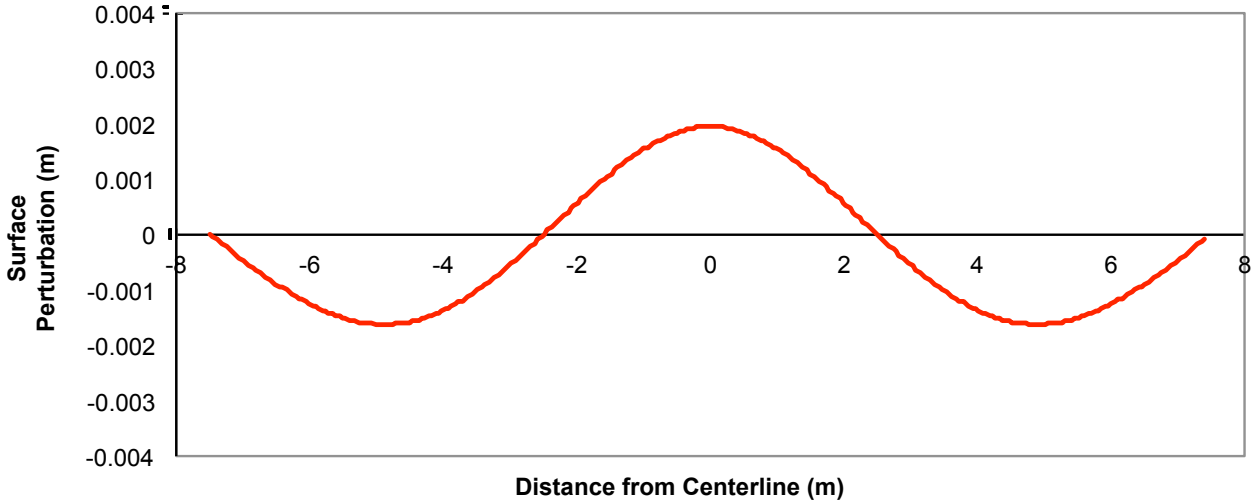

with a deflection of 1 mrad RMS slope error. The physical structure of the perturbations in the reflector surfaces were modeled after actual experimental measurements of inflatable reflectors performed by our partner L'Garde Incorporated of Tustin California. They report that the perturbations take the shape of a "W" or "M" as shown in Figure 2-20. The results of these calculations are shown in Figure 2-21. We checked these results against the closed form approach of eq. 41 by applying the rim angle of the secondary reflector in the formula and found excellent agreement, which gives us confidence in our approach. This calculation showed a peak ideal concentration ratio of 2,500:1 with a perfect reflector dropping to 2,000:1 when worst case surface perturbations were included, but not yet accounting for surface reflectivity effects. We also studied the effects of attitude control pointing error and found a barely detectable effect at 0.1° off Sun pointing, which is probably an achievable but aggressive ACS control requirement.

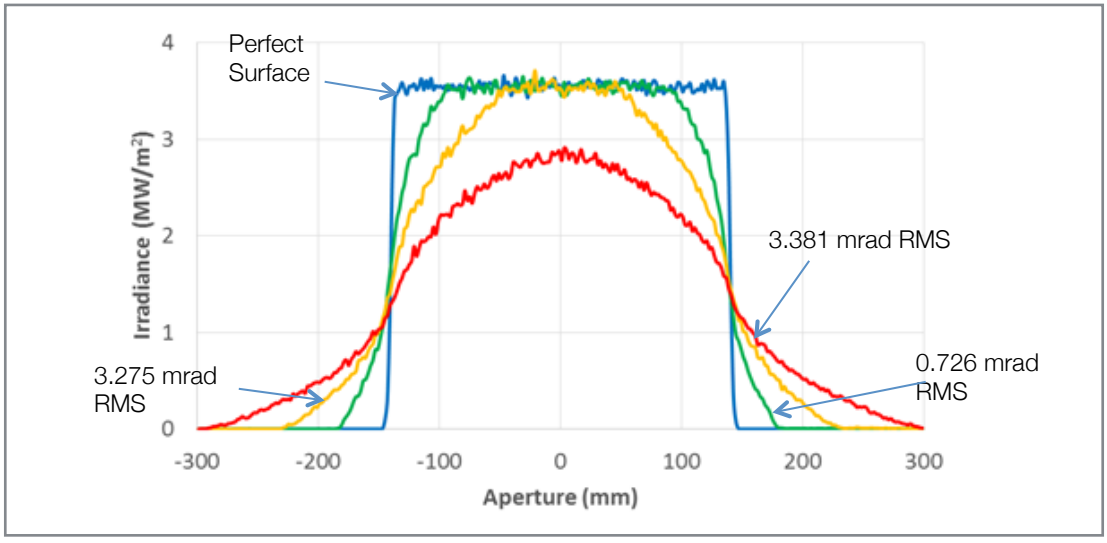

Figure 2-21: Results of Zemax Analysis of Geometry Shown in Figure 2-19

Figure 2-22: Zemax Model of Nonimaging Light Pipe Added to Cassegrain Reflector

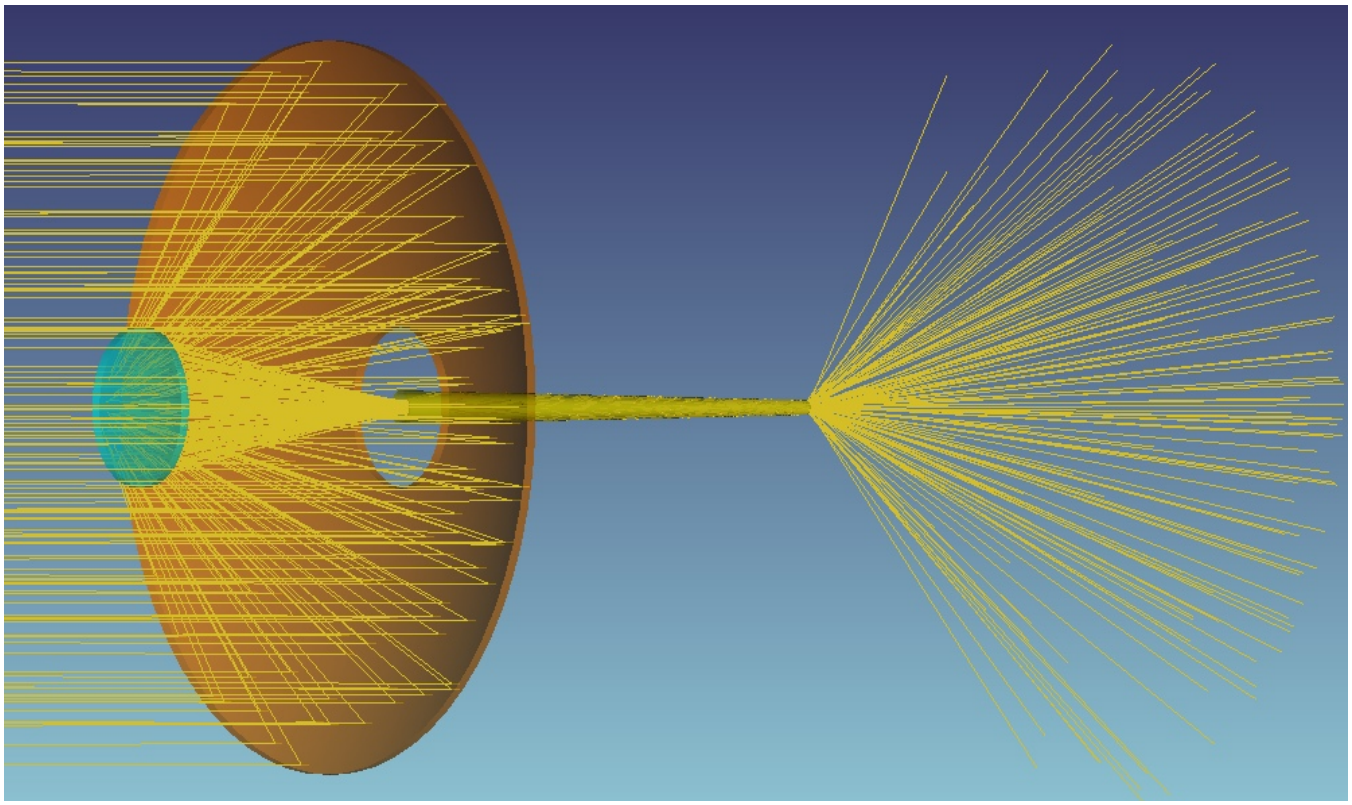

In the case in which we used a perturbed secondary reflector we found the perturbations to the secondary to have magnifying effects as we expected: the concentration ratio would be higher if only a primary reflector was used, but the effect was small. All Zemax simulations were done with one million rays.

When we initiated this research we anticipated that anidolic (non-imaging) optical design would yield the best results from a system perspective and had planned to design a system with horn type secondary concentrators and light pipes. The purported advantage of nonimaging optics were in reduced pointing requirements and higher concentration ratios. We investigated this approach and applied Zemax to model several design concepts of increasing complexity ranging with the simple example test design shown in Figure 2-22. Figure 2-22 was a simple test case to study line losses in a slightly tapered light tube tied to a solar concentrator. In Figure 2-22 all surfaces were treated as 100% reflective and ideal (without surface perturbations) roughly analogous to the green line in Figure 2-18. This simulation produced an average concentration gain factor of 2,120:1 over a 20 cm diameter focal spot and a peak gain factor of 13,000:1 near the central region of the spot, far higher than the single reflector focal arrangement of Figure 2-18, seeming to suggest promise for the nonimaging approach.

Figure 2-23: Early Design Concept of Traditional Focal Optical Architecture

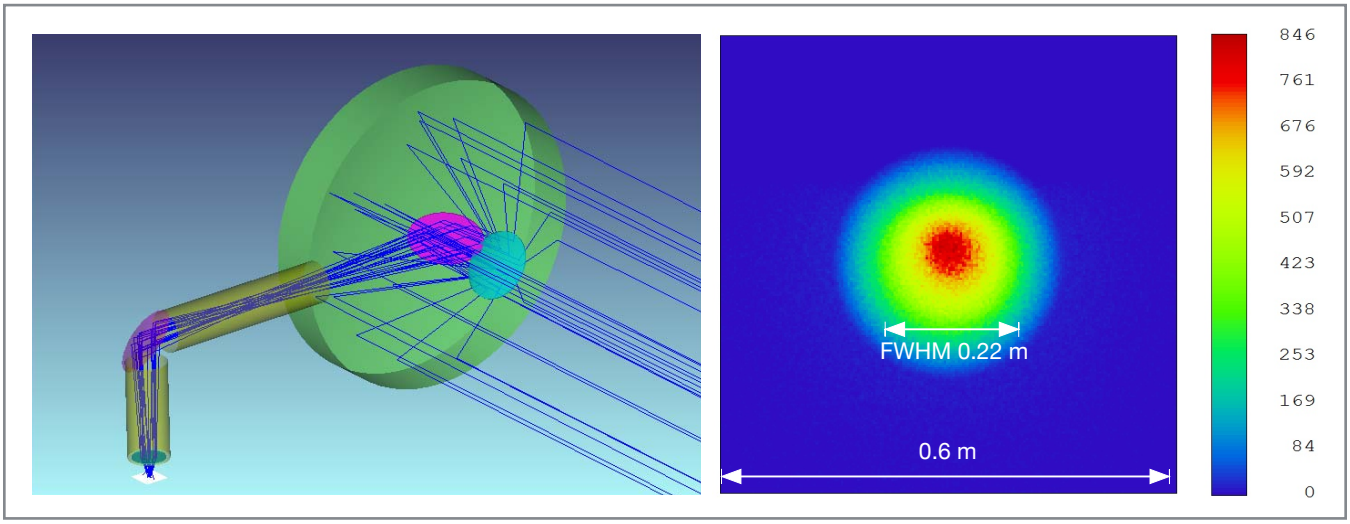

Figure 2-23 is an example of an early design concept we developed for a more traditional optical configuration modeling one arm of the dual reflector configuration of Figure 2-17. In this simulation optical surfaces were treated as perfect but the radial extent of the Sun was included correctly in the calculation as per the simulation of Figure 2-21. The optical design parameters were as follows:

- Primary Paraboloid Reflector
  Diameter: 15 m
  Focal Length 7.5 m
- Secondary Reflector
  Diameter 3.3
  Separation From Primary: 6 m
  Location of Ideal Focus; 16 m (midway down first tube)
- 1st Turning Mirror:
  Flat ellipse shape
  2.5m back from vertex of primary
- 2nd Turning Mirror (at “T”):
  Off-axis paraboloid (Lens Maker’s Radius, R= 5 m, k= -1)
- Terminal Fresnel Lens:
  Diameter 0.8 m, R= 0.707 m, k= 6.33e-6
- Tubes are Oversized to 2 m As Shown. Beam Fits in 1 m Diameter tubes.

Full width at half maximum (FWHM) minimum beam diameter in this case was about 22 cm and note from Figure 2-23 that the peak concentration ratio achieved in this case is nearly 6,200:1, considerably better than the idealized calculations of Figure 2-18 would suggest are possible. The reason for this excellent performance is the terminal fresnel lens placed at the end of the optical baffle as shown. This lens provides strong optical convergence near the target. There is a

corollary to the étendue property of a light beam that at best the cross sectional area of the beam area times the solid angle of the beam is a conserved quantity. Hence, by strongly converging the light near the target, the lens creates a large solid angle and allows the beam to become very narrow producing a high concentration ratio.

Figure 2-24: Geometry of Winston Cone or Compound Parabolic Concentrator (CPC)

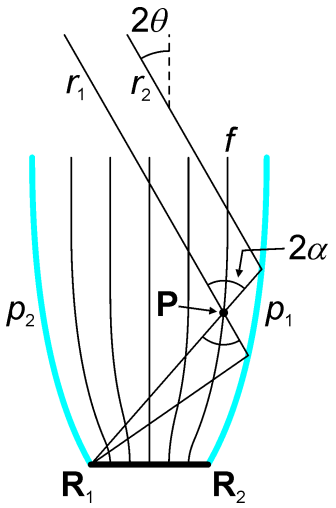

A Winston Cone (Figure 2-24) or Compound Parabolic Concentrator (CPC) is a non-imaging light collector in the shape of an off-axis parabola of revolution with a reflective inner surface. CPCs can be used to concentrate light passing through a relatively large entrance aperture through a smaller exit aperture. The collection of incoming rays is maximized by allowing off-axis rays to make multiple reflections before reaching the exit aperture. They are widely used for measurements in the far infrared portion of the electromagnetic spectrum in part because there are no suitable materials to form lenses in that wavelength range. Some of our investigations sought to determine if these devices can be usefully integrated with the Apis system design in a non-imaging configuration to replace the Fresnel lens from the design of Figure 2-23. In this trade study we considered three designs, each of which was a dual arm configuration like Figure 2-17, not a single arm configuration like Figure 2-23. The first was a non-imaging design terminating in a CPC, the second was a non-imaging system terminating in a Fresnel lens, and the third was an imaging system with an innovating design for mixing the beams from the two arms terminating in a lens.

Figure 2-25 shows the configuration for the two arm non-imaging design with CPC. This overhead/isometric view shows simulated rays visible on one arm, and the other arm without any rays for visibility of the optics. Both arms were simulated with one million rays and individual component parameters were numerically optimized to maximize overall system optical throughput and concentration ratio. In these calculations the primary reflector is once again a 15 m diameter paraboloid with focus 7.5 m (behind the secondary), but now we have introduced additional loss mechanisms which would be present in the real world. The primary reflector is taken to be 90% reflective as is appropriate for an aluminized polyamide material. The secondary (blue) is a 3.3 m diameter hyperboloid with the second focus placed at the entrance to the lateral tube and is 95% reflective which would be appropriate for silver coated composite structure with a thin fused silica coating. Separation between the primary and the secondary is 6 m. The turning mirror (green) is a flat elliptical reflector like the secondary also 95% reflective with dimensions 3.1 m by 4.2 m. The

Figure 2-25: Non-Imaging Configuration Modeled With Terminal CPC. This overhead/isometric view shows simulated rays visible on one arm, and the other arm without any rays for visibility of the optics. Both arms were simulated with one million rays.

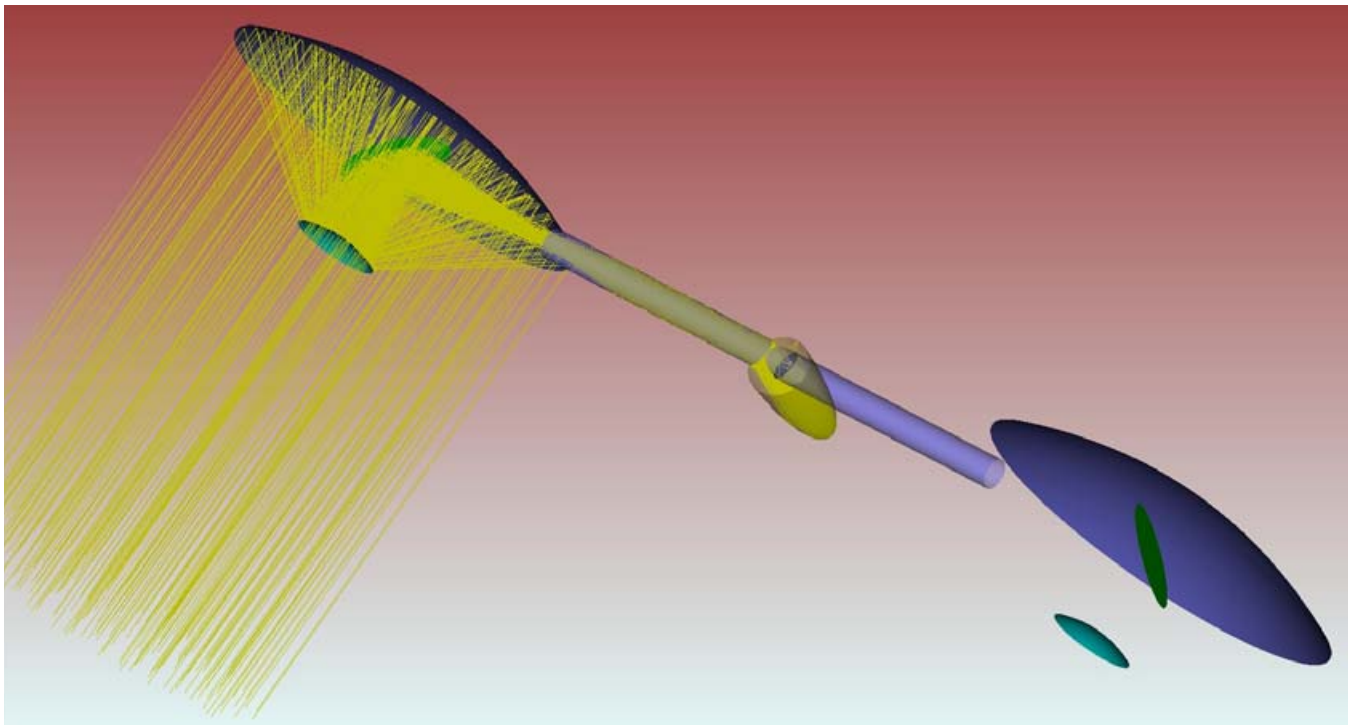

lateral tube (translucent violet in the Figure) is 1.18 m diameter, 10 m long, and offset 2.5 m from the plane tangent to the vertex of the primary (to clear the edge of the primary) also with 95% reflectivity. The rotary "T" mirror is a flat elliptical surface, 1.18 m by 1.67 m, 95% reflective. It is oriented not at 45º, but at 47.86º to tilt the two beams from the dual-arms towards a common center point. The CPC has a small end that is 0.5 m in diameter, is designed to accept rays up to 12º at the large opening, and is 5.4 m long with a 1.2 m diameter opening. The internal surface of

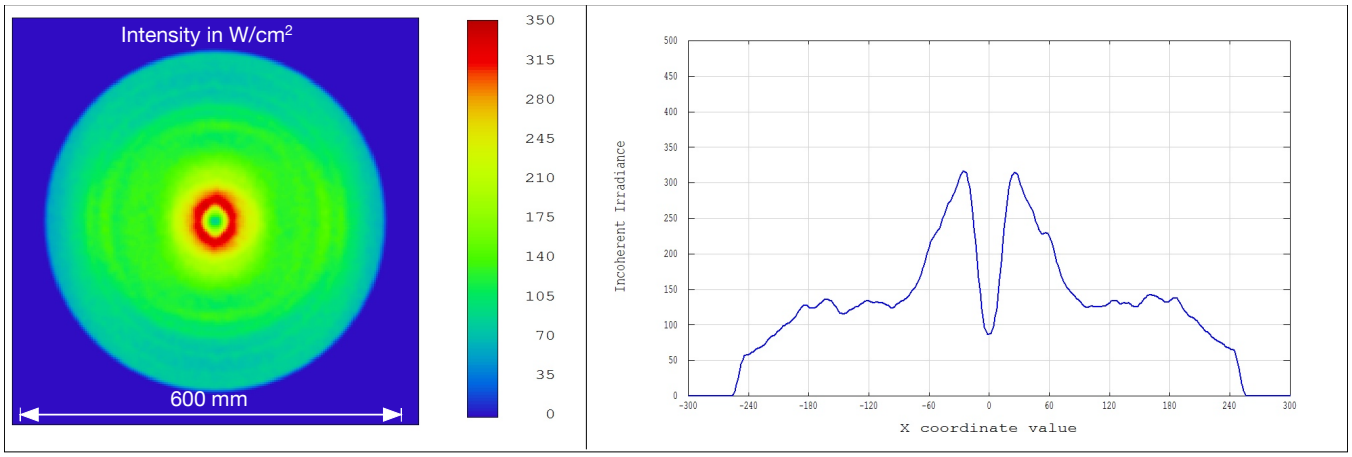

Figure 2-26: Simulation Results for the Design of Figure 2-25 With Terminal CPC. Results are expressed in W/cm^2. Average intensity is approximately 150 W/cm^2 which is sufficient for Optical Mining™, but not for high performance solar thermal propulsion.

Figure 2-27: Non-Imaging Configuration Modeled With Terminal Fresnel Lens. This overhead/ isometric view shows simulated rays visible on one arm, and the other arm without any rays for visibility of the optics. Both arms were simulated with one million rays.

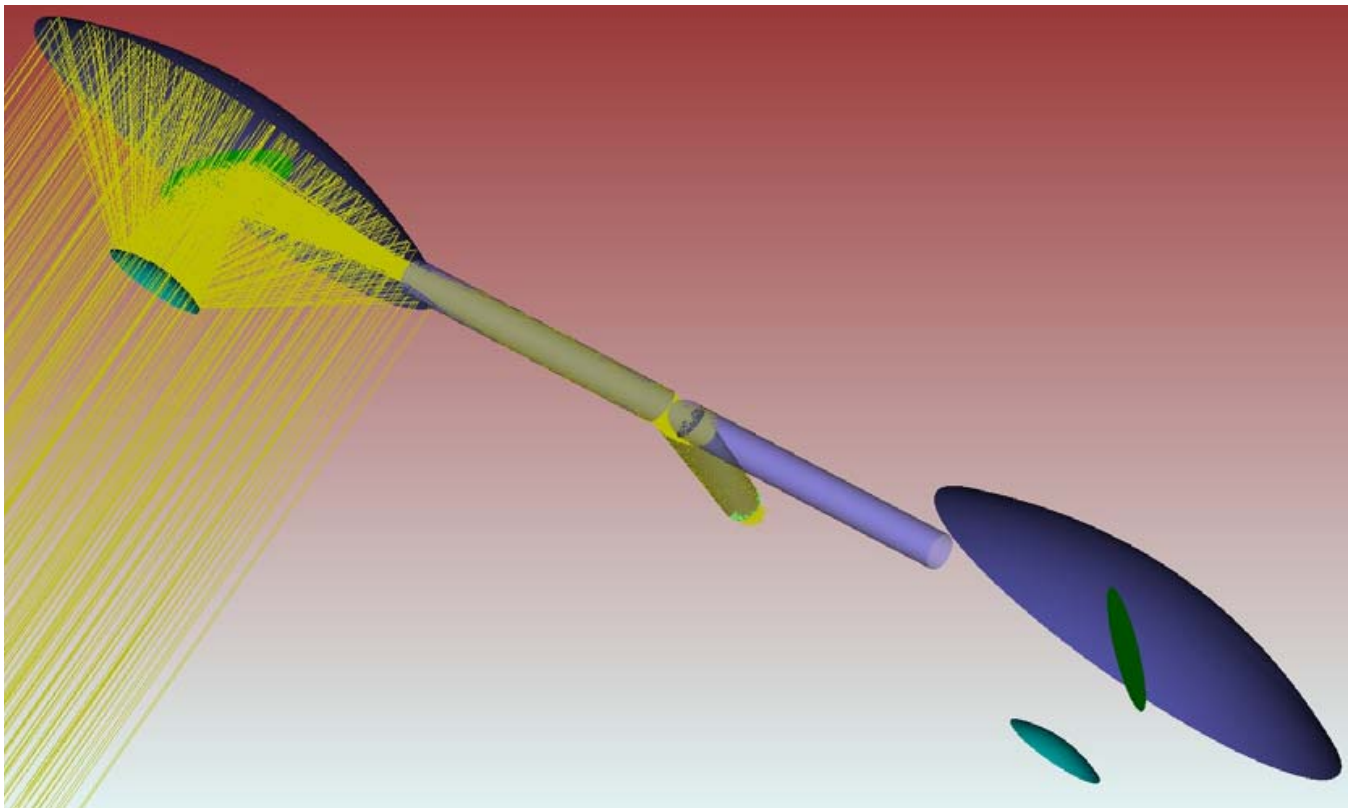

the CPC is assumed to have a 95% reflectivity. Figure 2-26 shows the simulation results. In Figure 2-26 intensity is expressed in W/cm^2. Average intensity is approximately 150 W/cm^2 which is sufficient for Optical Mining™, but not high enough for high performance solar thermal propulsion.

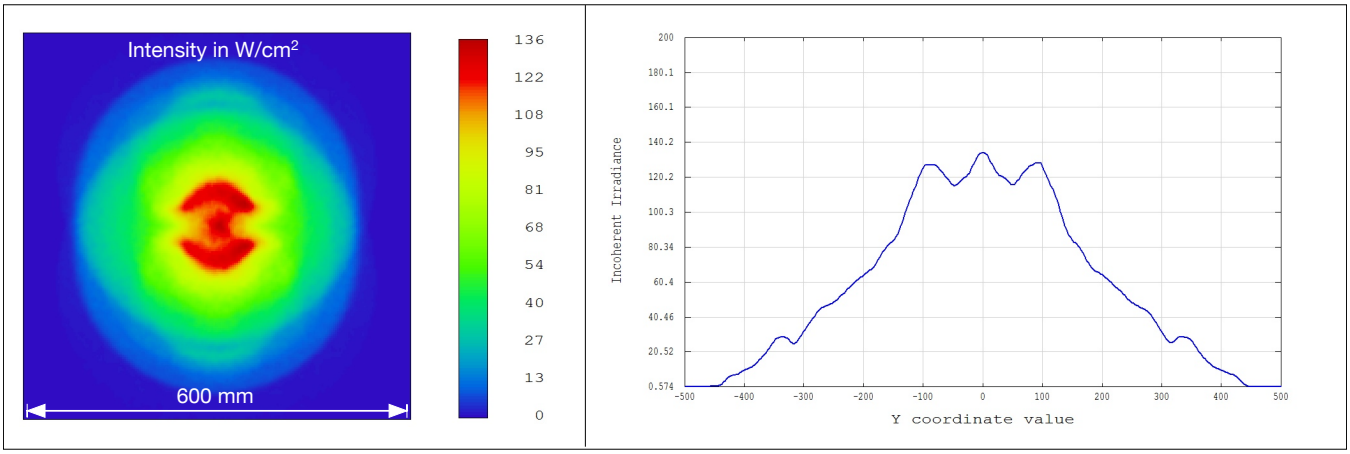

Figure 2-28: Simulation Results for the Design of Figure 2-27 With Terminal Sapphire Fresnel Lens. Results are expressed in W/cm^2. Average intensity is approximately 100 W/cm^2 which is sufficient for Optical Mining™, but not for high performance solar thermal propulsion.

Figure 2-27 shows the non-imaging configuration we designed with a Fresnel lens in place of the CPC. The CPC is replaced in this configuration with a linearly tapered tube (elliptical at *top near the tee* 1.2 m by 2.4 m tapering to 1.2 m diameter circular at bottom) 5.4 m long. This length was determined to be appropriate to allow the tube to end 6 m below the axis of the horizontal tubes as before. A numerically optimized Fresnel lens is positioned at the end of the tube. The tilt angles of the "T" mirrors are reduced to 46.5º to account for the longer throw. The working distance now is 1 m further away, 1 m below the tube end. The design of the Fresnel sapphire refractive optics includes a 1.2 m diameter and an *effective* radius of curvature of 1.5 m on one face, the other face being flat. Given the course geometric optical requirements of this system, it will be possible to assemble this lens in practice from individual arc shaped segments of each Fresnel ring with no segment being thicker than a few centimeters. Performance results shown in Figure 2-28 and are similar to the results for the CPC design. Total power throughput is acceptable at 219 kW (45% of incident) delivered on target out of a total theoretically available power level of 480 kW with significant power being lost to the walls of the tubes even at an optimistically assumed 95% reflectivity, but the spot is even larger than before with barely 100 W/cm^2 for the central 30 cm diameter, or an unacceptable concentration factor of about 730:1. Our analysis of the non-imaging optical designs shows that while in theory anidolic optics could work for this application, in practice it does not provide sufficient optical performance. The CPC outperforms the Fresnel lens in the nonimaging configuration, but wall losses in light tubes and CPCs are too high to merit further investigation of nonimaging optics for this application.

With this insight in hand we turned our attention to an imaging design in which we numerically optimized component shapes not for image quality as is the usual approach in imaging optics, but for maximum delivered power and concentration ratio. By moving to an imaging design, the tubes that run the long and short axes of the vehicle become structural members and light baffles and do not have to be reflective on the internal surface (with one exception as noted below). Moving from non-imaging to imaging optics introduced an interesting design challenge: how to combine the light from the two arms of the optical train in such a way as to maximize performance.

The design we came up with to solve this problem is shown in Figures 2-29. As before, the primary reflectors are 15 m diameter paraboloids with foci 7.5 m behind the secondary and are assumed to be 90% reflective. The secondary reflectors (blue) are once again hyperboloid and as before are assumed to be 95% reflective with diameters of 3.3 m, but now with the second focus placed 5 m beyond the entrance to the lateral tube. As before, they are placed 6 m from the primaries but the longer focal length reduces the beam diameter in the horizontal leg. The turning

Figure 2-29: Final Phase I Optical Design Concept.

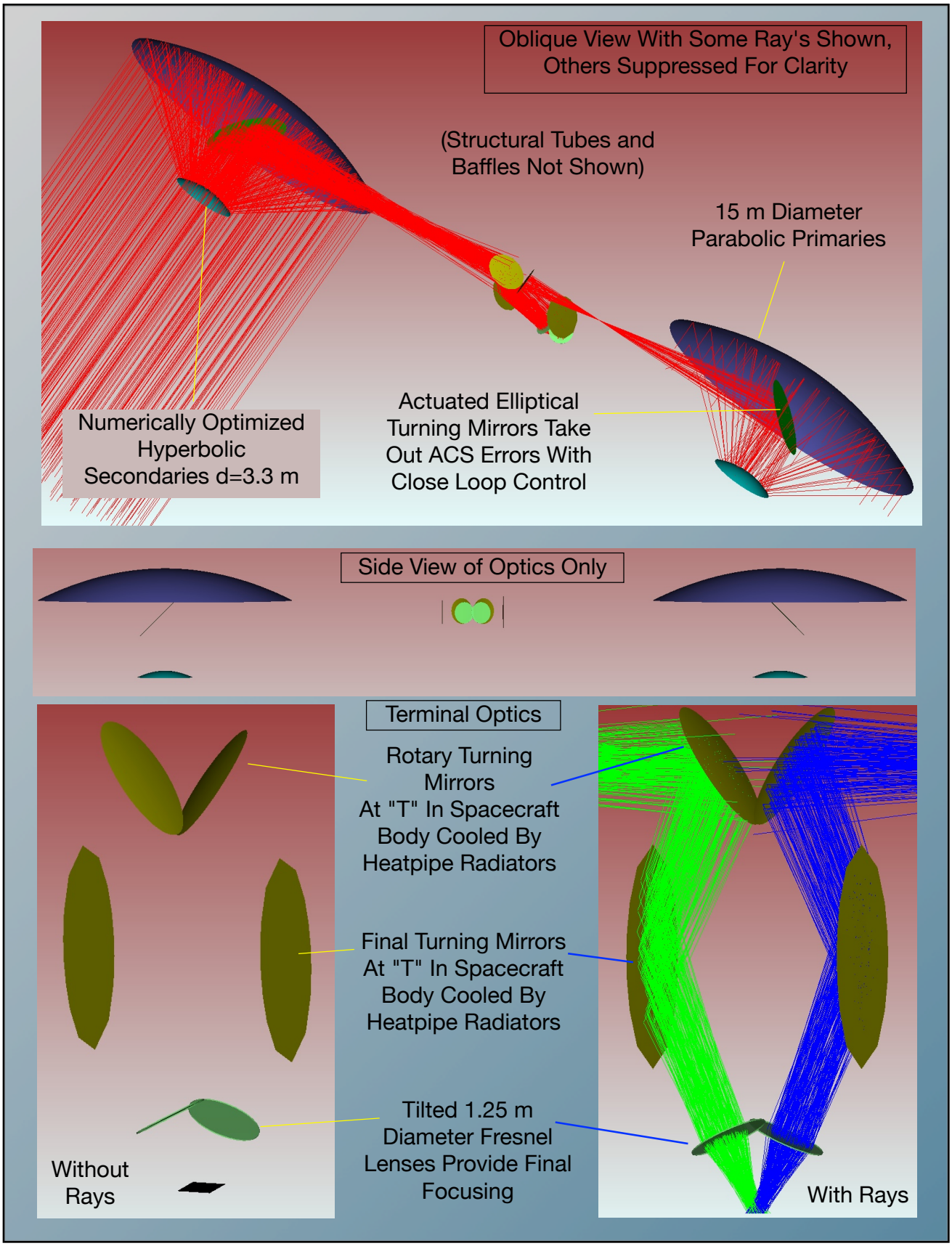

Figure 2-30: Simulation Results for the Imaging Optics Based Design of Figure 2-29

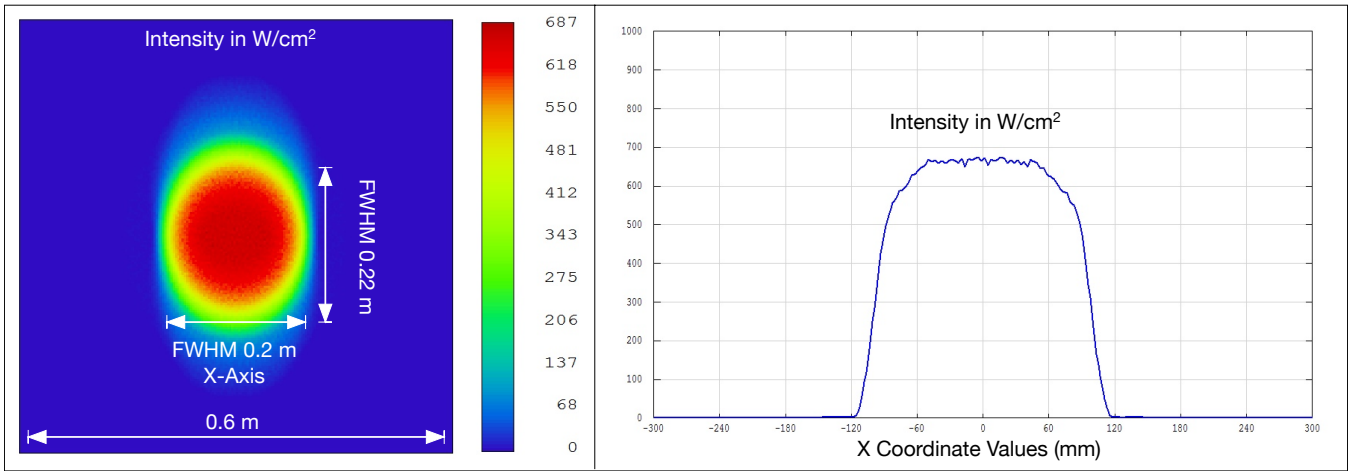

mirror (green) is flat with an elliptical cross section and is once again 95% reflective with dimensions 3.1 m by 4.2 m. The structural tubes are not shown. The rotating "T" mirrors are biconic concave ellipses approximating an off-axis paraboloid and are 95% reflective. The curvatures of these reflectors are numerically optimized to collimate the light and they are 1.1 m by 0.75 m, and tilted at 33.6º (instead of 45º) to facilitate aiming the beams at a common focus through an additional subreflector on each side. We have added two new subreflectors onto the sides of the vertical beamline which are to be integrated with the shroud assembly. In this design their shape has been numerically optimized producing a very slight concave curvature. They are nominally vertical in the diagram, spaced at ±1.81 m from the centerline, and are 95% reflective. The Fresnel lenses are tilted at 26.4º to be normal to the beam and are ±0.5 m from centerline and 1 m removed from the focus. Like the lenses in the nonimaging design they are sapphire with one flat surface. Design optimization resulted in an effective radius of curvature of 0.99 m and an aspheric conic constant of -0.88 with diameter 1.25 m. Standard antireflective coatings were assumed for efficiency calculations.

The performance of this design was outstanding as shown in Figure 2-30. With realistic losses included, this system delivers 250 kW on target (49% efficiency) with 687 W/cm^2 at peak intensity. The FWHM area is an ellipse with an area of 0.14 m^2 and dimensions of 20 cm by 22 cm exhibiting an average power density of 1,785 kW/m^2 with a peak intensity of 6,870 kW/m^2 for a peak solar concentration ratio of 5,440:1 and an average concentration ratio over the spot of 1,310:1. This system yields the potential to operate at spot temperatures approaching 3,000 Kelvin, enough for high performance solar thermal propulsion.

In addition to calculating baseline performance, we repeated our analysis of this design and performed a parametric analysis of performance with off nominal primary reflector distortions and

pointing errors. For primary reflector distortions we applied the same "W" shaped distortion of Figure 2-20 but varied the distortion parametrically between zero and 10 mrad. The result of this analysis was a modest reduction in power inside the FWHM area out to distortion levels of 10 mrad as shown in Figure 2-31. Note that actual distortion measurements in ground tests on the L'Garde 14 m diameter off axis reflector for the IAE program were 2 mrad RMS, so we expect a maximum distortion of no more than 2 mrad RMS after considerably more development. Reading from the figure, we expect to loose no more than 1% in terms of power and intensity due to primary reflector distortion. In terms of total power at the FWHM, the size of the focal ellipse did not change substantially, in agreement with our earlier analysis on the simple Cassegrain configuration. Note that there are two main reasons that primary reflector distortions do not substantially effect focal point intensity in the range we have considered in this study. First, the distortions that can be achieved with modern thin film fabrication techniques yield reflector surface slope errors which are substantially less than the divergence cone angle of sunlight, so most of the spot size is the irreducible image size of the Sun. Second, modern optical design and analysis tools have allowed us to optimize the shape of optical elements to produce performance which is better than could be achieved by simply applying the lens makers formulas, which were developed for imaging systems, not peak intensity solar concentrators. Our simulation of off-pointing conditions in which the elliptical turning mirrors are used to compensate for attitude control errors gave similar results with the primary effect of attitude control errors of the spacecraft being a cosine loss effect on total power as long as gross errors are less than about 2 degrees.

Figure 2-31: Results of Parametric Analysis of Primary Reflector Distortion

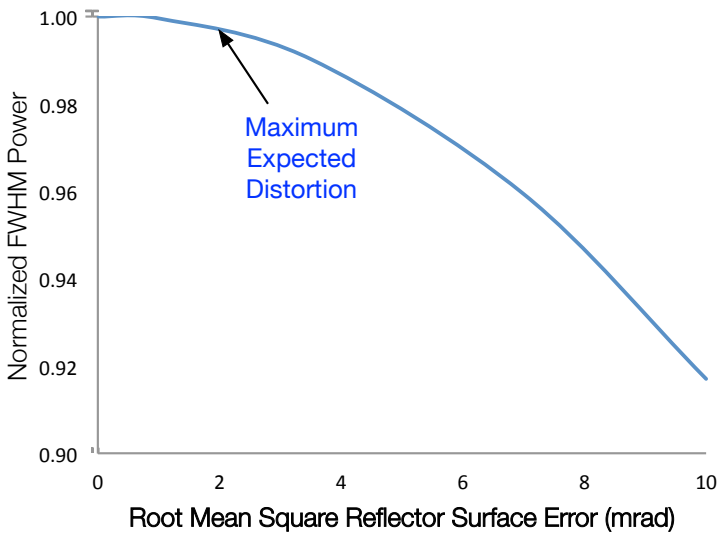

Conclusions of Optical Analysis Effort: This optical design and analysis work was performed as part of the technological analysis of the Apis™ architecture to advance the stage of technology, not just for mission analysis. This work confirms that the expected performance of inflatable structures technology, which has been in development in this country since the 1960s, is such that it can enable the Apis architecture if integrated with state of the art materials, controls, mechanism, and thermal control systems.

A solar thermal rocket that can take advantage of asteroid ISRU products as propellant is a key

2.4 Omnivore™ Thruster Invention and Performance Analysis

part of the Apis architecture. Our mission-systems analysis shows that there is high leverage to having a propulsion system that can use propellants that require minimal processing in space prior to use. Originally, we assumed that the minimal processing needed would be to separate the H_2O from the CO_2 and purify the H_2O so it can be run in a solar thermal rocket. However, as we started to analyze the problem, we realized that by using an innovative technical approach for the rocket engine design we can virtually forgo the propellant processing step and utilize all of the fluid products of the Optical Mining™ ISRU process as propellant. This has the dual benefit of minimizing the ISRU plant mass and complexity while maximizing the effective productive yield of the process. We call this new type of solar thermal rocket the Omnivore™ thruster because it will be able to consume virtually any fluid as the propellant source including the raw, unprocessed (filtered only), volatile products from the Optical Mining™ process. The Omnivore™ solar thermal rocket is a new breakthrough propulsion technology that ICS has been working on diligently under NIAC sponsorship since we conceived of it in November of 2015. Based on the work we have done so far, we have elevated the technology readiness of this invention from TRL-1 to TRL-2 and hope to have it to TRL 3-4 by September of 2016 if our Phase II NIAC is funded in the spring of 2016.

Table 2-5 - Omnivore™ Thruster Physical and Operational Characteristics

	5 kW H2O	10 kW H2O	250 kW H2O/CO2
Operating Regime	1 atm (lab)	1 atm (lab)	Vacuum
Thrust (N)	2.2	4.4	146
Chamber Diameter (cm)	4.6	6.5	33
Chamber Exit Diameter (cm)	5.6	7.5	36
Chamber Length (cm)	8.4	10	27
Nozzle Length (cm)	0.72	1.9	27
Throat Diameter (cm)	0.19	0.26	1.2
Exit Diameter (cm)	0.24	0.34	12
Inlet ID (cm)	0.2	0.2	0.6
Inlet OD (cm)	0.6	0.6	1.2
Injector Hole Diameter (cm)	0.02	0.02	0.04

As with any solar thermal rocket, the Omnivore™ thruster is positioned near the focus of a solar concentrator when in use. Innovations built into the Omnivore™ rocket include the use of advanced 3D printing of high temperature ceramics to form a monolithic thruster body with dual propellant inlets to individually control window cooling and regenerative heat capture from the thruster body along with the use of 3D printed low density ceramic foam as the solar absorber

Figure 2-32 - Concept Drawing of Omnivore™ Solar Thermal Rocket. Innovations include dual propellant inlets for window cooling and counterflow heat capture, replaceable ceramic foam solar absorbers for rapid prototyping and agile ground development program, and monolithic 3D printed ceramic thruster body.

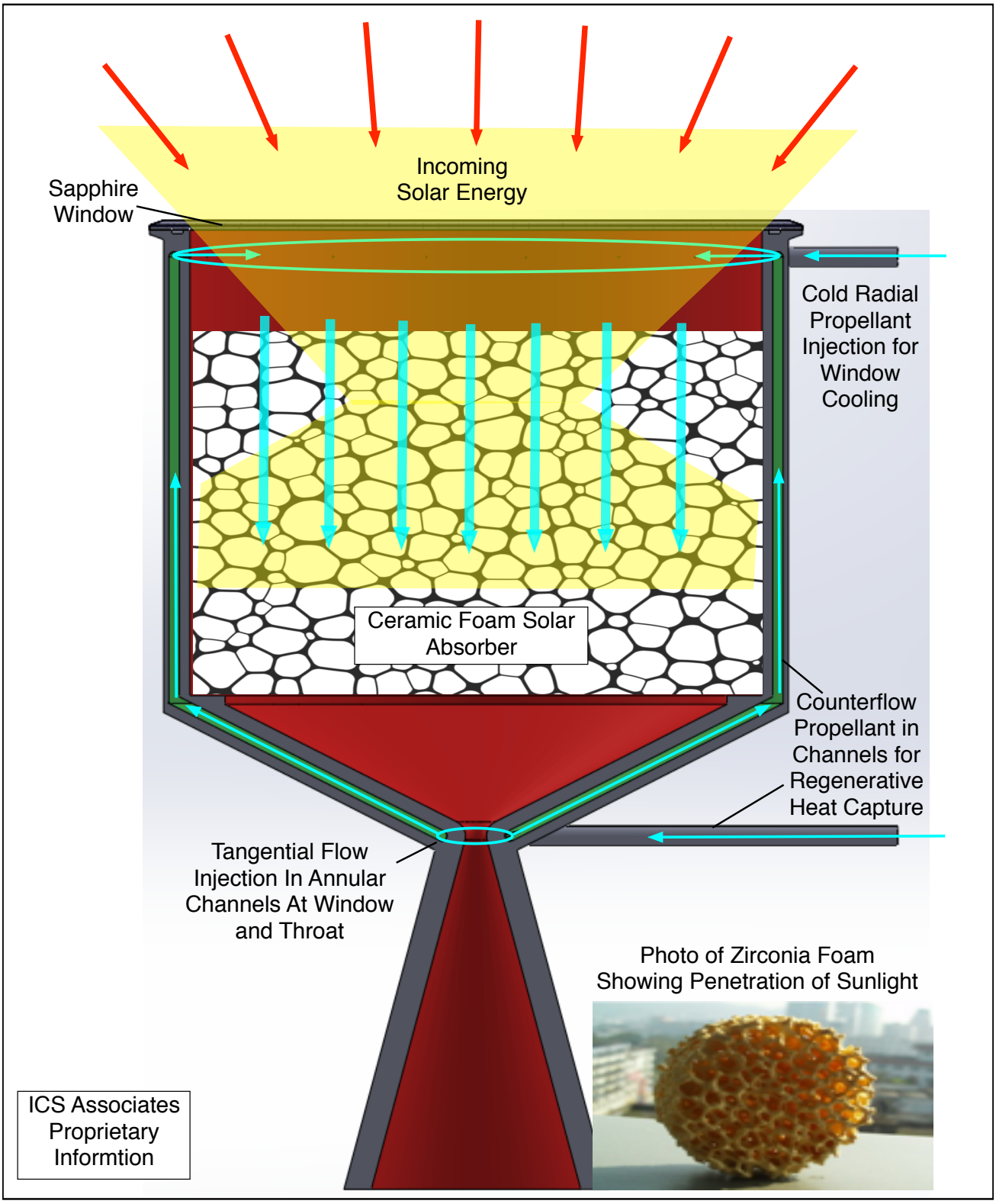

Figure 2-33 - Flight Scale Omnivore™ Thruster Concept Design

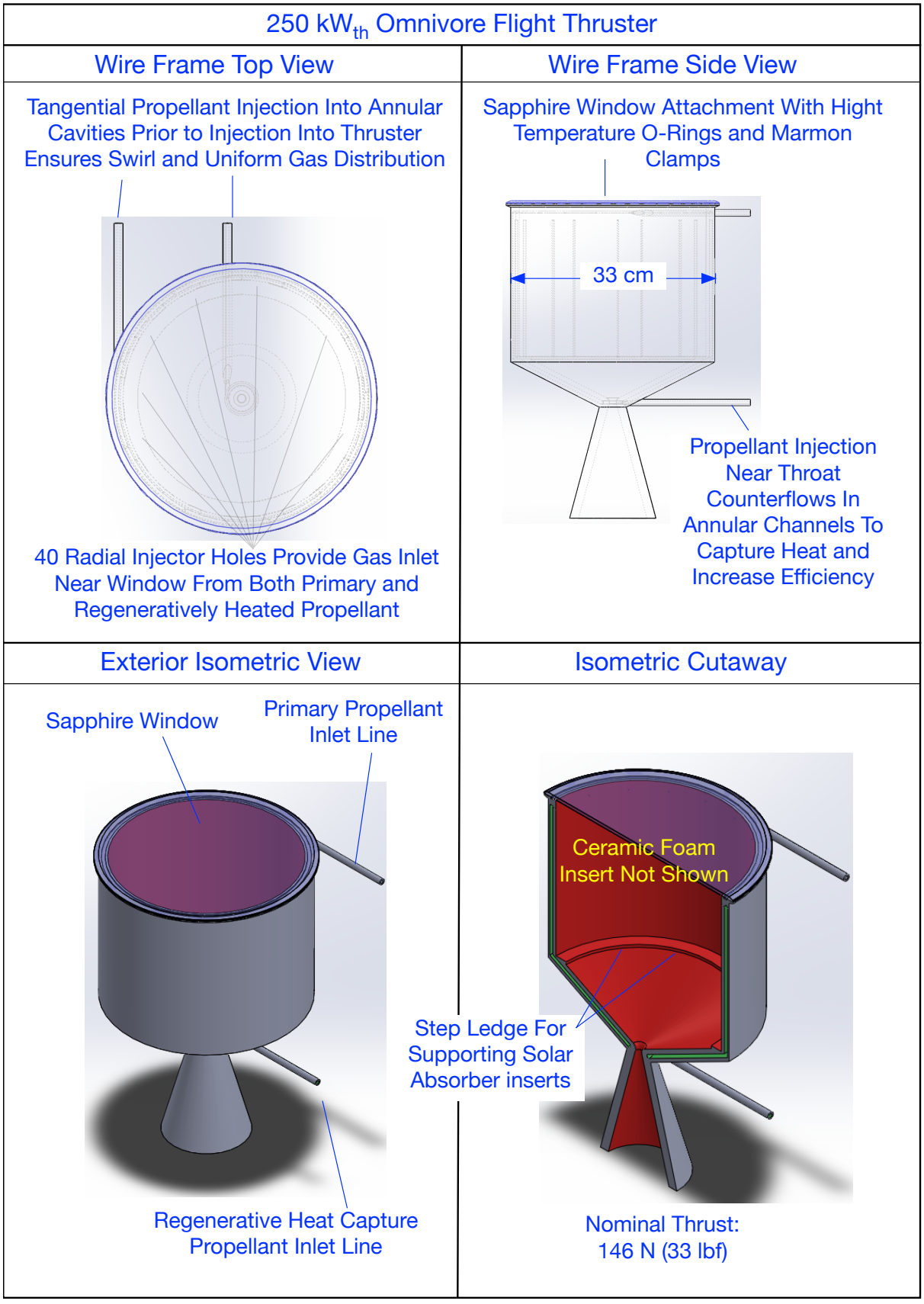

medium. As shown in Figure 2-32, the thruster design has only four primary parts: a 3D printed ceramic thruster body, a sapphire window, Marman clamps (not shown) to hold the window in place, and ceramic foam solar absorber inserts that absorb the solar energy and transfer the absorbed heat to the working fluid. For our laboratory development effort we will use zirconia ceramics including low density foam which has been developed for the steal industry and is in common use as filtering material for cleaning debris out of high temperature molten metals.

Figure 2-34 - Laboratory Omnivore™ Thruster Concept Design

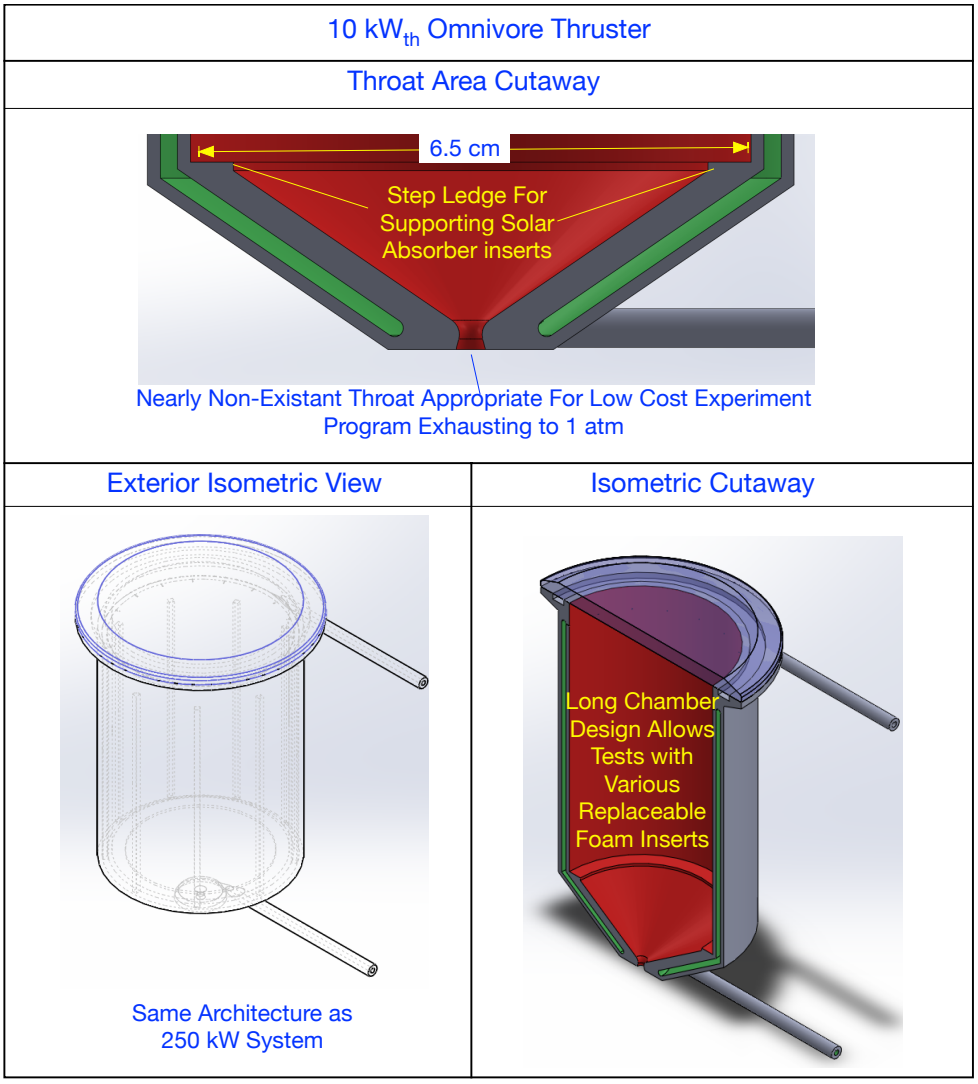

As previously indicated, the Omnivore™ thruster will need two work with contaminated propellants so that it can utilize the direct products of Optical Mining. Although large debris particles, more than 0.4 mm in diameter, will clog the foam solar coupler and will have to be filtered out, no other processing should be required. The ceramic materials we have selected are compatible with both SO_2 and hydrocarbon contaminants that we have found in the effluent of our Optical Mining™ experiments. We have performed modeling and simulation to determine the likely performance of the Omnivore™ thruster on mixture of CO_2 and H_2O and find that CO_2 rich mixtures produce higher thrust and efficiency, but lower specific impulse. An example of our performance analysis work is provided in Figure 2-35 which shows calculated specific impulse versus chamber temperature for water propellant expanding to vacuum from a chamber pressure

of 100 psi. Note that this is an ODK analysis that has been derated to account for nozzle losses.

Figure 2-35 - Derated ODK Specific Impulse Performance Analysis

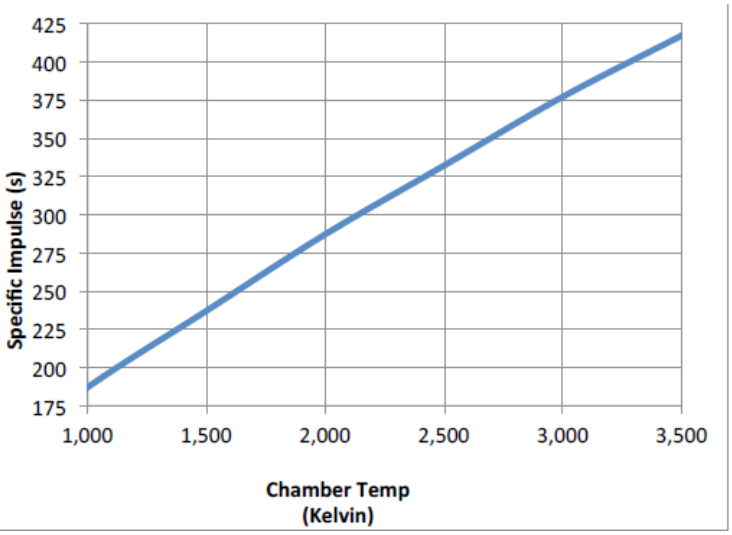

For flight applications we will switch to thorium oxide which is the highest temperature oxidation resistant ceramic in nature and can deliver specific impulse performance over 350 s with water propellant. Although generally safe to use, we can't use thorium oxide for our laboratory experiments because it is slightly radioactive and environmental regulations for its use would dramatically drive up early research and development costs. Also, while 3D printing of thorium oxide should not be a technical challenge for ceramic producers, they too are not equipped to produce parts from this material due to environmental regulations but could tool up quickly for a flight program if the budget were available. We have performed design studies of three Omnivore thrusters including two laboratory technology development scale devices and one full flight system scale devices. The laboratory technology development thrusters are 5 kW and 10 kW respectively. The full scale flight system design is 250 kW. CAD designs for the 250 kW flight Omnivore™ thruster are shown in Figure 2-33 and the 10 kW technology development design is shown in Figure 2-34. Table 2-5 provides a summary of physical scale parameters and operating characteristics of the three thrusters.

2.5 Omnivore™ Thruster Ground Test Development Plan

The solar thermal rocket is a compellingly elegant technical concept and simple in principle. Over the past 65 years many propulsion technologists have proposed solar thermal rockets of various different designs. The first serious work on this technology was done in the 1950s by the German rocket scientist Krafft Ehricke (Ehricke 1956). In the 1970s the Air Force Rocket Laboratory (now AFRL) spent considerable resources on the technology and proved that it has compelling mission benefits for space tug applications (Etheridge 1979). We know that the Air Force did considerable hardware development in this area funding work at Rockwell International in the 1980s (see Shoji 1985, 1986, 1992) and in the 1990s and that NASA did development in this area in the 1990s and early 2000s (personal communication with Harold P. Gerrish Jr December 2015).

Photographs of the Air Force (see Section 1 of this report) and NASA tests (see Figure 2-36) are available, but there are no publicly available reports or papers that we can find on the results.

Past attempts to develop solar thermal rockets have been fraught with difficulty. Neither the Air Force (personal communication with Jame Shoji 1993) nor the NASA (personal communication with Harold P. Gerrish Jr December 2015) test and development goals where met within budget. Key challenges that have plagued past work include:

a. the use of high temperature refractory metal engines that are highly oxidation sensitive with high parts counts and many sensitive leak-prone seals,
b. hydrogen propellant which imposes demanding requirements for safe storage and management, and
c. the use of solar thermal concentrators, which are not a reliable and consistent power source here on the Earth and which require the test stands to be located outdoors on towers or gantries or in cramped laboratory conditions.

These challenges are synergistically problematic. For example, the fact that the thrusters are made of refractory metals which are highly oxidation sensitive but have to be tested in an outdoor environment on a tower rather than in an indoor vacuum system causes practical test hurdles. Likewise, the presence of any oxidizer in the propellant feed system or down stream of the thruster in the diffuser or vacuum system can cause issues including detonation of the facility or oxidation and destruction of the thruster unit. This issue is a cost multiplier for the test effort. With its simple design, use of oxidation resistant materials, and use of H_2O and CO_2 propellants, the Omnivore™ thruster fully resolves items a. and b. above.

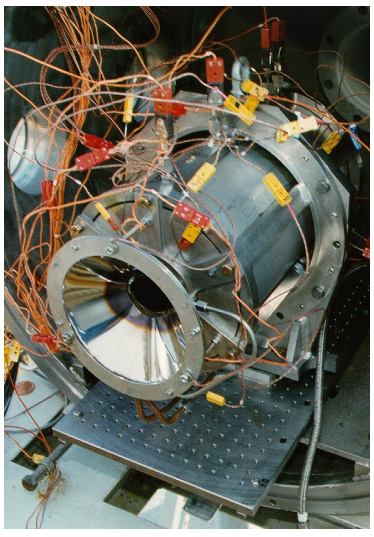

NASA Refractor Metal STR Designed for Hydrogen Propellant

NASA Solar Concentrator Facility at MSCF

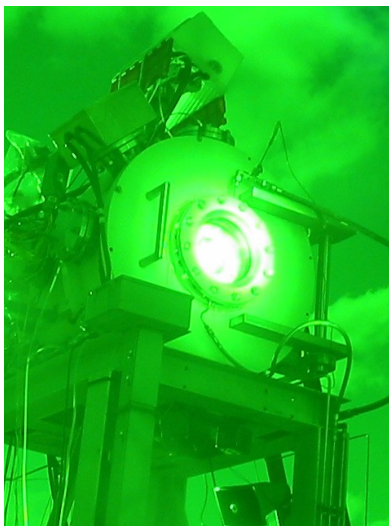

NASA Solar STR Under Test Viewed Through Welding Goggles

Figure 2-36 - Photographs of NASA's Attempt to Use An Outdoor Solar Thermal Furnace To Test and Develop a Hydrogen Solar Thermal Rocket (STR)

Figure 2-37 - Power Output Profiles of the ICS 10 kW Array on Typical Clear Days in Southern California. These profiles show that solar power through clear day weather is problematic for a careful propulsion research effort, which requires consistent and controllable power.

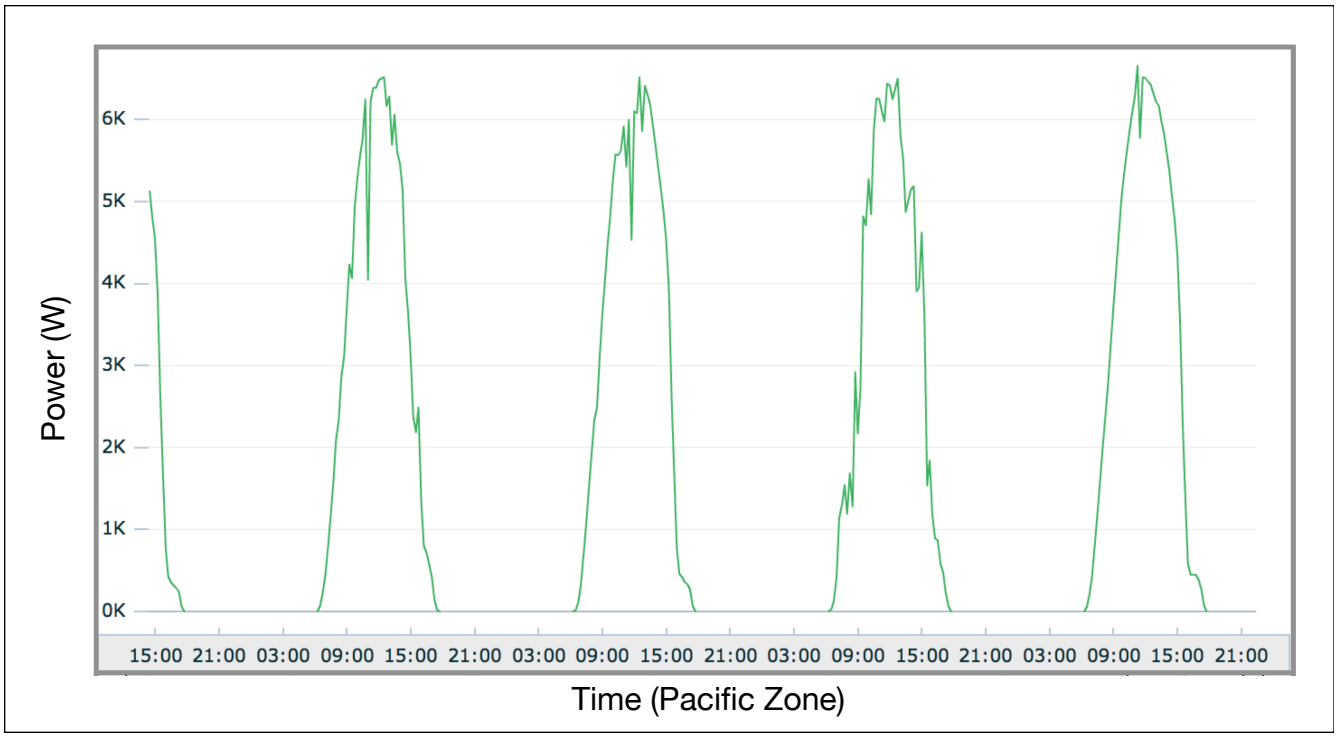

The PI of this work has personally observed the problems associated with outdoor solar concentrators in his work on the full scale Optical Mining™ demonstration as part of this Phase I NIAC research. While the Sun is a constant, steady and reliable power source in space, that same cannot be said of sunlight here on the ground. This fact significantly increased the time and difficulty associated with performing the full scale Optical Mining™ demonstration. Part of the issue with item c. is clearly depicted in Figure 2-37 which is a plot of AC power output from the 8.5 kW power inverter tied to a 10.2 kW solar array at ICS Associates Incorporated's office site in Southern California. This data was recorded on four consecutive days in late February and early March in 2016. A review of national weather service reports for the days will show that the weather was reported to be clear and sunny. Nonetheless, spikes and drops in power output can be seen in the graph. Note that on the first day shown in the graph power dropped from 6.2 kW to 4.0 kW in just a few minutes. Rapid upward spikes can also be seen in the data. These spikes are caused by transient clouds. If a STR test is being conducted and the system parameters are adjusted for maximum performance conditions and power output suddenly spikes upward, it could result in the failure of the apparatus. On the other hand, if power suddenly drops out, it would invalidate performance data and the test would have to be re-run.

The **ORTB** coupled with the Omnivore™ rocket concept **constitutes an innovative breakthrough in propulsion technology** because it will be the first laboratory apparatus that will allow **the rapid experimental demonstration and technological characterization of a high performance solar thermal rocket** in an indoor, shirtsleeve environment with simple and practical controls of the light source for the rocket. Moreover, it will allow the demonstration of a propulsion technology that can make direct use of asteroid ISRU products, **eliminating the need for propellant supply launched from Earth with a system that produces up to 100 times the thrust of SEP.**

Other issues with terrestrial solar concentrators for ground based propulsion research are cost, availability, geography, and performance. For example, we know of three government controlled high performance solar concentrators in the United States: one at Sandia, one at White Sands, and one at NASA MSFC. The one at Sandia is not available for commercial use and the one at White Sands is marginal in performance for use in solar thermal propulsion. Both the MSFC and White Sands facilities have quoted prices for use of the facilities in the range of multiple thousands of dollars per day. In the case of MSFC, use would have to be arranged through a Space Act

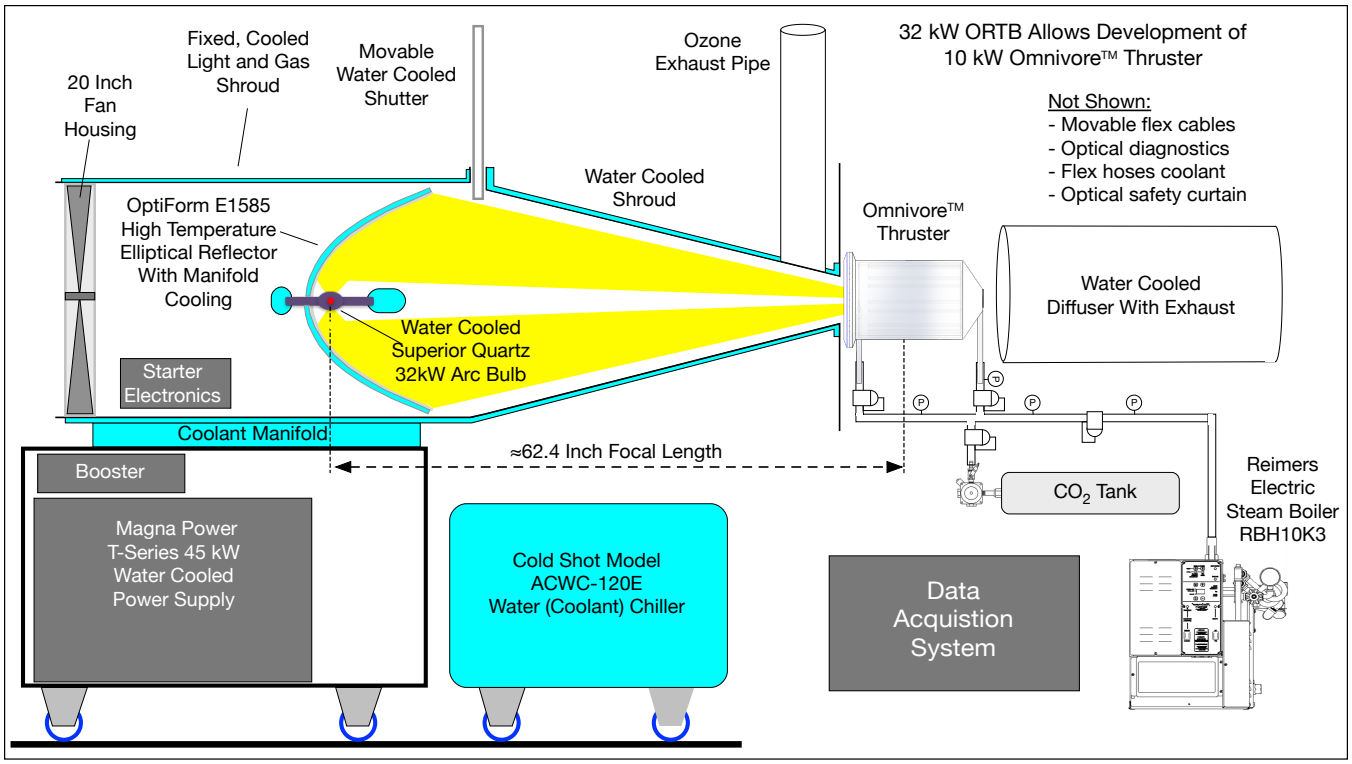

Figure 2-38 - Key Features of the 32 kW Variant of the Omnivore™ Rocket Test Bed (ORTB). This system is designed to demonstrate and characterize a 10 kW thruster that operates on mixtures of H_2O and CO_2.

Figure 2-39 - Key Features of the 10 kW Variant of the Omnivore™ Rocket Test Bed. This system is designed to demonstrate and characterize a 3 kW thruster that operates on CO_2.

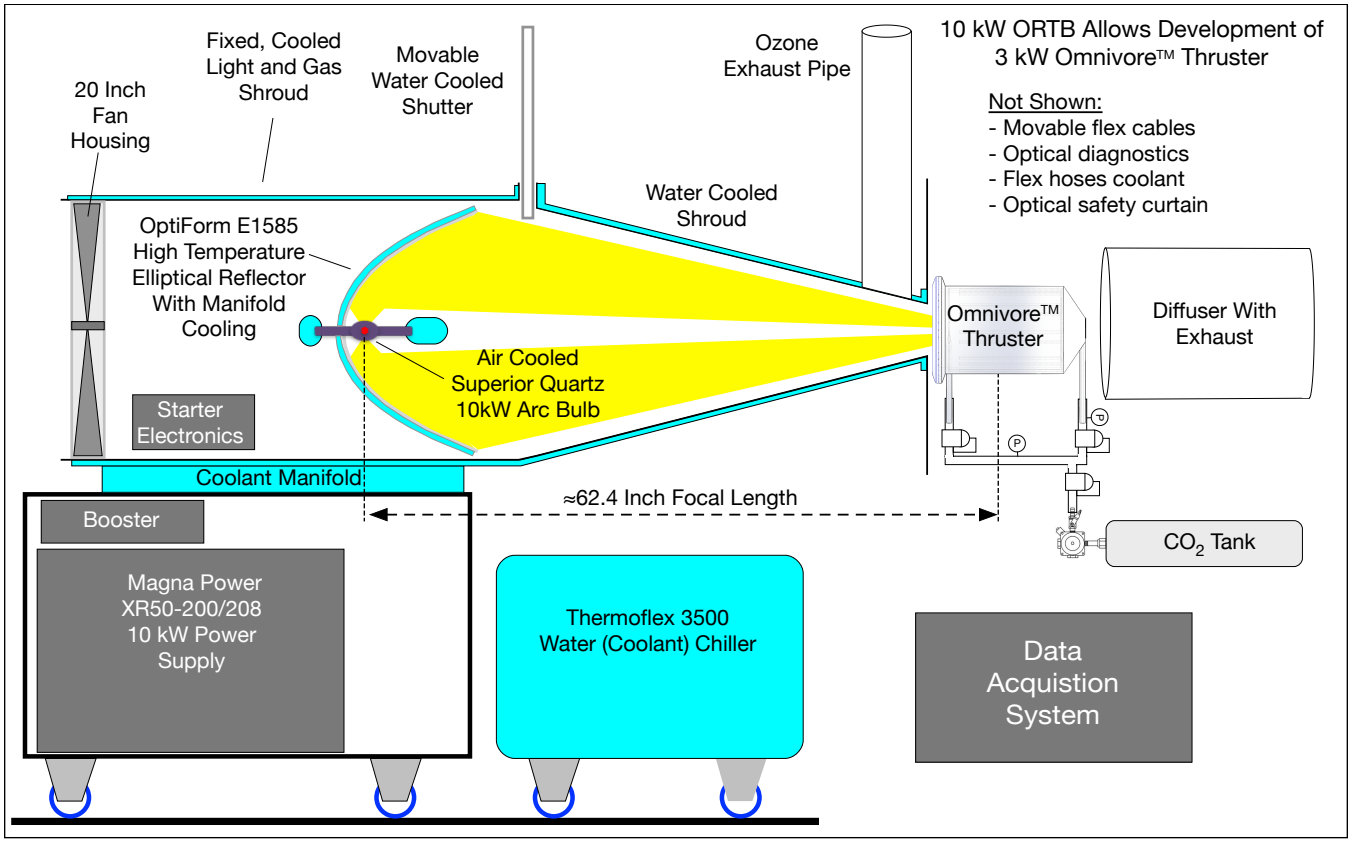

Agreement with White Sands through a contract. For a successful one year test program we would plan to have approximately 100 days of testing. This would require nearly a year of travel, relocation of laboratory equipment and hundreds of thousands of dollars in expense just for the facility. Instead, we found a better way.

Figure 2-40: Photograph Of Selected Superior Quartz Sx32000D High Pressure Short Arc Xenon Arc Lamp

During our recently completed Phase I SBIR contract we designed an innovative Phase II laboratory apparatus called the Optical Mining™ Test Bed (OMTB). Instead of using an outdoor solar concentrator for Phase I ISRU experiments, the OMTB uses an electrically powered laboratory light source which can be easily turned on and off or modulated as needed for experimental work. Late in this NIAC Phase I effort we realized that it makes sense to apply this same approach to our Phase II NIAC effort to demonstrate the Omnivore™ rocket. We call the innovative and highly practical and cost effective apparatus we have designed to do this in our Phase II NIAC effort the Omnivore™ Rocket Test Bed (ORTB). The design of the ORTB has benefited greatly from the work we did in our SBIR, especially in the design of the light source. We have designed two versions of the ORTB, a 32 kW system that allows the development of a 10 kW Omnivore™ thruster operating on varying mixtures of H_2O and CO_2 propellant, and a 10 kW system that allows the development of a 3 kW Omnivore™ thruster operating only on the easier to handle CO_2 propellant. The 32 kW system assumes that our related SBIR proposal is funded and uses the light source from the OMTB allowing more resources to go into the thruster,

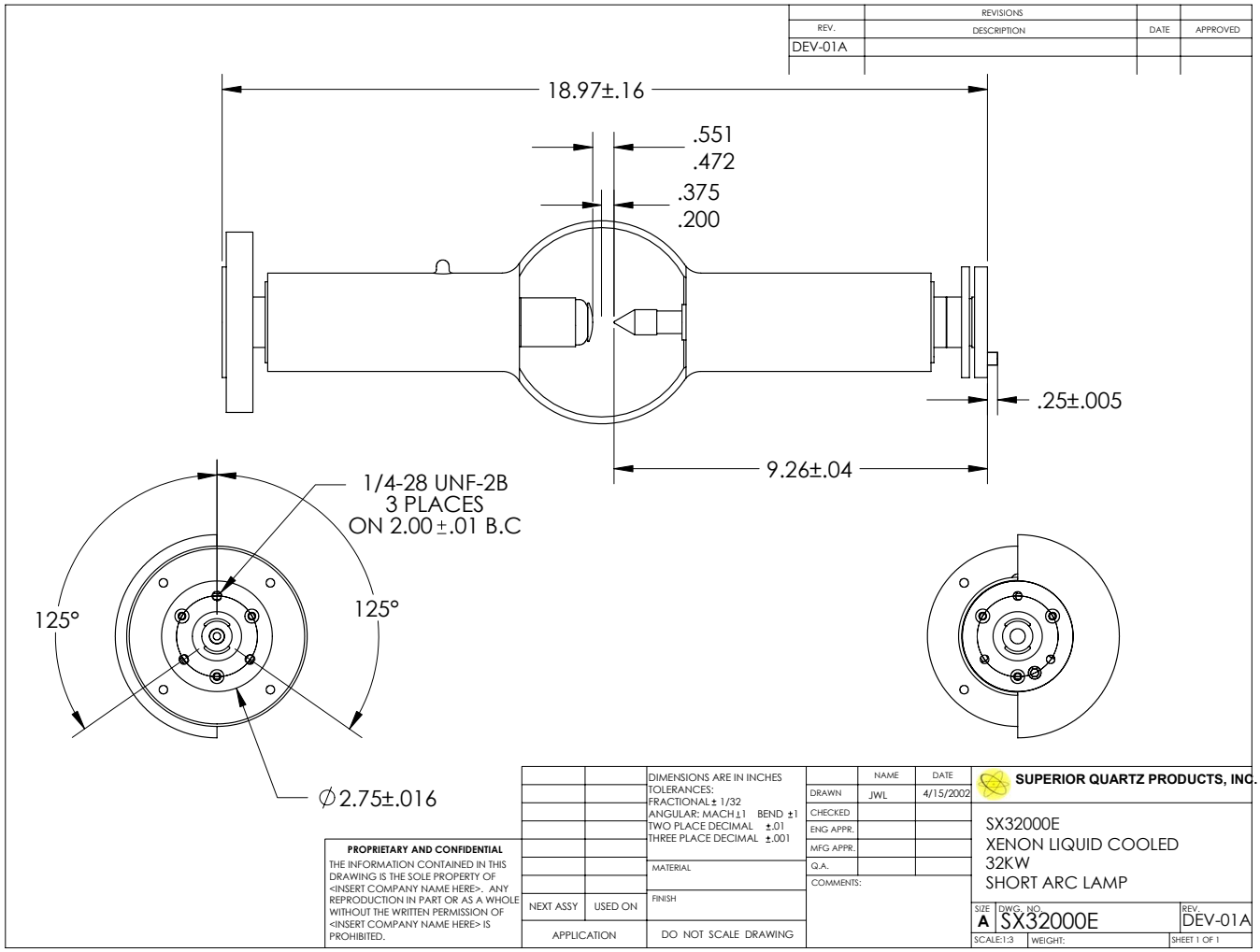

Figure 2-41: Drawing Of Selected Superior Quartz Sx32000D High Pressure Short Arc Xenon Arc Lamp

feed system and test program. The 10 kW system is a stand alone NIAC Phase II option which does not make the assumption of shared resources with our proposed SBIR effort. Key features of the 32 kW ORTB are shown in Figure 2-38 while the 10 kW option is shown in Figure 2-39. The difference between the two systems is that the 10 kW system uses smaller, lower cost components and eliminates the water boiler needed for H_2O vapor feed allowing a simpler CO_2 gas only feed system in order for the whole system to fit within a NIAC Phase II implementation plan. Other than the elimination of the water vapor gas handling components to allow testing on a variety of mixture ratios of water and carbon dioxide, other specific changes for the 10 kW system include a smaller thruster, elimination of the water cooling for the diffuser, and smaller main power supply and water chiller. Note that the 32 kW system will allow testing of both 10 kW and 5 kW Omnivore™ thruster designs to validate scaling models. The text and figures that follow describe only the 32 kW system for brevity. We cite adaptation of our SBIR work for much of this and repeat some of the text from our SBIR reports for the reader's convenience.

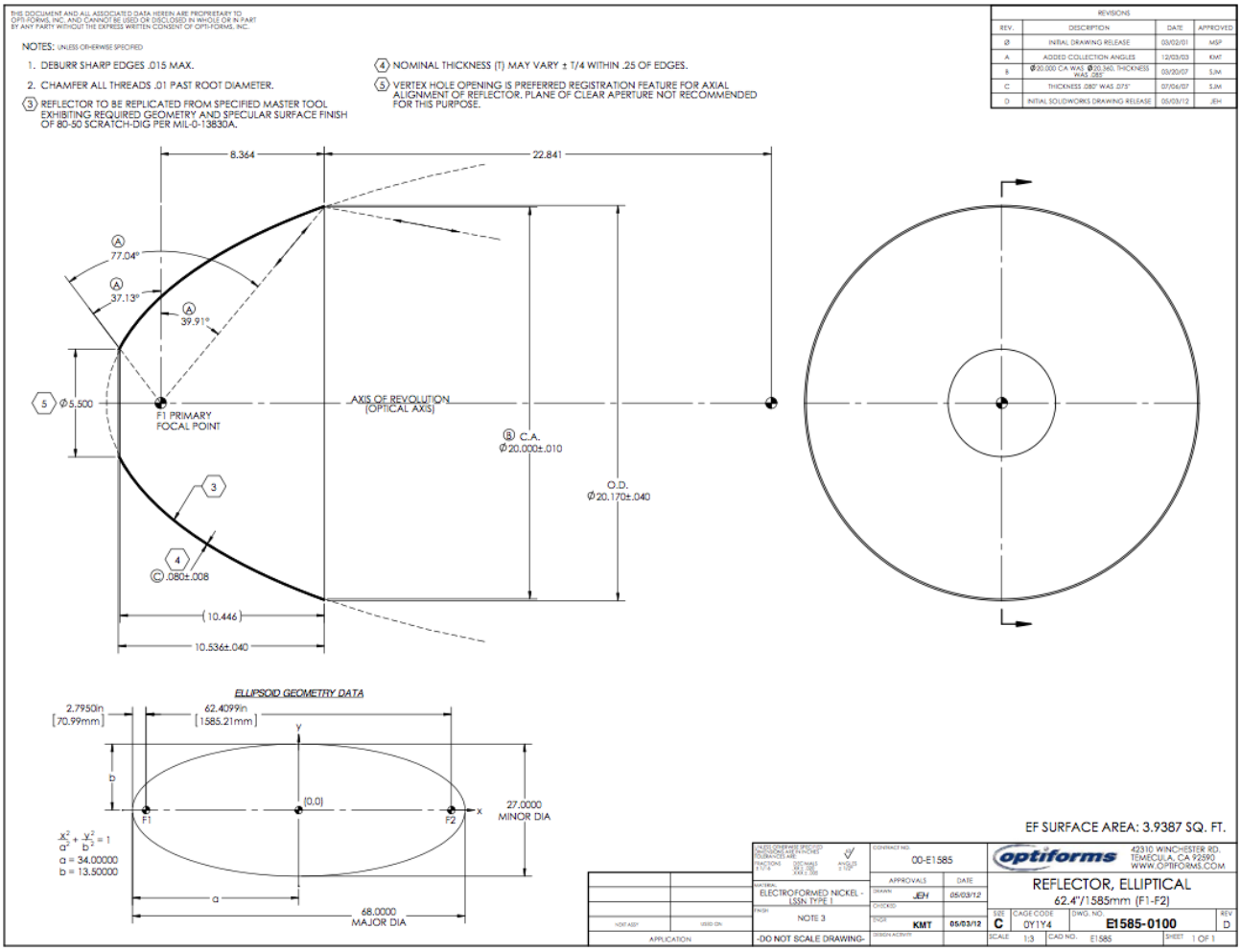

Figure 2-42: Drawing Of Selected OptiForm E1585 High Temperature Elliptical Reflector

The centerpiece of the illumination system will be the Superior Quartz SX32000D high pressure short arc xenon arc lamp bulb. This device is the highest rated power level light bulb made in the world today. It operates at 32 kW input DC power at a current of 700 amps and 45 volts in normal conditions. This bulb is 19 inches (48.3 cm) long and weighs 5.5 kg. A photograph of this bulb is provided in Figure 2-40 and a drawing of the bulb is provided in Figure 2-41. ICS Associates' Optical Systems Engineer has over 36 years of experience in optical design designing and building solar simulators and high powered light sources and has extensive experience designing systems for this class of bulb.

Figure 2-43: The Selected Power Supply Fits In Our 9U Rack On Rails, Is Water Cooled, Digitally Controlled And Has Excess Capacity For Margin

Another key feature of the lamp system is the OptiForm E1585 high temperature elliptical reflector. This nickel reflector is from a line of reflectors made by OptiForm and used extensively in the optics industry, for example in the reflector housings in IMAX theaters. This reflector is fabricated for high power applications and the elliptical design allows the arc lamp light to be brought to a focus far smaller than we will need for optical mining. The E1585 model we have selected for the ORTB has a focal length of 64 inches and is made with a highly reflective (95% across the white light spectrum) silver coating that is protected by a proprietary high temperature transparent silica layer to prevent oxidation and allow high temperature application. We have designed a custom water cooled manifold housing and support system for the E1585 reflector to physically support the reflector and the arc lamp bulb. Figure 2-42 is a specification drawing of the reflector we have selected for the ORTB. Note that the reflector material we plan to use in the laboratory experiment is also baselined for the Apis™ flight system subreflectors. In the flight system subreflectors cooling will be provided by heat pipe or pumped fluid loop radiators instead of water. Several pieces of equipment in the ORTB will require water cooling with a total water cooling load of about 35 kW. To enable this cooling we have selected a standard ColdShot ACW120E chiller which is rated as a 10 Ton chiller, meaning it can support the 120,000 BTU per hour cooling needs of the ORTB.

To run the lamp, three electrical components are needed. First we have selected a modified Magna Power T-Series 45 kW water cooled power supply (Figure 2-43) to provide the main power

during operation. This will be wired to the bulb via a double bundle of 4/O welding cables each of which is rated for 400 amps along with welding lugs and a terminal bar. This 9U power supply will be located in a 19" rack mounted on wheels on a rail in our laboratory. The other two electrical components are the starter and the booster circuits. The starter is the high voltage trigger that initially breaks down the gap between the electrodes in the bulb using a short 35KV pulse. The "Booster" is wired in parallel and contains a large capacitor that is charged up to about 220 volts and which is then made to discharge across the electrodes when the initial spark breaks it down. This 220 volt discharge produces a sustaining current for a short period of time (few 10s of msecs) to allow the main power supply to build up the current required to maintain the high current across the lamp. Required circuit elements include a 68,000 microfarad, 250 volt capacitor and a large diode that can hold off 300 volts and pass more than 800 amps continuously. It needs a terminal strip that can handle the 4 each 4/0 gauge wires that bring the current in and out of the enclosure. This will all be housed in a 19" rack enclosure for EMI shielding. These parts can be ordered from Allied Electronics. This is a custom circuit we will build.

ICS Associates employees have extensive experience building high powered light sources using these techniques and this is the standard way that arc lamps are started reliably. This method is used in IMAX movie theaters which are made with water cooled lamps of the same general type we will use in the ORTB. The starter and the booster are both boutique electrical devices made by small companies and we are familiar with their deign and construction. For example, the starter “brick” is made by LP associates, a company our team members have worked with in the past.

Mounted on top of the moving rack will be a cooling manifold and a structural support system for the lamp housing. The purpose of the lamp housing will be to support the lamp system and enclose it to contain ozone gas produced by the high intensity optical radiation and to provide stray light enclosure as an eye and skin safety measure. The movable water cooled shutter will serve two purposes and will be made from high temperature stainless steel with a high temperature black powder coating, although it will not operate near the intense focus of the beam. Its first purpose will be to provide a secondary light source “off switch” to allow optical power to be cut mechanically as part of normal operations or as a secondary safety measure. Second, the shutter will include thermocouples and water flow gauges to measure flow rate and temperature increase of the cooling water when the beam is blocked. Flow calorimetry will make this device an independent measure of system total optical power.

Table 2-6: Estimated Optical Power Output Of The ORTB Lamp Based On Best Case, Worst Case And Nominal Projections

Factor	Worst Case	Nominal	Best Case
Input Electric Power to Arc Bulb (W)	32,000	32,000	32,000
Arc Bulb Electrical to Optical Efficiency	0.3	0.5	0.65
Reflector Geometric Efficiency	0.5	0.62	0.8
Reflectivity of Reflector	0.9	0.95	0.95
Power Output (W)	**4,320**	**9,424**	**15,808**

A 20 inch blower fan will maintain a positive flow of air throughout the internal structure of the lamp shroud. This will provide convective air flow through the system to augment the water cooling system, minimize hot spots, and remove ozone that is known to build up in the presence of these high powered bulbs. The ozone is created because the lamp produces a small fraction of its optical output in the UV. When the UV radiation interacts with the oxygen in the air it produces ozone. Note that ozone ducting is a standard feature of high power light systems and such exhausting has no danger or environmental impact, as ozone gas is unstable breaking down to oxygen rapidly in the ductwork.

Small additional components for the light source system for the ORTB which we have designed and selected in detail include an X-Y scannable power meter, temperature sensors, and computer control for the power supply current, computer monitoring of the temperatures of key components, and computer monitoring of water flow rates and water temperatures. All of these functions can be easily implemented with off the self equipment from vendors such as ThorLabs and we have built up a detailed budget sheet which fits well within the Phase II limits. In addition to these major items there will be several minor subassemblies that we have identified that will require parts from McMaster-Carr and other similar vendors and welding and machining from local shops.

We performed an analysis of the power output of the lamp system in our related SBIR Phase I work. The results of this analysis are repeated here in Table 2-6 for the reader's convenience. The largest uncertainty in expected output power is the electrical to optical efficiency of the bulb. This uncertainty stems from the fact that the bulbs are rated in terms of lumens, not in terms of optical power or radiant flux and there is no clear mapping between brightness in lumens and radiant flux because lumen brightness depends on the color spectrum of the source and the sensitivity

response of the human eye. However large xenon lamps are known to produce a color spectrum very close to that of the Sun. An engineering rule of thumb for this color of light is that every 100 lumens of brightness corresponds to 1 watt of optical radiation with an uncertainty of ±20%. Using this rule of thumb, specifications for xenon arc lamps consistently project efficiencies higher than 50% at power levels above 5 kW with some manufacturers claiming efficiencies has high as 80% at 10 kW. In general, xenon lamp electrical to optical efficiency increases at higher power levels. We take a conservative, worst case, estimate for this parameter to be 30% and a best case optimistic estimate to be 65% with 50% being the most likely expected value. We would not be surprised to see efficiencies as high as 75% in operation.

Reflector geometric efficiency is the fraction of light output from the bulb that intersects the reflector. We performed an analytical point source geometric analysis for the OptiForm E1585 elliptical reflector and determined that it has a 62% geometric efficiency for an ideal isotropic point source at the focus. However, the arc lamp bulb we have selected emits its radiation radially, not axially. In fact, its geometric emission pattern is very well matched to the reflector we have chosen so the reflector efficiency for this configuration could be as high as 80%. On the other hand, the details of the emission pattern depend on anode and cathode geometry that may block the light path so we take a worst case reflector geometric efficiency to be 50% with a nominal 62% estimate. This reflector has a highly polished silvered surface with a 95% reflective specification from the manufacturer. In case the surface is contaminated we take a worse case reflectivity of 0.9 which would be appropriate for aluminum. All of these estimates are listed and summed in Table 2-6. As can be seen, the worst case projection is for somewhat more than 4 kW of optical energy and the best case is for almost 16 kW. We consider the worst case analysis to be extremely unlikely and are confident that the system will preform as per the nominal condition. Our technical judgement is that best case performance is more likely for this system than worst case. However, our research only requires worst case performance and will only benefit from higher power so we are confident that this design will be effective. We have taken a very conservative approach.

The purpose of the rail system in the ORTB is to allow the entire optical assembly to move back and forth relative to the thruster. This movement is needed to move the equipment out of the way for test setup and teardown. Between experiments we will want to “zoom” the light source in and out to provide varying spot sizes and illumination intensity levels as part of the research effort. Hence the rails are a critical part of the experiments we intend to perform in the ORTB.

The gas feed system we have designed will provide independently regulated gas flow to the front and back of the thruster with independently metered warm water vapor and carbon dioxide flows to allow measuring thruster performance and operating characteristics as a function of H_2O to CO_2 mixture ratio. The propellant flow rate we expect for the 3 kW thruster is 0.2 g/s under optimal conditions and 0.6 g/s for the 10 kW thruster. The CO_2 source will be a standard high pressure bottle from McMaster Carr with added pressure and flow regulators. The H_2O source will be a Reimers Electric Steam Boiler model number RBH10K3. Feed pressure will be 690 kPa (100 psi). The boiling point of water at this pressure is approximately 160° C (320° F) so the feed system lines will have to be electrically heated and insulated with a simple thermostat controller. By metering independent flow rate to the back of the thruster we can control how much propellant flow goes to the annular ring around the throat and then flows up the channels in the thruster body to the annual injector ring near the window. Note that this counterflow propellant is not there to cool the chamber or to assist in material survival. It is there to capture heat lost to the walls of the throat and chamber to increase thruster efficiency. This heated flow will mix with cooler gas injected directly into the annular channel near the window. Radially oriented pinhole sized injector orifices will inject the mixed propellent into the chamber downstream of the window and upstream of the solar absorber made of low density ceramic foam, effectively cooling the window and providing relatively cool gas stagnation conditions upstream of the solar absorber.

Note that there is no vacuum system or thrust stand incorporated into our baseline design. This is because we will be able to very well characterize thruster performance by measuring gas flow rate, chamber pressure, input power level, and temperatures at various places and then back out thruster efficiency and specific impulse with adequate accuracy using standard methods in common use from chemical rocket propulsion, especially for small attitude control thruster development. Note also that the laboratory thrusters we plan are nominally designed with tiny nozzles with expansion ratios of less than two as is appropriate for expansion to 1 atm. We view direct measurement of thrust in this effort as a “nice to have," but not critical. If the related SBIR on Optical Mining™ is funded, we will have a vacuum system capable of maintaining pressure levels of a few torr at these propellant flow rates but will not have a thrust stand capable of measuring fractional Newton variations in thrust for thrust levels in the 1 to 5 N range. We know that the electric propulsion group at JPL near our laboratory has such a thrust stand so if they or another NASA center could loan us a thrust stand it is possible that we could do direct thrust measurements to confirm nozzle efficiency. If this happens we would redesign the thrusters for larger expansion ratio for vacuum conditions.

2.6 Summary of Apis™ Technology Research and Development

We have completed a successful Phase I NAIC research and development effort accomplishing the following:

- demonstrated full scale Optical Mining™ confirming the validity of related (SBIR) theoretical modeling and subscale experiments;
- developed an analytical method to accurately predict the quantity of accessibility of asteroid resources for application to ISRU;
- completed analytical and computational simulations showing that both the Optical Mining™ and Omnivore™ propulsion aspects of the Apis™ architecture can be supported with optical systems that are feasible with current TRL-4 thin film inflatable reflector and structures technology;
- developed an innovative breakthrough in propulsion technology called the Omnivore™ solar thermal thruster which uses state of the art additive manufacturing technology and available high temperature ceramics in an innovative new thruster design that promises to harness astroid ISRU to eliminate the need for Earth launched propellant resupply while supplying nearly 100 times the thrust of Solar Electric Propulsion (SEP);
- designed an innovative new type of laboratory apparatus based on short arc, high pressure xenon lamp technology to make it feasible to quickly and successfully demonstrate and develop solar thermal rocket technology, especially the breakthrough Omnivore™ thruster.

3.0 Apis™ Mission-Systems Analysis

The mission systems analysis reported in Section 3 of this report shows that when the elements of the Apis™ mission system architecture are developed, they will provide a breakthrough level of benefit for NASA.

We have accomplished the following objectives:

- Defined the Apis™ mission system architecture and its component elements.
- Performed concept level flight system configuration studies of the Honey Bee™ Optical Mining™ spacecraft and the Worker Bee™ deep space tug to the level that includes definitions of major flight system components; system dimensions; and mass and performance estimates.
- Completed mission analysis showing performance benefit for two types of in space transport services: LEO to GEO transport in support of commercial business, and transport from launch to Lunar Distant Retrograde Orbit (LDRO) in support of NASA human exploration.
- Performed mission analysis for a version 1.0 Honey Bee™ flight system to deliver up to 100 tons of ice to LDRO from a three year mission post launch from Earth on a medium class rocket such as the SpaceX Falcon 9 and Optical Mining™ of a 1,000 ton water rich NEO.
- Performed a preliminary analysis of the cost savings Apis™ may provide to NASA in its use in cislunar space as a *Proving Ground* for future human exploration transitioning to *Earth Independence* in deep-space concluding that Apis™ may save NASA as much as $100B over a ten year period of human exploration beyond LEO.

Apis Architectural™ Concepts: Apis™ is named for the honeybee genus because like bees Apis™ efficiently gathers and returns useful resources and then utilizes those resources to perform useful work. In this case the resources are volatile materials from highly accessible asteroids and the useful work is transportation services for NASA's missions of human exploration of space. The Apis™ mission system architecture is depicted graphically in Figure 3-1. A space mission system architecture comprises hardware in the form of flight systems and the missions performed by that hardware. This architecture is designed with the objectives of enabling a far richer and simultaneously more affordable program of human exploration for NASA by putting in place a cis-lunar orbital infrastructure that will also enable massive new industries in space. Key new technologies invented by ICS Associates to enable the Apis™ architecture include the Optical Mining™ approach to ISRU and Omnivore™ solar thermal propulsion system. Other technologies uniquely embedded in Apis™ include thin film precision inflatable structures (currently at TRL-4), advanced optical systems design and analysis (currently at TRL-8), and advanced passive thermal control technology (currently at a range of TRLs from 4 to 8).

Figure 3-1: Graphical Representation of the Apis™ Flight System Architecture. Hardware elements of the of the Apis™ architecture include the reusable Honey Bee™ Optical Mining™ spacecraft; the reusable Worker Bee™ deep space tug, or Orbit Transfer Vehicle; and the Hive propellant depot in Lunar Distant Retrograde Orbit (LDRO). Missions supported include dedicated asteroid ISRU missions each of which brings back up to 100 tons of ice, NASA human exploration missions, commercial LEO to GEO satellite delivery and many others.

We have focussed most of our effort in this Phase I program on actual technology development as documented in Section 2 of this report. However, it is important to place our work in a mission-system context to show its benefit to NASA. To do that we have performed flight system conceptual level design as documented in Subsection 3.1 as needed to conduct mission performance and benefits analysis, which is documented in Subsection 3.2.

3.1 Apis Flight Systems Conceptual Design

The flight system elements of the Apis™ architecture include:

- the reusable Honey Bee™ Optical Mining™ spacecraft;
- the reusable Worker Bee™ deep space tug, or Orbit Transfer Vehicle; and
- the Hive propellant depot in Lunar Distant Retrograde Orbit (LDRO).

Within the scope of this Phase I effort we have applied some resources to the conceptual design of two flight systems, the Honey Bee™ vehicle and the Worker Bee™ vehicle. Our design philosophy is modular. Just as these two vehicles use the same underlying technologies, we have designed them so a Honey Bee™ vehicle is a Worker Bee™ vehicle with an Optical Mining™ module attached at the universal docking adapter on the Worker Bee™. Figure 3-2 shows the Worker Bee™ configuration design while Figure 3-3 shows the Honey Bee™ configuration. Note that important aspects of the Honey Bee™ optical configuration and design were presented in Section 2.3 of this report and will not be repeated here. It is assumed that the reader is familiar with the optical layout of the vehicle from the discussion in Section 2.

Key features of the vehicle design are the use of a standard universal docking adapter to connect the Worker Bee to payloads or to the Optical Mining™ apparatus when the unit is configured as part of a Honey Bee™ system; via ports that connect the ice storage bags to the Optical Mining™ apparatus; multi-strand guy wires that work with the inflatable structure to provide a ridged quasi-tensioned system in the deployed configuration; an inflatable thin film thermal shield that shield the ice bags from high temperature components during mining operations; and the 100 N class Omnivore™ solar thermal rocket. To drive terrestrial resupply requirements to an absolute minimum (enabling *Earth Independence*) and make maximum use of ISRU supplied resources, the attitude control functions on this vehicle use the same propellant as the primary solar thermal rocket but in an electric warm gas mode with lithium ion battery energy storage for burst power. The solar arrays are sized for 5 kW end of life power which is driven somewhat by the electric warm gas attitude control system. Note that the warm gas system includes a warm insulated accumulator which minimizes the battery requirement.

Figure 2-3: Worker Bee™ Space Tug Vehicle Configuration

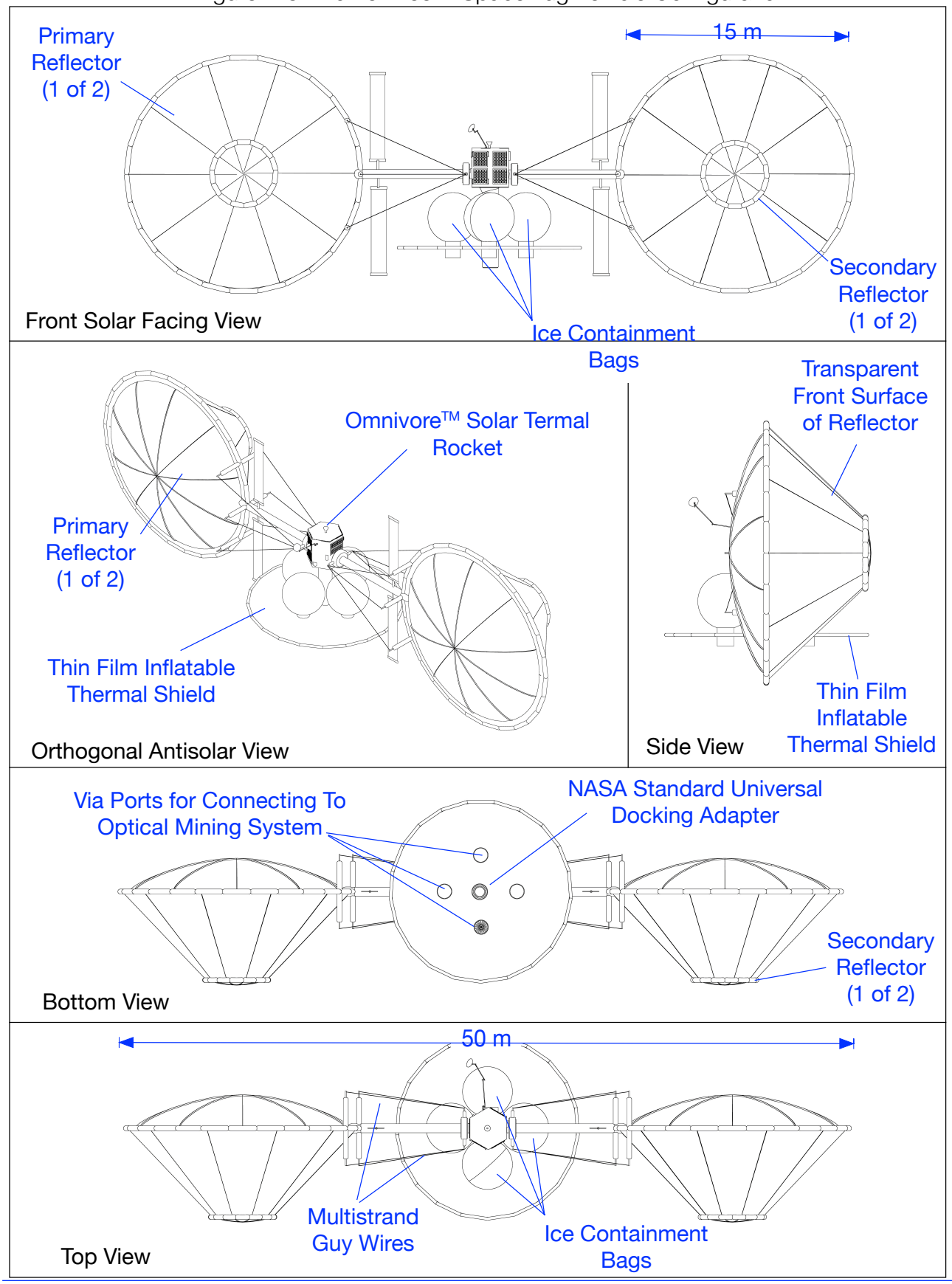

Figure 2-4: Honey Bee™ Asteroid ISRU Mining Vehicle Configuration

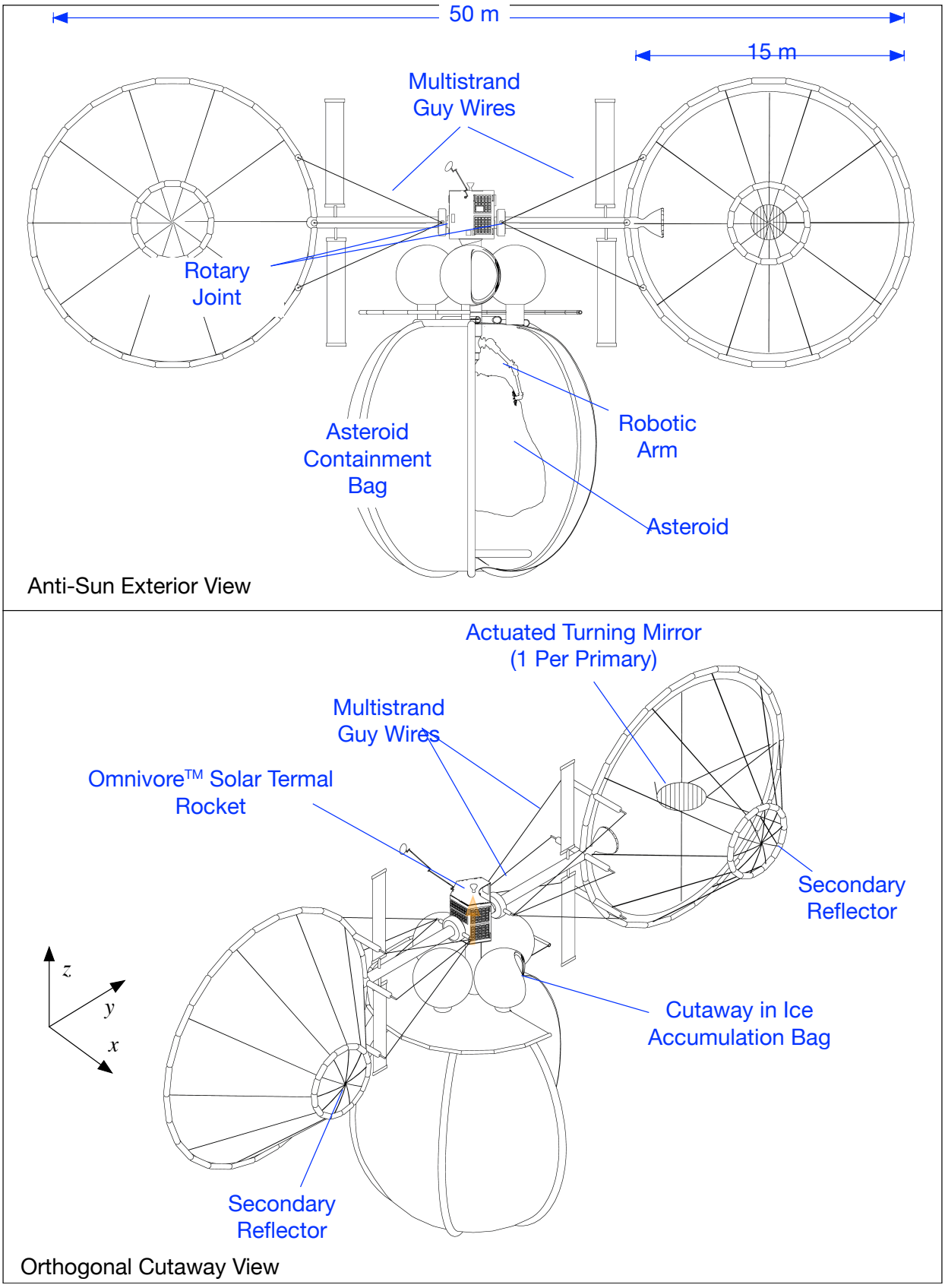

Figure 2-5: Terminal Configuration of Optical Train in Optical Mining Apparatus™. Key features include debris shield and counterflow gas to prevent contamination of the sapphire lens.

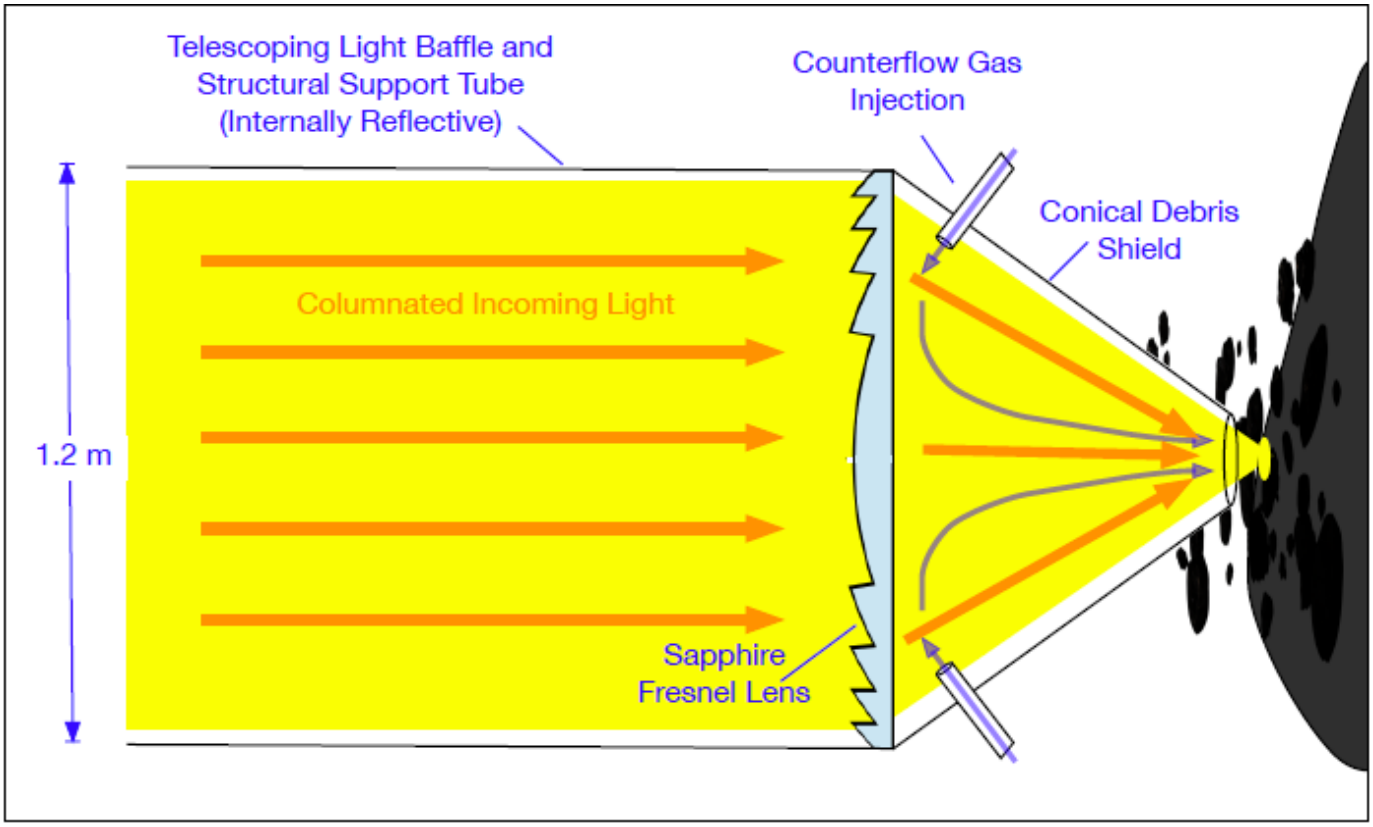

The primary additional feature of the Honey Bee™ vehicle relative to the Worker Bee™ is the Optical Mining™ apparatus comprising the asteroid containment bag, the telescoping optical baffle, and structural support tube that holds the sapphire lens that performs the final concentration of the optical beam, and the sapphire lens itself. The asteroid containment bag is based on the JPL design and technology development program for the ARM option "A" mission concept which has been documented in the open literature (see Wilcox 2015). After a significant investment in design and technology, JPL was able to elevate the readiness of this capture and containment system to TRL-4. The technology associated with the containment system includes the rendezvous and capture system, despin system, and systems for positive control of the asteroid once it is captured. Figure 2-5 shows some of the features of the Optical Mining™ apparatus not detailed elsewhere in this report. Note that to prevent contamination of the sapphire lens, it has considerable standoff distance from the actual surface of the asteroid being mined and is protected by a conical debris shield and counterflow gas which is injected behind the debris shield between the lens and the optical target. Note also that debris particles moving off the surface of the asteroid are strongly illuminated on the side opposite the asteroid. This will

Table 3-1 - Apis Mission and System Parameters Shown Relative to ARM

Mission Parameter	Baseline ARM Mission Concept	Apis™	Comment/Difference
Approximate Launch Mass (kg) to Low C3	17,000 kg (Heavy LV Required)	5640 kg (Falcon 9 FT)	Primarily Reduced By Elimination of Xenon and SEP
Development Cost	≈$1B	$500M	Large Cost Savings Through Reduction of Flight System SWAP and Elimination of SEP System
Total Flight Mission Duration (years)	3 to 8 years	1.5 to 3 years	Enabled by 5 day total STR burn time derived from higher thrust and mission to leave asteroid slag behind. Burn time increases to 50 days for full asteroid return.
Main Propulsion System Thrust (N)	1.6	68	Factor of 40 increase in thrust due to ≈4x increase in jet power and 10x reduction in specific impulse
Main Propulsion System Net Jet Power (kW)	24	100	Direct use of solar thermal energy allows for larger power at less mass
Main Propulsion System Specific Impulse (s)	≈3000	335	Electric propulsion specific impulse is mis-matched to low Delta-V mission
Delivered ΔV for Nominal 1000 MT Target (m/s)	290	290	Derived from NASA presentations, reports, and conference papers.
Required Burn Time For Nominal Mission (Days)	≈2000	<50	Enabled By High Propellant Flow Rate and Thrust of STR
Total System Cost	At least $3B including operations	Less than $1B	Reduced development cost, launch cost, and shorter mission duration.

cause them to outgas in such a way as to be propelled away from the lens. We plan to be validating these features of the Optical Mining ™ system in a related Phase II SBIR effort.

We will now present the component and system mass estimates for the Honey Bee system reminding the reader that the Worker Bee™ is the Honey Bee™ without the mining and asteroid capture and control equipment. For comparison purposes we have included the NASA ARM mission mass and performance parameters in our tables and have attempted to replicate the ARM system masses for all system elements that are similar. We are advocates of the ARM mission, and respect the work NASA has done on this mission, especially the Option “A” variant.

Table 3-2 - Top Level Honey Bee™ System Mass Rollup

	Our Estimate for ARM Option A		Honey Bee™		Comments
	Contingency	CBE Mass (kg)	Contingency	CBE Mass (kg)	
Total Launch Mass		16,916		4,714	Includes mass growth contingency as noted below.
Total Wet Element		11,869		729	Sum of other wet elements below.
Xenon		10,958		0	
Other Propellant		877		701	Bipropellant for ARM, water for Honey Bee
Pressurant		34		27	
Total Dry Element		5,047		3,986	We have applied a 30% mass growth contingency ARM on dry elements
ARM Asteroid Capture System		918			Based on Wilcox 2015 paper
Honey Bee Asteroid Capture and Extraction System				1,273	Based on Wilcox 2015 paper with added robotic arms, internal net system, and optical mining elements.
Instruments	0%	35	0%	35	Identical instrument payload taken from Brophy papers.
Power	30%	909	30%	151	Honey Bee power system sized for 5 kW spacecraft.
Propulsion – SEP		739			Taken as given in Brophy Paper
Honey Bee Reflector System			45%	189	Sized from L'Garde scaling equations based on dimensions provided in configuration drawings. Includes all hardware and inflatant.
Propulsion – STR			28%	574	See propulsion system mass detail.
Propulsion – RCS	10%	163	10%	163	We have been able to replicate top level masses of subsystems for ARM as provided in published Brophy papers based on component buildups.
ADACS	10%	44	10%	44	See buildup details in additional tables.
C&DH	13%	23	13%	23	See buildup details in additional tables.
Comm	14%	53	14%	53	See buildup details in additional tables.
Thermal	27%	324	30%	84	Radiators scaled for ARM to account for PPU thermal load
Structures and Mechanisms		674		476	Structures is close for ARM papers only if the LV adaptor (approx. 1120 kg) is removed. Honey Bee also excludes LV adaptor

We have tried to leverage the significant investment NASA and JPL have put into mission definition for the ARM mission. It is useful to compare the performance of the Honey Bee™ system with the ARM system to understand the power of the Apis architecture. We have created a conceptual-level design of the Honey Bee™ mission-system to be confident of system performance and mass based on spacecraft scaling laws, physics-based estimates of the unproven technologies, and conservative margins. ΔVs and trip times have been estimated based on ARM-like trajectories with higher thrust STR propulsion. Although neither NASA nor JPL have published detailed component mass breakouts for ARM, Brophy has published subsystem level mass estimates which we have been able to replicate within a few percent by using our proprietary Team X like scaling equations and component databases. We note that Brophy's papers on the Option "A" variant have a smaller mass for the asteroid capture mechanism than Wilcox's more recent paper on the subject, so we used Wilcox's capture system mass numbers in both our ARM comparison and our Honey Bee™ design.

Table 3-1 shows the top level results of this design and analysis, also showing ARM mission-system parameters for comparison. Total system launch mass for Apis™ with mass growth

Table 3-3 - Power System Mass Estimates

Item (ARM)	CBE Mass per Unit (kg)	# of Units	CBE Total Mass (kg)	Componen Contingenc	Predicted Mass (kg)	Comments
Total			699.10	30%	908.83	Sum
Li-ION (Secondary Battery)	7.90	4	31.60	30%	41.08	Based on standard scaling equations.
Solar Array	250.00	2	500.00	30%	650.00	Scaled from Ultraflex data plot
PPUs for EP	26.00	5	130.00	30%	169.00	Scaled from existing 5kW PPU
DC-DC (120V to 28V) converter	10.00	1	10.00	30%	13.00	Estimate from commercial units
Chassis	7.80	1	7.80	30%	10.14	Based on standard scaling equations.
Load Switches Boards	0.80	2	1.60	30%	2.08	Built up from component database
Thruster Drivers* Boards	0.80	2	1.60	30%	2.08	Built up from component database
Pyro Switches* Boards	0.80	2	1.60	30%	2.08	Built up from component database
Houskeeping DC-DC Converter Boards	1.00	2	2.00	30%	2.60	Built up from component database
Power/Shunt Control* Boards	1.00	2	2.00	30%	2.60	Built up from component database
Battery Control Boards	0.80	4	3.20	30%	4.16	Built up from component database
Diodes* Boards	0.80	8	6.40	30%	8.32	Built up from component database
Shielding	1.30	1	1.30	30%	1.69	Built up from component database

Item (Honey Bee)	CBE Mass per Unit (kg)	# of Units	CBE Total Mass (kg)	Component Contingency	Predicted Mass (kg)	Comments
Total			116.24	30%	151.12	Sum
Li-ION (Secondary Battery)	7.90	4	31.60	30%	41.08	Based on standard scaling equations.
Solar Array	28.57	2	57.14	30%	74.29	scaled from Ultraflex data plot
Chassis	7.80	1	7.80	30%	10.14	Built up from component database
Load Switches Boards	0.80	2	1.60	30%	2.08	Built up from component database
Thruster Drivers* Boards	0.80	2	1.60	30%	2.08	Built up from component database
Pyro Switches* Boards	0.80	2	1.60	30%	2.08	Built up from component database
Houskeeping DC-DC Converters* Boards	1.00	2	2.00	30%	2.60	Built up from component database
Power/Shunt Control* Boards	1.00	2	2.00	30%	2.60	Built up from component database
Battery Control Boards	0.80	4	3.20	30%	4.16	Built up from component database
Diodes* Boards	0.80	8	6.40	30%	8.32	Built up from component database
Shielding	1.30	1	1.30	30%	1.69	Built up from component database

Table 3-4 - Optical Mining™ System Mass Estimates

Item	Unit Mass (kg)	Units	Mass (kg)	Mass Growth Contingency	CBE Mass (kg)	Comments
Total					1872.67	
ARM Capture Module					918.3	From Wilcox paper. Includes structures and mechanisms, petal assemblies, actuators, soft goods, inflation system, thermal, harness, and sensors
Honey Bee Additions Total			636.25	50%	954.37	Sum
Honey Bee Robot Arm		2	135.72	50%	203.58	Sum from below
Arm Segments	11.31	4	45.24	50%	67.86	Titanium
Joints	22.62	4	90.48	50%	135.72	Titanium
Motors	1.00	4	4.00	50%	6.00	Ducommun commercial stepper motors
Telescoping Tube Assembly			500.53	50%	750.80	Sum from below
10m telescoping tube	100.53	1	100.53	50%	150.80	Assumes 5 mm thick nickel with silver coating on the inside covered with deposited fused silva liner. Outside surface thermal black
Sapphire Lens	400.00	1	400.00	50%	600.00	Based on 4 gm/cm^3 density and optical geometry

Table 3-5 - Inflatable Concentrator and Optics Mass Estimates

Item	CBE Mass per Unit (kg)	# of Units	CBE Total Mass (kg)	Component Contingency	Comment
Reflector(s) (Primary and Secondary)	40.57	2.00	81.15	45%	L'Garde Analysis 15m. SMCC with F/D of 0.5 including reflectors and booms. Sum from below
Wire support	1.50	1	1.50	45%	150 m of 220 kg breaking strength wire
Booms	5.10	4	20.39	45%	L'Garde flight system mass scaling equations.
Boom Rotary Joints	2.92	2	5.84	45%	see calculations below
Motor for Boom rotation	1.00	2	2.00	45%	Ducommun stepper motors and support hardware
Boom Rotation Gearbox	2.00	2	4.00	45%	Avoid Housed Brushless DC catalog V2 4
Couplers for Solar Array attachment	2.92	2	5.84	45%	Mass estimate based on mechanical layout
Fixed Mirrors	2.94	2	5.88	45%	One at the base of each reflector to send light down the boom tube
Rotating Mirrors	2.94	1	2.94	45%	Allows for switching modes between ISRU and STR
Motor for Rotating Mirrors	0.50	1	0.50	45%	Ducommun reversible stepper motors
Mirror Rotation Gearbox	0.50	1	0.50	45%	Avior Housed Brushless DC catalog V2 4
Total Mass			**130.53**	**45%**	

contingency is under 5640 kg, about 1/3 that of ARM and within the throw capacity of a Falcon 9 Full Thrust, the latest version of the Falcon 9. The primary areas of mass savings for Apis™ include the 10 tons of xenon propellant that Apis™ does not have to carry due to the plan to harvest propellant from the target, 500 kg of solar array, and 130 kg of power management hardware that we estimate ARM has to carry for the 40 kWe SEP system. Areas in which mass is higher for Apis include the inflatable structures and the Optical Mining™ assembly. The overall Honey Bee™ vehicle is lower in mass and thus structures, thermal control, and attitude control system masses are also all less. Shorter return trip time is afforded by obviating the need to bring back the entire asteroid and the 100x higher thrust of STR versus SEP. Focussing on just system mass, Table 3-2 is a rollup of total system mass estimates. Detailed mass summaries for key

Table 3-6 - Solar Thermal Propulsion and Omnivore™ Subsystem Mass Estimate

Item (Honey Bee)	CBE Mass per Unit (kg)	# of Units	CBE Total Mass (kg)	Component Contingency	Predicted Mass (kg)	Comment
STR System Total			437.86	28%	573.62	
STR Thruster	25.01	1	25.01	50%	37.51	Scaled from Sercel JANNAF paper equation. Includes 50% contingency
Fuel Tanks and Feed System			412.85	6%	536.11	Sum
Gas Service Valve	0.22	2	0.44	2%	0.45	Database of TRL-9 flight components
HP Latch Valve	0.37	1	0.37	2%	0.38	Database of TRL-9 flight components
Solenoid Valve	0.36	2	0.72	2%	0.73	Database of TRL-9 flight components
HP Transducer	0.27	1	0.27	2%	0.28	Database of TRL-9 flight components
Gas Filter	0.10	1	0.10	2%	0.10	Database of TRL-9 flight components
NC Pyro Valve	0.20	1	0.20	2%	0.20	Database of TRL-9 flight components
Temp. Sensor	0.01	2	0.01	2%	0.01	Database of TRL-9 flight components
Liq. Service Valve	0.30	1	0.30	2%	0.31	Database of TRL-9 flight components
Test Service Valve	0.24	1	0.24	2%	0.24	Database of TRL-9 flight components
LP Transducer	0.27	4	1.08	2%	1.10	Database of TRL-9 flight components
Liq. Filter	0.45	1	0.45	2%	0.46	Database of TRL-9 flight components
LP Latch Valve	0.36	2	0.72	2%	0.73	Database of TRL-9 flight components
NC Pyro Valve	0.17	4	0.68	2%	0.69	Database of TRL-9 flight components
Mass Flow Control	0.05	1	0.05	2%	0.05	Database of TRL-9 flight components
Temp. Sensor	0.01	10	0.10	2%	0.10	Database of TRL-9 flight components
Lines, Fittings, Misc.	5.00	1	5.00	50%	7.50	Mass estimate based on layout
Water Tanks	100.53	4	402.12	30%	522.76	Standard flight tank sizing equations. Note; These are accumulator tanks inside the spacecraft.

subsystems are provided in Tables 3-3 through 3-6. Table 3-3 is our power system mass buildup. Table 3-4 is the mass summary for the Optical Mining™ apparatus. The inflatable solar concentrators, booms, guy wires, and subreflector mass estimates are provided in Table 3-5. Finally, the Solar Thermal Rocket propulsion subsystem mass buildup is provided in Table 3-6 which also includes the Omnivore™ thruster mass estimate. The comments columns in these tables document the design philosophy or technical approach we took in each case. Mass buildups for standard subsystems such as avionics, thermal control and structures were performed using industry standard mass scaling equations and commercially available space qualified parts databases and are not repeated here.

3.2 Apis™ Mission Performance and Benefits Analysis

Although is not limited to just these missions, the Apis™ architecture has been designed primarily to support the following missions (in chronological order):

- the version 1.0 Honey Bee™ mission to deliver up to 100 tons of ice to LDRO from a three year mission after launch from Earth on a medium class rocket such as the SpaceX Falcon 9 and Optical MiningTM of a 1,000 ton water rich NEO;
- subsequent Honey Bee™ missions staged out of LDRO, each returning up to 100 tons of ICE to the Hive™(Each Honey Bee™ will fly its first ISRU mission directly from launch and then operate out of LDRO on subsequent missions);
- a variety of types of cis-lunar and planetary transportation services missions performed by the reusable Worker Bee ™ space tugs.

The types of cis-lunar and planetary transportation services missions performed by the Worker Bee ™ space tugs include:

- delivery of crew vehicles with astronauts and mission support hardware to LDRO in support of NASA human exploration (presumably a NASA outpost at LDRO);
- delivery of commercial satellites from LEO to GEO;
- delivery of crew vehicles with astronauts to NEOs on missions of exploration;
- delivery of crew vehicles with astronauts to trans-Mars injection on missions of exploration;
- delivery of unmanned planetary spacecraft on interplanetary injection.

Section 1 of this report provided an operational view diagram of the Honey Bee 1.0 mission profile in Figure 1-8 and showed that the Worker Bee™ space tugs will typically return to LDRO to replenish propellant between missions in Figure 1-7. It is conceivable that Worker Bees™ will be used in an expendable mode when propelling payloads on missions with high C_3 outside of cis-lunar space. When this is the case we anticipate that vehicles near end of life will be used. Although not unique to the Apis™ architecture, our approach also depends on sophisticated satellite servicing systems for transfer of payloads and propellant between robotic systems and upgrade or replacement of modular components robotically. This study did not delve deeply into

the question of robotic servicing as robotic servicing is known to be an active area of research both within and beyond NASA. Not all components of the Worker Bee™ and Honey Bee™ systems will be equally reusable. We anticipate that most hardshell components such as spacecraft bus structures, power systems, computers, and thrusters will be designed and qualified for a typical commercial spacecraft life of 10 to 15 years, but our analysis suggests that it will be more cost effective to replace certain key components such as the inflatable structures on shorter time scales using satellite servicing technology. All inflatable structures in this study have been sized based on a five year mission life and are assumed to be replaced after 3 years in the case of Worker Bee™ space tugs or after each 100 ton ISRU mission in the case of Honey Bees™.

However, this has a negligible effect on system economics as we project the recurring cost of the inflatable structures to be in the hundreds of thousands of dollars per unit based on commercial manufacturing processes. The mass of the reflector system for a full replacement is less than 150 kg. The mass of the inflatable Optical Mining™ equipment is larger, projected to be approximately 1,300 kg per vehicle which sets an upper limit on the Mass Payback Ratio of the Honey Bee™ ISRU system of about 100 to 1 in LDRO. We anticipate that over its lifetime each Honey Bee™ vehicle will be able to return about 400 tones of ice to LDRO. To do this will require one Falcon 9 or equivalent launch for the first mission and then the equivalent of one additional launch to supply the three sets of additional inflatable hardware modules over the lifetime of a Honey Bee™ vehicle. Hence, we anticipate that the equivalent of two Falcon 9 launches will be required to supply 400 tons of propellant at LDRO. Therefore, if NASA's human exploration program requires an average of 400 tons of propellant at the top of the cis-lunar gravity well per year, on average NASA will have to launch one reusable Honey Bee™ vehicle and one inflatable structures replenishment mission (to refurbish three Honey Bee™ vehicles) each year. The Honey Bee™ vehicle fleet size in steady state to supply 400 tons per year to LDRO is ten vehicles. It will probably make sense to build the Honey Bee™ fleet up to this size over a period years.

Alternatively, some of the resources of the Honey Bee™ fleet could be devoted to bringing the regolith slag left over from the Optical Mining™ process to LDRO for use as radiation shielding. If 25% of Honey Bee™ missions use all of their ISRU derived propellant to bring slag LDRO for building material and radiation shielding, the quantity of propellant provided drops to 300 tons per year but up to 1,000 tons of regolith slag can be delivered per year. This would yield up to 10,000 tons of radiation shielding or raw materials for station fabrication over a ten year mission model.

This early in an architecture driven technology effort it is difficult to make reliable cost estimates, but it is instructive to perform approximate or first order cost analysis to get an idea of the potential savings from a new system. We have performed such a simplified analysis. For comparison, a typical 15 kW GEO communications satellite cost on average about $250M and is more massive than a Honey Bee™. We anticipate that the first Honey Bee™ vehicle may cost as much a $500M to develop, but subsequent units will be considerably cheaper than communications satellites if developed and manufactured using commercial like methods. However, if each Honey Bee™ vehicle costs a liberal allocation of $250M, the cost of a fleet of ten vehicles including $500M of nonrecurring engineering could be as much as $3B. They would also require ten Falcon 9 launches at $80M each to get the vehicles into space and ten Falcon 9 launches at $80M each for inflatable structures resupply for a total launch cost of $1.6B This is assuming launch vehicle prices don't come down. We think they will. Using a commercial flight vehicle operations model but modified based on current JPL approaches, we think mission operations costs for the fleet of ten vehicles can be 100 $M/yr, or $1B over ten years. We project that the total cost for 4,000 tons of propellant delivered to LDRO over ten years to be $5.6B, or $1,400.00 per kilogram. Current projected launch costs for delivering payload to LDRO for the SLS is uncertain but typically estimated to be $40,000 per kilogram, or $160B for delivering 400 tons to LDRO. This would consume most of the NASA budget.

The Honey Bee system has the prospect of saving NASA about $155B or about $15B/yr if the ice the Honey Bee vehicles deliver can be used efficiently. Using that ice efficiently to deliver transportation services is the role of the Worker Bee™ system. The Worker Bee™ systems are to be used primarily in cis-lunar space where mission duration is much less than the Honey Bee™ ISRU missions. The ISRU missions will typically have round trip flight times in the 3 to 5 year range. For this reason, a much smaller Worker Bee™ fleet will be required. Assuming each Worker Bee™ can fly a round trip mission every two months a fleet of three vehicles will be able to perform 18 missions per year. We anticipate this number to be sufficient to meet any projected NASA cis-lunar mission model to LDRO, even considering the need for spares in the case of a vehicle failure. As described in section 3.2 of this report, the Worker Bee™ vehicles are simpler and lighter than the Honey Bee™ systems.

Worker Bee™ tugs eliminate the need for high energy upper stages and multiply rocket throw capacity by more than twice that which is possible with such stages, cutting resupply launch cost by up to a factor of 4. Aerobraking and use of Worker Bees™ for other elements of the transportation network are expected to bring a net 10x launch vehicle cost reduction.

If we assume the economics for the Worker Bee™ vehicles are the same as the Honey Bee™ systems, total development, recurring, launch and operations costs over a ten year period for performing up to 180 missions in cis-lunar space comes to $2.73B. We have no idea what it would cost to perform these missions with baseline NASA approaches, but we know that NASA has optimistically projected a cost of $500M per SLS mission. Our analysis suggests that by using reusable Worker Bee™ systems in place of expendable upper stages, or OTVs resupplied from propellant launched up from the Earth, we eliminate the need for approximately half of the SLS system launches. If than number is 90 launches, the savings are potentially as high as $45B. We are not claiming to have done a complete enough cost and mission analysis to defend these estimates (NASA spends millions every year on such studies across headquarters and its field centers) against those who would prefer a more conventional approach, but we do suggest that the work we have done shows promise. There is a very real possibility of large cost savings from the Apis™ system and the savings could be enough to multiply NASA's effective productivity considerably in the coming decades.

Figure 3-6 Worker Bee™ Performance for LDRO Cargo Mission

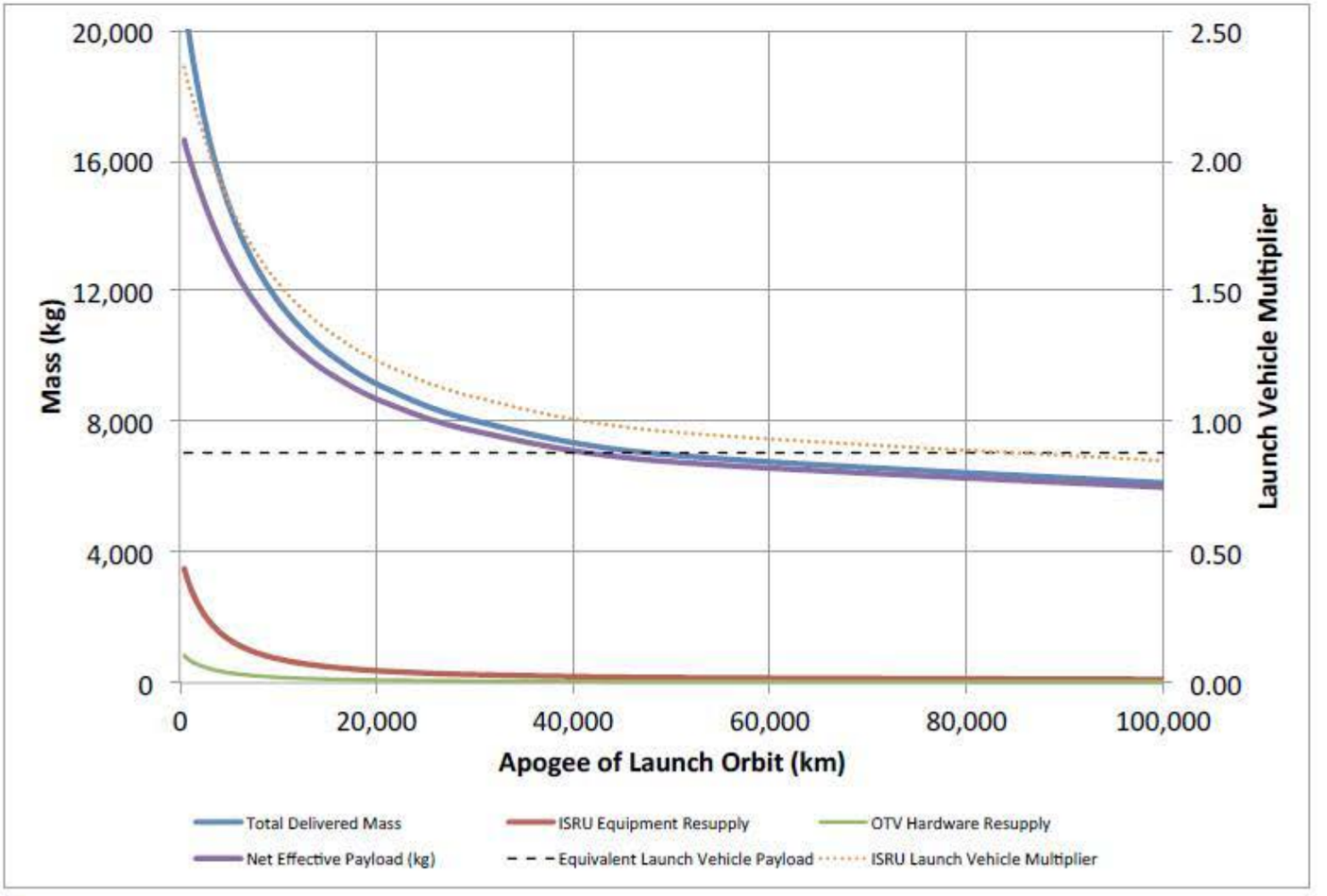

We have designed the Worker Bees™ transportation network to be confident of system performance and mass based on spacecraft scaling laws, physics-based estimates of the unproven technologies, and conservative margins. ΔVs and trip times have been estimated based on impulsive trajectory approximations with adjustments made for gravity loss and other factors. Figure 3-6 provides a parametric analysis of the effect of Worker Bees OTVs for cargo transfer between the injection orbit of a launch vehicle and LDRO. The OTVs are assumed to rendezvous with the launch vehicle payload and take it the rest of the way to LDRO. The apogee of the launch orbit is varied between 400 km (circular LEO) and 100,000 km to determine the optimum rendezvous altitude for payload transfer. Each Worker Bee is assumed to be able to complete the round trip 10 times prior to hardware retirement.

As stated previously, propellant for the Worker Bees is supplied from the Hive™ water depot in LDRO. The launch vehicle is modeled as a medium-heavy system based on LOX-RP1 with a LEO payload capability of 20,000 kg. For the comparison case without Worker Bees, the launch vehicle is assumed to use a LOX-LH2 high energy 3rd stage for direct delivery of cargo to LDRO.

Figure 3-7 Concept of Operations for GEO Satellite Transport

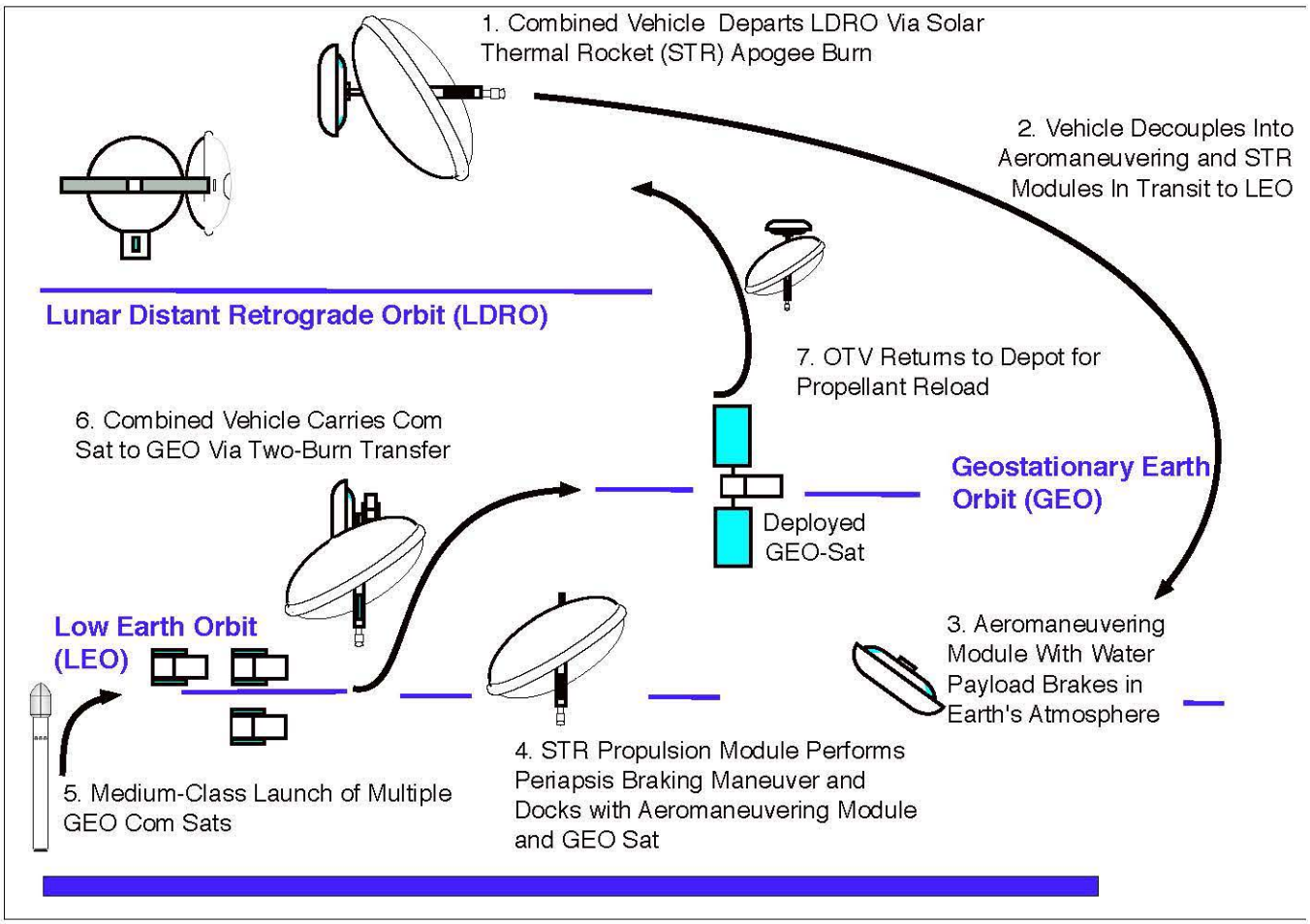

Worker Bees™ is fully penalized for ISRU equipment resupply and OTV equipment resupply in the purple line labeled "Net Effective Payload". The launch vehicle multiplier (read on the right-hand axis) is the ratio of the net effective payload with Work Bees to the payload of the launch vehicle with the expendable high energy upper stage. No aerobraking is assumed. The results of this study show that:

i) the optimum altitude for Worker Bees to pickup payload for delivery to LDRO is LEO, and
ii) even without aerobraking, the net effective launch vehicle payload is more than doubled by the use of Worker Bees supplied from LDRO in place of rocket 3rd stages.

We have also performed an aerobraking-based analysis for LEO-GEO transport in which Worker Bees are built in two modules, one of which aerobrakes as shown in Figure 3-7. We have found that on recirculating routes, aerobraking more than doubles the mass benefit.

4.1 Technology Readiness and Risk Assessment

The Apis™ architecture has been under development at the conceptual and mission concept level by the PI of this effort since 2013, but the critical technological innovations that will enable Apis™ to have a strong mission benefit for NASA's new evolvable exploration campaign came into being in 2015. These core innovations, each of which has been advanced by this NIAC study are:

- the Optical Mining™ method of asteroid ISRU which was originated in January of 2015,
- our new method of statistical analysis of asteroid resource accessibility which combines the Granvik NEO model with models of asteroid composition and taxonomies plus a mission design model,
- the Omnivore thruster which promises to virtually eliminate the need for propellant resupply from Earth by directly utilizing asteroid ISRU effluents and enable NASA's stated move to prove *Earth Independence* in space operations,
- the Omnivore Rocket Test Bed (MRTB) which will be the first low cost, practical, indoor laboratory facility for solar thermal propulsion and will enable the rapid proof of concept of the Omnivore™ thruster, and
- the Apis™ architecture concept including the design concepts for the Worker Bee™ and Honey Bee™ vehicles.

Each of these technologies was at TRL 1-2 at the beginning of this effort in the sense that the concepts had been formulated, but there had been no experimental proof or detailed analysis to prove feasibility. Now at the conclusion of this study their TRL's have been elevated as follows:

- Optical Mining™ is elevated to TRL-4 based on NIAC-funded conduct of full-scale demonstration validating analytical modeling and subscale experiments performed under separate SBIR sponsorship.
- Statistical analysis of asteroid resource accessibility is elevated to TRL-3 based on proof of concept computational demonstration of integration with mission taxonomic models.
- The Omnivore™ thruster has been elevated to TRL 2-3 based on conceptual level design and analysis of both full scale operational engines and laboratory scale development articles. Critical proof of concept studies completed here include gas dynamic performance analysis, thruster sizing analysis, and first order solar thermal coupling and thermal analysis. Achieving complete TRL 3-4 will require fabrication level optical, thermal, and mechanical design and analysis and initial test runs of low fidelity thrusters.
- ORTB to TRL-3 based on a complete test bed design including selection of all major components and systems. This facility concept will rapidly go from TRL-3 to full maturity when we build and operate it in our Phase II NIAC activity.
- The Apis architecture is at TRL-3 based on detailed modeling and simulation of the riskiest aspect of the vehicle concepts, namely the high performance optical train based on inflatable optical components.

Critical risks going forward in each of these areas as follows:

Optical Mining™: We need to confirm that the process can be scaled to even higher power levels and long durations (hours, days, and weeks) and that the process can be modulated to control the breakup of the asteroid in a systematic and controlled way. In addition, we need to confirm that methods to ensure that windows and lenses do not become fouled and fail will be successful. Achieving TRL-5 will require a microgravity demonstration in orbit. Achieving TRL-6 will require an in-space demonstration of a complete integrated flight system with a macroscopically large (≈100 kg) asteroid simulant. Achieving TRL-7 will require development and flight of a full scale Optical Mining™ asteroid ISRU mission such as the Honey Bee Version 1.0 mission described in other parts of this report.

Statistical Analysis Of Asteroid Resource Accessibility: This method is analogous to the technologies the mining and fossil fuel industries have established for the statistical assessment of mineral and energy reserves. They have developed standard techniques for reserve estimation based on a combination of scientific, engineering, and economic tools. In the work we have performed in this NIAC study we have retired most of the risk in this area in terms of proving that this process can be done with low computational cost and random error. The greatest risk in this area going forward has to do with the fundamental systematic error in asteroid distributions in terms of taxonomic type, composition, and orbital position. That systematic error or uncertainty is limited by our observational programs to locate, track and characterize the NEO population. Until now NASA's NEO observational programs have been targeting only bodies larger that about 100 m in diameter based on Earth impact risk mitigation. This observational effort will certainly help us reduce the systematic errors in our models, but if we are going to be successful we will need a more aggressive telescopic observation program including both ground and space based telescopes, better radar, and more high resolution spectroscopy. If NASA is going to move to an *Earth Independent* operational posture in cis-lunar space in the coming years, NASA will by necessity have to make use of asteroid resources and will need to step up its efforts in these areas.

The Omnivore™ Thruster: The greatest technical risk impeding mission application of the Omnivore™ thruster has to do with control of the thruster performance coupled with the control structures interactions in the physical and optical dynamics of the flight system. Retiring this risk will require that we first prove the operation of the Omnivore™ thruster in the ORTB, initially at power levels of a few to several kilowatts and then at power levels in the 100s of kilowatts. In parallel with the later full scale thruster development on the ground we will need to flight

demonstrate an Omnivore™ thruster integrated with an inflatable optical solar concentration system at a power level of a few to several kilowatts. Then in order to reduce this technology to practice at TRL 6-7 we will need to fly a complete integrated high power Omnivore™ solar thermal rocket mission in space.

ORTB: The ORTB is an important innovation that will make the ground based development of solar thermal rockets practical and affordable for the first time, but the technological risks in developing this system are not high. We will reduce the ORTB to practice in our proposed Phase II NIAC activity and in so doing elevate the TRL of the ORTB and the Omnivore™ thruster.

Apis™ Architecture: The Apis™ architecture cannot be separated from the risks associated with Optical Mining™ and the Omnivore™ thruster. Hence, the most important architectural risks are the risks we have identified in those two areas. In addition to those there is considerable risk still at the architecture definition and mission benefits level. To retire these risks we recommend that NASA initiate a multi-center mission system design activity focussed on the Apis™ architecture performing engineering design and analysis covering all aspects of the Apis™ system in collaboration with ICS associates and our industrial and university partners. NASA has articulated a powerful new strategy of *Earth Independence* in its policy documents. Given the clear benefits of asteroid ISRU and the power of the Apis™ concept it is critical that NASA work with us to perform these needed mission system design and benefits analysis.

4.2 Technology and Mission Development Roadmap

In this study we have developed a technology roadmap for achieving mission readiness for the Apis™ architecture. The roadmap addresses proposed focused technology developments (for example in a Phase II NIAC effort, a Phase II SBIR, a Game Changing Development (GCD), and a NextStep flight experiment), focussed studies, and a series of flight demonstration efforts.

The roadmap of technology development projects that build toward the Apis architecture includes the following:

1. Complete our SBIR and NIAC Phase II efforts, each of which we plan to be 14 month projects, faster than normal. The SBIR effort will be to perform a series of large scale (10 kW) demonstrations and tests of Optical Mining™ on a variety of asteroid simulants to gain high confidence in the technology and bring it to TRL 4-5. The NIAC Phase II effort will be to build and operate a multi kilowatt Omnivore thruster™ to prove operation with unrefined propellants.
2. Perform the flight experiment on ISS that we designed under our SBIR Phase I contract to demonstrate Optical Mining™ in space. We estimate this effort will cost $5M and take 18 months for experiment development. This demonstration involves the use of a small inflatable solar concentrator and Optical Mining™ of a 1 kg meteorite with mined water returned to Earth in a Dragon vehicle.
3. Build and fly a fully functional free flying but subscale (≈200 kg) Apis spacecraft in LEO demonstrating both Optical Mining™ on a 100 kg artificial asteroid and then use the mined propellant from that demonstration to maneuver the spacecraft in LEO flight demonstrating the viability of the Omnivore™ propulsion system. We estimate that this will be a two year development effort at a contract cost of approximately $50M.
4. Perform an ARM scale but ISRU-focused mission to a water rich 1,000 ton NEO, extract 100 tones of water and carbon dioxide, and use Omnivore™ propulsion to bring that water to LDRO. We estimate that this will be a $250M, three year spacecraft development if done using commercial methods and will require a Falcon 9 class launch vehicle and three years of mission operations.
5. In parallel to the above, complete the development of numerous ancillary but critical technologies such as complex inflatable structures, high powered optical systems designs for propulsion and mining, and remote asteroid prospecting technology. The cost of this technology work will be a few hundred million dollars if done using commercial, private sector methods under NASA contract.

The simplified technology roadmap is shown in Figure 4-1. We recognize that many elements of the Apis™ system that were only touched on in this limited Phase I study and report will require

efforts as large or larger than this entire Phase I effort. As part of out Phase II study we look forward to working with NASA to detail a more complete technology roadmap. However, we are confident that this roadmap provides the key features of an effort that can quickly be turned into a an innovative, advanced, game changing, next step for NASA. This technology is designed to create a *tipping point* for the space program. It is time to move the nation and the world into a new era of space exploration and development.

We understand that the cost and schedule of this roadmap seems optimistic, but it is possible to do this work for these costs at these schedules if the work is performed using private sector contracting methods akin to those NASA has used on the COTS program. With such an approach this roadmap can be completed in less than a decade for less than a billion dollars for in space cargo transport. As has been the case with COTS, crew transport would require an additional increment. Once this work is complete, Apis™ will open entire new vistas for NASA human exploration and for private sector businesses in space. The asteroids are the Stepping Stones to humanity's sustainable future in space. We urge NASA and STMD to aggressively pursue this historic opportunity. All of the technologies discussed in this RFI response are dual use, for commercial industry and NASA.

Figure 4-1: Simplified Technology Roadmap for Development of Apis™ Technologies and Systems Through First Use

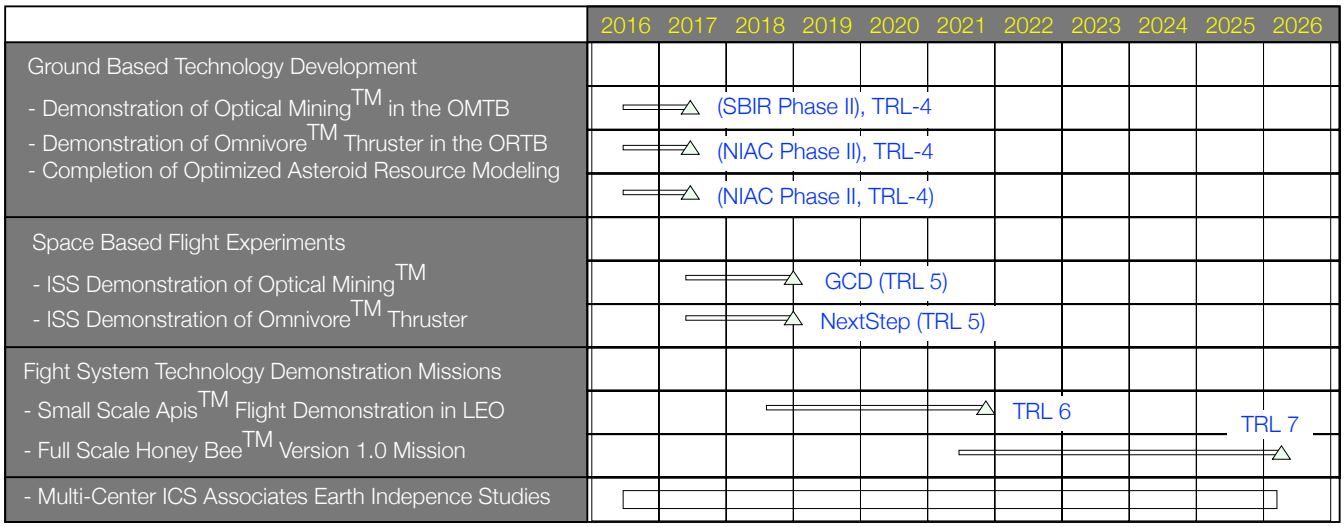

4.3 Suggested Approach for Public-Private Partnership

As we have stated previously in this report, the NASA Advisory Council has identified "a mismatch between NASA's aspirations for human spaceflight and its budget" to be "the most serious problem facing the Agency" (Squires 2014). Total cost of planned human exploration missions is strongly driven by the need to launch large quantities of rocket propellant, drinking water, oxygen, and radiation shielding. If made plentifully available in cis-lunar space, water can be used directly as propellant in Solar Thermal Rockets (STRs) to provide inexpensive transportation. Resources are available in highly accessible near Earth asteroids to enable a more cost effective approach. **The most effective way to build an asteroid supplied cis-lunar transportation architecture is through a public-private partnership model** with NASA funding technology development through approximately TRL-6. This NASA leadership can then be followed by joint NASA private sector sponsorship for development of commercially owned vehicles and systems that can provide NASA with asteroid resources and in-space transportation services. This model is somewhat like the current ISS Commercial Cargo and Crew programs but involves an earlier, lower TRL role for NASA. We call this joint public private approach to using the asteroids to open the solar system to humanity, the *Stepping Stones* model.

5. Key Findings and Conclusions

NIAC stands for **N**ASA **A**dvance **I**nnovative **C**oncepts. We believe that Apis™ is an ***Innovative Advanced Concept***, but more than that, it is realistic and potentially game changing. The work we have done in this effort coupled with our privately funded work and other NASA funded work as part of our larger collaboration establishes the technical credibility of this important breakthrough.

Innovation is a powerful force in the world today and America is still a leader in technological innovation in many sectors. The leading researcher and spokesman in the study of innovation is Prof. Clayton Christensen of Harvard Business School. Professor Christensen is the architect of and the world's foremost authority on *disruptive innovation*. According to Christensen, a *disruptive innovation* is an innovation that creates new markets and value networks and eventually disrupts existing markets and value networks, displacing established market leaders and alliances. Because NIAC was established to revolutionize NASA, we believe that more than just innovation, disruptive innovation is the ultimate purpose of the NIAC program.

Apis™ is designed to be the disruptive innovation that takes NASA to a new level. The new market will be a privately owned and operated transportation network that will supply NASA with far less expensive deep space and cis-lunar transportation services than could otherwise be possible potentially saving NASA $100B over a ten year period. This would make it possible for NASA to fulfill is human exploration ambitions within a politically realistic budget. More importantly, Apis™ will create new markets. With Apis™ it will be cost effective for the private sector to establish new industries such as asteroid mining, space solar power satellites, large scale high orbit space tourism, and ultimately homesteading of the solar system.

Bibliography of Asteroid Resources and Related Topics

Contents

Asteroidal Mining and Processing

Bellamy, D. and L. Pravica (2011) "Assessing the impact of driverless haul trucks in Australian surface mining" *Resources Policy* **36**, 149-158.

Brundrett, Scott (2014) "Industry Analysis Of Autonomous Mine Haul Truck Commercialization" MBA Thesis, Simon Fraser Univ.

Buet, M. et al. (2013) "Robotic Mining System for Rapid Return of Asteroid Resources" Presentation at the ISDC, San Diego, May 2013.

Carroll, K. A. (2015) "Asteroid Mineral Prospecting via Surface Gravimetric Surveying" Roundtable discussion, *http://www.isruinfo.com/index.php?page=srr_11_ptmss*

Ceruti, Alessandro et al. (2015) "Conceptual Design and Preliminarily Structural Analysis of Inflatable Basket for an Asteroid Capturing Satellite*" Strojniški vestnik - Journal of Mechanical Engineering* **61**, 341-351.

Court, R. W. and M. A. Sephton (2009) "Volatile Yields Upon Pyrolysis of Carbonaceous Chondrites as Determined by Quantitative Pyrolysis-Fourier Transform Infrared Spectroscopy" presented at the 40th Lunar and Planetary Science Conference.

Erickson, Ken R. (2006) "Optimal Architecture for an Asteroid Mining Mission: Equipment Details and Integration" Space 2006, 19 - 21 September 2006, San Jose, California, AIAA 2006-7504.

Fisher, B. S. and Schnittger, S. (2012) "Autonomous and Remote Operation Technologies in the Mining Industry" BAE Research Report 12.1.

Ge, Shen et al. (2013) "Economics of Asteroid Mining", presentation, *http://www.aiaahouston.org/Horizons/Shen%20Ge%20-%20Economic%20of%20Asteroid%20Mining%20%28Presentation%29%20V4.pdf*

Ge, Shen and Neha Satak (2014) "An Improved Economic Model for Asteroid Mining" *http://www.mendedreality.com/assets/docs/ECAPS%20-%20asteroidminingpaper.pdf*

Gertsch. Leslie (2013) "Adaptation of Mining Methods for Low- and Micro-gravity Environments: Part 1" Roundtable discussion, *http://www.isruinfo.com/index.php?page=srr_11_ptmss*

Lewis, John S. (1993) "Logistical Implications of Water Extraction from Near-Earth Asteroids", Proceedings of the Eleventh SSI-Princeton Conference, May 12-15, 1993.

Lynas, Danielle and Yim Horberry (2011) "Human Factor Issues with Automated Mining Equipment" *The Ergonomics Open Journal* **4**, (Suppl 2-M3) 74-80.

Moran, M. (1991) "Conceptual Study Of On Orbit Production Of Cryogenic Propellants By Water" AIAA-91-1844.

Mueller, R. P. and P. J. Van Susante (2012) "A Review of Extra-Terrestrial Mining Robot Concepts" Earth and Space 2012, Engineering, Science, Construction, and Operations in Challenging Environments (pp. 295-314) ASCE Press.

Nichols, C. R. (1993) “Volatile products from carbonaceous asteroids” *Resources of near-Earth space*, John S. Lewis et al. editors, University of Arizona, pp. 543-568.

NREL (2009) “Current (2009) State-of-the-Art Hydrogen Production Cost Estimate Using Water Electrolysis” NREL/BK-6A1-46676.

N-Science Corp. (2012) “Hummingbirds/CHARM” Roundtable discussion, *http://www.isruinfo.com/index.php?page=srr_11_ptmss*

Ross, Shane D. (2001) “Near-Earth Asteroid Mining” *http://www2.esm.vt.edu/~sdross/papers/ross-asteroid-mining-2001.pdf*.

Sonter, Marl J. (1997) “The Technical and Economic Feasibility of Mining the Near-Earth Asteroids” MS Thesis, University of Wollongong.

Sonter, Marl J. (1997) “Applying Mining Concepts to Accessing Asteroid Resources” TBD

Zacny, K. et al. (2012) “Mobile In-Situ Water Extractor (MISWE) for Mars, Moon, and Asteroids In Situ Resource Utilization” AIAA SPACE 2012 Conference & Exposition 11 - 13 September 2012, Pasadena, California, AIAA 2012-5168.

Zacny, K. et al. (2013) “Asteroid Mining” AIAA SPACE 2013 Conference and Exposition, September 10-12, 2013, San Diego, CA, AIAA 2013-5304.

Asteroid Missions

Alibay, Farah et al. (2011) “Finding NEO: A manned mission to a Near-Earth Object” *http://www.kiss.caltech.edu/study/space-challenge/Explorer%20Final%20Report_with_appendices.pdf*.

Bradley, Nicholas et al. (2013) “Optimized Free-Return Trajectories to Near-Earth Asteroids Via Lunar Flyby” AAS 13-937.

Brophy, J. R. et al. (2014) “Synergies of Robotic Asteroid Redirection Technologies and Human Space Exploration” 65th International Astronautical Congress, Toronto, Canada.

Brophy, J. R. et al. (2012) “Asteroid Retrieval Feasibility” *http://www.kiss.caltech.edu/study/asteroid/asteroid_final_report.pdf*

Brophy, J. R. and S. Oleson (2012) “Spacecraft conceptual design of returning entire near-earth asteroids” AIAA 20102-4067.

Brophy, J. R. et al. (2011) “Feasibility of capturing and returning small near-earth asteroids” IEPC-2011-277.

Cohen, Marc M. et al. (2013) “Robotic Asteroid Prospector (RAP) Staged from L1: Start of the Deep Space Economy” *http://www.nasa.gov/sites/default/files/files/Cohen_2012_PhI_RAP.pdf*.

Cutright, B. L. (2013) “The near-Earth asteroids on the pathway to Earth’s future in space” in W. A. Ambrose, et al. eds., Energy resources for human settlement in the solar system and Earth’s future in space: AAPG Memoir **101**, p. 75–97.

Dissly, Rich (2013) “Target NEO 2: Workshop Summary and Next Steps” *http://www.lpi.usra.edu/sbag/meetings/jul2013/presentations/WED_1015_Dissly_TN2_Summary.pdf*

Erickson, Ken R. (2006) “Optimal Architecture for an Asteroid Mining Mission: Equipment Details and Integration” Space 2006, 19 - 21 September 2006, San Jose, California, AIAA 2006-7504.

Gates, Michele et al. (2014) “The Asteroid Redirect Mission and Sustainable Human Exploration” 65th International Astronautical Congress, Toronto, Canada.

Hopkins, Josh and Adam Dissel (2009) “Plymouth Rock: An Early Human Asteroid Mission Using Orion” *http://www.lpi.usra.edu/sbag/meetings/sbag2/presentations/PlymouthRockasteroidmission.pdf*.

Jenniskens, Peter et al. (2015) “SHEPHERD: A Concept for Gentle Asteroid Retrieval with a Gas-Filled Enclosure” *New Space* **3**, 36-43.

Kuck, David L. (1997) “The Deimos Water Company” *http://www.nss.org/settlement/manufacturing/SM11.091.DiemosWaterCompany.pdf*

Mazanek, D. D. et al. (2014) “Asteroid Redirect Mission Concept: A Bold Approach for Utilizing Space Resources” IAC-14-D3.1.8, 65th International Astronautical Congress (IAC), Toronto, Canada.

Messidoro, P. et al. (2012) “Human Mission to Asteroids in the Context of Future Space Exploration Studies” Mem. S.A.It. Suppl. Vol. 20, 119.

Mueller, R. P. et al. (2014) “In--□Situ Resource Utilization (ISRU) Concepts for a Retrieved Asteroid in a Lunar Distant Retrograde Orbit (LDRO)” Roundtable discussion, *http://www.isruinfo.com/index.php?page=srr_11_ptmss*

NASA (2014) “Asteroid Initiative Ideas Synthesis Workshop” Final Report. *http://www.nasa.gov/content/asteroid-initiative-idea-synthesis-workshop/#.Vhqv_aK2SFo* *https://www.nasa.gov/sites/default/files/files/Asteroid-Initiative-WS-Final-Report-508.pdf*

Rodriguez, J. G. “ Low energy intercept orbits to NEO GU9” Roundtable discussion, *http://www.isruinfo.com/index.php?page=srr_11_ptmss*

Rudat, A. (2011) “HEXANE: Architecting Manned Space Exploration Missions beyond Low-Earth Orbit” M. S. Thesis, MIT, June 2013.

Sanks, W. A. (2014) “Kinetic Energy Transfer of Near-Earth Objects for Interplanetary Manned Missions” SpaceOps Conference 5-9 May 2014, Pasadena, CA.

Schweickart, Russell L. et al. (2003) “Asteroid Tugboat” *Scientific American*, November 2003.

Shoemaker, L. M. and L. E. Helin (1978) “Earth-Approaching Asteroids as Targets for Exploration” *http://www.clowder.net/hop/railroad/Shoemaker_Helin_1978.pd*f.

Wolters, S. D. et al. (2011) “Measurement Requirements for a Near-Earth Asteroid Impact

Mitigation Demonstration Mission" *Planetary and Space Science* **59**, 1506-1515.

Zimmerman, Daniel et al. (2010) "The First Human Asteroid Mission: Target Selection and Conceptual Mission Design" AIAA-2010-8370.

Asteroids and NEO Properties and Distribution

Carbonaceous Chondrites

Bell, J. F. (1988) "A probable asteroid parent body for the CV or CO chondrites" *Meteoritics* **23**, 256-257.

Britt D. T. and Consolmagno G. J. (2003) "Stony meteorite porosities and densities: A review of the data through 2001" *Meteoritics and Planetary Science* **38**, 1161-1180. Viewable at: *http://onlinelibrary.wiley.com/doi/10.1111/j.1945-5100.2003.tb00305.x/pdf*

Burbine, T. H., Binzel, R. P., Bus, S. J., Clark, B. E. (2001) "K asteroids and CO3/CV3 chondrites" *Meteoritics and Planetary Science* **36**, 245-253.

Clark, B. E., Ockert-Bell, M. E., Cloutis, E. A., Nesvorny, D., Mothé-Diniz, T., Bus, S. J. (2009) "Spectroscopy of K-complex asteroids: Parent bodies of carbonaceous meteorites?" *Icarus* **202**, 119-133.

Cloutis, E., Hiroi, T., Gaffey, M., Alexander, C. M. O'D. and Mann, P. (2011) "Spectral reflectance properties of carbonaceous chondrites: 1. CI chondrites" *Icarus* **212**, 180-209.

Cloutis, E., Hiroi, T., Gaffey, M., Alexander, C. M. O'D. and Mann, P. (2011) "Spectral reflectance properties of carbonaceous chondrites: 2. CM chondrites" *Icarus* **216**, 309-346.

Cloutis, E., Hiroi, T., Gaffey, M., Alexander, Gaffey, C. M. O'D. and Mann, P. (2012) "Spectral reflectance properties of carbonaceous chondrites: 3. CR chondrites" *Icarus* **217**, 389-407.

Cloutis, E., Hiroi, T., Gaffey, M., Alexander, C. O. D. and Mann, P. (2012) "Spectral reflectance properties of carbonaceous chondrites: 4. Aqueously altered and thermally metamorphosed meteorites" *Icarus* **220**, 586-617.

Cloutis, E., Hiroi, T., Hudon, P., Gaffey, M. and Mann, P. (2012) "Spectral reflectance properties of carbonaceous chondrites: 5. CI chondrites" *Icarus* **220**, 466-486.

Cloutis, E., Hiroi, T., Hudon, P., Gaffey, M., Mann, P. and Bell, J. F. (2012) "Spectral reflectance properties of carbonaceous chondrites: 6. CV chondrites" *Icarus* **221**, 328-358.

Cloutis, E., Hiroi, T., Hudon, P. and Gaffey, M., (2012) "Spectral reflectance properties of carbonaceous chondrites: 7. CK chondrites" *Icarus* **221**, 911-924.

Cloutis, E., Hudon, P., Hiroi, T., Gaffey, M. J. and Mann, P. (2012) "Spectral reflectance properties of carbonaceous chondrites: 8. "Other" carbonaceous chondrites: CH, ungrouped, polymict, xenolithic inclusions, and R chondrites" *Icarus* **221**, 984-1001.

Cloutis, E., Hudon, P., Hiroi, T., Gaffey, M. J., Mann, P. and Bell, J. F. (2012) "Spectral reflectance properties of carbonaceous chondrites: 6. CV chondrites" *Icarus* **221**, 328-358.

Grady, M. M., Verchovsky, A. B., Franchi, I. A., Wright, I. P. and Pillinger, C. T. (2002) "Light element geochemistry of the Tagish Lake CI2 chondrite: Comparison with CI1 and CM2 meteorites" *Meteoritics and Planetary Science* **37**, 713-735.

Hiroi T., Zolensky, M. E., and Pieters, C. M. (2001) "The Tagish Lake meteorite: A possible sample from a D-type asteroid", *Science* **293**, 2234-2236.

Mason, B. (1963) "The Carbonaceous Chondrites" *Space Science Reviews* **1**, 621-646.

Mittlefehldt, David W. (2002) "Geochemistry of the ungrouped carbonaceous chondrite Tagish Lake, the anomalous CM chondrite Bells, and comparison with CI and CM chondrites", *Meteoritics and Planetary Science* **37**, 703-712. Viewable at: *http://onlinelibrary.wiley.com/doi/10.1111/j.1945-5100.2002.tb00850.x/epdf*

Mothé-Diniz, T., J.M. Carvano, S.J. Bus, R. Duffard and T. Burbine (2008) "Mineralogical analysis of the Eos family from near-infrared spectra" *Icarus* **195**, 277–294.

Nelson, M. L., Britt, D.T., L. A. Lebofsky (1993) "Review of asteroid compositions" *Resources of near-Earth space*, John S, Lewis et al. editors, Univ. of Arizona Press, p. 493 – 522.

Norton, O. Richard (2002) *The Cambridge Encyclopedia of Meteorites*, Cambridge University Press, pp. 121–124.

Distribution

Adamo, Daniel R. (2013) "Known NEOs in Earthlike Orbits and their Accessibility for Exploration" Future In-Space Operations (FISO) 12 June 2013 Telecon Colloquium.

Binzel, Richard P. (2014) "Find asteroids to get to Mars" *Nature* **514**, 559-561.

Bottke, W. F. et al. (2002) "Debiased Orbital and Absolute Magnitude Distribution of the Near-Earth Objects" *Icarus* **156**, 399-433.

Britt, D. T., D. J. Tholen, J. F. Bell, and C. M. Pieters (1992) "Comparison of asteroid and meteorite spectra: Classification by principal component analysis" *Icarus*, **99**, 153-166.

Britt, D. T., Guy Consolmagno, S. J., and Lebofsky, L. (2014) "Main-Belt Asteroids," *Encyclopedia of the Solar System*, Chapter 26, T. Spohn, D. Breuer, and T. Johnson, editors, Elsevier, pp. 583-601.

DeMeo, F. E., and B. Carry (2013) "The taxonomic distribution of asteroids from multi-filter all-sky photometric surveys" *Icarus* **226**, 723–741. *https://www.researchgate.net/publication/247769539_The_Taxonomic_Distribution_of_Asteroids_from_Multi-filter_All-sky_Photometric_Surveys*

Elvis, Martin (2013) "How Many Ore--Bearing Asteroids?" *Planetary and Space Science*, in press.

Elvis, Martin et al. (2011) "Ultra-Low Delta-v Objects and the Human Exploration of Asteroids"

Planet. Sp ace Sci. **59,** 1408-1412.

Fowler, J., and J. Chillemi (1992) "Subaru Lightcurve Observations of Sub-km-Sized Main-Belt Asteroids. In The IRAS Minor Planet Survey" in *The IRAS Minor Planet Survey* (E. F. Tedesco, ed.) Tech. Rpt. PL-TR-92-2049, 17–43.

Grady, M. M., et al. (2002) "Light element geochemistry of the Tagish Lake CI2 chondrite: Comparison with CI1 and CM2 meteorites" *Meteoritics and Planetary Science* **37**, 713–735. *http://onlinelibrary.wiley.com/doi/10.1111/j.1945-5100.2002.tb00851.x/pdf*

Granvik, M. et al. (2012) "The population of natural Earth satellites" *Icarus* **216**, 262-277.

Granvik, M. et al. (2013) "A New Model of the Near-Earth-Object Population" European Planetary Congress 2013.

Greenstreet, Sarah et al. (2012) "The orbital distribution of Near-Earth Objects inside Earth's orbit" *Icarus* **217**, 355-366.

Ieva, Simone et al. (2013) "Surface composition of low delta-V near-Earth asteroids, a survey of future targets for space missions" EPSC Abstracts Vol. 8, EPSC2013-448, 2013, European Planetary Science Congress 2013.

Ieva, Simone et al. (2014) "Low Delta-V Near-Earth Asteroids: a survey of suitable targets for space missions" *Astronomy and Astrophysics* **569**, A59-A67.

Morbidelli, A. et al. (2002) "Origin and Evolution of Near-Earth Objects" *Asteroids III*, W. F. Bottke Jr., et al. (eds), University of Arizona Press, Tucson, p.409-422.

NASA (2006) "2006 Near-Earth Object Survey and Deflection Study" *https://www.hq.nasa.gov/office/pao/FOIA/NEO_Analysis_Doc.pdf*

Spaceguard "How many NEOs are there?" *http://spaceguard.rm.iasf.cnr.it/NScience/neo/neo-when/number.htm*

Stokes, G. H. et al. (2003) "Study to Determine the Feasibility of Extending the Search for Near-Earth Objects to Smaller Limiting Diameters" Report of the Near-Earth Object Science Definition Team, *http://neo.jpl.nasa.gov/neo/neoreport030825.pdf.*

Strange, N. J. et al. (2014) "Identification of Retrievable Asteroids with the Tisserand Criterion, AIAA 2014-4458. *http://arc.aiaa.org/doi/abs/10.2514/6.2014-4458*

Thomas, C. A. et al. (2011) "ExploreNEOs. V. Average Albedo by Taxonomic Complex in the Near-Earth Asteroid Population" *Astronomical Journal* **142**, 85-96.

Trigo-Rodriguez, Josep M. et al. (2013) "UV to far-IR reflectance spectra of carbonaceous chondrites - I. Implications for remote characterization of dark primitive asteroids targeted by sample-return missions" *Monthly Notices of the Royal Astronomical Society* **437**, October 2013.

Zavodny, M. et al. (2008) "The Orbit and Size Distribution of Small Solar System Objects orbiting the Sun interior to the Earth's Orbit" *Icarus* **198**, 284-293.

Generic

Michel, Patrick (2014) “Formation and Physical Properties of Asteroids” *Elements* **10**, 19-24.

National Academy (1998) “The Exploration of Near-Earth Objects”, National Academy Press, *http://www.nap.edu/catalog/6106/exploration-of-near-earth-objects*.

Rivkin, Andrew S. (2006) “An Introduction to NEOs” *http://www.jhuapl.edu/techdigest/TD/td2702/rivkin.pdf*

Schmitt, Harrison H. (?) “Asteroids and Comets: Potential Resources” Asteroids and Comets: Potential Resources, *http://fti.neep.wisc.edu/neep533/SPRING2004/lecture21.pdf.*

Trigo, Josep and M. Rodríguez (2009) “Deciphering The Internal Structure of Primitive Asteroids and Comets: Evidence from Meteoroids and NEO Follow-Ups”, International Symposium Marco Polo and other Small Body Sample Return Missions, Paris, 18-20 May 2009.

Internal Diffusion and Permeability

Bland, Philip A. et al. (2009) “Why aqueous alteration in asteroids was isochemical: High porosity ≠ high permeability” *Earth and Planetary Science Letters* **287**, 559-568.

Consolmagno, G. J. et al. (2008) “The significance of meteorite density and porosity” *Chemie der Erde* **68**, 1–29.

Corrigan, Catherine M. et al. (1997) “The porosity and permeability of chondritic meteorites and interplanetary dust particles” *Meteoritics & Planetary Science* **32**, 509-515

Hashizume, Ko and Naoji Sugiura (1998) “Transportation of gaseous elements and isotopes in a thermally evolving chondritic planetesimal” *Meteoritics & Planetary Science* **33**, 1181-1195.

Huebner, W. F. et al. (2006) “Heat and Gas Diffusion In Comet Nuclei” ISSI Scientific Report SR-004.

Marchi, S. et al. (2009) “Heating of near-Earth objects and meteoroids due to close approaches to the Sun” *Mon. Not. R. Astron. Soc*. **400**, 147–153.

Mitsui, T. et al. (1986) “Gas permeability of shocked condrites” *Meteoritics* **21**, 109-116. *https://www.researchgate.net/publication/234525087_Gas_permeability_of_shocked_chondrites*

Mommert, M. (2013) “Remnant Planetesimals and their Collisional Fragments: Physical Characterization from Thermal-Infrared Observations” Ph. D. Thesis, University of Berlin, Germany.

Paton, M. D. et al. (2012) “Investigating thermal properties of gas-filled planetary regoliths using a thermal probe” *Geosci. Instrum. Method. Data Syst*. **1**, 7–21.

Prialnik, Dina et al. (2004) “Modeling the Structure and Activity of Comet Nuclei” in Comets II, M. C. Festou, et al. (eds.), University of Arizona Press, Tucson, p.359-387.

Internal Structure and Mechanical Properties

Asphaug, Erik A. et al. (2003) “Asteroid Interiors” Lunar and Planetary Science XXIV, paper 1906, *http://www.lpi.usra.edu/meetings/lpsc2003/pdf/1906.pdf.*

Brophy, J. and Culik, F. (2012) “Asteroid Retrieval Feasibility Study” *http://www.kiss.caltech.edu/study/asteroid/asteroid_final_report.pdf.*

Bagatin, A. C. (2008) “On the internal structure of asteroids and comets” Mem. S. A. It. Suppl. **12**, 150-163.

Britt, D. T. et al. (1987) “Asteroid Density, Porosity, and Structure” *http://www.astro.ugto.mx/~papaqui/download/CursoR/2002_Britt.pdf*

Carry, B. (2012) “Density of Asteroids” *http://arxiv.org/pdf/1203.4336.pdf*

Cellino, A, (2011) “Determination of asteroid physical properties from Gaia observation” *https://www-n.oca.eu/workshop/Pise/slides/cellinoPisa.pdf*

Consolmagno, S. J., and D. T. Britt ( ) “Porosity and internal composition of asteroids” *http://irtfweb.ifa.hawaii.edu/~sjb/CD07/talks/Consolmagno_slides.pdf*.

Hirabayashi, Toshi (2014) “Structural Stability of Asteroids” Ph. D. Thesis, University of Colorado.

Licandro, J. (2008) “The surface properties of primitive asteroids and comet-asteroid transition objects” Marco Polo Workshop Cannes, 5-6 June, 2008.

Lomov, Ilya et al. (2013) “Influence of Mechanical Properties Relevant to Standoff Deflection of Hazardous Asteroids” *Procedia Engineering* **58**, 251-259.

Sanchez, P. and D. J. Scheeres (2013) “The Strength of Regolith and Rubble Pile Asteroids” *http://arxiv.org/pdf/1306.1622.pdf*

Yomogida, K. and T. Matsui (1983) “Physical properties of ordinary chondrites” *J. Geophys. Res*. **88**, 9513-9533.

Thermal

Anderson, W. W. and Y. J. Ahrens (1994) “An equation of state for liquid iron and implications for the Earth’s core” *J. Geophys. Res*. **99**, 4273-4384.

Bottke, W. F. et al. (2002) “The Effect of Yarkovsky Thermal Forces on the Dynamical Evolution of Asteroids and Meteoroids” *Asteroids III*, W. F. Bottke Jr. et al. (eds), University of Arizona Press, Tucson, p.395-408, 2002.

Capek, D. and D. Vokrouhlicky (2004) “The YORP effect with finite thermal conductivity” *Icarus* **172**, 526-536.

Cellino, A. and S. Bagnulo (2015-A) “Polarimetry: a primary tool for the physical characterization of the Asteroids” *https://www2.hao.ucar.edu/sites/default/files/users/whawkins/Thurs_Polarimetry-a%20primary%20tool%20for%20the%20physical%20characterization.pdf*

Cellino, A. and S. Bagnulo (2015-B) “Polarimetry: a primary tool for the physical characterization of asteroids” Polarimetry: From the Sun to Stars and Stellar Environments, Proceedings IAU Symposium No. 305, 2015.

Consolmagno, G. J. et al. (2013) “Low temperature heat capacities of solar system materials” EPSC Abstracts Vol. 8, EPSC2013-248, European Planetary Science Congress 2013.

Delbo, Marco et al. (2007) “Thermal inertia of near-Earth asteroids and implications for the magnitude of the Yarkovsky effect” *Icarus* **190**, 236-249.

Delbo, Marco and Paolo Tanga (2007) “Thermal Inertia of Near Earth Asteroids Implications for the Strength of the Yarkovsky & Yorp Effects” *http://irtfweb.ifa.hawaii.edu/~sjb/CD07/talks/Delbo_slides.pdf*

Delbo, Marco and Paolo Tanga (2008) “Thermal inertia of main belt asteroids smaller than 100 km from IRAS data” *Planetary and Space Science* **57**, 259-265.

Delbo, Marco et al. (2011) “The cool surfaces of binary near-Earth asteroids” *Icarus* **212**, 138-148.

Delbo, Marco et al. (2014) “Thermal fatigue as the origin of regolith on small asteroids” *Nature* **508**, 233-249.

Delbo, Marco et al. (2015) “Asteroid thermophysical modeling” *http://arxiv.org/pdf/1508.05575v1.pdf*

Ghosh, A. et al. (2003) “Importance of the accretion process in asteroid thermal evolution: 6 Hebe as an example” *Meteoritics & Planetary Science* **38**, 711–724.

Gilbert-Lepoutre, A. (2014) “Survival of water ice in Jupiter Trojans” *Icarus* **231**, 232-238.

Harris, A. W. and Lagerros, J. S. V. ( ) “Asteroids in the Thermal Infrared” *Asteroids III*, W. F. Bottke Jr. et al. (eds), University of Arizona Press, Tucson, p.205-218 *http://www.lpi.usra.edu/books/AsteroidsIII/pdf/3005.pdf*

Leyrat, C. et al. (2011) “Thermal properties of the asteroid (2867) Steins as observed by VIRTIS/Rosetta” *Astronomy and Astrophysics* **532**, A168-A178.

Lim, L. F. et al. (2011) “Mineralogy and thermal properties of V-type Asteroid 956 Elisa: Evidence for diogenitic material from the Spitzer IRS (5–35 lm) spectrum” *Icarus* **213**, 510-523.

Marchi, S. et al. (2009) “Heating of near-Earth objects and meteoroids due to close approaches to the Sun” *Mon. Not. R. Astron. Soc*. **400**, 147–153.

Marchis, F. et al. (2012) “Multiple asteroid systems: Dimensions and thermal properties from Spitzer Space Telescope and ground-based observations” *Icarus* **221**, 1130-1161.

Matter, Alexis et al. (2012) “New insights on thermal properties of asteroids using IR interferometry” *http://www.sciops.esa.int/SD/ESACFACULTY/docs/seminars/080312_Matter.pdf.*

McSween, H. Y. et al. (2002) “Thermal Evolution Models of Asteroids” *http://www.academia.edu/2745123/Thermal_evolution_models_of_asteroids*

Moskovitz, Nicholas and Eric Gaidos (2011) “Differentiation of Planetesimals and the Thermal Consequences of Melt Migration” *Meteorics and Planetary Science* **46**, 903-918.

Mueller, Michael et al. (2010) “Eclipsing Binary Trojan Asteroid Patroclus: Thermal Inertia from

Spitzer Observations" *Icarus* **205**, 505-515.

Opeil, C. P. et al. (2010) "The thermal conductivity of meteorites: New measurements and analysis" *Icarus* **208**, 449-454.

Opeil, C. P. et al. (2012) "Stony meteorite thermal properties and their relationship with meteorite chemical and physical states" *Meteoritics & Planetary Science* **47**, 319–329.

O'Rourke, L. et al. (2012) "Thermal and shape properties of asteroid (21) Lutetia from Herschel observations around the Rosetta flyby" *Planetary and Space Science* **66**, 192-199.

Szurgot, M. (2011) "On the Specific Heat Capacity and Thermal Capacity Of Meteorites" 42nd Lunar and Planetary Science Conference, Paper 1150.

Szurgot, M. (2012) "On the Heat Capacity of Asteroids, Satellites and Terrestrial Planets" 43rd Lunar and Planetary Science Conference, Paper 2626.

Szurgot, M. et al. (2012) "Thermophysical Properties of the Sołtmany Meteorite" *Meteorites* **2**, 53-65.

Trommsdorff, V. and J. Connolly (1996) "The ultramafic contact aureole about Bregaglia (Bergell) tonalite : isograds and a thermal model" *Schwiz. Mineral. Petrogr*. *Mitt.* **76**, 537-547.

Usui, F. (2013) "Mid-Infrared Asteroid Survey with AKARI" *http://pasj.oxfordjournals.org/content/63/5/1117.full*

Vokrouhlicky, D. et al. (2000) "Yarkovsky Effect on Small Near-Earth Asteroids: Mathematical Formulation and Examples" *Icarus* **148**, 118-138.

Williams, Quentin (2009) "Bottom-up versus top-down solidification of the cores of small solar system bodies: Constraints on paradoxical cores" *Earth and Planetary Science Letters* **284,** 564–569.

Yang, Jijin et al. (2010) "Thermal history and origin of the IVB iron meteorites and their parent body" *Geochimica et Cosmochimica Acta* **74**, 4493–4506.

Yomogida, K. and T. Matsui (1983) "Physical properties of ordinary chondrites" J. Geophys. Res. 88, 9513-9533.

Water, Volatiles and Chemical Composition

Albertsson, T. et al. (2014) "Chemo-dynamical deuterium fractionation in the early solar nebula: The origin of water on Earth and in asteroids and comets" *Astrophysical Journal* **784**, …

Cardiff, E. H. (2012) "Volatile Extraction and In Situ Resource Utilization for the Moon applied to Near Earth Objects" Annual Meeting of the Lunar Exploration Analysis Group, Paper 3041.

Cardiff, E. H. (2012) "Volatile Extraction and In Situ Resource Utilization for the Moon applied to Near Earth Objects" Annual Meeting of the Lunar Exploration Analysis Group, slides.

Garenne, A. (2014) "The abundance and stability of "water" in type 1 and 2 carbonaceous chondrites (CI, CM and CR)" *Geochimica et Cosmochimica Acta* **137**, 93–112.

Kelsey, Laura (2013) "Purifying Water Mined from Asteroids for In Situ Resource Utilization"

Roundtable discussion, *http://www.isruinfo.com/index.php?page=srr_11_ptmss*

Kuppers, Michael et al. (2014) "Localized sources of water vapor on the dwarf planet Ceres" *Nature* **505**, 525-533.

Krot, A. N. et al. (1995) "Mineralogical and chemical variations among CV3 chondrites and their components: Nebular and asteroidal processing" *Meteoritics* **30**, 748-775.

Kurat, G. et al. (1994) "Petrology and geochemistry of Antarctic micrometeorites. *Geochim. Cosmochim. Acra* **58**, 3879-3904.

Lewicki, C. et al. (2013) "Planetary Resources—The Asteroid Mining Company" *New Space* **1**, 105-108.

Lewis, J. S. (1987) *Space Resources*, John Wiley and Sons, Inc.

Lewis, J. S., and M. L. Hutson (1993) "Asteroidal Resource Opportunities Suggested by Meteorite Data," *Resources of Near-Earth Space*, J. S. Lewis, et al. editors, University of Arizona Press. pp. 523-542.

Lewis, J. S., M. S. Matthews, and M. L. Guerrieri (1993) editors, *Resources of Near-Earth Space*, University of Arizona Press.

Licandro, J. et al. (2011) "(65) Cybele: detection of small silicate grains, water-ice, and organics" *Astronomy & Astrophysics* **A34**, 525-531.

Nelson M. L., D. T. Britt and L. A. Lebofsky (1993) "Review of Asteroid Compositions," *Resources of Near-Earth Space*, Lewis, J. S., Matthews, M. S., and Guerrieri, M. L. editors, University of Arizona Press pp. 493-521.

Rivkin, Andrew S. (2009) "The Trojan Asteroids: Keys to Many Locks" *http://www.lpi.usra.edu/decadal/sbag/topical_wp/AndrewSRivkin-trojans.pdf*

Rivkin, Andrew S. and Joshua P. Emery (2010) "Detection of ice and organics on an asteroidal surface" *Nature* **464**, 1322-3.

Rivkin, Andrew S. et al. (2015) "Astronomical Observations of Volatiles on Asteroids" Chapter to appear in the (University of Arizona Press) Space Science Series Book: Asteroids IV, *http://arxiv.org/abs/1502.06442*.

Svetsov, V. V. and V. V. Shuvalov (2015) "Water delivery to the Moon by asteroidal and cometary impacts" *Planetary and Space Science* *http://www.sciencedirect.com/science/article/pii/S0032063315002615*

Taylor, G. J. (2015) "Water in Asteroid 4 Vesta" *http://www.psrd.hawaii.edu/Jan15/Vesta-water.html*.

Teague, S. and M. Hicks (2011) 2011 HP: A Potentially Water-Rich Near-Earth Asteroid" *http://www.lacitycollege.edu/academic/departments/physics/cure/reports/TeagueS_Sm11.pdf*

Wolters, S. D. et al. (2011) "Physical Characterisation of low delta-V asteroid (175706) 1996 FG3" *http://arxiv.org/pdf/1108.1831.pdf*

Asteroids as Stepping Stone to Mars

Binzel, Richard (2014) “Find asteroids to get to Mars” (Comment) *Nature* **514**, 559-561.

Binzel, Richard (2014) “Use asteroids as stepping stones to Mars: Richard Binzel on NASA's asteroid redirect mission” *http://phys.org/news/2014-10-asteroids-stones-mars-richard-binzel.html*.

Brophy, J. R. and L. Friedman (2012) “Returning an entire near-earth asteroid in support of human exploration beyond LEO”
http://www.kiss.caltech.edu/study/asteroid/papers/returning.pdf

Cordell, Bruce M. (1990) ”Transportation Approaches For Manned Mars Missions” AIAA 90-3892.

Crusan, Jason (2014) “An Evolvable Mars Campaign”

Foster, Cyrus and Matthew Daniels (2010) “Mission Opportunities for Human Exploration of Nearby Planetary Bodies” AIAA SPACE 2010 Conference & Exposition 30 August - 2 September 2010, Anaheim, California, AIAA 2010-8609.

Koelle, H. H. (1997) “Comparison of Future Launch Vehicle Concepts for Cargo Transportation to Low Earth Orbit and Lunar Destinations” Technical University Berlin Aerospace Institute Marchstr.14, D-10587 Berlin

Mazanek, Dan et al.(2013) “Considerations for Designing a Human Mission to the Martian Moons” 2013 Space Challenge California Institute of Technology March 25-29, 2013.

Oeftering, Richard (2011) “A Cis-Lunar Propellant Infrastructure for Flexible Path Exploration and Space Commerce” NASA/TM—2012-217235, AIAA–2011–7113.

Zegler, Frank and Bernard Kutter (2010) “Evolving to a Depot-Based Space Transportation Architecture” AIAA SPACE 2010 Conference & Exposition 30 August - 2 September 2010, Anaheim, California, AIAA 2010-8638.

Delta-Vee for Transport in Cis-Earth-Lunar-Mars Space

Elvis, Martin et al. (2011) “Ultra-Low Delta-v Objects and the Human Exploration of Asteroids”
http://arxiv.org/ftp/arxiv/papers/1105/1105.4152.pdf

Murphy, Max (2015) “Delta –V to Near-Earth Asteroids: an Examination of the Shoemaker - Helin Equations” B. A. Thesis, Harvard College April 11, 2015.

Early History of Asteroids as Resources

early history.asteroids.resource.docx

Mautner, Michael N. (2005) “Life in the Cosmological Future: Resources, Biomass and Populations” *Journal of the British Interplanetary Society* **58**, 167-180.

O'Neill, Gerard K. et al. (1979) “Space Resources and Space Settlements” NASA Report SP-428.

Tsiolkovsky, K. E. (1931) *Interplanetary Flight and Communication*, translated from Russian,

NASA TT F-646.

Electrolysis of Water

deGroot, W. A. and L. A. Arrington (1997) “Electrolysis Propulsion for Spacecraft Applications” NASA Technical Memorandum 113157, AIAA-97-2948.

Fuel Cell Today (2013) “Water Electrolysis and Renewable Energy Systems” *http://www.fuelcelltoday.com/media/1871508/water_electrolysis___renewable_energy_systems.pdf*.

Ivy, Johanna (2004) “Summary of Electrolytic Hydrogen Production Milestone Completion Report” NREL/MP-560-36734.

Moran, M. (1991) “Conceptual Study Of On Orbit Production Of Cryogenic Propellants By Water” AIAA-91-1844, NASA Technical Memorandum 103730.

National Renewable Energy Laboratory (2009) “Current (2009) State-of-the-Art Hydrogen Production Cost Estimate Using Water Electrolysis” NREL/BK-6A1-46676, September 2009.

Stechman, R. Carl et al. (1973) “Water Electrolysis Satellite Propulsion System” AFRPL Report AD-755 384.

Zoulias, Emmanuel et al. (2006) “A Review on Water Electrolysis” *http://www.cres.gr/kape/publications/papers/dimosieyseis/ydrogen/A%20REVIEW%20ON%20WATER%20ELECTROLYSIS.pdf*

Fuel Depots

Goff, Jonathan et al (2009) “Realistic Near-Term Propellant Depots: Implementation of a Critical Spacefaring Capability” AIAA-2009-6756.

Goff, Jonathan et al (2009A) “The case for orbital propellant depots” *http://www.slideshare.net/jongoff/sa08-prop-depot-panel-jon-goff*

Kutter, Bernard F. et al (2008) “A Practical, Affordable Cryogenic Propellant Depot Based on UCLA’s Flight Experience” AIAA-2008-7644.

Kutter, Bernard F. et al (2010) “Propellant depots made simple” *http://spirit.as.utexas.edu/~fiso/telecon10-12/Kutter_11-10-10/*

Larson, Wiley et al. (2012) “Operations and Service Infrastructure for Space Team Project: Spaceports” International Space University Final Report.

McLean, Christopher (2011) “Cryogenic Propellant Depots Design Concepts and Risk Reduction Activities” *http://spirit.as.utexas.edu/~fiso/telecon10-12/McLean_3-2-11/*.

NASA (2011) “Propellant Depot Requirements Study” *http://images.spaceref.com/news/2011/21.jul2011.vxs.pdf*

Notardonato, William et al. (20121) “In-Space Propellant Production Using Water” AIAA SPACE 2012 Conference & Exposition, AIAA 2012-5288.

Oeftering, Richard C. (2012) “A Cis-Lunar Propellant Infrastructure for Flexible Path Exploration

and Space Commerce" NASA/TM—2012-217235, AIAA–2011–7113.

Smitherman, David and Gordon Woodcock (2011) "Space Transportation Infrastructure Supported By Propellant Depots" *http://www.nss.org/articles/Space_Transportation_Infrastructure_Supported_by_Propellant_Depots.pdf*

Smitherman, David et al. (2001) "Space Resource Requirements for Future In-Space Propellant Production Depots" Space Resources Utilization Roundtable III October 24-26, 2001, Colorado School of Mines, Golden Colorado.

Street, David (2006) "A Scalable Orbital Propellant Depot Design" *http://soliton.ae.gatech.edu/labs/ssdl/papers/mastersProjects/StreetD-8900.pdf*

Tanner, Christopher et al. (2006) "On-Orbit Propellant Resupply Options for Mars Exploration Architectures" IAC-06-D1.1.01.

Taylor, Tom et al. (2009) "On-Orbit Fuel Depot Deployment, Management and Evolution Focused on Cost Reduction" AIAA SPACE 2009 Conference & Exposition 14 - 17 September 2009, Pasadena, California, AIAA 2009-6757.

Wilhite, Alan et al. (2012) "Evolved Human Space Exploration Architecture Using Commercial Launch/Propellant Depots" 63rd International Astronautical Congress, Naples, Italy, IAC-12,D3,2,3,x15379.

Zegler, Frank and Bernard Kutter (2010) "Evolving to a Depot-Based Space Transportation Architecture" AIAA SPACE 2010 Conference & Exposition 30 August - 2 September 2010, Anaheim, California, AIAA 2010-8638.

History of Stepping Stones Approach

Binzel, Richard (2014) "Use asteroids as stepping stones to Mars", *phys.org/pdf333871206.pdf*

Cassady, J. et al. (2014) "A Sustainable Concept for a Human Exploration Spacecraft", Space Exploration International Conference, October 29-31, 2014, Strasbourg (France).

Dunham, David D. et al. (2013) "New Approaches for Human Deep-Space Exploration" *J. of Astronautical Science* **60**, 149-166.

Ehrenfreund et al. (2012) "Toward a global space exploration program: A stepping stone approach" *Advances in Space Research* **49**, 2–48.

Harvey, Brian (2007) "Section 5.2 Stepping Stones to Mars", in *Space Exploration 2007*, Praxis Publishing Ltd.

Huntress, Wesley (2003) Testimony to Congressional Hearing on the Future of NASA, October 29, 2003. *http://history.nasa.gov/columbia/Troxell/Columbia%20Web%20Site/Documents/Congress/Senate/OCTOBE~1/huntress_testimony.html*

IAU (2016) "Near Earth Asteroids (NEAs) A Chronology of Milestones 1800 – 2200",

International Astronautical Union.

Intl. Academy of Astronautics (2004) “The Next Steps in Exploring Deep Space” Final Report, 9 July 2004, *http://www.space.noa.gr/esfesa/documents/IAAstudy.pdf*.

Kwong, Jeffrey et al. (2011) “Stepping Stones: Exploring a Series of Increasingly Challenging Destinations on the Way to Mars” AIAA 2011-7216.

Morgan, Daniel (2011) “The Future of NASA: Space Policy Issues Facing Congress” Congressional Research Service Report for Congress 7-5700, January 27, 2011.

Oberg, James (2007) Chapter 5 Stepping Stones to Mars – A New Strategy”, in *Space Exploration 2007*, Praxis Publishing Ltd.

Pengra, Patricia (2001) “A stepping stone approach to human and robotic exploration of space” AIAA 2001-4562.

Inflatable Concentrators

Bonometti, J. A. and C. W. Hawk (1994) “Solar Thermal Research Facility Design” AlAA 94-3028.

Bonometti, J. A. and C. W. Hawk (1995) “Solar Thermal Concentrator” AlAA 95-2637.

Carrasquillo, Omar (2013) “Design of Inflatable Solar Concentrator” M.S. Thesis, MIT.

Clayton, W. R. and A. Gierow (1992) “Inflatable Concentrators for Solar Thermal Propulsion” Solar Engineering 2, 795-800.

Colozza, Anthony J. et al. (2010) “Cassegrain Solar Concentrator System for ISRU Material Processing” *http://ntrs.nasa.gov/archive/nasa/casi.ntrs.nasa.gov/20120004046.pdf*

Freeland, R. E. and G. R. Veal (1998) “Significance of the Inflatable Antenna Experiment Technology”, AIAA-98-2104 published in the 39TH AIAA/ASME/ASCE/AHS/ASC STRUCTURES, Structural Dynamics and Materials Conference And Exhibit, April 1998

Freeland, R. E. et al. (1997) “Large Inflatable Deployable Antenna Flight Experiment Results,” IAF Paper 97-1.3.01, presented at the 48th Congress of the International Astronautical Federation, Turin, Italy, October 6-10, 1997.

Gordon, P. E. C. (2011) “Thermal Energy Process Heat for Lunar ISRU: Technical Challenges and Technology Opportunities” 49th AIAA Aerospace Sciences Meeting including the New Horizons Forum and Aerospace Exposition 4 - 7 January 2011, Orlando, Florida. AIAA 2011-704.

Grossman, G. and G. Williams (1990) “Inflatable Concentrators for Solar Propulsion and Dynamic Space Power” *Journal of Solar Energy Engineering* **112**, 229-236.

Jaffe, Leonard D. (1983) “Dish Concentrators for Solar Thermal Energy” *J. Energy* **7**, 304-312.

Kudirka, A. A. and L. P. Leibowitz (1980) “Advanced Solar Thermal Receiver Technology” AlAA 18th AEROSPACE SCIENCES MEETING January 14-16, 1980/Pasadena, California, AIAA-80-0292.

Laug, K. K. and M. R. Holmes (1999) “Paraboloidal Thin Film Inflatable Concentrators and their use for Power Applications” SAE Technical Paper 1999-01-2552.

Leigh, L. et al. (2001) “Dynamic Characterization of an Inflatable Concentrator for Solar Thermal Propulsion”
http://citeseerx.ist.psu.edu/viewdoc/download;jsessionid=D8F1BD6CB5B0B1106A3F24AFB735BEC2?doi=10.1.1.475.1348&rep=rep1&type=pdf

Lichodziejewski, David and Costas Cassapakis (1999) “Inflatable Power Antenna Technology“ AIAA 99-1074.

Lucas, J. W. and J. Roschke (1978) “Solar Thermal Power Systems Point-Focusing Distributed Receiver (PFDR) Technology: A Project Description” AIAA 78-1771.

Ma, Hongcai (2012) “Optical Design of a Solar Dish Concentrator Based on Triangular Membrane Facets“ *International Journal of Photoenergy*, *http://www.hindawi.com/journals/ijp/2012/391921/*.

Macosko, Robert et al. (2010) “Solar Concentrator Concept for Providing Direct Solar Energy for Oxygen Production at the Lunar South Pole” 48th AIAA Aerospace Sciences Meeting Including the New Horizons Forum and Aerospace Exposition 4 - 7 January 2010, Orlando, Florida, AIAA 2010-1167.

Nakamura, T. et al. (2005) “Solar Thermal Technology for ISRU” 3rd Intl. Energy Conversion Engineering Conf. San Francisco, CA 15-18 Aug. 2005.

Palisoc, A. L. and M. Thomas (1995) “A Comparison of the Performance of Seamed and Unseamed Inflatable Concentrators” *Solar Engineering* **2**, 855-864.

Palisoc, A. L. and Y. Huang (1997) “Design Tool for Inflatable Space Structures” AIAA-97-1378.

Sahara, Hironori et al. (2003) “Ultra-Light Concentrators for Solar Thermal Propulsion” IEPC-2003-84.

Thomas, M. and G. R. Veal (1991) “Scaling Characteristics of Inflatable Paraboloid Concentrators”, Presented at the Second ASME-JSES-JSME International Solar Energy Conference, Rena, Nevada, March 17-22, 1991.

Wen, L., Huang, L., Poon, P. and Carley, W. (1980) "Comparative Study of Solar Optics for Paraboloidal Concentrators" *Journal of Solar Energy Engineering* **102**, 305-315.

ISRU Generic

Blair, B. R. (1998) “Use of Space Resources – A Literature Survey” 6th Int. Conf. Engineering, Construction, and Operations in Space, Space 98; R. G. Galloway and S. Lokaj, editors; ASCE Press, pp. 651-665.

Chepko, Ariane (2006) “Technology Selection and Architecture Optimization of In-Situ Resource Utilization Systems” MS Thesis, MIT.

Cutright, Brue and William Ambrose (2014) “Economic Benefits of In Situ Resource Utilization in Near-Term Space Exploration” Search and Discovery Article #70163.

Hubbard, M. S., P. K. Davidian, D. Gump, J. Keravala, C. Lewicki, T. Gavin, and W. Hanson, (2013) “Deep Space Resources: Can We Utilize Them?” *New Space* **1**, 52-59.

Kuck, David R. (1997) “Decision Points”
http://www.nss.org/settlement/manufacturing/SM11.128.DecisionPoints%28Kuck%29.pdf

Linne, Dianne L. et al. (2015) “Capability and Technology Performance Goals for the Next Step in Affordable Human Exploration of Space” 8th Symposium on Space Resource Utilization AIAA 2015-1650.

Sanders, Gerald (2015) “Space Resource Utilization and Human Exploration of Space” Roundtable discussion, *http://www.isruinfo.com/index.php?page=srr_11_ptmss*

Lunar

Beyer, R. et al. (2011) “Feasibility And Definition of a Lunar Polar Volatiles Prospecting Mission” 42nd Lunar and Planetary Science Conference, paper 2735.

Bienhoff, D. G. (2011) “From Importing to Exporting: The Impact of ISRU on Space Logistics” AIAA 2011-7112.

Borowski, S. K. (1995) “Human Lunar Mission Capabilities Using SSTO, ISRU and LOX-Augmented NTR Technologies -- A Preliminary Assessment” AIAA 95-2631.

Charania, A. C. and DePasquale, Dominic (2007) “Economic analysis of a lunar ISRU propellant services market”, 58th Intl. Astro. Congress, IAC-07-A5.1.03.

French, J. R. et al. (2013) “Architecture for Lunar Return Using Existing Assets” *Journal of Spacecraft And Rockets* **50**, 838-847.

Heiken, G., D. Vaniman, and B. M. French (Eds.). (1991) “Lunar sourcebook: A user's guide to the Moon” Cambridge University Press, available on line at
http://www.lpi.usra.edu/publications/books/lunar_sourcebook/

Hofstetter, W. K. et al. (2007) “Analysis of Human Lunar Outpost Strategies and Architectures” AIAA 2007-6276.

Larson, W. and Sanders G. B. (2007) “NASA In-Situ Resource Utilization (ISRU) Project and Its Linkage To Lunar Science” Presentation to Lunar Science Workshop Tempe, AZ .February 29, 2007

Logsdon, John M. (1979) "An Apollo Perspective," *Astronautics and Aeronautics*, December 1979, pp. 112-17.

Mueller, R. P. et al. (2012) “Launch and Landing Infrastructure on the Moon”
http://commons.erau.edu/cgi/viewcontent.cgi?article=3426&context=space-congress-proceedings

Neish, C. D. et al. (2011) “The nature of lunar volatiles as revealed by Mini-RF observations of the LCROSS impact site” *Journal of Geophysical Research* **116**, E01005

O'Handley, D. A. et al. (2001) "ISRU Support Self-Sustaining Lunar Colony (SSLC)" AIAA 2001-0937.

Project Apollo: A Retrospective Analysis, *http://history.nasa.gov/Apollomon/Apollo.html*

Sanders, G. B. et al. (2013) "Lunar Polar In Situ Resource Utilization (ISRU) as a Stepping Stone for Human Exploration" Presentation to Lunar Exploration Analysis Group (LEAG) Workshop, Oct. 14, 2013.

Sanders, G. B. et al. (2010) "Lunar in-situ resource utilization in the ISECG human lunar exploration reference architecture" IAC-10.A5.1.7.

Sanders, G. B. et al. (2007) "NASA In-Situ Resource Utilization (ISRU) Project – Development & Implementation" *https://www.nasa.gov/pdf/203084main_ISRU%20TEC%2011-07%20V3.pdf*

Spudis, P. D. (2010) "Mini-RF Mapping of the Poles of the Moon" Space Resources Roundtable, Golden CO 9 June, 2010.

Spudis, P. D. and T. Lavoie (2010) "Mission and Implementation of an Affordable Lunar Return" *http://www.spudislunarresources.com/Papers/Affordable_Lunar_Base.pdf*

Woodcok, G. R. (2011) "An Early Lunar Outpost for Lunar Development" AIAA 2011-5096.

Woodcock, G. R. (2007) "Architectures and Evolutions to Enable Lunar Development" AIAA 2007-6080.

Mars ISRU

Muscatello, A. C. and Santiago-Maldonado, E. (2012) "Mars In Situ Resource Utilization Technology Evaluation" 50TH AIAA Aerospace Sciences Meeting; 9-12 Jan. 2012; Nashville, TN.

Ramohalli, K., W. Dowler, J. French, and R. Ash (1987) "Some Aspects of Space Propulsion with Extraterrestrial Resources" *Journal of Spacecraft and Rockets* **24**, 236-244.

Rapp, Donald (2012) *Use of Extraterrestrial Resources for Human Space Missions to Moon or Mars* (Springer Praxis Books / Astronautical Engineering)" published November 20, 2012

Zubrin, Robert et al. (2012) "Mars Regolith Water Extractor" Roundtable discussion, *http://www.isruinfo.com/index.php?page=srr_11_ptmss*

Miscellany

Aarnes, Ingrid et al. (2010) "How contact metamorphism can trigger global climate changes: Modeling gas generation around igneous sills in sedimentary basins" *Geochimica et Cosmochimica Acta* **74**, 7179–7195.

Blair, Brad R. (2000) "The Role of Near-Earth Asteroids in Long-Term Platinum Supply" *http://www.nss.org/settlement/asteroids/RoleOfNearEarthAsteroidsInLongTermPlatinumSupply.pdf*

Bosworth, M. L. (1999) “The Rise and Fall of 15th Century Chinese Sea Power” Available at: *http://militaryrevolution.s3.amazonaws.com/Primary%20sources/china.pdf*.

Bottke, W. et al. (2014) “Asteroid Resources Investigation, Engineering, and Science (ARIES)” SWRI Proposal, 10-31-2014.

Bonornetti, J. A. and C. W. Hawk (1994) “Solar Thermal Research Facility Design” AIAA 94-3028.

Kuck, David L. (2001) “Mining an iron NEA” *http://www.nss.org/settlement/manufacturing/SM13.249.MiningAnIronNEA.pdf*

Launius, R. D. (1994) *NASA*: *A History of the US Civil Space Program*. Krieger Publishing Co.

McCurdy, H. E. (1993) *Inside NASA: High Technology and Organizational Change in the US Space Program*, New Series in NASA History, Johns Hopkins University Press.

McCurdy, H. E. (1994) “The Cost of Space Flight” *Space Policy* **10**, 277-289.

Metzger, P. T., A. Muscatello, R. P. Mueller, and J. Mantovani (2012) “Affordable, Rapid Bootstrapping of the Space Industry and Solar System Civilization,” *Journal of Aerospace Engineering* **26**, 18-29.

Oh, David Y. (2006) “An Analytical Tool for Tracking and Visualizing the Transfer of Mass at each Stage of Complex Missions” AIAA 2006-7254.

Pyne, S. J. (2006) “Seeking Newer Worlds: An Historical Context for Space Exploration” *Critical Issues in the History of Spaceflight*, Steven J. Dick and Roger D. Launius (editors), NASA SP-2006-4702. Available at: *http://history.nasa.gov/SP-2006-4702/chapters/chapter1.pdf*.

Sercel, J. “Diaphanous Systems: A Compelling New Vision for America’s Future In Space” Report, ICS System, Sylmar, CA

Shepard, T. R. (1909) “Placer Mining Law in Alaska” *Yale Law Journal*, pp. 533-548.

Shinn, C. H. (1884) *Mining Camps: A Study in American Frontier Government*, Charles Scribner and Sons.

Zapata, Edgar and Carey McCleskey (2014) "An Analysis and Review of Measures and Relationships in Space Transportation Affordability" American Institute of Aeronautics and Astronautics, Joint Propulsion Conference, July 28-30, 2014. Available at: *http://science.ksc.nasa.gov/shuttle/nexgen/Nexgen_Downloads/AIAA_JPC_Paper_Review_Measure_Space_Trans_Afford_r8.pdf*.

Zapata, Edgar et al. (2014) "Life Cycle Analysis of Dedicated Nano-Launch Technologies," Commercial and Government Responsive Access to Space Technology Exchange (CRASTE), June 23-27, 2014. Available at: *http://science.ksc.nasa.gov/shuttle/nexgen/Nexgen_Downloads/CRASTE_Zapata_et_al_Paper_Assess_Dedicated_Nano-Launch_r8.pdf*

Zubrin, Robert M. (1993) “Nuclear Power and Propulsion for Missions to Mars and the Outer Solar System” AIAA 93-1814.

NASA Exploration Plans

Bowersox, Kenneth and the NASA Advisory Council Committee on Human Exploration and Operations (2014) "NASA Advisory Council Finding on NASA Human Exploration Strategy", from the Council Public Deliberation, July 31, 2014.

Craig, Douglas (2015) "Evolvable Mars Campaign Overview to FISO Telecon" *http://spirit.as.utexas.edu/~fiso/first.cgi*

Crusan, Jason (2014) Director, NASA Advanced Exploration Systems, Presentation, "The Evolvable Mars Campaign" *http://www.nasa.gov/sites/default/files/files/20140429-Crusan-Evolvable-Mars-Campaign.pdf*

Davis, Donald R. et al. (1993) "Role of Near-Earth Asteroids in the Space Exploration Initiative" *http://www.uapress.arizona.edu/onlinebks/ResourcesNearEarthSpace/resources23.pdf*

Emerging Space: The Evolving Landscape of 21st Century American Spaceflight, NASA Report from Office of the Chief Technologist, *http://images.spaceref.com/docs/2014/Emerging_Space_Report.pdf*

Lewis, James Andrew (2014) "Hard Choices for Manned Spaceflight: America as Icarus" *http://csis.org/files/publication/140508_Lewis_HardChoicesMannedSpaceflight_Web.pdf*

Mankins, John C. (2000) "Human Exploration Studies: A Review of the Trade Space" AIAA 2000-5316.

NASA (2014) "NASA's Efforts to Identify Near-Earth Objects and Mitigate Hazards" Office of Inspector General Report No. IG-14-030.

NASA (2012) "NASA's Challenges to Meeting Cost, Schedule, and Performance Goals" Office of Inspector General Report No. Report No. IG-12-021.

Sherwood, Brent (2011) "Comparing future options for human space flight" *Acta Astronautica* **69**, 346-353.

Steven Squyres and the NASA Advisory Council on Human Exploration and Operations (2014) "Recommendation Regarding Mismatch Between NASA's Aspirations for Human Space Flight and Its Budget, from the Council Public Deliberation, July 31, 2014.

Physics of Ceramic Foams and Water Vapor

Wu, Zhiyong et al. (2011) "Coupled radiation and flow modeling in ceramic foam volumetric solar air receivers" *Solar Energy* **85**, 2374–2385.

Biasetto, Lisa et al. (2007) "Gas Permeability of Microcellular Ceramic Foams" *Ind. Eng. Chem. Res.* **46**, 3366-3372.

Schmidt, B. E. (2015) “Compressible Flow Through Porous Media with Application to Injection” Internal Report for Caltech Hypersonics Group, FM 2014.001.

Fritzsch, Robert et al. (2015) “Investigation on permeability of ceramic foam filters” 2015 TMS Annual Meeting & Exhibition, *https://www.researchgate.net/publication/274653211_An_Investigation_on_Permeability_of_Ceramic_Foam_Filters_%28CFF%29*

Wu, Zhiyong et al. (2010) “Experimental and numerical studies of the pressure drop in ceramic foams for volumetric solar receiver applications” *Applied Energy* **87**, 504–513.

Moreira, E. A. et al. (2004) “Permeability of ceramic foams to compressible and incompressible flow” *Journal of the European Ceramic Society* **24**, 3209–3218.

Ferriso, C. C. et al. (1966) “Empirically Determined Infrared Absorption Coefficients of H,O From 300 To 3000 K” *J. Quant. Spectrosc. Radiat. Transfer* **6**, 241-273.

Younis, L. B. and R. Viskanta (1993) “Experimental determination of the volumetric heat transfer coefficient between stream of air and ceramic foam” *Int. J. Heat and Mass Transfer* **36**, 1425-1434.

Solar Electric Propulsion

Aspaugh, Erik and Lindley Johnson (2010) “Planetary Science Decadal Survey Near Earth Asteroid Trajectory Opportunities in 2020–2024” *http://sites.nationalacademies.org/cs/groups/ssbsite/documents/webpage/ssb_059327.pdf*

Brophy, John and Muirhead, Brian (2013) “Near-Earth Asteroid Retrieval Mission (ARM) Study” Presented at the 33rd International Electric Propulsion Conference, Washington, DC, October 6 – 10, 2013, IEPC-2013-82.

Brophy, John et al. (2011) “300-kW Solar Electric Propulsion System Configuration for Human Exploration of Near-Earth Asteroids” AIAA 2011-5514.

Gazarik, Michael J. (2013) “Asteroid Redirect Mission Solar Electric Propulsion” *http://www.nasa.gov/pdf/756160main_GazarikPresentation.pdf*

Ilin, Andrew V. et al. (2013) “VASIMR® Solar Powered Missions for NEA Retrieval and NEA Deflection” Presented at the 33rd International Electric Propulsion Conference, The George Washington University, Washington, D.C. USA October 6 – 10, 2013, IEPC-2013-336.

Lord, Peter W. and G. van Ommering (2015) “Evolved Commercial Solar Electric Propulsion: a Foundation for Major Space Exploration Missions” 31st Space Symposium, Technical Track, Colorado Springs, Colorado, United States of America, Presented on April 13-14, 2015.

North American (1970) “Solar Electric Propulsion Asteroid Belt Mission Study Final Report” Volume 1, Summary Report, SD-70-21-1, 112 pp.

North American (1970) “Solar Electric Propulsion Asteroid Belt Mission Study Final Report” Volume 2, Technical Report, SD-70-21-1, 670 pp.

North American (1970) “Solar Electric Propulsion Asteroid Belt Mission Study Final Report”

Volume 3, Asteroid Belt Mission Study, SD-70-21-1, 201 pp.

Solar Thermal (Water) Propulsion

Alexander, R. A. and H. W. Coleman (1999) “Thermal Characterization of a Direct Gain Solar Thermal Engine” *http://ntrs.nasa.gov/archive/nasa/casi.ntrs.nasa.gov/20000024853.pdf.*

Bérend, Nicolas (2003) “System Study for a Solar Thermal Thruster With Thermal Storage” 39th AIAA/ASME/SAE/ASEE Joint Propulsion Conference and Exhibit 20-23 July 2003, Huntsville, Alabama, AIAA 2003-5031.

Calabro, M. (2002) “Solar Thermal Propulsion” AAAF 6th International Symposium on Propulsion for Space Transportation of the XXIst century Versailles – May 2002

Cassarly, William (2002) “Taming Light” SPIE Magazine, December 2002.

Colonna, Gianpiero et al. (2005) “Model for Ammonia Solar Thermal Thruster” AFRL-PR-ED-JA-2005-343.

Ehricke, K. (1956) "The Solar Powered Space Ship", ARS Paper 310-56, Presented at the Semi-Annual Meeting of the American Rocket Society, Cleveland, Ohio, 18-20 June 1956

Etheridge, F. G. (1979) “Solar Rocket System Concept Analysis” Report on AFRPL Contract O46-1179-C-0007, AFRPL-TR-79-79, Rockwell International, Space Systems Group, Downey, CAY Nov. 1979. AFRPL-TR-79-79.

Fiot, D. et al. (2002) “Solar Thermal Upper Stage Technologies for Future Launcher Generation Program” *https://gsp.esa.int/documents/10192/43064675/C14022ExS.pdf/09ee40fc-1042-441c-9a8a-8d53af3a0df2*

Frye, Patrick E. and James M. Shoji (1992) “Innovative Applications of Solar Thermal Propulsion” AlAA 92-3081.

Hall, Christopher D. (2001) “Solar Orbit Transfer Vehicle” *http://www.dept.aoe.vt.edu/~cdhall/courses/aoe4065/OldReports/sotv.pdf*.

Holmes, Michael (2001) “Solar Rocket Propulsion Ground and Space Technology Demonstration” *http://oai.dtic.mil/oai/oai?verb=getRecord&metadataPrefix=html&identifier=ADA408537*

Jack, J. R. (1961) "Theoretical Performance of Propellants Suitable for Electrothermal Jet Engines", NASA-ND-682, March 1961.

Kennedy, Fred and Palmer, Phil (2003) “An Analysis of Preliminary Test Campaign Results for a Microscale Solar Thermal Engine” 17th Annual AIAA/USU Conference on Small Satellites, *http://digitalcommons.usu.edu/cgi/viewcontent.cgi?article=1794&context=smallsat*.

Kessler, Thomas L. et al. (2000) “Solar Thermal OTV-Applications To Reusable And Expendable Launch Vehicles” *Acta Astronautica* **47**, 215-226.

Lyman, R. W. et al. (2001) “Solar Thermal Propulsion for an Interstellar Probe” AIAA 2001-3377.

McNutt Jr., R. L. et al. (2004) “A realistic interstellar explorer“ *Advances in Space Research* **34**, 192-7.*http://www.sciencedirect.com/science/article/pii/S0273117704002698*

Mossallam, M. A. (2013) “Concentrated Solar Power Utilization in Space Vehicles Propulsion and Power Generation” *International Scholarly and Scientific Research & Innovation* **7**, 1541-1554.

Nakamura, T. et al. (2005) “Solar Thermal Propulsion for Small Spacecraft” PSI-SR-1228, *http://www.psicorp.com/pdf/library/VG05-189.pdf*.

Nakamura, T. et al. (2005) “Solar Thermal Technology for ISRU” *http://www.psicorp.com/pdf/library/VG05-236.pdf*.

Rault, 0. and Hertzberg, A. (1983) "Radiation Energy Receiver for Laser and Solar Propulsion Systems", AIAA Paper 83-1207, 19th Joint Propulsion Conference, Seattle, WAY 27-29 June 1983.

Scharfe, David and Marcus Young (2010) “A Study of Solar Thermal Propulsion System Enhancement via Thermal Storage and Thermal-electric Conversion” AFRL-RZ-ED-TP-2010-110.

Selph, C. C. and Naujohus, G. J., "AFRPL Solar-Thermal Rocket Activities", 1984 JANNAF Propulsion Meeting Proceedings, Vol. 1, pp. 379-384.

Sercel, Joel C. (1985) "Solar Thermal Propulsion for Planetary Spacecraft", presented at the JANNAF Propulsion Conference, San Diego, CA, April 9-12, 1985.

Shoji, James M. (1983) “Solar Thermal Rocket Concept Evaluation and Test Hardware Design” JANNAF Propulsion Meeting v370.

Shoji, James M. et al. (1985) “Solar Thermal Rocket Design and Fabrication” JANNAF Propulsion Meeting v425.

Shoji, James M. et al. (1986) “Windowed Porous Material Absorption Concept – A New Solar Thermal Propulsion Concept” JANNAF Propulsion Meeting v455.

Shoji, James M. (1985) “Solar Rocket Component Study” AFRPL TR-84-057, Final Report.

Shoji, James M. et al. (1992) “Solar Thermal Propulsion Status and Future”, AIAA-92-1719, AIAA Space Programs and Technologies Conference, March 1992.

Sippel, M. and J. Kauffmann (2008) “Solar Thermal Propulsion for Upper Stages”, Chapter 9, *Advanced Propulsion Systems and Technologies, Today to 2020*, *http://arc-test.aiaa.org/doi/abs/10.2514/5.9781600866937.0201.0222*.

Venkateswaran, Sankaran (1992) “Analysis of Direct Solar Thermal Rocket Propulsion” *Journal of Propulsion and Power* **8**, 541-7.

Wassom, S. R. (2000) “Focus Control System for Solar Thermal Propulsion” 2000 International ADAMS User Conference.

Wilner, B., Hays, L. and Buhler, R. (1963) "Research and Development Studies t o Determine the Feasibility o f a Solar LH2 Rocket Propulsion System", Electro-Optical Systems, Inc., Final Report, Contract AF04(611)-8181, RTD-TDR-63-1085, September 1963, AD345094.

Zuppero, A. C. (2005) “Propulsion to Moons of Jupiter Using Heat and Water Without Electrolysis Or Cryogenics” Space Exploration 2005 SESI Conference Series.

Zuppero, A. C. et al. (1997) “Nuclear-Heated Steam Rocket Using Lunar Ice” *http://arc.aiaa.org/doi/abs/10.2514/6.1997-3172*.

Zuppero, A. C. et al. (1999) “Origin Of How Steam Rockets Can Reduce Space Transport Cost By Orders *Of Magnitude” http://www.neofuel.com/staiff1999/zuppero-*1999_staiff99_steam_rocket_factor_1000_final_g.pdf